



**This electronic thesis or dissertation has been  
downloaded from Explore Bristol Research,  
<http://research-information.bristol.ac.uk>**

*Author:*  
**Bozzolan, Elisa**

*Title:*  
**Quantifying the influence of informal housing on rainfall-triggered landslides in the humid tropics**

**General rights**

Access to the thesis is subject to the Creative Commons Attribution - NonCommercial-No Derivatives 4.0 International Public License. A copy of this may be found at <https://creativecommons.org/licenses/by-nc-nd/4.0/legalcode> This license sets out your rights and the restrictions that apply to your access to the thesis so it is important you read this before proceeding.

**Take down policy**

Some pages of this thesis may have been removed for copyright restrictions prior to having it been deposited in Explore Bristol Research. However, if you have discovered material within the thesis that you consider to be unlawful e.g. breaches of copyright (either yours or that of a third party) or any other law, including but not limited to those relating to patent, trademark, confidentiality, data protection, obscenity, defamation, libel, then please contact [collections-metadata@bristol.ac.uk](mailto:collections-metadata@bristol.ac.uk) and include the following information in your message:

- Your contact details
- Bibliographic details for the item, including a URL
- An outline nature of the complaint

Your claim will be investigated and, where appropriate, the item in question will be removed from public view as soon as possible.



**This electronic thesis or dissertation has been  
downloaded from Explore Bristol Research,  
<http://research-information.bristol.ac.uk>**

*Author:*  
**Bozzolan, Elisa**

*Title:*  
**Quantifying the influence of informal housing on rainfall-triggered landslides in the humid tropics**

**General rights**

Access to the thesis is subject to the Creative Commons Attribution - NonCommercial-No Derivatives 4.0 International Public License. A copy of this may be found at <https://creativecommons.org/licenses/by-nc-nd/4.0/legalcode> This license sets out your rights and the restrictions that apply to your access to the thesis so it is important you read this before proceeding.

**Take down policy**

Some pages of this thesis may have been removed for copyright restrictions prior to having it been deposited in Explore Bristol Research. However, if you have discovered material within the thesis that you consider to be unlawful e.g. breaches of copyright (either yours or that of a third party) or any other law, including but not limited to those relating to patent, trademark, confidentiality, data protection, obscenity, defamation, libel, then please contact [collections-metadata@bristol.ac.uk](mailto:collections-metadata@bristol.ac.uk) and include the following information in your message:

- Your contact details
- Bibliographic details for the item, including a URL
- An outline nature of the complaint

Your claim will be investigated and, where appropriate, the item in question will be removed from public view as soon as possible.

# Quantifying the influence of informal housing on rainfall-triggered landslides in the humid tropics

by

**Elisa Bozzolan**

Department of Civil Engineering

University of Bristol



A dissertation submitted to the University of Bristol in accordance with the requirements for award of the degree of Doctor of Philosophy in the Faculty of Engineering.

February 2021





# Abstract

Rainfall-triggered landslides cause the greatest death toll in developing countries and such an impact might increase under climate change and ongoing urbanisation. In the humid tropics, rainfall is the main landslide trigger and climate change will likely change rainfall pattern and potentially landslide incidence rates. At the same time, rapidly expanding cities modify the natural environment, often increasing the susceptibility of slopes failure. This is particularly the case in informal settlements where unregulated slope cutting, vegetation removal and lack of surface water management can increase landslide occurrence. Landslide hazard assessment that accounts for the effect of both climate change and informal housing should therefore be used to inform disaster risk reduction decisions. However, climate and land cover change (from deforestation to informal urbanisation), if included, are generally analysed separately. This research gap might be explained by the lack of slope stability models that include hydrological slope dynamics, vegetation, and urbanisation, as well as a lack of methodologies that deal with the large uncertainty that such analysis involves. In particular, the uncertainty related to errors and incompleteness of the input data (common in developing countries) and future climate predictions often challenge the practical usefulness of current landslide hazard assessment approaches. This thesis addresses such data and methodological gap by providing a new methodological framework that includes informal housing and climate change in slope stability analyses. This new methodology is used to explore and quantify changes in slope stability under different natural and anthropogenic conditions while including a transparent representation of uncertainty (essential to support decision making) associated with both the slope properties and future climate predictions. First, the mechanistic model CHASM (Combined Hydrology And Stability Model) is extended to represent leaking pipes, septic tanks, and roof gutters (CHASM+). Secondly, CHASM+ is incorporated into the new methodology and applied in a typical data-scarce location of the humid tropics. The analysis demonstrates that informal housing increases landslide hazard and quantifies how the presence of informal housing modifies the natural susceptibility of slopes failure. Critical rainfall (intensity-duration) thresholds for triggering landslides are also evaluated, identifying a greater number of small-scale landslides for high intensity and short duration events when informal housing is included in the slope stability analysis. Finally, the results are transferred into regional hazard maps, which can be adjusted for different land cover and climate, demonstrating the importance of accounting for their joint effects on slope stability analysis when supporting environmental planning under changing conditions.



# Acknowledgments

My first and biggest thank goes to Elizabeth Holcombe, who has guided me through this PhD, shared passion and valuable advice while supporting me at both professional and person level. Thanks also to Francesca Pianosi and Thorsten Wagener who greatly improved this work with excellent suggestions and, together with Liz, shaped me as a researcher. It was a great pleasure to work with the three of them.

Thanks to Ivan Marchesini and his team who helped me with the work in Chapter 4, and for their availability to chat and consider me for future collaborations. Thanks also to EPSRC, as this work would not exist without their support.

Thanks to my officemates Rose and Shaini for the chats, laughs, Greek biscuits, moments of research panic, and mainly for being such a joyful daily company while rocking science; to the whole woodland road water research group and the, now legendary, lunch break debates on science, politics and reality perception; thanks to my (numerous) housemates, especially Ana, Suzanne, Alberto and to my favourite boys and friends Elia and Ivan, who fed me with good dinners, wine, films and music; thanks to my lifelong friends Fede, Cate, Silvi, Franca, Michi, Chiari, Gigio and Diego, for always being a home I can come back to.

A special thank then goes to 'the lads', Maria and Anna. Thanks for being such mad and hilarious friends. Meeting them was definitely one of the reasons why this Phd was worth doing. And a thank to Cain for standing by me through these four years, for the laughs (and the countless perplexed smiles) and for the list of memories that will stay with me as nice melodies do.

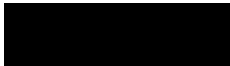
Most of all, thanks to my parents and my brother Nico for constantly supporting me while understanding or not my choices. Thanks for always being there no matter what.



## Author's declaration

I declare that the work in this dissertation was carried out in accordance with the requirements of the University's Regulations and Code of Practice for Research Degree Programmes and that it has not been submitted for any other academic award. Except where indicated by specific reference in the text, the work is the candidate's own work. Work done in collaboration with, or with the assistance of, others, is indicated as such. Any views expressed in the dissertation are those of the author.

**Signed:**



**Date:** 26/02/2021



# Table of Content

Abstract .....	1
Acknowledgments .....	3
Author’s declaration.....	5
Table of Content .....	7
List of figures .....	10
List of Tables .....	19
List of Acronyms .....	20
Chapter 1 : Introduction .....	21
1.1 Landslide risk in developing countries and a changing climate .....	21
1.2 Lack of scientific methodologies to quantify the influence of informal housing on landslide probability .....	27
1.2.1 Review of methods for landslide hazard assessment .....	30
1.2.2 Uncertainties and current techniques to handle them .....	36
1.2.3 Summary of advantages and limitations of current approaches .....	39
1.3 Research goal and objectives .....	43
1.4 Research outline .....	45
Chapter 2 : A methodology to include informal housing into slope stability analysis under uncertainty .....	46
2.1 A new methodology outline .....	47
2.2 CHASM – Description of its hydrology and stability routines .....	50
2.2.1 Integrating slope water management (point water sources) into CHASM: new CHASM+ .....	58
2.2.2 Assumptions and limitations of the model .....	62
2.3 Methods for uncertainties quantification and attribution.....	63
2.3.1 Regional sensitivity analysis (RSA).....	64
2.3.2 Classification And Regression Tree (CART).....	65
2.4 Assessing the performance of the newly extended CHASM+ .....	66
2.4.1 Sanity checks for the new point water source functions and for the modified grid search .....	66
2.4.2 Using GSA to benchmark the new slope water point source functions in CHASM+ .....	69
2.5 Conclusions.....	78
Chapter 3 : Including informal housing in slope stability analysis – an application to a data-scarce location in the humid tropics .....	79
3.1 Introduction.....	80
3.2 Method .....	82
3.2.1The case study: Saint Lucia, Eastern Caribbean .....	83
3.2.2Definition of the input factors and their probability distributions.....	84

3.2.3	Creation of synthetic combinations of input factors and model simulation .....	90
3.3	Results .....	91
3.3.1	Regional sensitivity analysis .....	92
3.3.2	CART analysis .....	94
3.4	Discussion .....	96
3.4.1	Slope cutting is the urban construction activity most detrimental to slope stability .....	96
3.4.2	The rainfall threshold for triggering landslides is lower when informal housing is included .....	97
3.4.3	Guidelines for landslide mitigation actions to tackle the main instability drivers .....	100
3.5	Conclusions.....	101
Chapter 4	: Mapping landslide hazard in a data scarce region under changing urbanisation and climate ..	103
4.1	Introduction.....	104
4.2	Method workflow and components needed.....	107
4.2.1	Available land cover map, Digital Elevation Model and landslide inventory .....	109
4.2.2	Automatic creation of slope units for Saint Lucia .....	110
4.2.3	Definition of the input factors and their probability distributions.....	112
4.2.4	Creation of synthetic combinations of input factors and model simulation.....	117
4.2.5	Analysis of model simulations to associate each SU with a failure rate and create a hazard map .....	118
4.2.6	Evaluation of the quality of the hazard map .....	119
4.3	Analysis and results .....	120
4.3.1	Identify the most influential input factors for slope stability.....	120
4.3.2	Define the probability of failure for a slope unit as a function of the most influential input factors .....	121
4.4	Discussion .....	129
4.4.1	Thickness and cohesion of the first layer of soil, slope angle and rain properties are the most influential input factors at regional scales .....	129
4.4.2	The five most influential input factors identified create accurate hazard maps .....	130
4.4.3	When and where the combined effect of land cover and climate change mostly increases landslide hazard.....	131
4.5	Limitations .....	132
4.6	Conclusions.....	134
Chapter 5	: Summary and Conclusions.....	135
5.1	Research Summary .....	135
5.1.1	Summary of Chapter 2.....	137
5.1.2	Summary of Chapter 3.....	138
5.1.3	Summary of Chapter 4.....	138



5.1.4 Overall thesis conclusions .....	139
5.2 Directions for future work .....	140
5.2.1 Bringing this research into practice .....	140
5.2.2 Possible ways to improve landslide hazard assessment: a scientific outlook .....	141
5.3 Concluding remarks .....	143
Appendix A – Supporting information for Chapter 2 .....	144
Appendix A1: Description of the new text files for running CHASM+ .....	144
Appendix A2: Stochastic creation of input files to run CHASM .....	146
A2.1 Geometry file .....	147
A2.1.1 Modify coordinate of the slope profile when cut slopes are present .....	148
A2.1.2 Insert houses according to the selected urban expansion model .....	149
A2.1.3 House loading .....	150
A2.1.4 Modify the initial soil suction to maintain the water table height where initially set .....	150
A2.2 Vegetation file .....	152
A2.3 Water leakage file .....	153
A2.4 Modify the stability file to include the new search grid .....	155
Appendix B – Supporting information for Chapter 3 .....	156
Appendix B1: CART performance without auxiliary variables .....	156
Appendix B2: CART pruning .....	158
Appendix B3: Calculation of the rainfall threshold by multi-objective optimisation .....	159
Appendix C - Supporting information and results for Chapter 4 .....	162
Appendix C1: The influence of urban density on slope stability .....	162
Appendix C2: Predict soil thickness by using inherently unstable slopes .....	163
Appendix C3: Exponential relationships between the most influential input factors .....	167
Appendix C4: Differences in failure rates between land covers .....	170
Appendix C5: Sensitivity rank for different classes of slope angle .....	172
Bibliography .....	174
Curriculum Vitae .....	189

# List of figures

- Figure 1.1: distribution and number of reported fatalities associated with approximately 10,804 rainfall-triggered landslides from 2007-2017. White dots represent 8,369 incidents with zero fatalities. Source: the Global Landslide Catalog, available at <https://catalog.data.gov/dataset/global-landslide-catalog-export>. The white lines represent the Tropics of Cancer, framing the regions of the humid tropics..... 22
- Figure 1.2: Examples of informal housing affecting land stability. Panels (a) and (b) show examples of unsupported cut slopes, respectively, in DumsiPakha (Kalimpong, India) and Saint Lucia (Caribbean). Panel (c) shows the effect of the lack of water management in an informal community of Saint Lucia (Caribbean). Source: the AGU Landslide Blog (<https://blogs.agu.org/landslideblog/2016/03/14/managing-urban-landslides-1/>, last access: 21 November 2020) and the community-based project Mosaic (Management of Slope Stability In Communities; Anderson and Holcombe, 2013).**Errore. Il segnalibro non è definito.**
- Figure 1.3: (a) Framework describing the traditional top-down approach used to derive future landslide hazard predictions based on the climate scenario selected; (b) the bottom-up approach used in this study, which starts by defining many feasible combinations of the input factors to then identify the regions in such input space that lead to a certain output (e.g. high or low probability of failure – high or low vulnerability). \*In this context, the term ‘vulnerability’ is used to define critical hazard thresholds that identify a change in slope stability response (e.g. FoS passing from above to below 1). ..... 39
- Figure 2.1: The new methodology developed which addresses the gaps outlined in Fig. 1.4 (Chapter 1). The innovative components are highlighted in bold. .... 48
- Figure 2.2: Main workflow that will be used throughout this thesis. To include informal housing into the analysis, the mechanistic model CHASM is extended, and the generation of the input files required to run the model is automated with a Matlab script. To assess the uncertainties associated with the model’s outputs, the two methods RSA and CART are selected. All these components are described in more detail in the following sections, as reported in the figure. .... 50
- Figure 2.3: Geometrical and process representation of CHASM (after Wilkinson 2000).....51
- Figure 2.4: On the left, a schematic representation of the negative pressure defining soil suction. The surface tension of water in between particles creates menisci, a force that pull fine particles together (apparent cohesion). Such negative pressure becomes the more significant the finer the soil particles (e.g. on clays). On the right, the SWCCs proposed by Hodnett and Tomasella (2002), for different soil textural classes for tropical soils. The curve presents an ‘S’ shape, with maximum water moisture content corresponding to the minimum (in absolute value) suction and vice versa..**Errore. Il segnalibro non è definito.**

Figure 2.5: Circular slip surface analysis with method of slices (after Wilkinson 2000)..... 54

Figure 2.6: Representation of rainwater intercepted by the roof discharged onto the top cells of the slope to the sides of the house for (a) double pitch roof; (b) single pitch roof discharging downslope; (c) single pitch roof discharging upslope. .... 61

Figure 2.7: (a) Example of search grid that CHASM could represent before the modifications apported (only square or rectangular shapes are possible); (b) example of search grid that the new CHASM+ can represent. The letter ‘L’ represents the length of the slope; ‘H’, the height; ‘X’ represents the portion of the grid tilted of  $\delta$ ; ‘r’ portion of horizontal grid (see Appendix A1). .... 62

Figure 2.8: Difference between FoS calculated on slopes with houses with roof gutters versus those without (10 houses in total). The FoS is always higher in the case houses are provided with roof gutters. The shading refers to the legend in Fig. 2.12. The simulated slopes are 70 m long and 30° steep. The SWCC refer to Sandy Clay loam (from Hodnett and Tomasella, 2002). The soil is 7 m deep, overlying an impermeable surface, also 7 m deep. Rainfall duration is 24 h. The roofs are simulated as double pitch. .... 67

Figure 2.9: Difference between FoS calculated on slopes with houses without versus with superficial leaking pipes (10 houses and leaking pipes in total). The FoS is always higher in the case pipes are not leaking. The shading refers to the legend in Fig. 2.12. The simulated slopes are 70 m long and 30° steep. The SWCC refer to Sandy Clay loam (from Hodnett and Tomasella, 2002). The soil is 7 m deep, overlying an impermeable surface, 7 m deep. Rainfall duration is 24 h. The leak of the pipe is constant and equal to  $1 \times 10^{-6} \text{ m}^3 \text{ s}^{-1}$ . .... 67

Figure 2.10: Legend of shading used to categorise the difference between FoS. The division in classes is arbitrary..... 67

Figure 2.11: Difference between FoS calculated on slopes with or without leaking buried septic tanks (10 houses and septic tanks in total). The FoS is always higher in the case where houses have a septic tank that does not leak. The colours refer to the legend in Fig. 2.12. The simulated slopes are 70 m long and 30° steep. The SWCC refer to Sandy Clay loam (from Hodnett and Tomasella, 2002). Rainfall duration is 24 h and rainfall intensity is  $30 \text{ mm s}^{-1}$ . The leak of the tank is constant and equal to  $1 \times 10^{-6} \text{ m}^3 \text{ s}^{-1}$ ..... 68

Figure 2.12: Difference between FoS calculated on slopes with varying slope and cut angles using the traditional square-shaped search grid (old grid) and the new search grid that runs parallel to the slope. FoS is always higher in the case the old search grid is used. The colours refer to the legend in Fig. 2.12. The simulated slopes are 70 m long. The SWCC refer to Sandy Clay loam (from Hodnett and Tomasella, 2002). The soil is 7 m deep, overlying an impermeable surface. Rainfall duration is 24 h and rainfall intensity is  $30 \text{ mm h}^{-1}$ . .... 69

Figure 2.14: the methodology developed for this thesis (described in Section 2.1) is used to compare the results obtained with CHASM+ and GeoSlope for an urban landslide occurred in Sao Jose’ dos Campos (Brazil) in 2016, described in Mendes et al. (2018). The input factors that are known (because of field measurements and lab tests, or because assumed – such as the leak rate) are kept constant, while the input factors that were not specified in Mendes et al. (2018) but are necessary to run CHASM+ as well as those differently implemented in CHASM+, are stochastically varied. .... 74

Figure 2.15: Factor of Safety calculated considering only rainfall and load of the tank for both CHASM+ and GeoSlope (this latter is referred as Mendes et al. 2018, and it corresponds to the grey line with square markers in Fig. 2.13). .... 75

Figure 2.16: The input factors used in CHASM+ are varied within the ranges defined in Table 2.3. The whole ranges are represented in this figure as ‘range all simulations’ (light grey bars). These are compared to the ranges of values that produce ok and best performing simulations (darker greys) which correspond to the FoS trends shown in Fig. 2.15 in the same colour. The black horizontal lines reported on the upper plots (a, b, c and d) identify the discrete values used by Mendes et al. 2018 in the GeoSlope analysis (see Table 2.1). Note as in plot (d) the black line is at zero level..... 76

Figure 2.17: a) shows Factor of Safety calculated considering both rainfall and the leaking tank with CHASM+ and GeoSlope (referred as Mendes et al. 2018); b) shows the parallel plots of the ok (lighter grey) and best performing (darker grey) simulations. The lines identify how the input factors are distributed within their variability ranges. The black dots are the values used by Mendes et al. (2018). .... 77

Figure 3.1: Two population of slopes are stochastically generated and analysed in this chapter: urbanised and non-urbanised slopes. .... 80

Figure 3.2: scheme of the main workflow of Chapter 3. .... 82

Figure 3.3: Rainfall intensity–duration–frequency (IDF) curves for Saint Lucia developed by Klohn-Crippen (1995) using Gumbel analysis of 40 years of daily rainfall data from 15 rainfall gauges. The light grey section includes rainfall events from observed data (below IDF curves); the dark grey section represents combinations of rainfall intensity-duration not recorded in the past but that might occur in the future (above IDF curves). .... 87

Figure 3.4: Urban properties of informal housing included in the slope stability analysis. Each house corresponds to a cut on the slope. Cut slope angle varies according to its probability distribution, defined in Table 3.1. Vegetation, roof gutters, leaking tanks/pipes are stochastically inserted or not. The house on the cut slope is always present and its load is not varied. The height of the cut slope varies relatively to the cut slope angle, but it is forced to be maximum 4 metres. .... 88

Figure 3.5: Example of slope generated by stochastically sampling from the ranges of input factors specified in Table 3.1. H is the slope height resulting from the fixed slope length and varying slope angles. The dimensions of the slip circle search grid are fixed, with initial height of 20 m, and width equal to the slope length. The grid extends downslope parallel to the slope as shown..... 91

Figure 3.6: Percentage of predicted stable and failed slopes per each urban property. An urban property will be influencing slope stability if the percentage of the predicted failures changes with the variation of that urban property..... 92

Figure 3.7: Sensitivity index for each input factor in the urbanised (full colour) and not urbanised (pale colour) cases. The bars correspond to the mean value of sensitivity for each input factor calculated with bootstrapping, while the black vertical lines at the top of the bars represent the confidence interval (Number of bootstrap resampling N = 100; significance level for the confidence intervals 0.05). ..... 93

Figure 3.8: Percentage of slope failures for urbanised and non-urbanised slopes for different categories of input factors. Throughout, urbanised slopes show higher failure rates than non-urbanised slopes. In the upper plots (a), (b), (c), the distribution of failure rates for urbanised slopes are more uniform for variations of input factors than the non-urbanised case, while in the lower plots (d), (e), it is more pronounced. Panels (a-c) represent the input factors whose sensitivity indices are smaller when urbanisation is introduced in Fig. 3.7, while the (d-e) show the input factors whose sensitivity gets larger when urbanisation is introduced in Fig. 3.7. .... 94

Figure 3.9: Classification tree of slope response for non-urbanised slopes (a) and urbanised slopes (b). Black branches represent the paths that lead to simulations predicted as failed, while grey branches lead to simulations predicted as stable. The bar under each leaf shows the proportion of simulations that resulted as failed (black) or stable (grey) for that leaf. The thickness of the branch is proportional to the number of simulations following that path. Note as 14% and 22% of the simulated slopes have been excluded respectively for the non-urbanised and urbanised case, because failed before the start of the precipitation. .... 96

Figure 3.10: In figure (a) and (b) the red line represent the minimum rainfall thresholds calculated from our stochastic sample (99.9% of the failed slopes in the sample are above the thresholds). Figure (c) represents the radius of the slip surfaces of the recorded landslides plotted against the corresponding triggering rainfall intensity/duration ratio. Note as in (a) and (b) the x and y axis are in logarithmic base 10 scale, but the notation is linear for an easier readability..... 99

Figure 4.1: Slopes stochastically generated for the analysis of this chapter to compute regional hazard maps for Saint Lucia. .... **Errore. Il segnalibro non è definito.**

Figure 4.2: scheme of the main workflow of Chapter 4..... 107

Figure 4.3: (A) Land cover map where different land cover types have been grouped into 4 classes: forest, shrub, urban and water bodies. The original version can be downloaded at <http://www.charim.net/stlucia/maps.>; (B) Slope steepness map derived from the DEM available at 5m resolution; the DEM is available at <http://www.charim-geonode.net/layers/geonode:dem>; the black polygons in Fig. 4.3 (B) represent the landslides recorded after the Hurricane Tomas (2010) by Mott MacDonald (2013). The corresponding GeoNode can be downloaded at [http://www.charim-geonode.net/layers/geonode:landslides\\_2010\\_2014](http://www.charim-geonode.net/layers/geonode:landslides_2010_2014). Of the 1025 landslides available for the year 2010, only the 714 landslides fully contained within the slope units are displayed..... 110

Figure 4.4: Slope Units (SUs) of Saint Lucia. On the right hand side, a zoom-in of the map, showing the SUs overlaying the terrain aspect (derived from the DEM described in Section 4.2.1). The minimum area and circular variance values are varied until the shape of the SUs is as much as possible homogeneous with the terrain aspect. .... 1122

Figure 4.5: Rainfall intensity–duration–frequency (IDF) curves for Saint Lucia developed by Klohn-Crippen (1995) using Gumbel analysis of 40 years of daily rainfall data from 15 rainfall gauges. The light grey area includes rainfall events from observed data (below IDF curves); the dark grey area (above IDF curves) represents combinations of rainfall intensity-duration not recorded in the past but that might occur in the future..... 115

Figure 4.6: Example of urban slope generated by stochastically sampling from the ranges of input factors specified in Table 4.1. The dimension of the slip circle search grid depend on the slope height (H) and length (L) as shown in the figure. The grid extends downslope parallel to the slope as shown. Its size has been reduced compared to the analysis of Chapter 3 to constrain the computational time. On the right hand side of the figure, a zoom-in box shows the urban properties included in the slope stability analysis. The urban properties that are stochastically varied are written in black, whereas those that are kept fixed are written in grey. Cut slope angle varies according to its probability distribution, defined in Table 4.1. Vegetation, roof gutters, leaking tanks/pipes are stochastically inserted or not. The house on the cut slope is always present and its load is not varied. The height of the cut slope varies relatively to the cut slope angle, but it is constrained to a maximum of 4 metres. .... 118

Figure 4.7: Accuracy statistics for the calculation of the ROC curve..... 119

Figure 4.8: Sensitivity index for each input factor in the 4 land covers considered. The bars correspond to the mean value of sensitivity for each input factor calculated with bootstrapping, while the black vertical lines at the top of the bars represent the confidence interval (Number of bootstrap resampling N = 100; significance level for the confidence intervals 0.05). .... 120

Figure 4.9: Representation of the window (red cube) used to calculate the frequency of failure across the variability space. The letters (a), (r), (s) represent the ranges of the three combined input factors whose

intersection define such window. The initial width of these ranges is defined in the box on the left hand side of the figure as well as the rate of increase. Initial width and rate of increase are chosen heuristically according to the total range of variability, input factor type and after visual inspection of the results. When the window includes a number of simulations less than M, the rate of increase is used to iteratively widen the ranges (a), (r), and (s) in the direction of the black arrows until M simulations are included. .... 1233

Figure 4.10: Landslide hazard map corresponding to the Hurricane Tomas rainfall event. The landslides recorded after the event (black polygons) are plotted on the map. On the top right-hand side corner, we show the success rate curve, overlying the ROC curve. These curves are used to evaluate the capability of the map to reproduce the hazardous areas under the rainstorm event. The performance of the model increases the more the curve gets closer to the point (0,1). Points that fall on the bisector are associated with a model that randomly predicts stable or unstable slope units with the same rate. .... 124

Figure 4.11: Hazard maps obtained for varying rainstorm severity and two hypothetical scenarios: 1) vegetation is removed (middle panel) and 2) informal housing is inserted (bottom panel) on all slopes with angle less than 50°. The framed map is the same reported in Fig. 4.10. The arrows between the maps highlight the change in percentage of SUs predicted with high frequency of failure ( $\geq 0.5$ ). Between the maps, each SU is defined by the same two input factors - slope angle, soil ratio but varying rain index. A moving window (see section 4.3.2) is then used to identify the frequency of failure of the simulated slopes most similar to each SU, within the library of simulations corresponding to the SU's landcover. The windows size used for the maps are kept equal to those used for calculating the hazard map of Fig. 4.10 in order to facilitate the comparison..... 125

Figure 4.12: Example for forested slope: in the upper panel the scatter plot of failed (black dots) and stable (grey dots) slopes at variations of soil ratio, slope angle and rain index. The lower plots represent the frequency of failure calculated with the moving window from the corresponding scatter plots of the above panel. These scatter plots represent the 2D planes of the 3D plots shown in Fig. 4.9. The frequency of failure calculated for the other land covers are reported in the Appendix C3. .... 1277

Figure 4.13: difference in frequency of failure between the three land covers considered. The title of each plot defines the calculation made in the image subtraction (e.g. bare – forest: frequency of failure of bare slopes minus frequency of failure of forested slopes). The colour identifies the increase in landslide frequency (from 0 difference in white to 40% more failures in black). The other combinations of image subtraction can be found in Appendix C4. .... 128

Figure 5.1: Landslide drivers found to most influence urban slope stability in the three analyses performed in this thesis, and their respective spatial scales. The drivers are ranked in order of influence. .... 1366

Figure A.1: Typical content of a steering file. CHASM reads the text files not preceded by the symbol #... 144

Figure A.2: Example in support of Table A.1. ....	1455
Figure A.3: Geometrical and process representation of CHASM (after Wilkinson 2000). ....	147
Figure A.4: representation of the input factors required for the representation of houses on slopes. The physical meaning of the letters are reported on the legend on the right hand side of the figure. The colour grey refers to those input factors that are treated as fixed within the Matlab code (as specified in Table A.3). ....	148
Figure A.5: representation of different urban expansion models (regulated by the input factor: urban_model). The numbering shows how cut slopes are generated according to the urban model selected. ....	149
Figure A.6: (a) Example of slope with initial soil suction equal to -0.5 m. (b) Example of soil water characteristic curve (SWCC), user defined. The example shows that the cell above the water table is defined by an initial suction equal to -0.065 m which is smaller than the maximum value defined in SWCC (max value = -0.1 m). The maximum value of soil moisture content is then assigned to that cell, thus resulting saturated. ....	151
Figure A.7: List of functions in the Matlab code generating the new geometry file. ....	152
Figure A.8: List of functions in the Matlab code generating the new vegetation file. ....	153
Figure A.9: representation of possible options that can be inserted to model water management at household scale. ....	154
Figure A.10: List of functions in the Matlab code generating the new water leakage file. ....	154
Figure A.11: representation of the new search grid, modified to look for both small and large slip surfaces. ....	155
Figure B.1: Cross-validation error of the CART for increasing pruning level for non-urbanised (a) and urbanised (b) slopes. The cross-validation error is computed by randomly dividing the dataset in 10 subgroups. Ten trees are then constructed by using 9 subgroups as training set. The excluded subgroup is used to calculate the misclassification error (in percentage). The average value of the ten misclassification errors so obtained gives the cross-validation error (at given pruning level). The 'chosen minimum' (in blue) represents the pruning level and corresponding misclassification error to build the CART in Fig. B.2; in black (values pointed by the arrows), the pruning level used to build the trees reported in the chapter 3 (Fig. 3.9 a and b) and the corresponding misclassification error resulted if the auxiliary variables (A.V.) were not considered. ....	156
Figure B.2: CART tree obtained for urbanised slopes without considering auxiliary variables. Black branches represent the paths that lead to simulations predicted as failed, while grey branches lead to simulations predicted as stable. The bar under each leaf shows the proportion of simulations that resulted as failed (black) or stable (grey) for that leaf. The thickness of the branch is proportional to the number of	



simulations following that path. The pruning level used is 17, with 16% simulations misclassified (Fig. B.1).....	1577
Figure B.3: Cross-validation error of the CART for increasing pruning level. The cross-validation error is computed by randomly dividing the dataset in 10 subgroups. Ten trees are then constructed by using 9 subgroups as training set. The excluded subgroup is used to calculate the misclassification error (in percentage). The average value of the ten misclassification errors so obtained gives the cross-validation error (at given pruning level).....	1588
Figure B.4: Combinations of rainfall intensities (I) and durations (D) resulted into stable (grey dots) or failed (black dots) slopes, for the non-urbanised (a) and urbanised (b) case. The plots show how the recorded landslides follow the typical descending trend found in empirical rainfall thresholds. The x and y axis are in logarithmic base 10, but the notation is linear for an easier readability. ....	1599
Figure B.5: Illustration of the two objectives functions used in the optimisation, for a given threshold line: (a) maximise the number of failed slopes above the threshold and (b) minimise the area above the threshold. ....	16161
Figure C.1: Percentage of failure rates (a) between land covers and (b) for varying percentage of urban density. ....	1633
Figure C.2: Simulated slopes failed before the triggering event at variations of their slope angle and thickness of layer 1. The plots show how the recorded landslides follow a linear descending trend (i.e. exponential without the log. transformation) until $\sim 50^\circ$ for then decreasing more rapidly with steeper angles. The 30 thresholds obtained with the multi-objective optimisation tool are plotted in grey and red colour. The dashed red lines represent the lower and upper thresholds, with respectively 99% (lower th1), and 70% (upper th3) of simulations above them. The continuous red line is the threshold used in the analyses presented in chapter 4. 85% of simulations are above this threshold and it is defined by equation C.4. The y axis of the figure is in logarithmic scale, but the notation is linear for an easier readability.....	165
Figure C.3: Hazard maps representing the Hurricane Tomas (rain index = 0.89 – see chapter 4), calculated using different cohesion and soil thickness values. Specifically, cohesion values equal to 8 – 5 – 11 kPa respectively represent the mode, and the mode $-/+$ half standard deviation of the probability distribution of soil cohesion of layer 1 used for the stochastic sampling. The thresholds th1, th2, and th3 are respectively the lower, mid, and upper thresholds calculated with the optimisation algorithm and represented in Fig. C.2. The figure shows how the lower (higher) the threshold the lower (higher) the number of slopes predicted with high frequency of failure ( $\geq 0.5$ ). The framed map is the same shown in chapter 4 (Fig. 4.10) calculated with the mid threshold (th2) and cohesion equal to 8 kPa. ....	167
Figure C.4: Frequency of failure at variation of the most influencing combined input factors. Only slopes with angles below $50^\circ$ are shown (urbanisation is not simulated for steeper slopes). ....	169

Figure C.5: Frequency of failure at variation of the most influencing non-combined input factors. The example represent the failure rates of forested slopes..... 1699

Figure C.6: difference in frequency of failure between the four land covers considered. The title of each plot defines the calculation made in the image subtraction (e.g. bare – forest: frequency of failure of bare slopes minus frequency of failure of forested slopes). The colour identifies the increase in landslide frequency (from 0 difference in white to 40% more failures in black). ..... 17171

Figure C.7: Sensitivity index for each input factor in the 4 slope angle categories and land covers considered. The bars correspond to the mean value of sensitivity for each input factor calculated with bootstrapping, while the black vertical lines at the top of the bars represent the confidence interval (Number of bootstrap resampling N = 100; significance level for the confidence intervals 0.05). ..... 173

# List of Tables

Table 1.1: Summary of advantages of statistical- and mechanistic-based modelling approaches, and their limitations with respect of the four modelling requirements (Req. 1-4) set for this research.....	41
Table 3.1: Input factors of CHASM+ and their probability distributions .....	89
Table 3.2: values defining the vegetation parameters for trees. The values refer to the work presented in Holcombe et al. 2016 (online Supplement, Table S5). .....	90
Table 4.1: Input factors of CHASM+ and their probability distributions. ....	116
Table A.1: Format of the new text file describing surface water management. ....	145
Table A.2: Format of the new text file describing the modified search grid (the modifications are reported in italic) .	146
Table A.3: Input factors to be inserted to include cuts and/or houses on slopes. All the input factors in the table, their ranges and probability distributions, can be defined in Step1_InputSampling_VaryUrbanDegree. ....	148
Table A.4: input factors that define the water management options shown in Fig. A.9.....	154

# List of Acronyms

**CART:** Classification And Regression Tree

**CHASM:** Combined Hydrology And Stability Model

**DEM:** Digital Elevation Model

**DRR:** Disaster Risk Reduction

**EM-DAT:** Emergency Events Database

**FoS:** Factor of Safety

**GIS:** Geographic Information System

**GSA:** Global Sensitivity Analysis

**IPCC:** Intergovernmental Panel on Climate Change

**LAI:** Leaf Area Index

**MC:** Monte Carlo

**ROC:** Receiver Operating Characteristic

**RSA:** Regional Sensitivity Analysis

**SA:** Sensitivity Analysis

**SWCC:** Soil-Water Characteristic Curve

**UN:** United Nation

# Chapter 1 : Introduction

## 1.1 Landslide risk in developing countries and a changing climate

One of the challenges of the 21<sup>st</sup> century is how to reconcile worldwide rapid urban growth with the prevention and mitigation of environmental disasters, such as those caused by landslides. Urban population currently represents 55% of the total global population and this proportion is expected to reach 68% by 2050 (UN, 2019). At the same time, landslides have a great impact on cities worldwide (IFRC, 2020). Current estimates of global landslide records reveal that 300 million people are exposed to landslides every year, with over 4,000 fatalities (Froude and Petley, 2018; Haque et al., 2019), 250,000 of people affected (CRED, 2019), and billions of US dollars of economic damage (Dilley et al., 2005). The International Disaster Database (EM-DAT) suggests that landslides accounted for 5% of all natural disaster events and 1% of all natural hazard fatalities between 1998 and 2017, although these estimates are likely to be greatly underestimated, given that landslides have been recognised to be the least well reported disaster type (CRED, 2019). Rainfall is a major landslide trigger and the impact of rainfall-triggered landslides might be expected to increase under climate change as rainfall patterns change (Seneviratne et al., 2012; CRED, 2019). Slope susceptibility to failure might also be increased by the increasing urban development activities accompanying urban population growth, such as vegetation removal, construction of buildings and roads, and altered drainage (Smyth and Royle, 2000). Given that 90% of urban expansion is projected to take place in the economically developing world (UN, 2019), low- and middle-income countries play a key role in the challenge of urban landslide risk mitigation and climate change adaptation.

Developing countries<sup>1</sup> face the greatest death toll from rainfall-triggered landslides today (Froude and Petley, 2018b; Sepúlveda and Petley, 2015). Figure 1.1 shows all type of mass movements triggered by rainfall and the corresponding fatalities from 2007 to 2017 (Kirschbaum et al., 2010). It is clear from the figure that developing countries are greatly affected by this natural hazard, especially in the tropics (Kirschbaum et al., 2015; Petley, 2009; Alexander, 1989; Froude and Petley, 2018a). To understand the reasons behind such disproportionate impact, landslide risk needs to be analysed in all its components (UNISDR, 2015b). Risk is commonly defined (e.g. in Varnes, 1984) as: *“the expected number of lives lost, persons injured, damage to properties or disruption of economic activities due to a particular phenomenon”*. With respect to landslides, risk is a function of the physical **landslide hazard (H)** expressed as the probability of landslide occurrence within a specific time period (e.g. a year), the **exposure (E)** of people or properties to that hazard, and their

---

<sup>1</sup> In this thesis, developing countries refer to lower-middle-income and low-income countries as defined in (UN, 2019).

**vulnerability (V)**, i.e. the potential for loss, and it can be represented by the following formula (e.g. Van Westen et al. 2016):

$$Risk = \sum (H \sum (EV)) \quad (1.1)$$

When the hazardous event leads to one or more human, material, economic and environmental losses that exceeds the capacity of the system to cope, it is classified as ‘disaster’ (<https://www.undrr.org/terminology/disaster>).

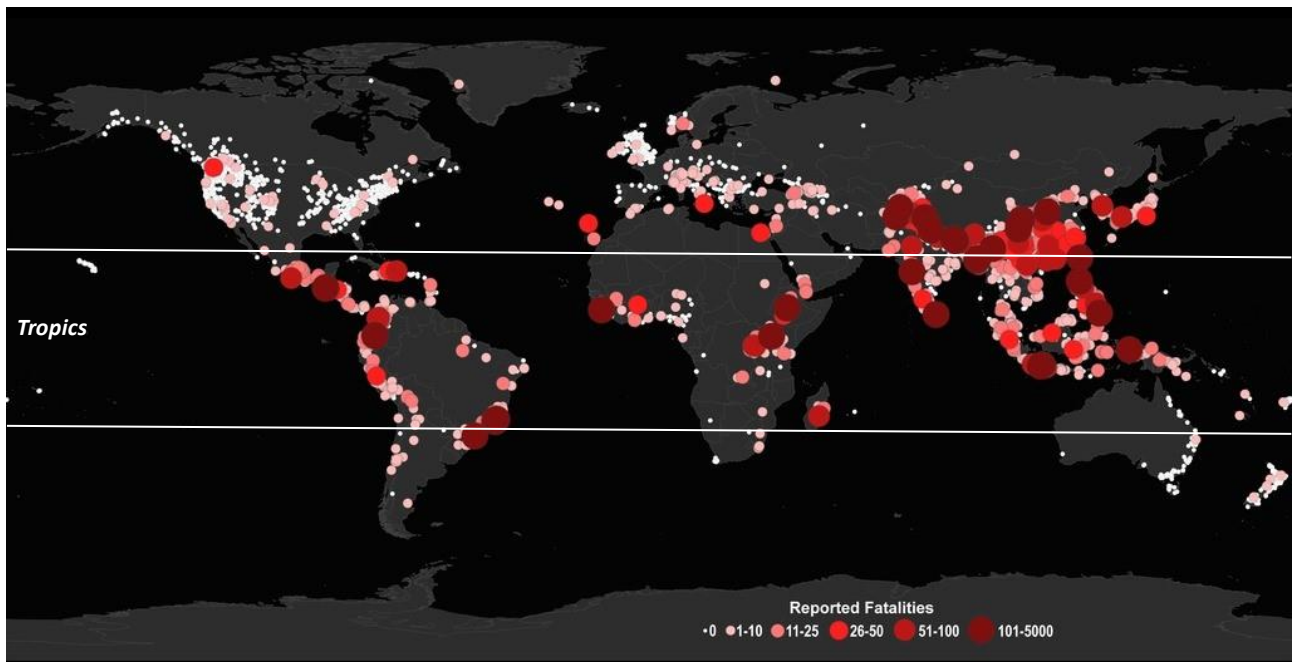


Figure 1.1: distribution and number of reported fatalities associated with approximately 10,804 rainfall-triggered landslides from 2007-2017. White dots represent 8,369 incidents with zero fatalities. Source: the Global Landslide Catalog, available at <https://catalog.data.gov/dataset/global-landslide-catalog-export>. The white lines represent the Tropics of Cancer, framing the regions of the humid tropics.

Landslide *hazard*, *exposure* and *vulnerability* are particularly high in developing countries, because of:

- Location. Most developing countries (80%) are located in the humid tropics. These regions are generally characterized by high annual precipitation totals, recording very intense and prolonged precipitations (e.g. over 100 mm in an hour in both the tropical cyclone- and the monsoon-affected regions), which might initiate landslides because of the progressive build-up of positive pore pressures, additional downward (rainwater) weight forces, reduction in soil capillary suction (i.e. reduction in cohesion) and, in some instances, reduction in soil internal friction (Crozier et al. 2010).

Rainfall has, in fact, been recognised as the main landslide trigger in these regions (Lumb, 1975). Tropical climate also leads to a progressive weathering of the parent bedrock, i.e. the progressing breakdown and alteration of materials near the earth's surface. Consequences of rock weathering can be the reduction of effective strength, the formation of minerals which are susceptible to swelling when wet (as smectite), and the opening or formation of discontinuities, which increase the susceptibility to slope failure (Parise et al., 2004; Regmi et al., 2013), mainly when disturbed by urban development (Petley, 2009).

- Growing urban population. Between 1970 and 2018, the population in developing countries increased from 680 million to 3.2 billion, accounting for 76% of the world's urban population and 84% of the total world population. By 2050, these countries are expected to grow up to 5.6 billion, with 83% of the world's urban population and 87% of the total world population (UN, 2019). The expanding urban population increases landslide exposure in two ways: there is a higher number of elements (e.g., people or buildings) concentrated in the same location (i.e. urban centres) and potentially exposed to the same landslide event; and an increasing number of people that live on landslide-prone areas. Urban centres often expand up to the surrounding steep slopes, which were originally left unbuilt because they were unsuitable for construction. Furthermore, urban construction in such locations modifies the landscape in a way that slope susceptibility to failure might also be enhanced (e.g. by removing vegetation, or cutting the hills).
- Social, economic, political and cultural context (Alcántara-Ayala, 2002). Vulnerability has been defined as *"the characteristics of a person or group and their situation that influence their capacity to anticipate, cope with, resist and recover from the impact of a natural hazard"* (Wisner et al., 2004). Vulnerability involves a combination of factors, grouped in terms of 'root causes' (e.g. historical and cultural development), 'dynamic pressure' (e.g. due to rapid urbanisation, extensive deforestation) and 'fragile livelihood and unsafe locations' (e.g. lack of natural, human, economic and political resources as well as a lack of physical infrastructures) (Wisner et al., 2015). High vulnerability can, in turn, increase landslide exposure and hazard (e.g. low financial capacities might lead to a lack of appropriate construction practices or slope stabilising measures on landslide-prone areas).

Within rapidly developing countries, informal settlements, sometimes called 'slums' (although they are not necessarily the same<sup>2</sup>) are the most at risk of landslides (e.g. Castro et al., 2015; O'Hare and Rivas, 2005).

---

<sup>2</sup> Here we follow the note on the terminology reported in UN-Habitat (2018) for which informal settlements and slums can be used interchangeably and refer to settlements characterized by at least some of the following features: a lack of formal recognition on the part of local government of the settlement and its residents; the absence of secure tenure for residents; inadequacies in provision for infrastructure and services; overcrowded and sub-standard dwellings; and location on land less than suitable for occupation.

Today one billion people live in informal settlements around the world, and represent a substantial percentage of the urban population within some regions (59% of the urban population in sub-Saharan Africa, 28% in Asia and 21% in Latin America and the Caribbean). This type of urban settlements are a by-product of rapid urban expansion without economic growth, the “*exploding cities in unexploding economies*” of Smith (1996). In developing countries, the rapid population influx into urban centres often exceeds government capacity to create the required land regulations and basic services. As a result, the incoming urban dwellers bypass these deficits by adopting their own parallel structures, often ignoring existing land planning and building codes (Fekade, 2000; UN-Habitat, 2003; Castro et al., 2015). Poverty forces low-income households to overcrowd areas of low land value, such as steep slopes susceptible to landslides (Diaz, 1992; O’Hare and Rivas, 2005). Their location, the high population density and the low quality of the housing standards increase both the *exposure* and the *vulnerability* of informal settlements to landslide disasters (Alcántara-Ayala, 2002; Castro et al., 2015).

However, empirical evidence shows that unregulated urban construction activities and lack of infrastructure within informal settlements can also increase the occurrence of rainfall-triggered landslides, i.e. landslide *hazard*. Landslide hazard is defined as the probability of a specific landslide type and magnitude to occur. And a landslide can occur when the destabilising forces (function of the shear component of the gravitational forces and pore pressure) are greater than the resisting forces (function of the normal component of the gravitation force, the failure plane friction and the additional cohesive strength). These forces depend on the inherent susceptibility of the slope to failure (governed by natural factors such as slope angle, material geotechnical and hydrological properties, material strata depths and land cover) and the severity of a triggering event. Within an unregulated urban environment, such as informal settlements, human modifications can increase the destabilising forces (e.g., via steepening the slope gradient via cut slopes) and/or decreasing the resisting forces (e.g., via pipe leakages which increase pore water pressure and consequently decrease soil strength) acting on a slope (Terzaghi, 1950), potentially directly triggering landslides or increasing the susceptibility of slopes to landsliding (Fig. 1.2).





Figure 1.2: Examples of informal housing affecting land stability. Panels (a) and (b) show examples of unsupported cut slopes, respectively, in DumsiPakha (Kalimpong, India) and Saint Lucia (Caribbean). Panel (c) shows the effect of the lack of water management in an informal community of Saint Lucia (Caribbean). Source: the AGU Landslide Blog (<https://blogs.agu.org/landslideblog/2016/03/14/managing-urban-landslides-1/>, last access: 21 November 2020) and the community-based project Mosaic (Management of Slope Stability In Communities; Anderson and Holcombe, 2013).

A review of the literature reveals that **hillslope cutting** (with the side-hill cuttings up-slope and the side-hill embankments of fill down-slope) has often been recognised to increase landslide rates (Sidle et al., 2006; Sidle and Ziegler, 2012; Barnard et al., 2001; Hencher and Lee, 2010; O'Hare and Rivas, 2005). According to Sidle et al., (2006), for example, landslides frequency along roads can be two orders of magnitude higher than in undisturbed steepland forests in Southeast Asia. Similar conclusions were drawn in Nepal, Caribbean and Bangladesh for both road networks and 'cut-and-fill' terracing (Dahal et al., 2006; Rahman et al., 2017; Anderson, 1983; Gerrard and Gardner, 2006; Petley, 2009; Smyth and Royle, 2000). Another major driving factor reported for landslides in the built environment is the **inadequate surface and household water management**. Laws and Murray (2001) highlight that, while in some regions of New Zealand almost 60% of the observed landslides could be directly attributed to unsupported cuts, in other regions almost 50% was related to poor stormwater management. Other field surveys within informal settlements in Latin America indicate that topographic soil water convergence and the consequent potential reduction of soil strength is enhanced by a lack of surface water management (Anderson and Holcombe, 2013, 2006; Smith et al., 2020; Larsen, 2008; O'Hare and Rivas, 2005; Diaz, 1992). Finally, **land cover mismanagement** can promote slope failure in some regions (Cui et al., 2019; Gerrard and Gardner, 2006; Glade, 2003; Reichenbach et al., 2014).

Extensive deforestation in South Auckland district (New Zealand), for example, has been estimated to have increased the probability of landslides occurrence by about three times (Selby, 1976).

Unregulated slope cutting, changes to drainage patterns and surface water concentrations due to increasing impermeable areas and surface water mismanagement, as well as loss of natural vegetation are, therefore, identified as major anthropogenic contributors to rainfall-triggered landslides. In this thesis, the combinations of these urban activities is defined as 'informal housing'. Informal housing generally promotes small (a few metres deep), but frequent landslides (e.g., 250 landslides were recorded in 6 years in the metropolitan area of Caracas between 1974-1979, corresponding to ~42 landslides per year – Diaz, 1992), and they are, for this reason, also defined as 'everyday disasters' (Bull-Kamanga et al., 2003).

While there is a large body of evidence that unregulated urban constructions can enhance landslide hazard, the impact of predicted climate change on slope stability remains equivocal (Gariano and Guzzetti, 2016; Parker et al., 2016; Crozier, 2010). Global warming increases the capacity of the atmosphere to hold water, which might lead to a greater frequency and magnitude of heavy precipitations (IPCC, 2018). More severe and frequent precipitations might then increase landslide activity (Seneviratne et al., 2012). Rainwater infiltrating into the slope, in fact, influences the relation between soil shear and stresses by decreasing soil suction and effective strength, while increasing soil bulk density. Changes in climatic factors can also influence the initial slope conditions (e.g. the soil might be wetter throughout the year and therefore less rainfall might be required to achieve critical conditions) and, in the longer term, promote weathering processes (which can decrease soil cohesion and friction). However, the direction, the magnitude and rate of change in landslide activity due to climate change will depend on specific site conditions (such as the soil hydrological properties which effectively determine how much rainwater can infiltrate and resides into the slope), or landslide type (Crozier 2010) and it is, in general, difficult to predict because of the high level of uncertainties involved in the analysis (Gariano and Guzzetti, 2016; Crozier, 2010).

In the humid tropics, climate projections predict an increase in the frequency of extreme precipitation by 2100 (IPCC, 2018; Seneviratne et al., 2012), which might further increase landslide risk within informal settlements (UN-Habitat, 2018). A better understanding of the joint and relative effect of informal housing and climate change (and their associated uncertainty) on landslide hazard could increase risk awareness, better address investments for hazard mitigation, and built the basis for more sustainable urban development (Smyth and Royle, 2000; Wong and Ko, 2005; Harari et al., 2017). These goals are in line with the 2015-2030 Sendai Framework for Disaster Risk Reduction (DRR) program which aims for the prevention of new, and the reduction of existing “*small scale and large scale, frequent and infrequent*” disasters (UNISDR, 2015a). DRR policies must, by definition, be part of upgrading programs for improving the living conditions

of urban dwellers within informal settlements (Harari et al., 2017). With respect to landslides, researchers involved in field investigations within informal settlements recognise that to facilitate such a sustainable future, municipal authorities require more effective strategies than have hitherto been followed (Smyth and Royle, 2000). In particular, there is the need for objective criteria that identify sets of environmental and urban conditions that enhance landslide hazard (Wamsler, 2006; Anderson and Holcombe, 2013). These tools should support DRR decision and actions, by, for example, more effectively identifying the areas that are most suitable for development and those that require specific infrastructure improvements (Gaillard and Mercer, 2013; Smyth and Royle, 2000; Diaz, 1992).

However, the relative role of informal housing in landslide hazard is rarely investigated and therefore still poorly quantified. This means that as these local urban landslide drivers cannot be identified, the actions to tackle those drivers cannot be explored, and the choice of appropriate landslide mitigation measures cannot be (economically) justified. While such gaps between knowledge and mitigation actions still exist (Gaillard and Mercer, 2013), landslide risk within informal settlements will keep accumulating (UN-Habitat, 2015; Delfin and Gaillard, 2008; Anderson and Holcombe, 2006; UN-Habitat, 2003; Wisner et al., 2004).

## 1.2 A lack of scientific methodologies to quantify the influence of informal housing on landslide probability

Risk accumulation occurs when potential hazards are unaccounted for during urban construction development, and when “*momentary urban development gains [are prioritised] at the expense of increased disaster risk*” (UNDP, 2004). Within informal settlements, a major unaccounted-for hazard is represented by small-scale, high-frequency rainfall-triggered landslides, such as those associated to poorly designed construction activities (Sepúlveda and Petley, 2015; Smyth and Royle, 2000; Diaz, 1992; Bull-Kamanga et al., 2003). These ‘small to medium’ disasters (the ‘every-day’ disasters) are often not recognised in regional and international landslide statistics. For example, the EM-DAT international database records only disasters in which 10 or more people are killed, 100 or more affected, or where damage is sufficient for international agencies to be called in (CRED, 2019), systematically excluding the small-medium disasters causing landslide risk accumulation within informal settlements. When compared to an independent dataset, EM-DAT was found to underestimate the number of fatal landslides by ~2000% and fatalities by 430% between 2004 and 2010 (Petley, 2012). Other studies undertaken within informal settlements highlighted how small-medium scale disasters might not only be highly underestimated by local and regional landslide inventories but also that their adverse impact (economically or in terms of fatalities) might be larger than those events classified as disasters (Bull-Kamanga et al., 2003). It is, therefore, crucial to include such ‘small-medium’ scale disasters

into landslide mitigation programs and urban development planning. Specifically, understanding the drivers of these every-day rainfall-triggered landslide hazards within informal settlements represent the first step to tackle risk accumulation, by providing the basis for hazard mitigation actions and future disaster prevention.

However, landslide hazard management in informal settlements has tended so far to be limited to rescue and recovery post disaster (Delfin and Gaillard, 2008; O'Hare and Rivas, 2005; UN-Habitat, 2003, 2015; Wisner et al., 2004). Landslide hazard prevention, instead, usually involves relocation rather than hazard mitigation (Satterthwaite et al., 2020; Smith et al., 2020). Obstacles for delivering hazard mitigation measures are partly related to the complex social, economic, and political context informal settlements are caught in. For example, there could be a political unwillingness to engage with informal communities<sup>3</sup> (Diaz, 1992; Castro et al., 2015; Satterthwaite et al., 2020); or a lack of trust or communication between the communities members and local authorities, both necessary to deliver any disaster mitigation actions (Rivera et al., 2015; Wamsler, 2007; Smith et al., 2020).

Besides the social and political barriers, **there is also a lack of scientific methodologies to support the prioritisation of what could be done on the ground.** There have been a number of studies that have assessed maps at regional scale of landslide susceptibility (the likely spatial distribution of landslides based on preparatory factors such as slope angle, soil strength or land cover), hazard (spatial and temporal probability of landslides of a certain size) and risk (a function of the hazard, the element at risk and their vulnerability) (for example, Table 3.3 p. 94 in Glade and Crozier, 2005). However, the scale of such mapping does not match with the scale of the human and physical triggering mechanisms, which is critical for practical risk reduction implementation. As Anderson et al., (2011) argue, wide-area landslide maps may identify the part of the community at risk but it does not identify the triggering cause of a landslide. The need is therefore to look *within* the community to examine and model the processes that cause landslides. Once the natural and urban causes behind increasing (every-day) landslide hazard are identified, effective mitigation measures can be deduced or justified. Such understanding is particularly relevant where informal housing takes place, given that planning policies alone (e.g., derived from susceptibility maps), might not be sufficient to control landslide risk because informal housing often outstrips urban regulations.

Landslide hazard assessment within informal communities (the focus of this thesis), thus requires a methodology capable of representing the highly localised effect that informal housing (hill cutting, vegetation removal and surface and subsurface water management) might have on slope stability. Given the fast urban growth within developing countries and the potential of more severe rainstorms in the future, such analysis

---

<sup>3</sup> Throughout this thesis we use the definition of community suggested by (Mercer et al., 2009): a community is defined as “a group of people sharing common ideals, resources, environment and aspirations while living in the same geographical location”.

should also include considerations on the changing environment (e.g., how landslide probability is affected within a community if the urban density becomes higher and/or if rainfall intensity increases).

Another methodological requirement for landslide hazard assessment within informal communities (and in any other context) is the quantification of the uncertainty that such analysis involves. Source of uncertainty can relate to the inherent variability and/or errors in the measurement of the input parameters used in the slope stability modelling (i.e. *aleatory uncertainties* – such as soil properties or landslide inventories, Cho et al. 2007; Steger et al., 2017); or to a lack of knowledge, for example, of the natural processes analysed or of what could happen in the future (i.e. *epistemic uncertainties*; Beven et al. 2018). Aleatory uncertainty can be larger when data are sparse. This is often the case in developing nations, where adequate landslide, soil and rainfall records are often lacking (Sepúlveda and Petley, 2015; Monsieurs et al., 2017). Scarce data contexts can also challenge the evaluation of the epistemic uncertainty associated to climate change - a topic that received a significant attention within the scientific community in the last decades. The standard approach to include climate change in landslide hazard assessment is via scenario-led approaches: future climate projections are obtained from global or regional climate models (e.g. General Circulation Models – GCMs) according to the greenhouse gas concentration scenarios of interest; then, the derived climatic variables (e.g. rainfall intensity and duration) are used to drive slope stability models to assess potential future changes in landslide frequencies (e.g., Bernardie et al., 2020; Melchiorre and Frattini, 2012). However, significant uncertainties exist in evaluating the causal relationship between climate change and landslides (Gariano and Guzzetti, 2016), particularly where sufficient field measurements (e.g. necessary to calibrate downscaled climate models) or landslide inventories (e.g. necessary to train statistical or empirical landslide probability models) are not available (Alvioli et al., 2018). Besides the data availability and the climate model used, there is low confidence in the projections for shallow landslide activity in temperate and tropical regions because of the coincident effect of human land use practice (Seneviratne et al., 2012). A methodology that quantifies and attributes uncertainty including both the urban and the natural environment is thus required.

In summary, a scientific methodology that can assess landslide hazard within informal communities in a data-scarce contexts such as developing countries and that can then be used to deliver evidence and tools for identifying effective landslide hazard reduction strategies, should satisfies the following four requirements:

- 1) Include in the slope stability analysis the urban construction activities typically found within informal settlements, reaching a balance between the level of urban landslide process representation and the data requirements and availability (i.e. the model used should be parsimonious).
- 2) Quantify the relative role of the urban and the natural environmental processes driving landslide hazard from household to hillside scales and across regions, in order to deduce landslide hazard mitigation practices at different stakeholders' decision levels (e.g., cut slope reinforcement at

household scale, drainage implementation within an informal community, urban planning at city scale).

- 3) Include possible future urban expansion scenarios and climate change.
- 4) Quantify the uncertainties related to both data (aleatory uncertainties) and future changes (epistemic uncertainties), associated to both the urban and the natural environment.

In the next sections, a review of the current methods used for landslide hazard assessment and for uncertainty quantification and attribution, reveals that none of the available methodological frameworks satisfy the four requirements above listed. There is a methodological gap between data availability, the scale of the processes controlling slope failure and the models available. Such gap is both scientific and practical because the lack of understanding of how informal housing could be detrimental for slope stability, challenges the deduction of which landslide hazard mitigation actions could be most effective, as well as the limits the delineation of better urban construction practices for the future.

### 1.2.1 Review of methods for landslide hazard assessment

Landslide hazard assessment within a specific period of time and within a given area, is based on the recognition of the conditions that caused the slope to become unstable and the processes triggering that movement (Dai et al. 2002). The factors which determine the probability of landsliding can be defined as: 1) preparatory (generally referred to the natural slope properties) or aggravating (generally referred to the urban properties) factors, which define whether a slope is susceptible to fail, without actually initiating the movement (e.g., slope topography, geology, or land cover); and the 2) the triggering factors (in the case of this thesis, the rainfall properties) which initiate the landslide. The probability of landsliding depends on both factors. However, the triggering variables might change over very short time spans and they are difficult to estimate (Dai et al., 2002; van Westen et al., 2006). If the triggering component is not considered, the term “susceptibility” is employed, which defines the spatial probability of a landslide to occur, but does not specify its temporal probability (e.g. how many times a year a slope is likely to fail).

Numerous methods have been developed to assess landslide hazard. In general, approaches for landslide hazard assessment can be classed as qualitative, which provide hazard zoning or slope stability scores in relative terms; or quantitative which provide numerical estimates of the probability of occurrence of slope movements in a given zone or location (Guzzetti et al., 1999; Van Westen, 2000). Landslide hazard assessments can also be divided into five broad categories according to the data and methods used, as follows (van Westen et al., 1997; Guzzetti et al., 1999): (i) geomorphological hazard mapping which are qualitative methods that rely on the ability of the investigator to identify past and future potential landslides; (ii) heuristic or index based methods which are mostly qualitative and also depend on the ability of the

investigator to understand the underlying causes of the landslide processes in a considered area; (iii) analyses of landslide inventories which are empirical-statistical, quantitative methods that seek to predict future distribution of landslides based on the spatial density and frequency of past landslides; (iv) statistically based models which are quantitative methods that assess the statistical relationship between combination of variables (such as slope angle, lithology, land cover) and observed landslides to evaluate the likelihood of future landslide occurrence for areas where similar conditions exist; and (v) mechanistic/physically based models which are quantitative methods that represent the physical laws regulating slope stability and use numerical models and software to simulate these processes.

Qualitative methods produce subjective estimates of landslide hazard assessment. This subjectivity challenges the evaluation of the degree of uncertainty, making difficult, or impossible, to compare landslide hazard maps produced by different investigators (Guzzetti et al., 1999). For this reason, quantitative methods are generally preferred for both research and decision support applications (Reichenbach et al., 2018; Pardeshi et al., 2013). The choice of the most appropriate quantitative method then depends on the purpose of the assessment, the scale of the area analysed and the data availability (Chowdhury, 1999; Guzzetti et al., 1999). These elements are often interrelated. For example, regional scales can be adopted for land use planning purposes, whereas hillslope scales are more appropriate for site-specific engineering design and construction.

If preparatory and triggering factors associated with substantially complete landslide inventories (i.e. landslide inventories that include a substantial fraction of all landslides at all scales; Malamud et al., 2004) were available in sufficient detail, then landslide inventory-based methods would be probably the best choice for a quantitative hazard estimation, assuming that the occurrence of past landslide events is a good indication for future landslide probabilities (van Westen et al., 2006). However, such inventories, with the exception of particular regions such as Hong Kong, are rare (van Westen et al., 2006). Two other quantitative methods are therefore generally employed: statistical and mechanistic approaches (both spatially distributed and site-specific).

**Statistical approaches** mainly operate at regional scale (< 1:100,000 – p. 87 in Glade and Crozier 2005) and they generally attempt to quantify only the spatial probability of landslides, i.e. where a landslide might occur in a study region (landslide susceptibility - see Reichenbach et al., 2018 for a recent review on the topic), or only the temporal probability, i.e. when landslides might occur, in the form of rainfall thresholds for landslide triggering (e.g., Caine, 1980; Guzzetti et al., 2007). Landslide susceptibility is evaluated by computing the statistical relationship between landslides ('dependent variable') and a set of geo-environmental conditions ('independent variables'), generally available from earth observation data (e.g. lithological maps, or Digital Elevation Models - DEMs with derived slope angle, elevation etc.). Initially, bivariate statistical analysis can

be used to compare landslide locations and each geo-environmental parameter separately, for then computing and assigning to each parameter weighted factors on this basis. Nevertheless, multivariate statistics is generally preferred (Reichenbach et al., 2018) because it employs combinations of geo-environmental parameters, thus considering the interdependence that such parameters might have in influencing slope stability. The resulting matrix is then analysed using statistical tests (such as the multiple regression or discriminant analysis - e.g. Guzzetti et al., 2006a), which provide information of which combination of geo-environmental parameters score equivalent to those for areas associated with landslides. These areas are, for this reason, considered prone to future slope failures. Other statistical methods (e.g. Bayesian probability, fuzzy logic) have also been used (e.g., Lee et al., 2002; Pourghasemi et al., 2012). For example, the fuzzy method simply applies 'if-then' rules (based on expert opinion, frequency ratio or through analytical hierarchy process) to the geo-environmental conditions, and is thus based on a decision tree approach (e.g. Ercanoglu and Gokceoglu, 2002).

On the other hand, statistical models can be used to draw empirical thresholds for the initiation of landslides. A threshold *"might define the rainfall, soil moisture, or hydrological conditions that, when reached or exceeded, are likely to trigger landslides"* (Guzzetti et al., 2007). Thus, statistical approaches (e.g. via Bayesian statistical or frequentist approaches) are used to define the thresholds that best separate the rainfall conditions that resulted in landslides from those that did not (when available) (Brunetti et al., 2010; Guzzetti et al., 2007). Given that there is a direct relationship between rainfall levels and the occurrence of landslides (Finlay et al., 1997), which in turn depends on the slope susceptibility to fail, the link between rainfall thresholds and susceptibility maps could be used to design early warning systems. However, such link can only be assessed where a system of real-time rainfall information and a substantially complete (Malamud et al., 2004) multitemporal inventories are available (see for example, Dai and Lee, 2003; Guzzetti et al., 2006; Zêzere et al., 2004), which, as mentioned before, is not common in developing countries. Nevertheless, statistical approaches have the advantage to be simple, no data-intensive and reproducible (Glade and Crozier, 2005), and the derived susceptibility maps can be used for numerous applications in land use planning, policymaking, and civil defence, even when not combined to rainfall thresholds (Guzzetti, 2000; Varnes, 1984; Glade and Crozier, 2005).

However, in the attempt of assessing landslide hazard within informal communities and evaluating the role of informal housing in landsliding probability, wide-area susceptibility maps are less useful. As mentioned before, a first limitation is that urban planning (derived by susceptibility maps) is often outstripped by informal urbanisation and therefore susceptibility maps alone might not be sufficient to reduce landslide risk. A second limitation is that, despite the rapid progress in topographic remote sensing, it is difficult to generate maps that account for urban factors such as hill cutting (Van Westen et al., 2016). Only the presence (or



absence) of different vegetation covers (e.g. from forest to bare due to human activities), drainage and road networks have been analysed (Meusburger and Alewell, 2008; Galve et al., 2015; Persichillo et al., 2016; Reichenbach et al., 2014; Rahman et al., 2017). Yet, the physical reason behind the increase or decrease of landslide susceptibility is only deduced, for example suggesting that an increased slope stability might be due to a likely better water management in cultivated areas (Persichillo et al., 2016). Furthermore, basic assumptions in statistical approaches are static environmental and triggering boundary conditions (Glade and Crozier, 2005). Considering the continuous change of the catchment conditions following landslide events (Samia et al., 2018; Parker et al., 2016), the ongoing debate on future climate change (Crozier, 2010; IPCC, 2018), and the current fast urbanisation growth and land cover change in developing countries (UN, 2019), the assumption of time stationarity influences the interpretation of the landslide susceptibility assessment.

**Mechanistic models** generally operate at more localised scales (< 1:10,000 – p. 87 in Glade and Crozier 2005) than statistical models. These models rely upon the understanding of the physical laws controlling slope stability. Thus, if they adequately represent the mechanisms acting in a slope system, they are capable of identifying (and disentangling the effect of) the main slope instability drivers. The physical problem involves understanding the resisting and destabilising forces that govern slope movement. Their ratio (resisting/destabilising) constitute the factor of safety (FoS) which quantifies the stability of a slope: stable if greater than one, otherwise failed. Typically, the Mohr-Coulomb failure criterion is assumed, in which the shear strength of the slope material is characterised by its cohesion, angle of friction as well as the normal stress on the slope (a function of the unit weight of the material and pore water pressure). When rainwater infiltrates, the resulting change in pore water pressure modifies the shear strength of the material and therefore the FoS. A realistic prediction should therefore capture these dynamic processes, ideally in the three-dimensional space.

In the case of **spatially distributed mechanistic models** such three-dimensional dynamics are generally simplified to different degrees. Models such as TIGRIS, SHALTAB, SINMAP, TOPOG, and tRIBS-VEGGIES, for example, that couple two or three-dimensional steady and transient groundwater flow with infinite slope stability models are the most common (e.g. Arnone et al., 2016; Baum et al., 2002; van Beek, 2002; Godt et al., 2008; Montgomery and Dietrich, 1994; Pack, 1999; Raia et al., 2014; Burton and Bathurst, 1998; Simoni et al., 2008). These models assess the stability of each mapping unit assuming independence from its neighbours. Only one homogeneous (colluvium) soil layer is generally represented, with its stability calculated along an imposed translational slip surface (although, models with more sophisticated failure surface representation also exist; Anagnostopoulos et al., 2015; Lizárraga and Buscarnera, 2019; Simoni et al., 2008; Formetta et al. 2014). The input factors required to run the model, such as geotechnical and

hydrological parameters, are gathered from field work, laboratory tests and literature (e.g. van Beek, 2002; Vanacker et al., 2003; Godt et al. 2008). Field measurements are then either interpolated or uniformly distributed within the study area (mostly at catchment scale), using 'optimal' values when calibration is possible (Simoni et al., 2008; Gorsevski et al., 2006; van Beek, 2002). The FoS is eventually computed for each mapping unit, providing the predicted stability for the imposed rainfall histories and boundary conditions. By modelling dynamic rainfall interception and infiltration, evapotranspiration, the lateral moisture transfer in the unsaturated and saturated zones, and runoff routing, such theoretical models have the advantage over statistical models to give insights about the hydrological processes involved in a rainfall triggered landslide, potentially improving the understanding of landslide dynamics. For example, Vanacker et al. (2003) identified that the change in landslide hazard due to changes in vegetation cover was regulated by the slope steepness in a fully forested catchment, whereas seepage forces became a more important failure driver on slopes where vegetation was removed. Several other studies suggest that landslides in forested areas occur in steeper slopes than those in unforested areas and that root reinforcement is the main reason for this shift (Rickli and Graf 2009). Another advantage of mechanistic slope stability models is their smaller reliance on observations of past events. This characteristic allows assessment of the impact of predicted and/or hypothetical future climate and urbanization scenarios (e.g. Van Beek and Van Asch, 2004; Alvioli et al. 2018).

While changes in landslide hazard due to changes in vegetation cover are often analysed with spatially distributed mechanistic models, there are no examples where urban construction activities are also considered. This might be related to the scale at which these models operate as well as to their substantial degree of simplification. Urban construction activities (e.g. cut slopes or leaking pipes) are highly localised and therefore difficult to be detected from the satellite images used to define the modelled landscape (e.g. from DEMs). Furthermore, the assumption of infinite slope stability limits the understanding that one can gain on slope stability dynamics between mapping units. For example, in the context where informal housing is modelled, it would not be generally possible analysing how the urban constructions at the top (e.g. loading or water leaking) and at the bottom of a slope interact to determine its stability. Moreover, the assumption of one homogeneous soil layers might represent a limitation when modelling tropical soils, where soil weathering generates overlying soil strata with different geotechnical and hydrological properties, which may in turn influence landslide initiation (Rahardjo et al., 2004; Hencher and Lee, 2010).

**Mechanistic models at site-specific scales** are generally more sophisticated than spatially distributed models. Site-specific mechanistic models typically perform Limit Equilibrium (LE) analysis, which makes the assumption of a critical slip surface of a certain shape (e.g. planar, circular, composite), along which the factor of safety is calculated. The method of slices is then generally used to divide the sliding mass into slices and to calculate the shear and normal forces solving the equilibrium equations in two or three dimensions. LE

analysis can be simplified to different degrees. There are models that apply static limit equilibrium with hydrostatic conditions (e.g. GALENA); models in which two or three dimensional slope hydrology is dynamically integrated into slope stability modelling (e.g. CHASM); and models that perform a dynamic limit equilibrium also simulating two and three dimensional soil deformation (e.g. PLAXIS). Another widely used approach is the analysis of continua, which describe the behaviour of a particular soil type under dynamic stress and strain conditions (e.g. using Finite Elements (FE) analyses as in GeoSlope). These models use constitutive equations to describe the response of a particular soil type under dynamic forces. In contrast with LE, where the slip surface is imposed in terms of geometry and location, models using analysis of continua dynamically assess the most likely failure surface according to the geometry of the slope, initial conditions and the rheology of the material. These approaches could be therefore seen as more sophisticated in terms of physical mechanisms represented, but they are more complex and data intensive than LE methods. Choosing between these two methods therefore depends on the purpose of the analysis and data availability. In general, site specific mechanistic models are used to design new slopes, assess the effectiveness of landslide mitigation actions, or perform back-analyses of observed landslides, on sites where the input factors can be defined via field work and laboratory tests.

While spatially distributed models have the advantage of simulating wide-areas, where the drainage convergence and divergence based on upslope surface morphological conditions (derived from DEM) can be captured, site-specific mechanistic models can be used to evaluate the factor of safety of slopes, also including the effect of informal housing (although none of the models currently available can represent together hill cutting, water surface and subsurface management and vegetation). Such slope stability analyses have, for example, been applied to quantify how vegetation, via the representation of root reinforcement, rain interception, evapotranspiration, plant loading and increased soil hydraulic conductivity in the root zone, could influence (or not) the slopes' landslide probability (Wilkinson et al., 2002b; Greenwood et al., 2004); how leaking tanks, via modelling both the load of the tank and the water leakage, could have influenced the initiation of observed rainfall-triggered landslides (Mendes et al., 2018); how increasing building load and, therefore, increasing urban density, could affect the bearing capacity of the soil (El Kechebour, 2015); and how cut slopes could decrease the slope's FoS (Zhang et al., 2012; Anderson and Lloyd, 1991). Some combinations of these urban construction activities were also investigated under scenarios of dynamic urban expansion (Holcombe et al., 2016). When applied to slopes with different geometries, soil properties, and rainfall forcing, these models can lead to a greater understanding of the system interactions (Wilkinson et al. 2002). Such analysis quantifies how the FoS may change across landscapes, an information that can be particularly useful in the design of the type and magnitude of mitigation measures required to reach an acceptable FoS according to the site specific conditions (Wilkinson et al., 2002b; Collison et al., 1995; Anderson and Lloyd, 1991).

However, the detailed representation of slope processes within these models (both spatially and site-specific mechanistic models) requires an equally exhaustive model parameterization. The more sophisticated the model, the more data it demands to perform the slope stability analysis, and detailed information on the geotechnical and hydrological parameters of soils is generally available only at specific study sites. In data-scarce contexts such as those characterising the analyses performed in this thesis, parsimonious models that balance the ratio between process representation and data requirements should be selected. However, even for parsimonious models, data are rarely available in sufficient detail, introducing uncertainty into the modelling chain. Such uncertainties need to be accounted for throughout the modelling process, and their influence on the model outputs has to be quantified. The next section hence describes different sources of uncertainties affecting slope stability assessments (including those associated with climate change) as well as available techniques currently employed for their quantification and attribution.

## 1.2.2 Uncertainties and current techniques to handle them

Regardless of the model used (e.g. statistical or mechanistic), **aleatory and epistemic uncertainties need to be evaluated** (Corominas et al., 2014; Guzzetti et al., 2006a). Aleatory uncertainties represent the variability, imprecision and randomness of all the factors composing the modelling chain (Beven, 2016; Beven et al., 2018). These uncertainties can be modelled as random variables and represented in terms of probabilities. Epistemic uncertainties, instead, arise from a lack of knowledge about the nature of the phenomenon being considered (the 'severe' or 'deep' uncertainties) (Ben-Haim, 2006). These are more difficult to be evaluated ("*for good epistemic reasons*") (Beven et al., 2018). Any landslide susceptibility or hazard prediction is subjected to some level of aleatory and epistemic uncertainty. Sources of uncertainties include: (i) errors and incompleteness of the input data (e.g. input factors or landslide inventories); (ii) an imperfect understanding of landslide processes and their spatial and temporal evolution; (iii) uncertainties associated with limitations in the methods and models used for the landslide hazard assessment; and (iv) the inherent variability of the landslide phenomena (Wechsler and Kroll, 2006; Guzzetti et al., 2006a; Steger et al., 2017; Beven et al., 2018).

A standard approach to quantify the effect of **aleatory uncertainties** is via Monte Carlo (MC) sampling (Cho, 2007; Eckhardt et al., 2003; Gorsevski and Jankowski, 2010; El-Ramly et al., 2006; Melchiorre and Frattini, 2012; Raia et al., 2014; Wechsler and Kroll, 2006). For example, multiple slopes or catchments scenarios with varying geotechnical and hydrological properties can be created by stochastically sampling from their probability distributions (derived, for example, by literature, or by fitting available field data). In the case of mechanistic models, the output may represent the probability of the FoS. Different statistics can then be calculated to quantify the uncertainties of the outputs given the variability of the input data (Saltelli et al.,

2008). The uncertainty analysis can be followed by a sensitivity analysis, which determines which input factors are more important in influencing the uncertainty of the model output (Wagener and Pianosi, 2019).

Amongst all the **epistemic uncertainties** that can be present in a landslide hazard assessment, those associated to future climate change have received particular attention in the last decades (see Gariano and Guzzetti, 2016 for a review). Given that global warming is indubitable and that the capacity of air to hold moisture is a function of temperature, a greater frequency and magnitude of heavy precipitation might be observed in the future (IPCC, 2018). Many researchers have then tried to quantify the potential impact of future climate change on landslide hazard. This is generally done by introducing climate projections derived from general circulation models (GCMs) into slope stability assessments. As mentioned in the previous sections, these approaches are sometimes referred to in the literature as **'top-down' or 'scenario-led' approaches** (Fig. 1.3a). Climate projections are chosen according to the greenhouse gas concentration scenarios of interest. Given that the GCMs outputs' resolution is quite coarse (the horizontal resolution generally ranges between 100 and 600 km) downscaling techniques are used to obtain local meteorological series (Wilby and Wigley, 1997). Downscaled precipitation predictions are then either compared to empirical and statistical rainfall thresholds to examine changes in the probability of their exceedance (e.g. Dixon and Brook, 2007), or used as forcing for mechanistic models to derive future landslide rates (e.g. Melchiorre and Frattini, 2012). Results broadly vary between locations, with some studies, for example, predicting a significant increase (Jakob and Lambert, 2009; Ciabatta et al., 2016) or decrease (Jomelli et al., 2009; Dehn et al., 2000) in landslide activity in the 21<sup>st</sup> century. Though, researchers have also shown the high degree of uncertainty in the results, outlining the limitations in the use of scenario-driven projections in assessing changes in landslide activity. Uncertainties relate to the projection itself, as well as to limitations of the GCMs and downscaling techniques (Collins et al., 2012; Dehn and Buma, 1999). To reduce such uncertainty, climate model predictions can be run over past time periods (e.g. between 2002 and 2015 in Alvioli et al. 2018), calibrating their prediction capabilities over rainfall observations. However, such approach requires the existence of precipitation gauges and records, often not available in developing countries (Monsieurs et al., 2017; Redshaw et al., 2020). Other investigators compared the outputs of different GCMs scenarios to quantify their uncertainty (Melchiorre and Frattini, 2012; Ciabatta et al., 2016). Yet, diverging slope stability results could be found (e.g. one model predicting no increase and another predicting a significant increase in landslide hazard), hindering the use of the outcomes for decision making or for identifying an 'optimal' management solution (Wilby and Dessai, 2010; Melchiorre and Frattini, 2012).

Alternative, **'bottom-up' or 'vulnerability-based' approaches** (Fig. 1.3b) have been suggested for dealing with decision making under large uncertainties such as future climate change (Groves and Lempert, 2007;

Singh et al., 2014; Wilby and Dessai, 2010). These approaches allow to explore the vulnerability<sup>4</sup> of the system by finding those combinations of environmental properties that lead to unwanted outcomes. In landslide hazard assessment, this translates into exploring a wide range of plausible slope stability scenarios in order to identify thresholds of environmental conditions (e.g., above which slope angle, rainfall intensities or urban densities) that, if crossed, can lead to unacceptable outcomes (e.g. exceedance of a certain landslide probability, decided by stakeholders). These thresholds can then be compared to available projections on future climate (from GCMs) or land cover trends (e.g. from socio-economic scenario modelling) to assess their plausibility and to identify the most robust planning strategies (e.g., identify the strategies that perform well across many scenarios simulated).

The generation of multiple, feasible slope stability scenarios can be achieved by applying MC sampling. The sampling allows generation of ensemble of representative populations of slopes or catchments, with varying environmental conditions. Mechanistic slope stability models applied in this context can identify for which environmental conditions a large number of slope failures is predicted, as well as the main instability drivers (e.g. via sensitivity analysis). Almeida et al. 2017 have shown how this can be done on a single slope. They used a site-specific mechanistic model and a MC approach to create slopes with varying input factors, i.e., slope, soil, initial boundary conditions and rainfall intensity and duration. Instead of choosing one or more downscaled climate projection scenarios, possible future climates were simulated by uniformly (i.e. by using uniform distributions) increasing the severity of observed rainfall events (as in the intensity and duration graph in Fig. 1.3b). This approach allowed generation of many intensity-duration combinations, representative of past observations but also of potential future unobserved rainstorms. By varying all the input factors of the mechanistic model and by including a wide range of possible design rainstorms, it was possible to 1) quantify the uncertainty of all input factors and, therefore, quantify how hillslope uncertainty (e.g., slope thickness or soil cohesion) compared to climate uncertainty; and 2) identify for which values of current or future rainfall intensity and duration landslide hazard started to significantly increase. These rainfall intensity-duration combinations could then give insight of ‘how much’ change in precipitations is needed to have, for example, a much greater number of slopes at risk within a region.

---

<sup>4</sup> The term ‘vulnerability’ in this context is used to define critical hazard thresholds above/below which a certain hazard is expected to occur (e.g., above/below which slope angle, soil cohesion, and rainfall intensity, the FoS is predicted below one), consequently provoking adverse effects within the community. The term therefore differs from the definition given by the UNDRR within a risk assessment context, where vulnerability represents: *“the conditions determined by physical, social, economic and environmental factors or processes which increase the susceptibility of an individual, a community, assets or systems to the impacts of hazards”* (UNDRR, 2009).

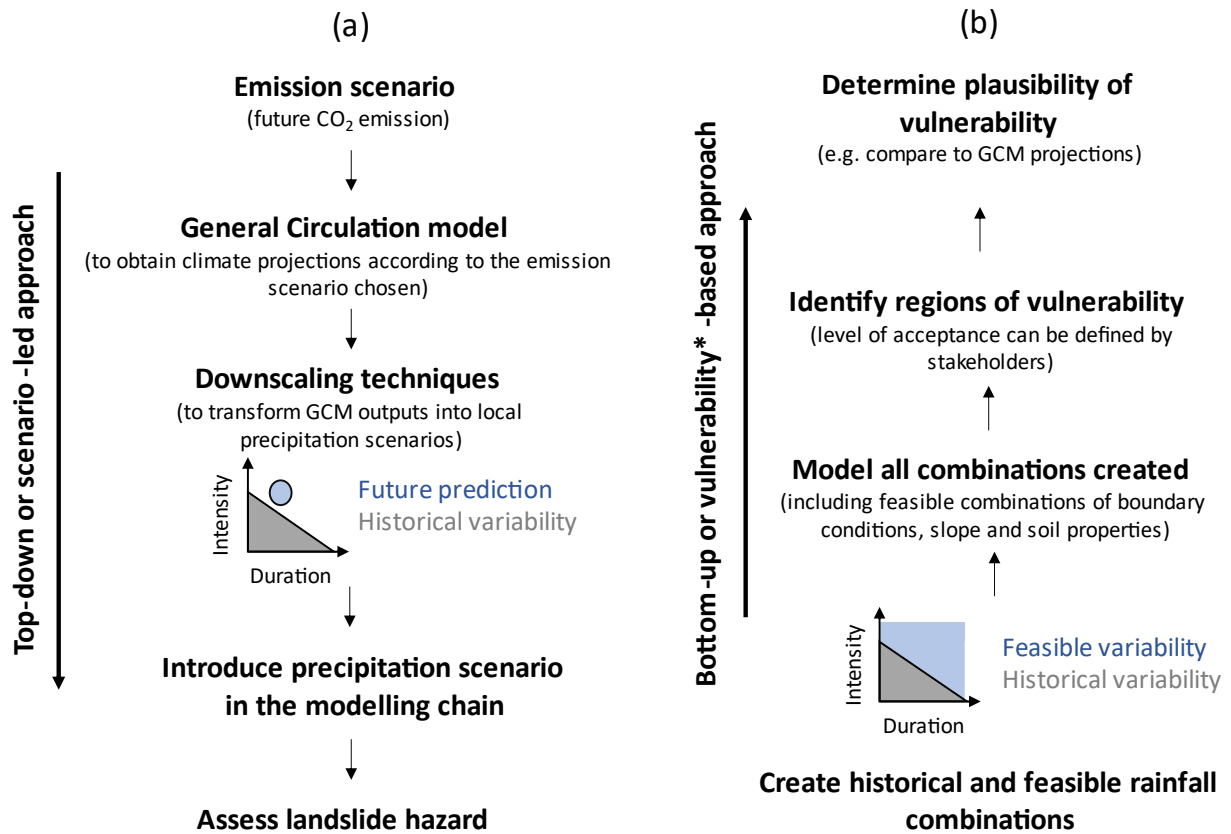


Figure 1.3: (a) Framework describing the traditional top-down approach used to derive future landslide hazard predictions based on the climate scenario selected; (b) the bottom-up approach used in this study, which starts by defining many feasible combinations of the input factors to then identify the regions in such input space that lead to a certain output (e.g. high or low probability of failure – high or low vulnerability). \*In this context, the term ‘vulnerability’ is used to define critical hazard thresholds that identify a change in slope stability response (e.g. FoS passing from above to below 1).

### 1.2.3 Summary of advantages and limitations of current approaches

In Section 1.2, four modelling requirements for assessing landslide hazard within informal communities, have been outlined:

- 1) Include in the slope stability analysis the urban construction activities typically found within informal settlements, reaching a balance between the level of urban landslide process representation and the data requirements and availability (i.e. the model used should be parsimonious).
- 2) Quantify the relative role of the urban and the natural environmental processes driving landslide hazard from household to hillside scales and across regions, in order to deduce landslide hazard mitigation practices at different stakeholders’ decision levels (e.g., cut slope reinforcement at household scale, drainage implementation within an informal community, urban planning at city scale).

- 3) Include possible future urban expansion scenarios and climate change.
- 4) Quantify the uncertainties related to both data (aleatory uncertainties) and future changes (epistemic uncertainties), associated to both the urban and the natural environment. To do so, the model requires to be efficiently run in a probabilistic (MC) framework, as discussed in Section 1.2.2.

This translates into two sub-requirements:

- a. Automatically generate tens of thousands of hillslopes with changing properties.
- b. Assess the stability of the generated hillslopes within reasonable time windows.

Figure 1.4 represents the approaches described in the previous sections (statistical and mechanistic), reporting the spatial scale at which they usually operate, data required and purpose. The figure also highlights the methodological gap at community scale (grey band), which relates to data availability, the scale of the processes controlling slope failure and the models available. Table 1.1, instead, provides a summary of advantages and limitations of such approaches, with respect of the four modelling requirements abovementioned.

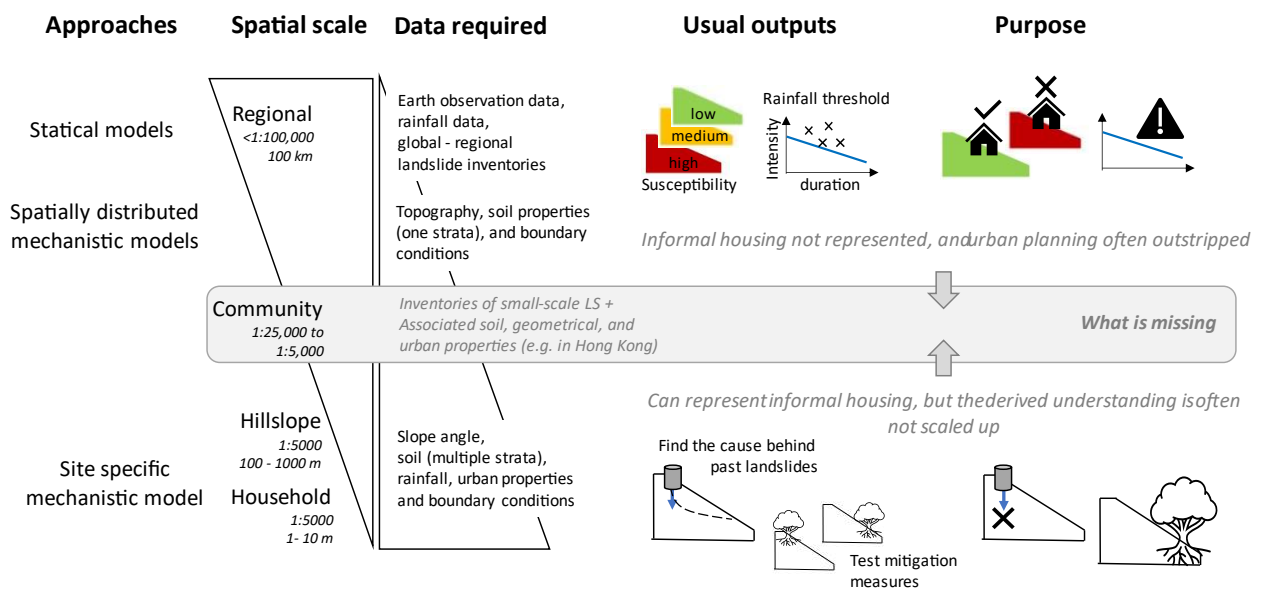


Figure 1.4: Scheme for the two main methodological approaches currently employed for landslide hazard assessment within informal settlements; the scale at which they generally operate; the data they generally require; usual outputs and usage. The grey box highlights the scale at which current approaches are failing in supporting effective landslide hazard mitigation actions. In italics, the components missing to achieve such purpose within the informal communities of developing countries (the data required reported as missing in the grey box, might be available in data-rich countries, such as Hong Kong, China).



Table 1.1: Summary of advantages of statistical- and mechanistic-based modelling approaches, and their limitations with respect of the four modelling requirements (Req. 1-4) set for this research.

	Statistical models	Spatially distributed mechanistic model	Site-specific mechanistic models
<b>Advantages</b>	These models find patterns in existing data and can provide insights on the nature of, and relation between slope stability processes even when such processes are not well understood. They are based on simple equations and they are easily reproducible. The data necessary to run such models are generally available (e.g. DEM or geological maps). They provide susceptibility maps and rainfall thresholds useful for urban planning and early warning systems (top Fig.1.4)	These models can assess the spatial and temporal landslide probability. They are capable of evaluating the effects of environmental changes through adaptations in their parameters. They can assess the causal relations between environmental conditions and landslide occurrence and simulate areas of drainage convergence and divergence across the landscape. They generally provide susceptibility maps and rainfall thresholds useful for urban planning and early warning systems (mid Fig.1.4).	As for spatially distributed models, site specific models can assess the spatial and temporal landslide probability; evaluate the effects of environmental changes on slope stability; and assess the causal relations between environmental conditions and landslide occurrence. The more detailed representation of the slope stratigraphy and the use of LE analysis allows a more sophisticated representation of the slope and its stability, useful in the design of the type and magnitude of mitigation measures (bottom Fig. 1.4).
<b>1. Include informal housing?</b>	<b>NO</b> - The resolution of the available topographic data does not capture localised features such as hill cutting. The landslide inventories used for the analysis should include small scale landslides associated with localised urban activities such as hill cutting or leaking pipes in order to establish their correlation – such inventories are not available within informal communities (and in the majority of places) (grey gap in Fig. 1.4).	<b>PARTLY</b> - Only vegetation removal is modelled. The assumption of infinite slope stability may limit considerations on urban construction activities. More sophisticated models could be too computationally demanding (see Req. 4).	<b>YES</b> - They can potentially include all the urban construction activities defining informal settlements. However, there are no examples in the literature where all of them are analysed conjointly.
<b>2. Quantify the role of informal housing at different scales?</b>	<b>NO</b> - Given the resolution at which these models operate (Fig. 1.4), informal housing is not included and therefore its relative role in influencing landslide probability is not quantified.	<b>PARTLY</b> - It has been done only for vegetation (see Req. 2) – the models could identify the relative role of the main landslide triggering mechanisms and therefore support decision makers for landslide mitigation actions, from catchment to hillslope scale.	<b>YES</b> - Through multiple applications of the model to different representative combinations of input factors (e.g. varying slope angles, soil strata and urban density), the understanding gained at hillslope scale can be transferred to wide areas. However, this has never been done while considering informal housing (grey gap in Fig. 1.4).
<b>3. Include future scenarios?</b>	<b>NO</b> - The statistical relation computed based on past landslide records may not hold under changed conditions, i.e. the hypothesis of stationarity ('time invariant') is challenged.	<b>PARTLY</b> - Only vegetation cover and climate change can be effectively modelled (not urban expansion scenarios, see Req. 1).	<b>YES</b> – although climate and land cover change are often analysed separately and only using top-down GCMs projections.
<b>4. Quantify aleatory and epistemic uncertainty?</b>	<b>PARTLY</b> - Mainly the uncertainty associated with landslide inventories, which are particularly important because they are used for both calibration and validation.	<b>YES</b> - Aleatory uncertainties are sometimes assessed using the MC stochastic sampling; epistemic uncertainties are sometimes assessed by comparing multiple GCMs projections. However, these models can be computationally demanding limiting the number of model trials. For this reason, only a limited number of parameters used to run the model are varied (and thus their uncertainty quantified) and only few future scenarios analysed.	<b>YES</b> - as in spatially distributed models. However, site-specific models are less computationally demanding, thus more suitable for an effective uncertainty evaluation. On the other hand, they are more sophisticated models. The more complex the model is, the more data will be required to set its parameters and the more uncertainty might be introduced into the analysis.

Site-specific mechanistic models can satisfy all the requirements set for this research. These models applied in a probabilistic framework, in which slope, soil, rainfall and urban properties (defined as input factors) are varied, have the potential to both identify the main failure drivers and quantify the inputs' uncertainties. In Finite Elements (FE) models (such as GeoSlope) addition of point water sources and cut slopes can be inserted manually, for example by modifying the slope geometry. However, these changes can be done one slope at the time, while we need to be able to represent all these urban effects stochastically, generating slopes with different properties automatically. An automatic and fast model's implementation is therefore necessary. Furthermore, FE models are generally more data demanding than Limit Equilibrium (LE) models, making them less parsimonious in data-scarce contexts. Parsimonious models are also advantaged in terms of uncertainty quantifications. First, less input factors are necessary to run such models, and therefore less sources of uncertainty are introduced in the analysis. Then, parsimonious models can be computationally fast, thus many models' trials can be performed to assess the uncertainty of all varying input factors. In terms of epistemic uncertainty, those associated with climate change are often analysed. Currently, the impact of climate change on landslides is assessed via top-down approaches based on GCMs projections (Section 1.2.2), which produce a wide range of possible outcomes, making the landslide hazard evaluation of little practical use.

The goal of this thesis is therefore to outline a new methodology which addresses both the four modelling requirements set, as well as the mentioned methodological shortcoming.

## 1.3 Research goal and objectives

The goal of this thesis is to provide a new methodological framework that includes informal housing in landslide hazard assessments and quantify its relative influence on the occurrence of rainfall-triggered landslides. In particular, the aim is to gain a better understanding of how, where and when informal housing has the potential to become most detrimental for slope stability, also considering hypothetical scenarios of urban expansion and climate change. To pursue these goals, the new suggested methodology aims to gain such understanding across scales (from household to regional scale), while quantifying the uncertainties arising from both the input data and future climate projections (aleatory and epistemic). This will allow assessment of the relative role of the natural, urban, and climatic factors affecting landslide predictions (which might change when looking at household scale where, for example, the effect of households' pipe leakages might be evident, or at regional scale where, topography instead might dominate on other factors).

Specifically, the thesis focuses on the following research questions:

- 1) How can we include informal housing in a slope stability analysis that also considers the uncertainties due to both slope (geometrical, geotechnical, hydrological<sup>5</sup>) properties and potential future climate changes?
- 2) How can we quantify the relative role of informal housing, natural slope susceptibility and rainstorm severity in increasing rainfall-triggered landslide hazard within a community?
- 3) How can we incorporate the understanding of slope stability gained at the hillslope scale, into regional hazard maps under changing urban expansion and rainfall conditions?

To address these questions, we select as a case study a region in the Eastern Caribbean, which represent a typical data-scarce and resource-limited location in the humid tropics. The main landslide trigger in this region is rainfall (Lumb, 1975; De Graff et al., 1989), and shallow rotational landslides dominate on both steep and shallow slopes (Migon, 2010). Furthermore, empirical evidence suggests that landslide risk is increased by informal housing which occupies steep slopes and employs unregulated engineering practices. Various sources of information on the slope, soil, rainfall, and urban properties are available from previous studies and community-based projects (Mott MacDonald, 2013; Anderson and Holcombe, 2006; Klohn-Crippen, 1995; Anderson and Holcombe, 2013). This region therefore represents a suitable setting for testing the objectives of this thesis and for the mechanistic model selected (CHASM, Combined Hydrology and Stability Model; Anderson and Howes, 1985). Such a model is particularly suited for tropical environment, and it has

---

<sup>5</sup> Geometrical, geotechnical and hydrological properties are terms that will be used throughout this thesis. As it will be explained in the results chapters, geometrical properties refer to the slope gradient and soil material strata.

been previously used with satisfactory outcomes in other similar tropical regions (see for example, Anderson 1990; Holcombe et al. 2016).

In a context where expanding urbanisation in developing countries has the potential to increase landslide hazard, this research addresses the growing need to include both the natural and the urban component in landslide hazard assessments. With the example in the Eastern Caribbean, we give evidence of how the methodology suggested can provide directions for effective hazard mitigation practices across scales (from better urban practice at hillslope scale to island-wide maps representing the change in landslide predictions under different land cover and climate change scenarios), despite the limitations arising within data-scarce, resource-limited locations and the uncertainties associated with changing environments. Given that such context is typical of all informal settlements in developing countries, we believe that this methodology can become a useful tool for similar research elsewhere.

## 1.4 Research outline

*Q1) How can we include informal housing in a slope stability analysis that also considers the uncertainties due to both slope (geometrical, geotechnical, hydrological) properties and potential future climate changes?*

### **Chapter 2.**

- Describe the proposed new methodology.
- Extend the selected mechanistic model to include all the unregulated urban activities commonly employed within informal settlements.
- Verify the consistency of the results of the newly extended model.



*Q2) How can we quantify the relative role of informal housing, natural slope susceptibility and rainstorm severity in increasing rainfall-triggered landslide hazard within a community?*

### **Chapter 3.** Apply the methodology described in Ch.2 to a population of slopes of the study area.

- Identify the most detrimental urban construction activities for slope stability.
- Identify the relative role of informal housing in triggering landslides compared to other environmental properties (such as soil strength and rainfall) and for which slope, soil, and climate conditions informal housing most increase the probability of slope failure.
- Calculate the rainfall threshold for triggering landslides including the impact of informal housing.
- Suggest hazard mitigation actions to tackle the main landslide drivers identified.



*Q3) How can we incorporate the understanding of slope stability gained at the hillslope scale, into regional hazard maps under changing urban expansion and rainfall conditions?*

### **Chapter 4.** Apply the methodology described in Ch.2 to all slopes of the study region.

- Identify the input factors (e.g., soil or climate properties) that most influence landslide hazard at regional scales.
- Use these input factors to create a regional hazard map that represents landslides associated with a past hurricane (rainfall) event and verify its quality with available landslide records.
- Present more hazard maps under hypothetical urban expansion and climate change scenarios with their relative change in landslide rate.
- Quantify the relative effect of land cover and climate change on regional landslide hazard.



### **Chapter 5.**

- Summary of the previous chapters and discussion about how to improve knowledge transfer from research to practice in landslide hazard mitigation within informal communities.

## Chapter 2 : A methodology to include informal housing into slope stability analysis under uncertainty

Sections 2.2.1 and 2.4.2 of this chapter are adapted from the supplementary material of a published, peer-reviewed work:

*Bozzolan, E., Holcombe, E., Pianosi, F. and Wagener, T.: Including informal housing in slope stability analysis – an application to a data-scarce location in the humid tropics, Nat. Hazards Earth Syst. Sci. Discuss., 1–20, doi:10.5194/nhess-2020-207, 2020.*

## 2.1 A new methodology outline

This chapter outlines the new methodology developed for this thesis which answers the first research question of the thesis:

- 1) How can we include informal housing in a slope stability analysis that also considers the uncertainties due to both slope (geometrical, geotechnical, hydrological) properties and potential future climate changes?

Figure 2.1 shows how this new methodology is designed to address the data, methodological and outputs gaps at community scale, as identified in Fig. 1.4 (Chapter 1). The main and novel components involved are:

- The **site-specific mechanistic model CHASM** (Combined Hydrology and Stability Model) which assesses the stability of the simulated slopes also including dynamic hydrological components and localised urban construction activities characteristic of informal housing. In particular, new functions are developed to represent surface and subsurface slope water management (new CHASM+).
- The use of **data gathered from governmental lab testing and community-based projects** across different locations in the case study context of Saint Lucia (Eastern Caribbean).
- The representation and, therefore, the **inclusion of the uncertainty related to all the data and properties representing the slope** (i.e. all input factors), i.e. geometrical, soil, rainfall and urban properties. In particular, a **bottom-up approach** is used to deal with the uncertainty related to climate change.
- Finally, the use of global sensitivity analysis and data mining techniques to **quantify the uncertainty of each input factors**.

Such new methodology allows determination of slopes stability response at three different scales ('new usage' in Fig. 2.1):

- *At hillslope scale*, where one single hillslope with known characteristics can be represented, for example, to back-analyse the main triggering mechanisms of observed landslides (as shown in section 2.4.2).
- *At community scale*, where a subset of simulated slopes representing, for example, the most hazardous areas of a community can be selected and analysed (as in Chapter 3, where slopes with gradient between 20° and 45° are selected), to then quantify the relative role of the natural slope susceptibility and urban activities on the slope stability response, and consequently deduce the most effective mitigation practices to reduce landslides probability.

- *At regional scale* where all slopes within a country can be analysed (as in Chapter 4 – where slope gradients range between 5° and 70°, aiming to represent all slopes in Saint Lucia Island), and the slope stability results spatially distributed to then create regional hazard maps that compare landslide probabilities under different land cover and climate change scenarios.

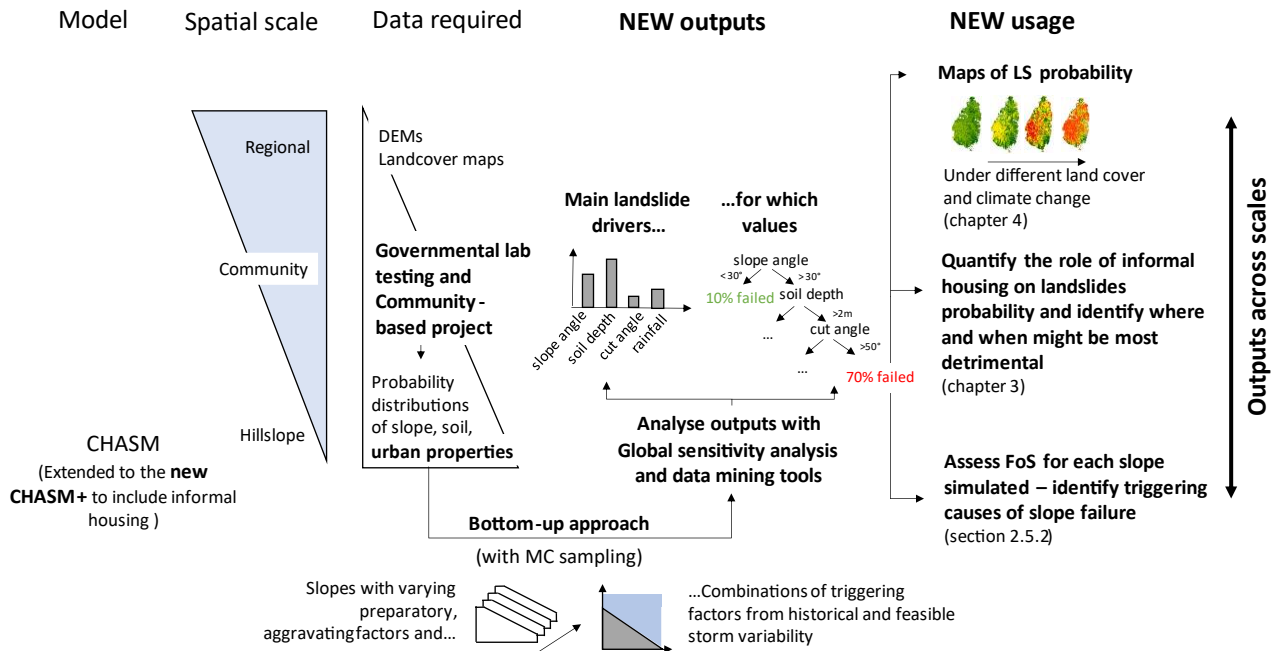


Figure 2.1: The new methodology developed which addresses the gaps outlined in Fig. 1.4 (Chapter 1). The innovative components are highlighted in bold.

Figure 2.2 shows the operational workflow used to perform such analyses.

First, the probability distributions of the slope, soil, climate, and urban properties (which represent the input factors of CHASM) are defined. The distributions aim to represent the uncertainty of the input factors and they are chosen based on literature, on available data collected from different sources (critically including previous studies in informal communities, with highly localised information such as soil strata depths, cut slope angles, and other type of urban construction practices), or to best represent our lack of knowledge (e.g., using a uniform distributions for no a priori knowledge). Definitions of the probability distributions and their parameters are given in Chapter 3 and 4.

A Monte Carlo (MC) approach is employed to stochastically sample different values of input factors from their probability distributions. This is done by using a Matlab script (Mathworks, 2018) and the open source toolbox SAFE (<https://www.safetoolbox.info/>). Thousands of combinations of input factors are so generated, each one defining a hillslope that will be simulated in CHASM+. To run the model, these combinations are first translated into appropriate input files that CHASM+ can read. Such step is performed in Matlab, and the



scripts are described in Appendix A2. Then, CHASM+ is run to determine the stability of each simulated slopes. CHASM+ is a unique two-dimensional mechanistic model because capable of representing the dynamic changes in unsaturated and saturated groundwater flow as well as cutslopes, vegetation (and thus vegetation removal), additional (house and septic tank) loading, rainwater and wastewater management (i.e., informal housing). CHASM and the new functions developed to include point water sources, which include the presence or absence of roof gutters on houses, as well as the localised water leakages from buried septic tanks and superficial water supply pipe networks, are described in Section 2.2.1.

Given the large number of simulations (equal to the number of combinations of input factors generated by the MC sampling), CHASM+ is run using high performance computers at the University of Bristol: the BlueCrystal Phase 3 which contains  $16 \times 2.6$  GHz Sandy Bridge cores; and Catalyst – an ARM (Advanced RISC Machines) based system which contains 64 cores and 256 GBytes of RAM in each node and runs at 2.2 GHz. At the end of the simulation time, each slope analysed is associated with the minimum FoS recorded, and the corresponding position of the slip surface.

Finally, Regional Sensitivity Analysis (RSA - a global sensitivity analysis method) and Classification and Regression Tree (CART – a data mining, machine learning method) analyse the simulations results and identify the main landslide drivers and combinations of input factors that most increase landslide hazard. It is then possible to identify the natural conditions (e.g. classes of slope angles or rainfall intensity) where informal housing might most increase landslide occurrence (Chapter 3), as well as to generate maps of landslide probability under different land cover and climate conditions (Chapter 4).

In the next sections, CHASM, its extension into CHASM+, as well as the RSA and CART methods are described in more detail. Furthermore, at the end of this chapter, the methodology presented above is used to assess the performance of the newly extended CHASM+. Specifically, CHASM+'s results are compared to another widely used mechanistic model, which was employed to analyse the role of a leaking water tank in triggering a landslide occurred in Brazil in 2016 (Mendes et al. 2018).

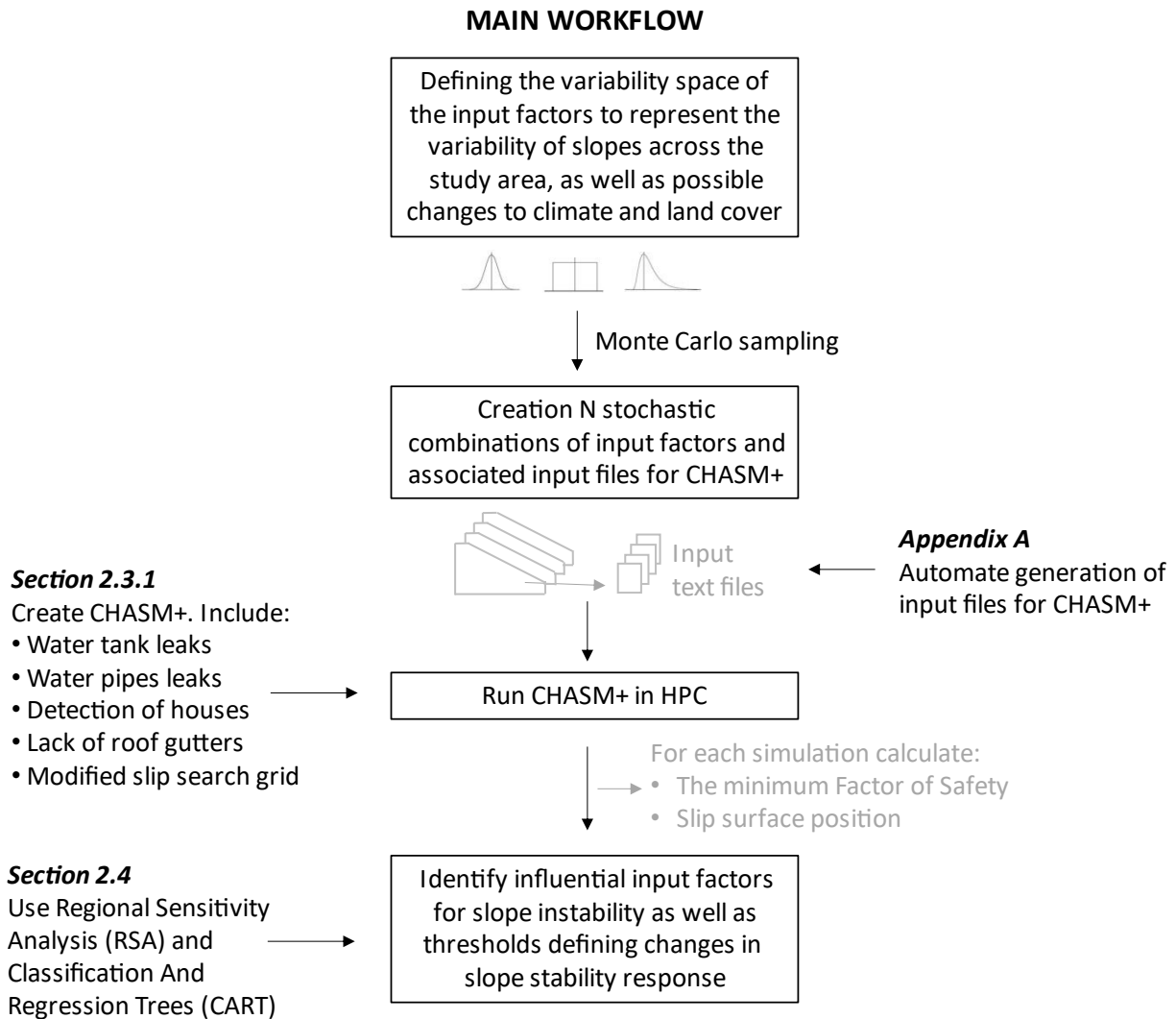


Figure 2.2: Main workflow that will be used throughout this thesis. To include informal housing into the analysis, the mechanistic model CHASM is extended, and the generation of the input files required to run the model is automated with a Matlab script. To assess the uncertainties associated with the model’s outputs, the two methods RSA and CART are selected. All these components are described in more detail in the following sections, as reported in the figure.

## 2.2 CHASM – Description of its hydrology and stability routines

CHASM (Combined Hydrology and Stability Model) is a two-dimensional mechanistic model which analyses dynamic slope hydrology and its effect on slope stability over time. The slope cross section is divided into a regular mesh of columns and cells as shown in Fig. 2.3. The initial hydrological conditions defining the position of the water table and the surface matric suction are specified as input data as well as the hydrological and geotechnical parameters for each cell, assigned according to their material type. Moisture within the slope flows through the unsaturated and saturated zones according to the hydraulic conductivity of the soil and

when rainfall is simulated the water infiltrates the top cells of each column. The moisture content, hydraulic conductivity and pore water pressure are iteratively assessed and updated for each cell at each time step (here fixed at 60 seconds). At the end of each simulation hour, the resulting pore water pressures are included in the stability routine where shear strength and stresses are assessed using a limit equilibrium analysis. Given that we are interested in rotational failures, the Bishop's simplified circular method is used and the slip surface corresponding to the minimum Factor of Safety (FoS) is assessed by using an automated algorithm.

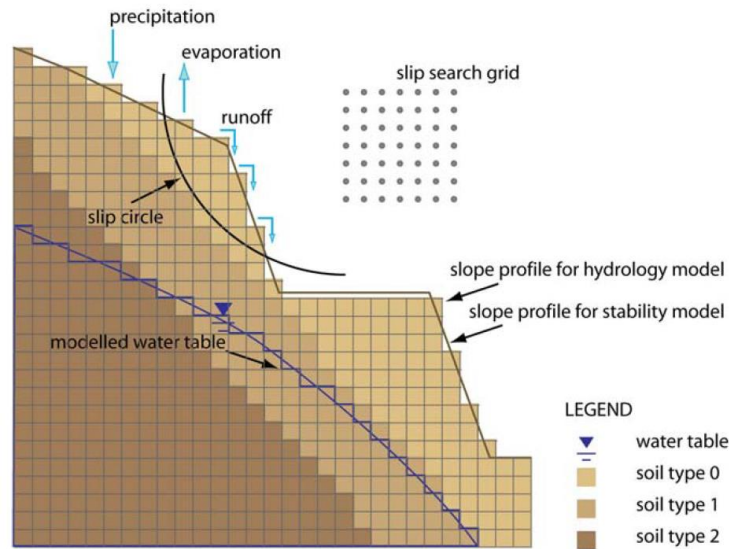


Figure 2.3: Geometrical and process representation of CHASM (after Wilkinson 2000).

## Hydrology routine

The physical basis and numerical scheme for CHASM are described in detail in Anderson and Howes, 1985; Wilkinson et al., 2002a and are summarised as follow.

The centres of each cell form computational points for a forward explicit finite difference scheme to solve the Richard's and Darcy's equations that regulate, respectively, unsaturated and saturated flow. The Richard's equation (Richards, 1931) in its one dimensional form solves the vertical infiltration through the unsaturated zone:

$$\frac{\partial \theta}{\partial t} = \frac{\partial}{\partial z} \left[ K(\theta) \left( \frac{\partial \psi}{\partial z} + 1 \right) \right] \quad (2.1)$$

where:  $\theta$  = volumetric moisture content ( $\text{m}^3 \text{m}^{-3}$ )  
 $K$  = unsaturated hydraulic conductivity ( $\text{m s}^{-1}$ )

$\psi$  = matric suction (m)  
 $z$  = vertical distance (m)  
 $t$  = time step (s)

Unsaturated hydraulic conductivity varies in time according to the volumetric water moisture content and soil suction. The plot of the relationship between water moisture content and soil suction is known as the soil-water characteristic curve (SWCC) and an example is shown in Fig. 2.4 (right-hand side).

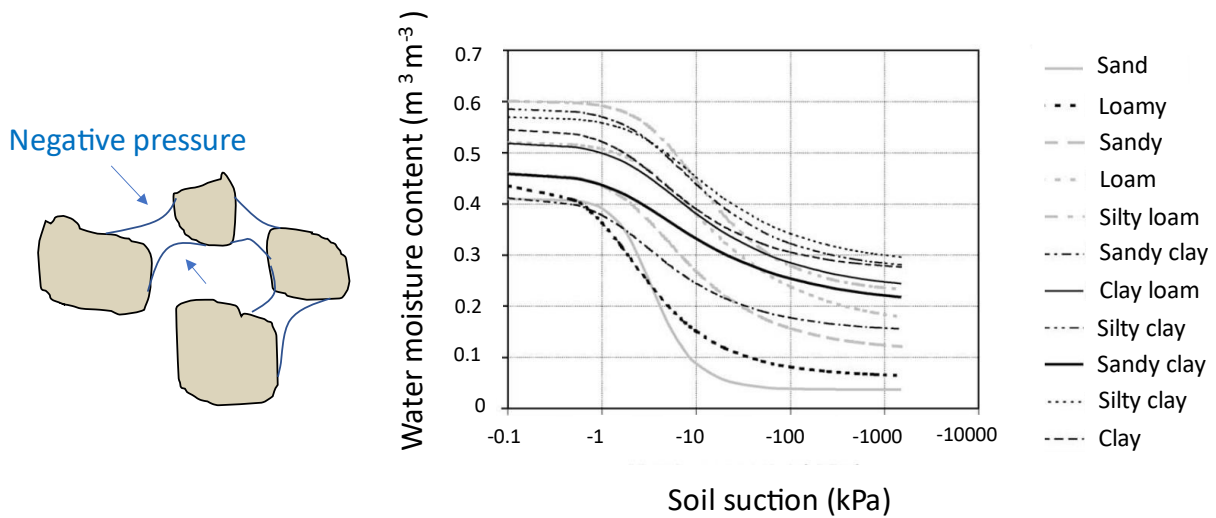


Figure 2.4: On the left, a schematic representation of the negative pressure defining soil suction. The surface tension of water in between particles creates menisci, a force that pull fine particles together (apparent cohesion). Such negative pressure becomes the more significant the finer the soil particles (e.g. on clays). On the right, the SWCCs proposed by Hodnett and Tomasella (2002), for different soil textural classes for tropical soils. The curve presents an 'S' shape, with maximum water moisture content corresponding to the minimum (in absolute value) suction and vice versa.

In CHASM, SWCCs are defined as input factors, specifying the saturated and the residual moisture content (shown in Fig 2.4) as well as other shape parameters (specifically, we will refer to those parameters reported by Hodnett and Tomasella, 2002). Variations of the water moisture change the value of unsaturated hydraulic conductivity in each cell. In CHASM, this value is iteratively calculated using the empirical Millington – Quirk procedure (Millington and Quirk, 1959):

$$K_i = \frac{K_s(\theta_i/\theta_s)^p \sum_{j=i}^m (2j + 1 - 2i)\psi_j^{-2}}{\sum_{j=i}^m (2j - 1)\psi_j^{-2}} \quad (2.2)$$

where:  $K_i$  = unsaturated hydraulic conductivity (m s<sup>-1</sup>)

- $K_s$  = saturated hydraulic conductivity provided as an input factor ( $m s^{-1}$ )
- $p$  = pore interaction term here considered equal to 1
- $\theta_i$  = unsaturated moisture content
- $\theta_s$  = saturated moisture content provided as input factor
- $\psi_j$  = suction value at moisture content  $\theta_i$
- $j$  = index to make summation over the  $m$  points at which the suction moisture curve has been divided

When the water table is reached, the explicit solution of the Darcy's equation (Darcy, 1856) for saturated flow is used to calculate lateral flow between columns in two-dimensions:

$$Q = K_s h \frac{dh}{dz} \quad (2.3)$$

- where:
- $K_s$  = saturated hydraulic conductivity ( $m s^{-1}$ )
  - $h$  = height of the water table above basal impervious surface layer (m)
  - $\frac{dh}{dz}$  = water table gradient at that point (m)

## Stability routine

At the end of each hour of a simulation, the pore water pressures (both positive and negative) calculated by the hydrology routine are incorporated into the limit equilibrium analysis, specifically into the Mohr-Coloumb equation for soil shear strength (Eq. 2.4). The limit equilibrium method investigates the forces that maintain in equilibrium a soil mass. By calculating both the effective shear stresses along the failure surface and the soil shear strength, it is possible to determine the FoS. In the Bishop's simplified circular method (Bishop, 1955) used for this analysis, the slope is subdivided into vertical slices as shown in Fig. 2.3. The effective stresses are estimated along a failure surface assumed to be circular and centred in the point 'O'. The shear strength for the slice is expressed as:

$$s = c' + (\sigma - u)\tan\phi' \quad (2.4)$$

- where:
- $s$  = soil shear strength ( $kN m^{-2}$ )
  - $c'$  = effective cohesion of the soil ( $kN m^{-2}$ )

- $\phi'$  = angle of internal friction (degrees)
- $\sigma$  = normal stress acting on the plane ( $\text{kN m}^{-2}$ )
- $u$  = pore water pressure ( $\text{kN m}^{-2}$ )

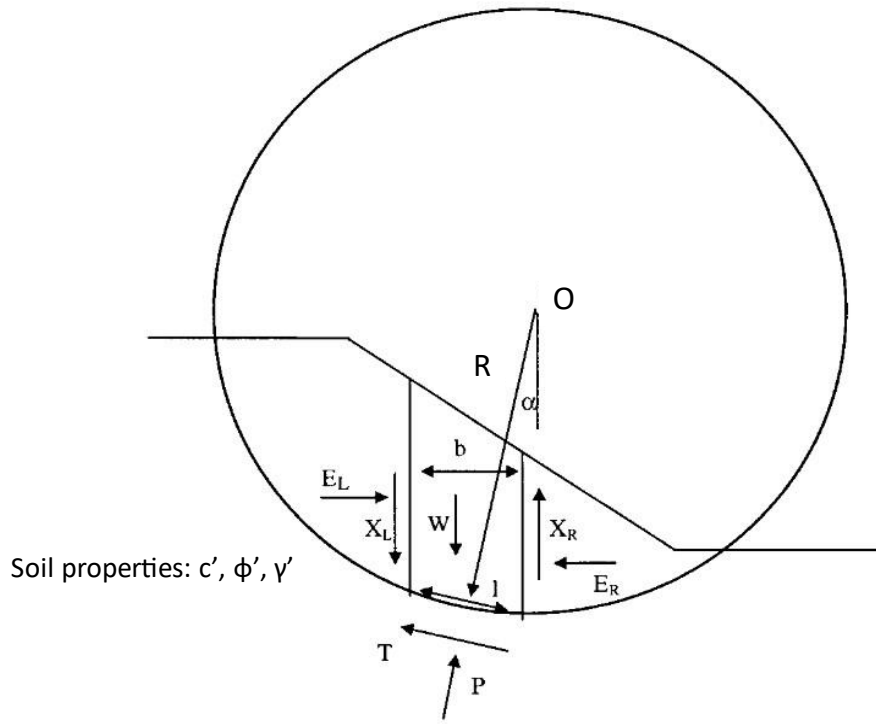


Figure 2.5: Circular slip surface analysis with method of slices (after Wilkinson 2000).

The mobilised shear strength is  $\tau = s / \text{FoS}$ . By expressing the normal stress  $P = \sigma \cdot l$  and shear strength  $T = \tau \cdot l$  (where  $l$  is the length of the slice), it follows that:

$$T = \frac{1}{\text{FoS}} (c'l + (P - ul)\tan\phi') \quad (2.5)$$

With the assumption that the left and right vertical interslice forces ( $\text{kN m}^{-2}$ ) are equal  $X_L = X_R$ , the forces are solved vertically:

$$P\cos\alpha + T\sin\alpha = W \quad (2.6)$$

and around the centre O:

$$WR\sin\alpha = TR \quad (2.7)$$

$\alpha =$  slope angle (degrees)  
 where:  $R =$  radius length (m)  
 $W =$  the weight of the slice (kN)

By replacing the expression of T derived from Eq. 2.7 into Eq. 2.5, we obtain:

$$FoS = \frac{\sum_{i=1}^n c'l + (P - ul)\tan\phi'}{\sum_{i=1}^n W\sin\alpha} \quad (2.8)$$

where P is expressed as a function of T (derived from Eq. 2.6). Therefore, the term 'FoS' appears in both sides of the equation, which is solved iteratively. The method also requires a large number of trial slip surfaces to be investigated. The lowest value of FoS identifies the most likely failure surface. Within CHASM it is possible to perform an automated search of the most critical circular failure surface. This is achieved by setting a two-dimensional grid above the slope, composed by evenly spaced points. These points provide potential centres of the slip circle. An initial radius and radius increment are specified. The search begins from the bottom left-hand point of the grid and generate new slip surfaces by successively incrementing the radius. For each new slip surface generated, the FoS are calculated, stored in an array and eventually compared to find the minimum value. The same procedure is repeated for all the other points available within the grid. The absolute minimum FoS is output at each simulation hour along with the x-y co-ordinates of the centre of the slip surface and the circle radius.

## Vegetation

Given that vegetation is included in this research, a brief description of its hydrological and geotechnical components is given below (more details can be found in Wilkinson et al., 2002a). Vegetation contributes to slope stability via hydrological and mechanical processes. Within the hydrological effect, vegetation can intercept rainfall (which is stored on leaves and stems and then loss via the process of evaporation) and deplete soil moisture via root uptake and transpiration. The result is a decrement of the volume of rainfall that reaches the ground and infiltrates into the soil as well as a reduction of soil moisture because of the plant uptake. A consequence of such processes is the reduction of pore water pressure within the slope, which can potentially lead to an increased slope stability. At the same time, transpiration can lead to drier soils and enhance desiccation cracking. Cracks as well as root networks increase the permeability and the infiltration capacity of the upper soil layer (e.g. via macropores which form after the roots die). When the soil hydraulic conductivity is low, root-permeated upper soil layers can induce the formation of a transitory,

infiltration induced, perched water tables, which can lead to a local increase in pore water pressure and to a consequent decrease of the FoS (Collison et al., 1995).

In addition to a change in soil moisture regime, vegetation influences the geotechnical properties of the slope. Vegetation surcharge increases the total weight of material acting on the slip surface while roots embedded in soil add tensile strength and adhesion, which may be compared to a reinforced soil system (Wu, 1995). Whether the effect of vegetation surcharge and root reinforcement increase slope stability depend on the relative position of vegetation in respect with the failure surface. In most cases vegetation surcharge has a detrimental effect on slope stability since it acts as an additional downslope force. However, a beneficial effect might be provided when trees create a restoring vertical load (e.g., trees located on the lower part of the slope, which create a positive momentum in respect to the centre O in Fig. 2.5), increasing the frictional resistance along the slip surface (Collison et al., 1995). The shear strength of the rooted soil mass is enhanced due to the presence of a root matrix. Fibres and roots act as a supplemental cohesion that is added to the soil shear strength in the Mohr Coulomb equation (Eq. 2.4). Whether the reinforcing effect is significant to slope stability depends primarily on whether roots intersect the potential failure surface. In situations of deep-seated landslides, their stabilising effect may be therefore limited, but may be considerable for deep penetrating roots and shallow failures (Wilkinson, 2000).

Within CHASM, vegetation is represented with the following processes:

- Rainfall interception divided into a canopy and a grass interception model. *Canopy interception* is described as: (i) rainfall that is retained by the plant and then it evaporates (interception loss); (ii) rainfall that does not hit the plant surface (free throughfall), or that hits the plant and then reaches the ground by flowing down branches and stems (stemflow). Stemflow and throughfall (free throughfall and drips) define the net rainfall. The structure of the canopy is therefore described by the free throughfall coefficient  $p$  (which is function of the canopy cover and ranges between 0 – no canopy cover – to 1 – complete canopy cover); the stemflow-partitioning coefficient  $p_t$ , the canopy storage capacity ( $S$ ) and the trunk storage capacity ( $S_t$ ). Throughfall, stemflow and interception loss (via evaporation) are then estimated from input rainfall and meteorological data using the method proposed by Rutter et al., (1971) and the Penman-Monteith equation (Monteith, 1973), with the canopy resistance set to zero since leaf stomata close under saturated conditions and the process of transpiration is halted (Wilkinson et al, 1998).

$$Ep = \frac{\Delta R_n + \rho c_p VPD / r_a}{\lambda [\Delta + \gamma (1 + \frac{r_c}{r_a})]} dt \quad (2.9)$$



Where  $E_p$  is the potential evapotranspiration rate ( $\text{m s}^{-1}$ ),  $\Delta$  is the slope of the saturation vapour pressure temperature curve ( $\text{kg m}^{-3} \text{K}^{-1}$ ),  $R_n$  is the net radiation ( $\text{W m}^{-2}$ ),  $\rho$  is the air density ( $\text{kg m}^{-3}$ ),  $c_p$  is the specific heat of air ( $\text{J kg}^{-1} \text{K}^{-1}$ ),  $VPD$  and  $r_a$  and  $r_c$  are the aerodynamic and canopy resistances, respectively ( $\text{m s}^{-1}$ ),  $\lambda$  is the latent heat of vaporisation of water ( $\text{J kg}^{-1}$ ),  $\gamma$  is a psychrometric constant ( $\text{kg m}^{-1} \text{s}^{-2}$ ), and  $dt$  is the time step (s). It is assumed that evaporation from the trunk and the leaves occurred at the same rate. However, the actual volume of water evaporated will be different because of the different surface area. Furthermore, it is also assumed that evaporation is allowed to occur only after the cessation of the rainfall period (Wilkinson, 2000). *Grass interception* is based on the thatch effect for which dense patches can flatten under the weight of rainfall and create a semi-impermeable barrier. The thatch effect is simulated by reducing the hourly rainfall intensity of a rate that is in accordance with the studies of Lamb and Premchitt (1990). These authors demonstrated through experimental plots in Hong Kong, that between half and three quarters of all rain formed runoff without the infiltration capacity of the soil having been reached. Amongst the investigated surface covers there were long grass and turfed grass.

- Evapotranspiration and root water uptake. Plant transpiration is controlled by environmental conditions above and below the ground. Soil flow is dependent on the amount of water of the soil (which determines the hydraulic conductivity). Under dry soil conditions, where suction values are high, the movement of water toward the root is limited and the plant reaches wilting point. A similar process is observed in saturated soil where there is an oxygen deficiency. Plant water uptake is therefore governed by these soil conditions (which determine the resistance offered by the soil to moisture extraction) as well as the extent of the root development, and the ease of the internal sap movement by the vascular system of the xylem. The principal variables that determine transpiration are then the leaf layer conductance (reciprocal of the aerodynamic resistance) and the stomatal conductance (Roberts et al. 1990). To determine the magnitude of transpiration the Penman-Monteith equation (Eq. 2.9) is adopted with the inclusion of the canopy resistance term  $r_c$ . This process is coupled with the spatial distribution of the roots and of the soil moisture content to determine the rate of water uptake from the roots. First, the amount of moisture extracted from the roots is calculated at each time step by distributing the rate of transpiration throughout the depth of the roots; then, the moisture of the cell where the roots are present is altered by subtracting the generated sink term to the equation 2.1. By changing the moisture content of those cells to account for the root uptake, alterations of the soil water pressure, hydraulic conductivity and fluxed will follow as a consequence. The transpiration model was evaluated by comparing CHASM results to measured transpiration rates of, amongst others, Amazonian rainforest in Brazil.

- Increased permeability given by the root network and determined by the root area ratio and root network distribution. This is calculated using an empirical equation formulated by Collison (1993) based on fieldwork in Malaysia. The equation determines the increase in saturated hydraulic conductivity as a function of the root area ratio (RAR).
- The interaction between roots and soil can be quantified using a perpendicular root model (Wu et al., 1979; Wu, 1995), where roots cross the slip plane perpendicularly. The mobilisation of the tensile resistance of roots can be represented by an increment of the effective cohesion ( $\Delta c'$ ) in vegetated soil, which is added to the soil shear strength in the Mohr-Coulomb equation (2.4). The magnitude of the reinforcement can be modelled using the following equation:

$$\Delta c' = t_r(\cos\theta \tan\phi + \sin\theta) \quad (2.10)$$

Where  $\theta$  is the angle of shear rotation (degrees),  $\phi$  is the angle of internal friction (degrees) and  $t_r$  is the average tensile strength of roots per unit area of the soil, which can be calculated as the average tensile strength of roots ( $T_r$ , kN m<sup>-1</sup>), multiplied by the root area ratio (RAR, m<sup>-2</sup>) (Wilkinson 2000). The parameter  $\theta$  depends on the thickness of the shear zone and the amount of shear displacement. According to field observations, Wu et al. (1979) indicate that the bracketed value of Eq. 2.10 can be replaced by a mean value equal to 1.15, so that Eq. 2.10 can be simplified as  $\Delta c' = 1.15 t_r$  (equation implemented in CHASM).

- Vegetation surcharge is accounted by adding the weight of vegetation on the slope surface which is then distributed through the soil profile according to the vertical and horizontal distance from the source of loading and eventually it is added to the weight of the slice. Estimates of tree surcharge can be estimated from the literature. Approximately, surcharge values of a mature forest stand range between 1-10kN m<sup>-2</sup> (O'Loughlin, 1974; Wu et al. 1979).

In this thesis, the parameters that define these hydrological and mechanical processes of vegetation are fixed (e.g. the tensile strength of roots or the canopy cover) and are defined according to values found in literature. This assumption translates into assessing the effect of vegetation on slope stability only by comparing slope with and without trees or shrub.

### 2.2.1 Integrating slope water management (point water sources) into CHASM: new CHASM+

A new functionality is developed in CHASM (new CHASM+) to include slope surface water management. This

has been included in the source code of CHASM (written in C++). The new CHASM+ provides the modelling platform to analyse the effect of roof gutters on houses, leaking tanks and superficial pipes on slope stability. These model components are activated when the water leakage file is present (see Appendix A1).

### Leaking buried septic tank

The user can determine the position of the tanks, their dimensions (width and depth), the leakage rate ( $\text{m}^3 \text{s}^{-1}$ ) and the type of leakage (local or evenly distributed, see Appendix A1). Considering that the slope cross section is represented with a mesh of columns and cells, a tank will occupy some of these cells according to its dimensions and position. These cells are modelled as being impermeable and heavier than the surrounding soil. The water leakage is added to the moisture content of the cells underneath the tank, through the following water balance equation:

$$\frac{\partial(Q + Q_{\text{leak}})}{\partial z} = \frac{\partial \theta}{\partial t} \quad (2.11)$$

where,  $\theta$  is the moisture content (evaluated with Eq. 2.1), changing over time according to the water flow  $Q$  and  $Q_{\text{leak}}$ .  $Q_{\text{leak}}$  represents the water leaked by the tank, constant throughout the simulation time. The unsaturated hydraulic conductivity, which depends on the moisture content, locally increases because of the water leakage and is iteratively calculated with the Millington-Quirk formulation (Eq. 2.2). The maximum value is reached when soil is saturated (saturated hydraulic conductivity, fixed by the user). Note as buried leaking pipes can also be simulated by using this option by not considering the load of the tank.

### Leaking pipes on slope surface

Pipes are simulated as discharging water onto the slope surface. This can occur because of low pipe maintenance or when water collectors are poorly designed and not properly connected to formal drainage or sewerage system (Ortuste, 2012). As previously mentioned, in CHASM the slope cross section is represented by a two-dimensional mesh of columns and cells for the purposes of the hydrology calculations. Therefore, the water leakage from the pipe is added to the surface water where the pipe is positioned. This water infiltrates into the slope according to the infiltration capacity of the top cell of that column, which is a function of its (saturated or unsaturated) hydraulic conductivity. The water that does not infiltrate because it exceeds the infiltration capacity, is stored on the surface as ponding water. The maximum storage of ponding water is determined by the user as detention capacity of that cell. If the ponding water exceeds this value, it is removed from the calculation because surface water runoff is not included in the CHASM hydrology scheme. The leakage when present is constant throughout the simulation time.

## Roof gutters on houses

Where houses are present, rainfall does not reach the top cell of the slope underneath the house, and the amount of rain intercepted by the roof is calculated and discharged onto the top cells of the slope to the sides of the house. If the roof is dual pitch (Fig. 2.6a), half of the intercepted rain is discharged upslope and half downslope of the house, and it is equal to the rainfall rate multiplied by half of the roof area. This means that the surface water being added to the cells immediately adjacent to the house is the sum of the rainfall that would fall in that cell plus the intercepted rainfall discharged from the roof. The same calculation is used for the mono pitch roof, but in this case the rainwater that falls on the roof is entirely discharged downslope or upslope of the house and it is equal to the rainfall rate multiplied by the whole roof area (Fig. 2.6b and c). The surface water will then infiltrate into the slope as described for the case of the leaking pipe. If gutters are present, the rainwater intercepted by the roof is removed, consequently decreasing the rainfall rate infiltrating into the slope.

The localised addition of point water sources can induce soil pipe erosion in response to increasing water inputs. This could be simulated for example with a dual permeability model, but then it would be difficult to implement the pore pressure calculated into the slope stability analysis (Bogaard and Greco, 2016). Furthermore, the inclusion of preferential flows requires the definition of additional input factors which may be difficult in data-scarce contexts. So, given the spatial scale, the purpose of the analysis and the data available, the current CHASM+ representation can be considered sufficient to depict landslide initiation due to flow accumulation around the point water source.

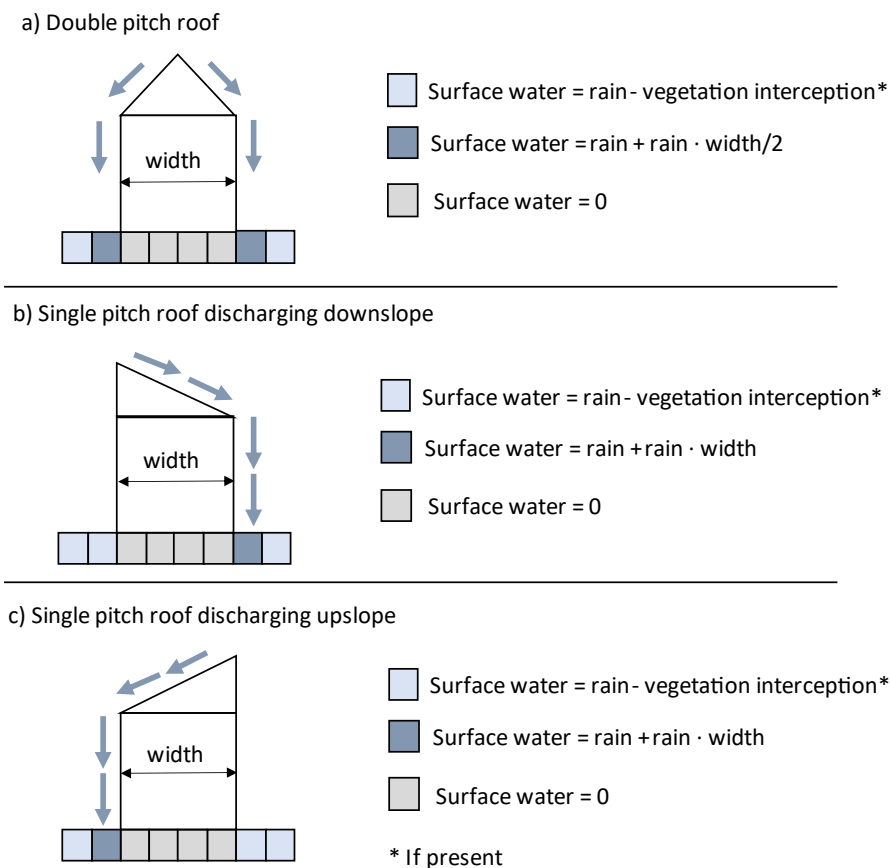


Figure 2.6: Representation of rainwater intercepted by the roof discharged onto the top cells of the slope to the sides of the house for (a) double pitch roof; (b) single pitch roof discharging downslope; (c) single pitch roof discharging upslope.

## Modify the slip search grid algorithm for detecting small-scale landslides

The Bishop's circular stability analysis in CHASM employs an automatic slip search to determine the slip surface with minimum FoS. Currently the CHASM search grid is defined as a square or rectangular shape composed of evenly spaced points (Fig. 2.7a). The search grid location and size as well as the initial radius and radius increment of the circular slip surface are specified by the user. The search procedure is then carried out in successive steps: the slip circle is centred on each generated grid points and the shear and strength forces are calculated along the slip surfaces generated at each radius increment. When all the available grid nodes have been tested, only the minimum calculated FoS is given as output.

In previous applications, grid size and position were defined according to the local slope morphology and failure mechanisms to be analysed. For example, Thiebes (2012) positioned the lower left hand corner of the grid (red point in Fig. 2.7) close to the top of the slope surface (at one-third of the slope length) to detect potential failure surfaces on the upslope section. Almeida et al. (2017) sets the same corner close to the toe of the slope (two-third of the slope length, Fig. 2.7a) because more interested to potential failures at the

lower slope sections. Rainfall-triggered landslides occurring on cut slopes are usually characterised by circular slip surfaces with a relatively small radius (Lam et al., 2006). In this thesis, the aim is to make sure that the grid search algorithm generates slip surfaces that are capable of detecting both small- (as those associated by hill cutting) and large-scale landslides. A new function is, therefore, developed in the stability routine of CHASM+ to modify the grid dimensions, position, and shape used in previous analyses. Figure 2.7b shows the new grid compared to the grid used by Almeida et al (2017). The new search grid runs parallel to the slope, at a distance above the slope surface that is user defined. The modifications made in the input file that allow to use the new search algorithm are shown in Appendix A1.

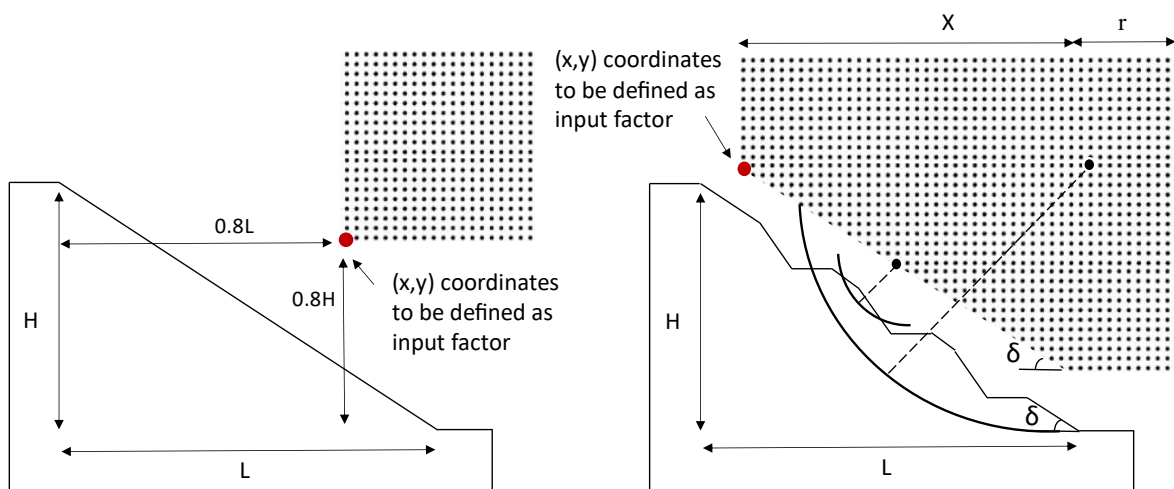


Figure 2.7: (a) Example of search grid that CHASM could represent before the modifications made (only square or rectangular shapes are possible); (b) example of search grid that the new CHASM+ can represent. The letter 'L' represents the length of the slope; 'H', the height; 'X' represents the portion of the grid tilted of  $\delta$ ; 'r' portion of horizontal grid (see Appendix A1).

## 2.2.2 Assumptions and limitations of the model

CHASM presents a series of limitations, affecting both the hydrology and stability routine:

- 1) The horizontal suction is assumed negligible, thus the horizontal fluxes in the unsaturated zone is neglected. Water infiltration is therefore modelled in one (vertical) dimension. This is justified by the use of CHASM in 'worst case' scenarios where low frequency and high magnitudes storms are often considered. In these conditions, soil surface rapidly saturates, and infiltration gets defined by the vertical suction gradient, which results higher than the horizontal.
- 2) Hysteresis is not modelled, thus different suctions associated with the wetting and drying process are not considered. This could affect the value of the hydraulic conductivity in unsaturated soils and therefore the infiltration rate. However, the unsaturated hydraulic conductivity in CHASM is a

function of the moisture content, which has been found to be much lesser affected by hysteresis compared to suction (Poulovassilis, 1969).

- 3) In the first model's iteration, the suction gradient distribution is assumed to be uniform, linearly decreasing from the slope surface to the water table set as initial boundary condition. This is physically unrealistic, but it is used to calculate the initial moisture content distribution. Equilibrium will be then reached according to the soil hydrological properties.
- 4) The surface run-off is not calculated, and the excess of rainwater is lost rather than being redistributed downslope. This can happen mainly for high intensity rainfall events when the rainfall rate is likely to exceed the soil infiltration and detention capacity.
- 5) Darcy's law is used to describe water movement in both saturated and unsaturated soil (Richard's equation for unsaturated seepage is, in fact, a derivation of Darcy's equation). Darcy's law assumes that: the flow is laminar and the effect of the pressure differences at the soil and air interface is negligible. By assuming laminar flow, the effect of macropores, such as those created by decay of plant roots or animal burrows, cannot be represented. Macropore flows can lead to lower or higher water pressures depending on their location within the slope, thereby affecting slope stability thresholds.

## 2.3 Methods for uncertainties quantification and attribution

Assuming that CHASM can represent landslide processes in a consistent way, its prediction of slope stability behaviour could still be erroneous because of the uncertainties in its input factors. It is, therefore, important to investigate how such uncertainties propagate through the model into its output. This task can be achieved via Monte-Carlo based methods for quantification and attribution of uncertainty, such as Global Sensitivity Analysis (GSA) (Pianosi and Wagener, 2015; Wagener and Pianosi, 2019; Saltelli et al., 2008). GSA is a set of statistical techniques that provide a structured approach to diagnose the impact of input uncertainties by:

- Quantifying which input factors influence the model's predictions the most. This might help to verify whether the model's behaviour is consistent with the modeller's expectation (e.g. by comparing the outputs to empirical evidence, to our conceptual understanding of the system or to another model's prediction, as shown in Section 2.4.2). Or it can be useful for targeting the efforts for uncertainty reduction (as will be discussed in Chapter 3).
- Identifying thresholds of the uncertain inputs that map the model output into regions of particular interest (e.g. regions where the threshold of acceptable risk is exceeded). This is a way to implement the 'bottom-up' strategy used in our modelling framework (Fig. 1.3b), to identify regions of the input

space associated with high probability of slope failure (regions of vulnerability) (as we will show in Chapter 3 and 4).

Application of GSA include three steps (Fig. 2.2):

- sampling of the space of variability, defined by the range/probability distribution of the input factors
- model evaluation (CHASM+ running in HPC)
- post-processing.

As anticipated in Section 2.1, we use a MC sampling for the first step. We create thousands of slopes with varying properties. Each slope is then associated with the minimum predicted FoS. To evaluate the differences in environmental and urban conditions defining the failed ( $FoS < 1$ ) and stable ( $FoS > 1$ ) slopes, we use two methods: regional sensitivity analysis (RSA) and Classification and Regression Trees (CART).

### 2.3.1 Regional sensitivity analysis (RSA)

In this thesis, we want to identify which input factors – among geometry, soil, hydrology, rainfall, and urban properties – have the strongest impact on slope stability. Since in our case the model output is binary as simulated slopes are categorised as failed (if  $FoS \leq 1$ ) or stable ( $FoS > 1$ ), we use the regional sensitivity analysis (RSA) approach (Hornberger and Spear, 1981), which is particularly suitable when dealing with categorical outputs. In the RSA approach, the cumulative marginal distribution ( $F$ ) of each input factor is computed for each output category, i.e. in our case 'stable' and 'failed' slopes. If the distributions significantly separate out, it is taken as evidence that the model output (slope stability) is significantly affected by variations in the considered input factor. The level of separation between the cumulative distributions can be formally measured by the Kolmogorov–Smirnov (KS) statistic (Kolmogorov, 1933; Smirnov, 1939) and used as a sensitivity index (Pianosi et al., 2016). The sensitivity index  $S$  for the  $i$ -th input factor  $x_i$  varies between 0 and 1 and it is then expressed as follows:

$$S_i = \max | F_i^{\text{Stable}}(x_i) - F_i^{\text{Fail}}(x_i) | \quad (2.12)$$

The confidence intervals of the sensitivity indices can be estimated via bootstrap technique (Efron and Tibshirani, 1994). The bootstrap randomly draws  $N$  samples (with replacement) from the available data to compute  $N$  KS statistics for each input factor. The magnitude of fluctuations in the KS statistic from one sample to another represents the level of confidence in the estimation of the sensitivity indices. For this



application, we use the SAFE (Sensitivity Analysis For Everybody) toolbox (Pianosi et al., 2015) to perform RSA and to calculate the sensitivity indices and their confidence intervals by bootstrapping.

### 2.3.2 Classification And Regression Tree (CART)

Classification and regression tree (CART; Breiman et al., 1984) is a supervised machine learning method which we will use here to predict critical thresholds in input factors over or below which a particular slope is more likely to fail. Starting from the whole set of simulations, the CART algorithm finds the best possible input factor (e.g. slope angle or rainfall intensity) and the best possible threshold of that input factor (e.g. slope angle greater or less than 30°) that divide the simulations into stable and failed simulations. This process is recursively repeated, creating at every split two branches and two ('child') nodes of the tree, until all stable and failed simulations are split or some pre-defined criteria is satisfied. In choosing the best splitter, the model seeks to maximise the 'purity', i.e. to maximise the number of stable or failed simulations at the two generated nodes. Amongst the different measures of purity available, we use the Gini purity index defined as:

$$1 - \sum_{i=1}^m p^2(i) \quad (2.13)$$

where  $m$  is the number of categories for the output (in this case two: stable or failed), and  $p(i)$  is the fraction of simulations in the node belonging to category  $i$ . The Gini purity index is 0 when all the simulations in the considered node belong to the same category (a 'pure' node, i.e. all stable or failed). The splitting process typically continues until all final leaf nodes show Gini purity indices below a chosen threshold. The final nodes express the prediction for the corresponding branch.

While a high number of nodes increases predicting accuracy, it also makes the model more difficult to interpret and generalise to other datasets (i.e. the problem of overfitting). A pruning technique can be applied to avoid this overfitting and to identify an acceptable trade-off, between predictive power and number of nodes. In this thesis, we use the CART algorithm implemented within the MATLAB Statistics and Machine Learning Toolbox (Mathworks, 2018) using the K fold cross-validation to better estimate its predictive power. In particular, we use 10-fold cross-validation (default option), which randomly divides the original dataset (the N thousands of simulations) into 10 subgroups. A total of nine subgroups are used to construct 10 CARTs, while the remaining subgroup is used to test the CARTs' performance. The average value of the 10 misclassification errors so obtained represents the cross-validation error, which can be used to select suitable pruning levels. To reduce the number of nodes without increasing the misclassification errors,

auxiliary variables can be used to combine correlated input factors. Auxiliary variables can simplify the tree's structure (by using fewer combined input factors) and potentially modify the input space in a way that the division of failed and stable simulations is more effective (see rotation of the coordinate systems in Dalal et al., 2013).

## 2.4 Assessing the performance of the newly extended CHASM+

The original CHASM code has previously been shown to successfully represent landslides in humid tropical weathered soils, correctly classifying 78 % of failed slopes and 68 % of stable slopes (Anderson, 1990). In this section we verify the consistency of the results provided by the newly extended software CHASM+. We first perform simple 'sanity checks' to evaluate whether the stability of the modelled slopes respond to the inclusion of surface water management and of the new search grid in a physically realistic way and in accord with reported observations of urban landslide processes (Section 1.1). Then, we compare the results of CHASM+ with the peer-reviewed results of simulations from another slope stability model (GeoSlope), which is assumed to give sensible results given its extensive use within the engineering community.

### 2.4.1 Sanity checks for the new point water source functions and for the modified grid search

A preliminary assessment of CHASM+ is presented in this section in order to verify the consistency of the simulations results. Water infiltration into the slope from leaking tanks and pipes as well as the absence of roof gutters increase soil moisture content and consequently pore water pressure. When these point water sources are present, slope stability is therefore expected to be lower compared to the same slopes without the water additions. To verify such assumption, we run CHASM+ on slopes with and without surface water management.

Roof gutters and leaking pipes modify the amount of surface water that can infiltrate into the slope (Section 2.2.1). If rainfall is very intense, the top soil strata may rapidly saturate, limiting the water infiltration to the rate of the maximum infiltration capacity while deleting the excess (which would in reality become run-off, but it is not included in CHASM, Section 2.2.2). We would, therefore, expect that an urbanised slope without roof gutters on houses and with pipes leaking on the slope surface would have a different slope stability response under different hydraulic conductivities and rainfall intensities. We, then, simulate a set of slopes with fixed geometry (soil height, slope angle and thickness of soil layers) and geotechnical properties but varying soil hydraulic conductivity and rainfall intensity. A comparison is made between the FoS derived for the urbanised slope with and without roof gutters and leaking pipes. The net destabilising effect (difference between FoS) is shown in Fig. 2.8 and Fig. 2.9 (the legend of the colour scheme is reported in Fig. 2.10). These

charts represent areas of sensitivity where the discharge of superficial water can be more detrimental for slope stability.

**Decrease in FoS when houses have no roof gutters**

		Rain Intensity mm h <sup>-1</sup> (m s <sup>-1</sup> )				
		10 (2.7E-6)	20 (5.5E-6)	30 (8.3E-6)	40 (1.1E-5)	50 (1.4E-5)
K <sub>sat</sub> (m s <sup>-1</sup> )	1.00E-05					
	1.00E-06					
	1.00E-07					

Figure 2.8: Difference between FoS calculated on slopes with houses with roof gutters versus those without (10 houses in total). The FoS is always higher in the case houses are provided with roof gutters. The shading refers to the legend in Fig. 2.10. The simulated slopes are 70 m long and 30° steep. The SWCC refer to Sandy Clay loam (from Hodnett and Tomasella, 2002). The soil is 7 m deep, overlying an impermeable surface, also 7 m deep. Rainfall duration is 24 h. The roofs are simulated as double pitch.

**Decrease in FoS when pipes are leaking**

		Rain Intensity mm h <sup>-1</sup> (m s <sup>-1</sup> )				
		10 (2.7E-6)	20 (5.5E-6)	30 (8.3E-6)	40 (1.1E-5)	50 (1.4E-5)
K <sub>sat</sub> (m s <sup>-1</sup> )	1.00E-05					
	1.00E-06					
	1.00E-07					

Figure 2.9: Difference between FoS calculated on slopes with houses without versus with superficial leaking pipes (10 houses and leaking pipes in total). The FoS is always higher in the case pipes are not leaking. The shading refers to the legend in Fig. 2.10. The simulated slopes are 70 m long and 30° steep. The SWCC refer to Sandy Clay loam (from Hodnett and Tomasella, 2002). The soil is 7 m deep, overlying an impermeable surface, 7 m deep. Rainfall duration is 24 h. The leak of the pipe is constant and equal to 1x10<sup>-6</sup> m<sup>3</sup> s<sup>-1</sup>.

**Legend (Decrease of FoS)**

No change	0	
Slight change	0 - 0.05	
Moderate change	0.05 - 0.1	
Significant change	0.1 - 0.15	
V. significant change	0.15 - 0.3	

Figure 2.1: Legend of shading used to categorise the difference between FoS. The division in classes is arbitrary.

Figure 2.8 shows that the lack of roof gutters is more detrimental in slopes with higher hydraulic conductivity. This is expected because in absence of roof gutters, most of the rainwater infiltrates into the slope, reducing the shear strength along the slip surface. Significant changes (decrease of FoS between 0.1 and 0.15) occur for combinations of high soil permeability ( $1 \times 10^{-5} \text{ m s}^{-1}$ ) and medium rainfall intensity (between 20-30  $\text{mm h}^{-1}$ ). For higher rainfall intensity or less permeable soil the effect of roof gutter interception is more negligible or null. This is because the infiltration capacity of the soil is exceeded and most of the incident rainfall would become run-off (which is deleted in CHASM).

Similar consideration can be made for Fig. 2.9. Leaking pipes decrease slope stability in all cases considered. This is expected because the leak is released throughout the whole simulation time. As for the previous case, the most detrimental effect occurs for the most permeable soil, whereas the influence of leaking pipes on slope stability decreases for higher rainfall intensities and lower soil permeabilities.

Leaks from buried tanks increase the amount of soil moisture content within the slope. The water will infiltrate depending on the hydraulic conductivity of the soil, but it is not directly influenced by the infiltration capacity of the soil surface (in turn influenced by rainfall intensity, as previously shown). Thus, for these simulations, rainfall intensity and duration are maintained as constant, while we vary the hydraulic conductivities of the soil depth (i.e. the distance to the underlying impermeable layer). Figure 2.11 shows that slope stability decreases in all the simulations considered. However, the most detrimental effect occurs for water leaks of the same order of magnitude of the soil permeability ( $1 \times 10^{-6} \text{ m s}^{-1}$ ). Soil locally saturates and the high pore water pressures decrease slope stability. In the other two cases ( $1 \times 10^{-5}$  and  $1 \times 10^{-7} \text{ m s}^{-1}$ ), the water flows respectively too fast (with highly permeable soil) or too slow (with more impermeable soil) to reach local soil saturation. Moderate changes are also observed when soil is 2 metres deep. The shallow soil leads to a progressive accumulation of water above the impermeable surface, eventually saturating most of the soil layer and consequently decreasing the FoS.

**Decrease in FoS when tanks are leaking**

		Depth to bedrock (m)				
$K_{\text{sat}} (\text{m s}^{-1})$		2	4	6	8	10
1.00E-05						
1.00E-06						
1.00E-07						

Figure 2.2: Difference between FoS calculated on slopes with or without leaking buried septic tanks (10 houses and septic tanks in total). The FoS is always higher in the case where houses have a septic tank that does not leak. The colours refer to the legend in Fig. 2.10. The simulated slopes are 70 m long and 30° steep. The SWCC refer to Sandy Clay loam (from Hodnett and Tomasella, 2002). Rainfall duration is 24 h and rainfall intensity is 30  $\text{mm s}^{-1}$ . The leak of the tank is constant and equal to  $1 \times 10^{-6} \text{ m}^3 \text{ s}^{-1}$ .

Finally, we test the modified grid (Section 2.2.1) used to search slip surfaces with minimum FoS. In this case, we vary both the angle of the slope and of the cut slopes. As Fig. 2.12 shows, the FoS calculated with the new grid are lower than those calculated with the traditional algorithm. This is because the new grid can better identify the circular slip surfaces with small radius in the proximity of the cut slopes. When the slope angle is steep (40°), both types of grid can detect low slope stability levels, making the difference between the FoS more negligible. These initial results, therefore, highlight that the slope stability assessment is improved with the modified shape of the search grid, mainly for those slopes characterised by a low natural susceptibility to failure (e.g. natural angle 20°).

**Decrease in FoS when the new search grid is used**

Slope angle $\delta$ (°)	Cutslope angle $\beta$ (°)		
	50	60	70
20			
30			
40			

Figure 2.3: Difference between FoS calculated on slopes with varying slope and cut angles using the traditional square-shaped search grid (old grid) and the new search grid that runs parallel to the slope. FoS is always higher in the case the old search grid is used. The colours refer to the legend in Fig. 2.10. The simulated slopes are 70 m long. The SWCC refer to Sandy Clay loam (from Hodnett and Tomasella, 2002). The soil is 7 m deep, overlying an impermeable surface. Rainfall duration is 24 h and rainfall intensity is 30 mm h<sup>-1</sup>.

### 2.4.2 Using GSA to benchmark the new slope water point source functions in CHASM+

To benchmark the new functionality introduced, we compare the results obtained with CHASM+ with an example found in the literature. Mendes et al., (2018) analysed the natural and anthropogenic drivers of a rainfall-triggered landslide event happened in the city of Sao Jose’ dos Campos (Brazil) on March 5<sup>th</sup>, 2016. Their analysis demonstrated that rainfall could only have initiated the observed landslide if combined with water tank leakage at the top of the slope. Mendes et al. used the Seep/w and Slope/w modules of the GeoSlope software to analyse the hydrology and the stability component of the landslide (from now on we will refer to the model as GeoSlope for simplicity). Rainfall records for the time of the landslide were available from nearby weather stations and were used to reproduce a daily accumulated rainfall graph for the 31 days prior to the landslide occurrence. These 31 days were used in the simulation to predict the landslide. The soil properties of the three soil layers used for the analysis are reported Table 2.1. Their characterisation was

based on in situ inspection and on previous studies carried out in the same location (Mendes, 2014; Mendes and Filho, 2015). The soil water characteristic curves (SWCC) and the conductivity functions are estimated from this data. The slope was 55 m high with an average slope angle of 40 degrees. The boundary conditions were set according to field observations and to considerations made by Rahardjo et al., (2007) in regarding the position of the water table and retaining walls at the bottom of the slope.

Table 2.1: Geotechnical and hydrological characterisation of the soil layers of the failed slope from Mendes et al. (2018), re-adapted according to the unit of measure used in this analysis.

Layer in soil profile	Depth sample (m)	USCS*	Bulk specific weight (kN m <sup>-3</sup> )	Effective cohesion (kPa)	Effective internal friction angle (°)	Hydraulic conductivity (m s <sup>-1</sup> )	Initial pore water pressure (m)
Soil 1	0.5	SM	17	10	33	2.8 e-6	-1
Soil 2	3.0	CL-ML	18	15	35	1.15 e-6	-1.5
Soil 3	6.5	SM	19	21	37	1.3 e-5	-2

\*USCS: Unified Soil Classification System

The observed landslide occurred in a 6 m high cut slope, at the bottom of the hillslope. A water tank of 1000 litres capacity (10 kN m<sup>-2</sup>) was found to be leaking just above the cut slope. Since the leakage rate at the moment of the failure was unknown, a linearly increasing leak of 0.5, 1.0 and 1.5 m<sup>3</sup> per day was assumed from day 16 until day 31. The Factor of Safety (FoS) was then calculated for three cases: i) including just the rainfall, ii) including just the leaking tank, and iii) including both. The analysis by Mendes et al. (2018) demonstrated how their modelling approach predicts failure (FoS ≤ 1) for the condition where the rainfall is combined with the leaking tank, but not for rainfall alone.

We want to emulate the above analysis with the new extended version of CHASM for the cases: i) including just rainfall and case iii) including both rainfall and the water leakage. With this aim, the analysis entails the following steps:

- 1) CHASM+ is compared to the GeoSlope models to evaluate how the two modelling approaches differ in the process representation and input factor specification. Some of the input factors not specified in Mendes et al. (2018) but necessary to run CHASM+ will be assumed (Section 2.4.2.1).
- 2) CHASM+ is run using both the input factors specified in Mendes et al. (2018) and the input factors assumed in step 1. The results obtained in this (deterministic) simulation are compared to the results presented in Mendes et al. (2018) (Section 2.4.2.2).
- 3) CHASM+ is run stochastically, where the input factors specified in Mendes et al. (2018) are fixed and the input factors assumed are stochastically varied within reasonable ranges. This allows to take into account the uncertainties introduced by the different input factors specification (Section 2.4.2.3).

### 2.4.2.1 Comparing CHASM+ with GeoSlope

The two models CHASM+ and GeoSlope present similarities and differences with respect to their process representation and in their specification and implementation of the input factors. Both models are based on limit equilibrium method of slices; they can represent unsaturated and saturated soil conditions using the Darcy equations; and they allow to define a grid of slip surface centres to analyse trial slips with different minimum FoS. GeoSlope operates on finite elements meshes for computing soil stresses with two-dimensional seepage. CHASM+ employs a forward explicit finite difference method to analyse the effective stresses at each computational node, with two-dimensional seepage on saturated soil conditions and one dimensional seepage on unsaturated soil conditions. Table 2.2 reports the differences in the governing equations and input factors specifications. The input factors not specified in Mendes et al. (2018) but necessary to run CHASM+ are assumed. These assumed values are fixed for the deterministic analysis (step 2) and varied within ranges for the stochastic analysis (step 3).

Table 2.2: differences between GeoSlope and CHASM+. The table specifies both the input factors used for the first deterministic comparison (step 2 – Section 2.4.2.2) and the space of variability for the input factors in the stochastic analysis (step 3 – Section 2.4.2.3).

	GeoSlope	CHASM+	Assumed values for the deterministic analysis	Assumed ranges for the stochastic analysis
<b>Initial suction</b>	Assigned per each cell with different values per soil type	Assigned only at the top cell and interpolated linearly until reaching the water table (where suction = 0 m)	-2 m at the top cell	U (-5; -0.5) m
<b>Soil water retention curves</b>	Specified by the parameters derived from lab tests	Use Van Genuchten model to calculate the soil water retention curve.	Hodnett and Tomasella (2002) Soil 1 = sandy clay loam Soil 2 = silty clay Soil 3 = loam	Varied according to the standard deviation suggested by Hodnett and Tomasella (2002) *
<b>Unsaturated Hydraulic conductivity</b>	Calculated with Van Genuchten interpolation	Calculated with the Millington-Quirk equation (Millington and Quirk, 1959)		
<b>Unit weight</b>	Only bulk specific weight specified	Need to specify both dry and saturated unit weight	Dry unit weight specified. Saturated unit weight = (dry unit weight + 2) kN m <sup>-3</sup>	Dry unit weight: Soil 1 = Soil 2 = Soil 3 U (12; 24) kN m <sup>-3</sup>
<b>Impermeable surfaces</b>	Applied impermeable barriers (software available option)	Obtained by decreasing the soil permeability of the cells occupied by the tank and walls	10e-13 m s <sup>-1</sup>	Ln (-11.654 0.898) m s <sup>-1</sup>
<b>Tank leaking</b>	Linearly increasing	Constant throughout the simulation time	Function modified to reproduce the same linear increment in the water leakage	As in the deterministic analysis

U = Uniform distribution; Ud = Discrete uniform; N = Normal distribution; Ln = Log-normal distribution.

VG: Van Genuchten parameters for defining suction moisture characteristics curve.

\*Probability distributions assumed: N (Saturated water content –  $\theta_{sat}$ ) m<sup>3</sup> m<sup>-3</sup>; Ln (Residual water content –  $\theta_{res}$ ) m<sup>3</sup> m<sup>-3</sup>; Ln (VG  $\alpha$  parameter) m<sup>-1</sup>; Ln (VG n parameter).

#### 2.4.2.2 Deterministic analysis: CHASM+ predicts lower slope stability than GeoSlope

The slope presented in Mendes et al. (2018) is reproduced in CHASM+, maintaining the same geometry, initial hydrological conditions, leak rate from the water tank and daily accumulated rainfall specified in the paper (the 31 days prior to the landslide occurrence). We use the soil properties reported in Table 2.1, and Table 2.2 (column: ‘assumed values for the deterministic analysis’). The Factor of Safety (FoS) predicted by GeoSlope and CHASM+ under these conditions, are presented in Fig. 2.13 (for CHASM+ only the case that includes both rainfall and the water leakage is shown). Both the models predict an early failure: in GeoSlope,



the FoS falls below 1 the 26<sup>th</sup> day (5 days before the landslide occurrence) while CHASM+ predicts failure the 21<sup>st</sup> day (10 days before). Furthermore, the FoS calculated with CHASM+ appears to be lower than the FoS calculated with GeoSlope throughout the whole simulation time. This might indicate that the assumed input factors used in CHASM+ or/and the different numerical implementation could have led to a different hydrological and stability response. We therefore use a stochastic framework to perform a back analysis that explores which combination of input factors allow CHASM+ to give similar results to GeoSlope, and if this combination is physically consistent with the observed landslide event and data.

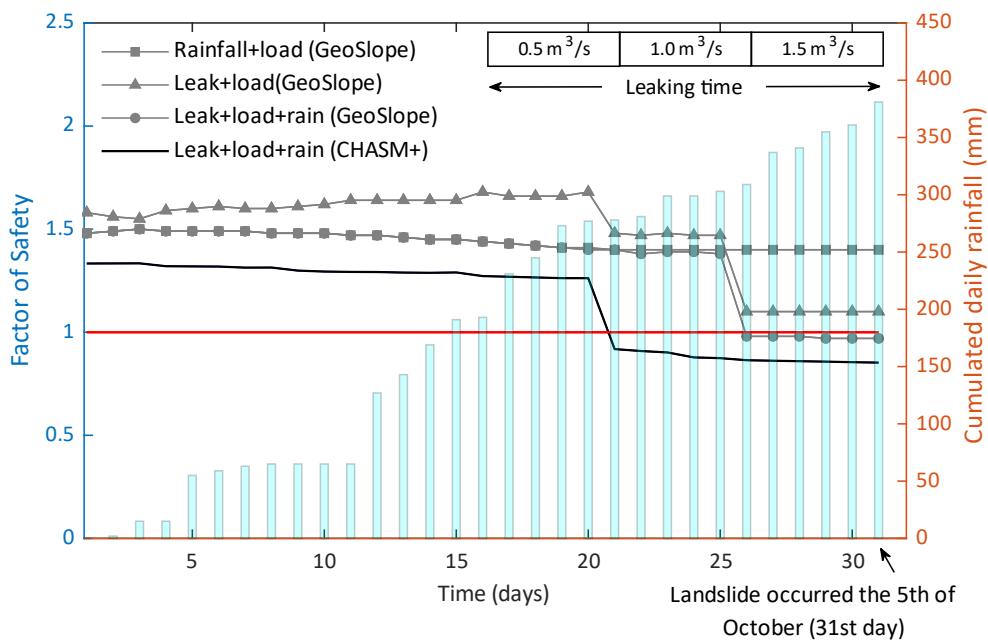


Figure 2.4: In grey the results obtained by Mendes et al. using GeoSlope for the three cases analysed (with and without rain and leaking tank); in black the results obtained with CHASM+ for the case where rainfall, leakage and load are considered. The light blue bars represent the cumulated rainfall of the 31 days preceding the landslide.

### 2.4.2.3 Stochastic analysis: CHASM+ presents consistent results with GeoSlope

To explore what it could have led CHASM+ to have a different stability response in step 1, the input factors specified in Mendes et al. are kept fixed while the input factors assumed are varied within reasonable ranges (Fig. 2.14). SWC curves, initial soil suction, soil unit weight and the hydraulic conductivity representing impermeable surfaces are varied according to the ranges specified in Table 2.2 (last column). 10,000 different combinations of these input factors are created by stochastically sampling from those day. The stochastic analysis aims to explore for which values of the varying input factors CHASM+ produces similar stability response to GeoSlope.

### Site-specific analysis of a known urban landslide

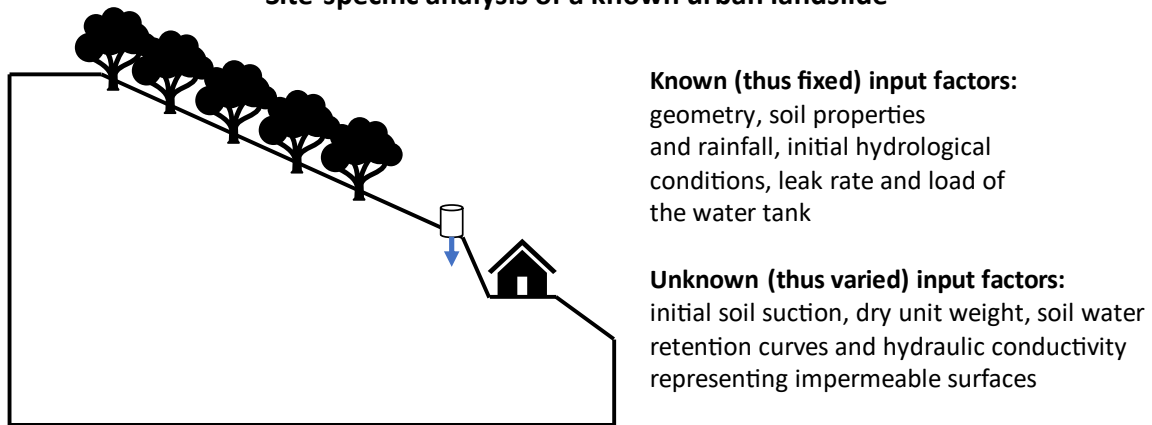


Figure 2.5: the methodology developed for this thesis (described in Section 2.1) is used to compare the results obtained with CHASM+ and GeoSlope for an urban landslide occurred in Sao Jose' dos Campos (Brazil) in 2016, described in Mendes et al. (2018). The input factors that are known (because of field measurements and lab tests, or because assumed – such as the leak rate) are kept constant, while the input factors that were not specified in Mendes et al. (2018) but are necessary to run CHASM+ as well as those differently implemented in CHASM+, are stochastically varied.

Figure 2.15 shows the comparison between the simulations obtained with CHASM+ and with GeoSlope when only rainfall is considered. The best performing 10% CHASM+ simulations are identified by comparing the Root Mean Square Error (RMSE) between the FoSs obtained with CHASM+ (dark grey lines) and the FoS obtained with GeoSlope (black line, indicated as Mendes et al. 2018). The values of input factors that create a hydrological response not compatible with the initial conditions used in Mendes et al. because creating a sudden decrease in FoS (light grey lines) are identified through sensitivity analysis. Those simulations that do not use these values are called 'ok simulations' in Fig. 2.15 (approximately 85% of the total simulations).

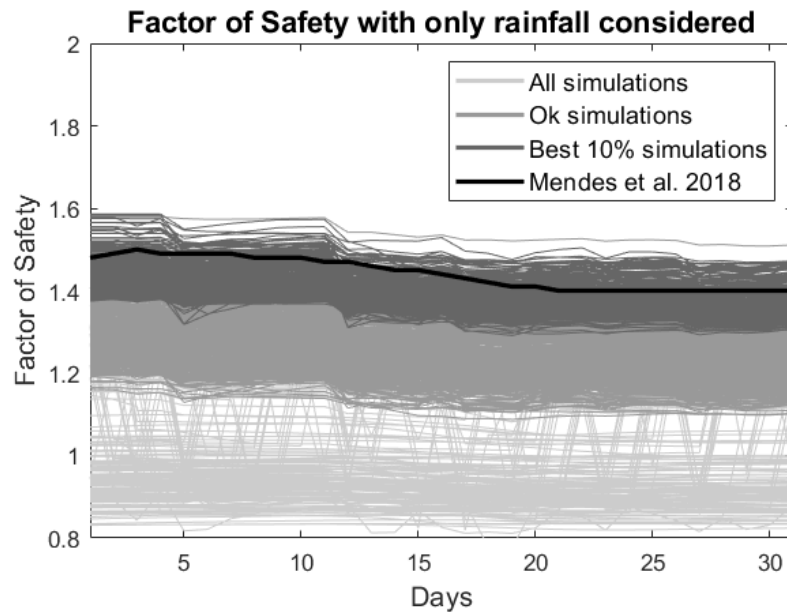


Figure 2.6: Factor of Safety calculated considering only rainfall and load of the tank for both CHASM+ and GeoSlope (this latter is referred as Mendes et al. 2018, and it corresponds to the grey line with square markers in Fig. 2.13).

Figure 2.16 shows how the ranges of the varied input factors are differently constrained when obtaining the ‘ok’ and the best performing simulations. The bars represent the ranges of the input factors. If the bars reduce in size, part of the values of the given range has not been used to create the corresponding response. For example, the best performing simulations never use values of initial soil suction equal to -1 m (Fig. 2.16b). The black horizontal lines represent the values used by Mendes et al. (present only for the upper plots). These values are amongst those used to produce the best performing simulations in CHASM+ (i.e. they are within the dark grey bars), except for the initial soil suction. CHASM+ performs best with low saturated hydraulic conductivity values when representing impermeable surfaces which is physically consistent (the value used in Mendes et al. is assumed to be equal to  $0 \text{ m s}^{-1}$  for impermeable surfaces, Fig. 2.16d), and with low values of the Van Genuchten (VG) parameters defining the SWCCs (saturated moisture content  $\theta_{\text{sat}}$ , residual moisture content  $\theta_{\text{res}}$ , and parameters  $n$ ,  $\alpha$ , Fig. 2.16c, e, f and g). Low values of the VG parameters correspond to steeper SWCCs, a preferred condition for the hydrological numerical stability in CHASM+. The initial soil suction values used to obtain the best performing simulations ranges between -5 m to -2 m (Fig. 2.16b). These values are lower than those used in GeoSlope. The difference is due by the assumptions governing the initial water content distribution in CHASM+, which is determined by the cell resolution 1x1 m of the slope, and by the suction gradient. In the first time step, the initial suction, defined at the top cells of the slope, linearly decreases until reaching the water table. The matric suction for each cell is therefore calculated by dividing the surface suction into the number of cells above the water table. When the initial suction is low (i.e. closer to 0) and the SWCCs are smooth (i.e. with little changes of saturated water content

for different suction values), more cells at the proximity of the water table result close to saturation, and the water level can increase up to 5 - 6 metres. High water table heights can intersect the cut slope and lead to an early failure (the sudden decrease in FoS in Fig. 2.13, represented by the light grey lines in Fig. 2.15). The uniform suction gradient assumed in CHASM+ is physically unrealistic, but it is used for the initial distribution of water moisture content across cells. The hydrological equilibrium is then regulated by the Richard's equation for unsaturated soil. However, this assumption leads to a different initial hydrological condition when compared to GeoSlope. High values of initial suctions are therefore necessary to maintain the water table levels in CHASM+ in the same position simulated in GeoSlope.

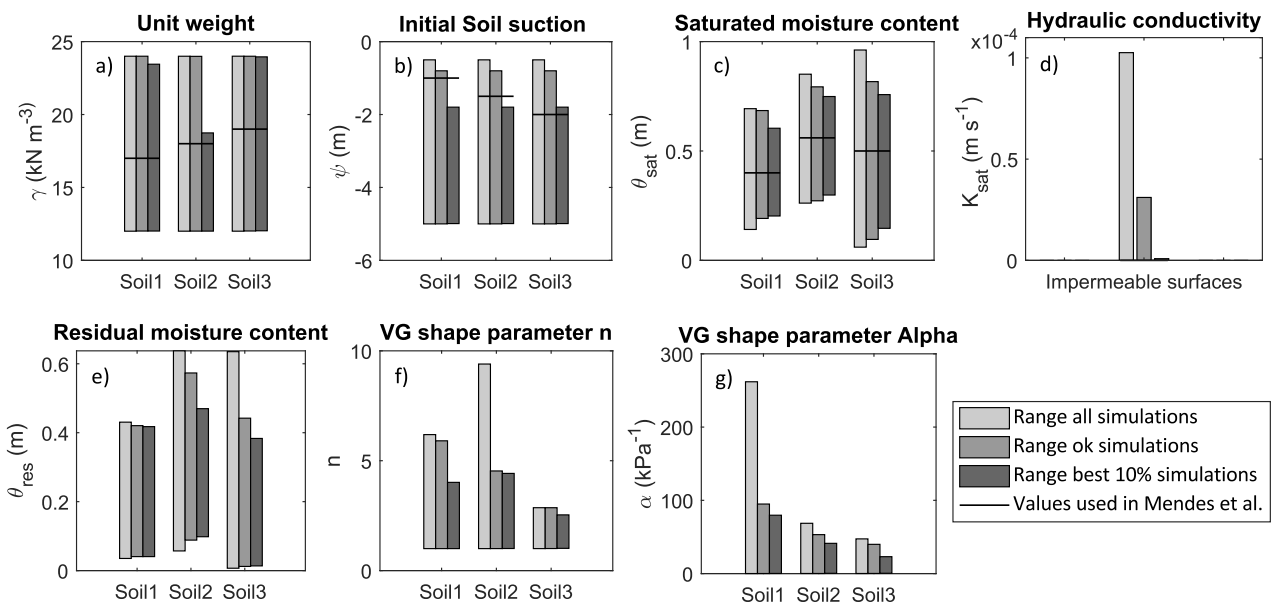


Figure 2.7: The input factors used in CHASM+ are varied within the ranges defined in Table 2.2. The whole ranges are represented in this figure as ‘range all simulations’ (light grey bars). These are compared to the ranges of values that produce ok and best performing simulations (darker greys) which correspond to the FoS trends shown in Fig. 2.15 in the same colour. The black horizontal lines reported on the upper plots (a, b, c and d) identify the discrete values used by Mendes et al. 2018 in the GeoSlope analysis (see Table 2.1). Note as in plot (d) the black line is at zero level.

For the second case the leaking tank is also considered. Other 10,000 simulations are created by sampling from the ranges previously identified as those producing the best performing simulations. Figure 2.17a shows the calculated FoSs. This time, the number of ok simulations differ from the total number of simulations of just 4%. This is because the values of the input factors that were not compatible with the assumptions of the model (i.e. initial soil suction set too low) were excluded in the initial ranges. Amongst the ok simulations, CHASM+ predicts slope failures ( $\text{FoS} \leq 1$ ) for a variety of different times (from Day 17 to Day 31). We want to explore which are the combinations of input factors that produce a most similar response to GeoSlope (dark grey lines in Fig. 2.17a, i.e. the best 10% performing simulations). The parallel plots in Fig. 2.17b show the

distribution of the input factors within their variability range. Ranges are standardised to allow for comparison across the factors. Each line corresponds to a simulation. The darker lines identify the combinations of input factors corresponding to the 10% best performing simulations and thus to the 'correct' timing of the failure. If the dark lines concentrate in a subrange, that factor is influencing the distinction between ok and best performing simulations. This is evident for the VG alpha parameter for the three soil types, and the hydraulic conductivity of the cells representing the impermeable surfaces (IS). Values of hydraulic conductivity close to 0 are consistent with the representation of impermeable surfaces. Low values of alpha correspond to steep SWCCs. The other VG parameters counterbalance their effect to obtain the same result (Van Genuchten, 1980). For example, when the saturated water content of soil 2 is high, the corresponding residual water content is low. Steep SWCCs mean that the water content of the soil increases slower with the decrease of soil suction. This explains their influence on the timing of the failure. The values used by Mendes et al. (black dots) are all part of the lines that corresponds to the best performing simulations of CHASM+ and therefore they are values used to create similar responses to GeoSlope. Furthermore, with these combinations of input factors, CHASM+ predicts the same failure position as GeoSlope (not shown). We have therefore demonstrated that using the sets of input factors identified as best performing, we can create similar responses to GeoSlope, a widely used dynamic slope hydrology and stability software. We use this analysis as an evidence that CHASM+ can correctly represent leakages from buried tanks.

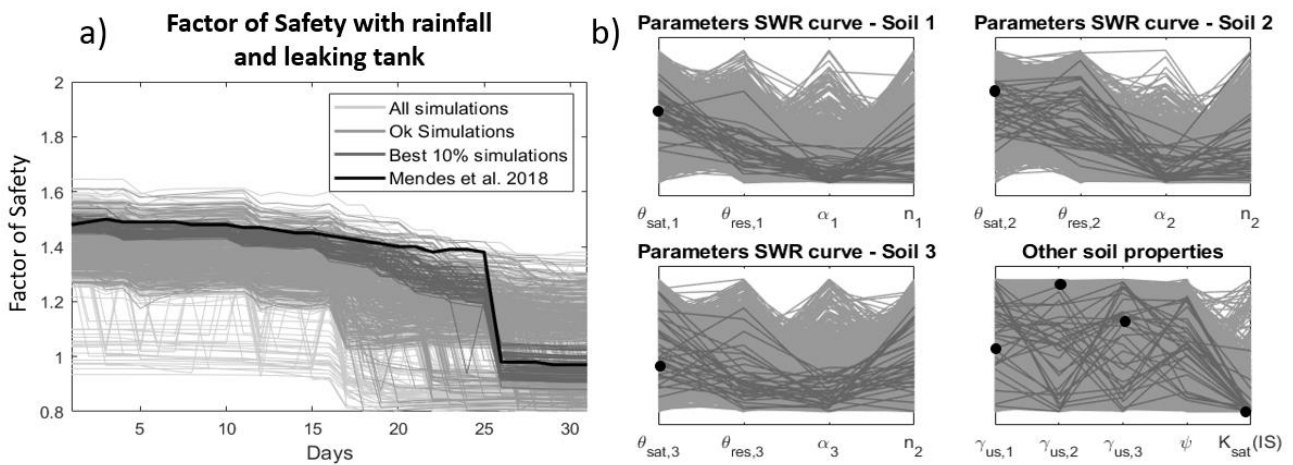


Figure 2.8: a) shows Factor of Safety calculated considering both rainfall and the leaking tank with CHASM+ and GeoSlope (referred as Mendes et al. 2018); b) shows the parallel plots of the ok (lighter grey) and best performing (darker grey) simulations. The lines identify how the input factors are distributed within their variability ranges. The black dots are the values used by Mendes et al. (2018).

## 2.5 Conclusions

This chapter addresses the first research question by delineating the new methodology developed for this thesis. Such methodology aims to include informal housing into slope stability analyses, while quantifying the uncertainty deriving from sparse data (both at hillslope of larger – e.g. community scales), as well as from future climate predictions (therefore, addressing the first research question). In particular, CHASM has been extended (new CHASM+), and it is now capable of representing vegetation removal, slope cutting, house loading, and point water sources (leaking septic tank and pipes, as well as house roof guttering). The capability of representing informal housing (i.e., the combinations of these urban construction activities just mentioned) makes this slope stability model unique. The new methodology also allows quantification of the uncertainty of all input factors, including those representing the urban and climate properties. This is a step forward, because generally the uncertainty of only few input factors (which are heuristically known to influence slope stability) is evaluated, due to the high computational cost that stochastic analyses require (via Monte Carlo sampling). However, CHASM+ is a computationally fast and parsimonious mechanistic slope stability model, and the evaluation of tens-of-thousands of slope stability analyses can be performed in a relatively short time window. Furthermore, the uncertainty related to climate change is included by using a ‘bottom-up’ approach, which has been rarely applied for slope stability and landslide hazard analyses. Such approach does not employ the future probability distributions of rainfall properties derived by climate models which are highly uncertain, but it uses uniform distributions which vary rainfall intensity and duration widely. This assumption allows generation of many intensity-duration combinations representative of past observations but also of potential future unobserved rainstorms. The slope stability analysis then aims to quantify how much change is required in the current (observed) rainfall conditions before landslide probability starts to significantly increases - a useful information to identify which might be the least regrettable climate policy one might take.

The steps of the new methodology is outlined in Section 2.1 and it will be used throughout this thesis. The end of this chapter shows a first application, where the methodology has been used to verify the consistency of the results provided by the newly extended software CHASM+. In the two next chapters, we test the new methodology in Saint Lucia, a typical data-scarce location of the humid tropics.

## Chapter 3 : Including informal housing in slope stability analysis – an application to a data-scarce location in the humid tropics

This chapter is adapted from a published work that has been partially modified to improve the consistency throughout the thesis:

*Bozzolan, E., Holcombe, E., Pianosi, F. and Wagener, T.: Including informal housing in slope stability analysis – an application to a data-scarce location in the humid tropics, Nat. Hazards Earth Syst. Sci. Discuss., 1–20, doi:10.5194/nhess-2020-207, 2020.*

### 3.1 Introduction

In this chapter, the methodology is applied in the context of Saint Lucia (Eastern Caribbean), a typical data-scarce, resource limited location in the humid tropics. The analysis seeks to address the second research question of this thesis:

- 2) How can we quantify the relative role of informal housing, natural slope susceptibility and rainstorm severity in increasing rainfall-triggered landslide hazard within a community?

Specifically, a Monte Carlo sampling is used to generate a population of slopes representative of Saint Lucia which have the potential to be particularly susceptible to landslides and might be a location for informal urbanisation (slopes with angles between 20° and 45°). The urbanisation scenarios are modelled as having a moderate density of informal housing (30% slope surface coverage by houses). The slopes are characterised by varying topographic (here called geometrical), soil, climate, and urban properties (Fig. 3.1, left hand side) and their stability is assessed with CHASM+. The same procedure is then repeated without including the urban properties (non-urbanised slopes; Fig. 3.1, right-hand side) to facilitate considerations about the role of informal housing in slope stability.

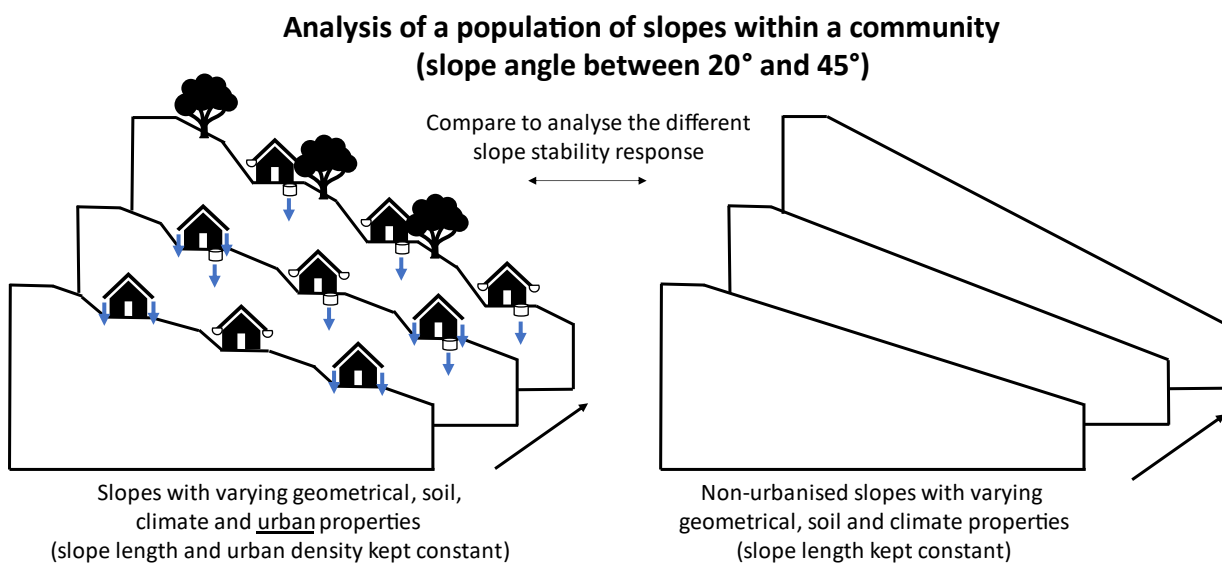


Figure 3.1: Two population of slopes are stochastically generated and analysed in this chapter: urbanised and non-urbanised slopes.

In this chapter we therefore diagnose how slope stability response is modified under a wide range of different natural, climate and urban combinations, aiming to identify the urban construction activities most detrimental for slope stability (e.g. cut slopes vs roof gutters on houses) as well as the natural conditions (e.g. slope angle, soil thickness, or rainfall intensity) in which the probability of rainfall-triggered landslides is most



increased by the presence of informal housing. This is useful information for engineers to prioritise slopes that are currently at risk, to identify those at higher risk of being impacted in the future, and to deduce appropriate hazard mitigation or preparedness actions. Furthermore, the inclusion of informal housing in slope stability analysis allows considerations about the reliability of those rainfall thresholds for triggering landslides calculated that have been calculated without including the human factor and might result in underestimating the hazard.

In particular, this chapter addresses the following three sub-questions that arise from Research question 2:

2a) How can we identify which informal urban construction activities are most detrimental to slope stability?

2b) How is the rainfall threshold for triggering landslides modified when informal housing is considered?

2c) Which landslide mitigation strategies and practices can be deduced from the analysis for current and potential future scenarios of urbanisation and rainfall?

The core of the new methodology used for this analysis is the one illustrated in Chapter 2. The following section schematically reports and briefly describe each methodological step, setting the basis for the results analysis and discussion.

## 3.2 Method

Figure 3.2 shows the main workflow of the analysis reported in this chapter.

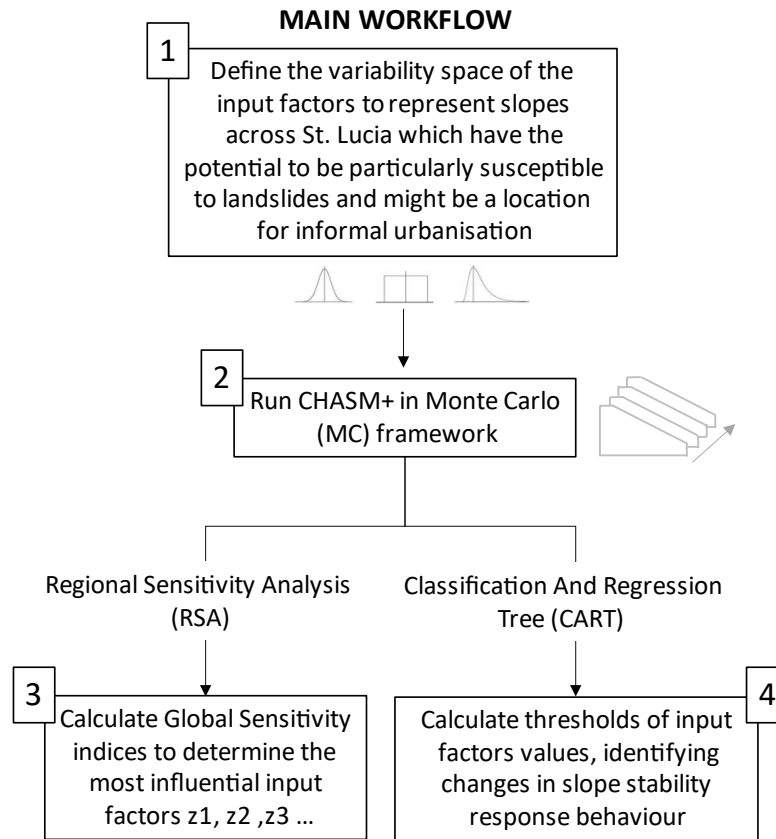


Figure 3.2: scheme of the main workflow of Chapter 3.

Specifically, the method entails the following steps:

- 1) Define the inputs factors necessary to run the model and their variability space. In our case study, the input factors are the parameters defining the geometrical, soil, urban characteristics, as well as rainfall forcing data. Each input factor is considered a random variable and associated with a probability distribution. The probability distributions (described in Section 3.2.2) are defined based on the physical meaning of the input factors, available data and information gathered from fieldwork in Saint Lucia and literature review.
- 2) Create synthetic combinations of input factors by stochastically sampling from their probability distributions (Monte Carlo simulations) and run CHASM+ to generate an equivalent number of model outputs. We repeat the stochastic sampling with and without the urban properties among the input factors in order to facilitate considerations about the role of informal housing in land stability. We

use the minimum factor of safety (FoS) calculated by CHASM+ to classify each slope as stable (FoS > 1) or failed ( $\leq 1$ ) as well as the slip surface where the minimum FoS is calculated to compare the landslides size between urbanised and non-urbanised slopes.

- 3) Identify the input factors that most influence slope stability using global sensitivity analysis (Wagener and Pianosi, 2019). In particular, we use a regional sensitivity analysis (RSA) approach (Hornberger and Spear, 1981; described in Chapter 2, Section 2.3.1) to identify which input factors are most influential in leading to slope failure.
- 4) Identify parameter thresholds beyond which the slopes become unstable. We use CARTs (Classification And Regression Trees; described in Chapter 2, Section 2.3.2) to develop a set of decision rules that predict the combination of soil, geometry, urbanisation, and rainfall input values for which a particular slope is more likely to fail.

In the following sub-sections, we describe in detail the data used to implement our analysis on the context of Saint Lucia.

### 3.2.1 The case study: Saint Lucia, Eastern Caribbean

Saint Lucia is an eastern Caribbean island with a humid tropical climate. The island covers an area of 616 square kilometres, with a population of 184,147 (<https://www.worldometers.info/world-population/saint-lucia-population>). The main landslide trigger is rainfall, and shallow rotational landslides dominate on both steep and shallow slopes (Migoń, 2010; Anderson and Holcombe, 2013). The geology is almost entirely comprised of volcanic bedrock and deep volcanic deposits. Due to the tropical climate, these volcanic parent materials are subjected to deep weathering, which decreases their strength and increases landslide susceptibility. The strata of a typical slope cross section comprise weathered residual soils overlying decomposed rock and volcanic bedrock. These three types of strata typically correspond, respectively, to the weathering grades V–VI, III–IV, and I–II of the Hong Kong Geotechnical Engineering Office weathering grade classification (GEO, 1988). The typical cross-sectional profile modelled in CHASM is therefore discretised into three parallel layers of materials, with a layer of residual soil at the surface (layer 1), underlain by a layer of weathered material (layer 2) and then unweathered bedrock (layer 3) (see Fig. 3.5).

There is a high variability in terms of engineering soils, but they can broadly be classified as fine-grained soils such as silty clays, clayey silts, and sandy clays (DeGraff, 1985). The combination of tropical climate, steep topography, and volcanic geology renders the region particularly susceptible to rainfall-triggered landslides. Saint Lucia exhibits the highest precipitation of the year from May to December and most of the disaster events occurred in the past concentrated in this period. Furthermore, empirical evidence suggests that

landslide risk is increased by informal housing which occupies steep slopes and employs unregulated engineering practices (World Bank, 2012, p. 226-235).

### 3.2.2 Definition of the input factors and their probability distributions

CHASM+ requires information on two-dimensional slope cross-section geometry (e.g. slope angle, slope height and slope material strata – particularly depth of weathered materials and soil that are the focus of this study), soil properties (geotechnical and hydrological), boundary conditions (e.g. initial water depth), rainfall (i.e. intensity and duration) and urban properties. The variation of these input factors can have a significant impact on the calculation of the factor of safety. Uncertainties in their definition can arise from the natural variation of soils, measurement techniques, and lack of reliable information.

In this chapter, the variation of 30 input factors, characterising our case study area, are analysed. Table 3.1 reports the full list of these input factors and the probability distributions that define their range of variability, while Fig. 3.5 shows an example of a slope derived from a combination of input factors.

The parameters of the probability distributions are defined based on various sources of information. These include:

- Literature on tropical soils to define the parameters delineating the soil water retention curves. In particular, we use the parameters (and associated probability distributions) suggested by Hodnett and Tomasella (2002) for sandy clay soil. This type of soil best represents the particle size distribution of the soil samples collected across the island and rendered available by the Government of Saint Lucia in 2016, as part of a collaboration with a World Bank funded public infrastructure asset risk management project ('Vision 2030').
- Previous studies carried out by government engineers and planners, the local water company, and consultants (e.g. CHARIM, 2015; Mott MacDonald, 2013) as well as from community-based projects for the improvement of slope stability with surface water drainage works (Anderson and Holcombe, 2013). Estimates of soil strength values are based on direct shear tests of local soils undertaken by Government of Saint Lucia geotechnical engineers and consultants, now part of a prototype national soil database (Anderson and Kemp, 1985; Holcombe, 2006; Shephard et al., 2019; DIWI, 2002). Soil hydraulic conductivity measurements were also collated from previous field tests by Anderson and Kemp (1985) and Holcombe (2006). These soil mechanical and hydrological parameter values were verified against secondary data sources on similar volcanic tropical residual soils such as those in Hong Kong (Anderson, 1982; Anderson and Howes, 1985). The probability distribution of effective cohesion, effective angle of friction and hydraulic conductivity, is assumed to be lognormal. Lognormal distribution is often chosen to avoid the generation of negative values of soil parameters

(Choudhuri and Chakraborty, 2021; Griffiths et al., 2002) and it has previously been considered as the best representation for these parameters in tropical regions (Hamm et al., 2006; Bello, 2015). However, recent studies have shown that, if sufficient soil information can be compiled, it is worthwhile exploring the possibility that another distribution might give a better fit (e.g., the Weibull distribution shown in Shephard et al., 2019).

- Information about soil type (e.g. residual or weathered), soil depth, type of house construction, cut slope angles, and the management of surface run-off and wastewater on slopes was based on community-based mapping and elicitation of local expert knowledge undertaken by Anderson and Holcombe (2013), who codeveloped these datasets with community residents, government, and local experts. The soil depths are varied uniformly (no a priori knowledge), within ranges defined by minimum and maximum observed depths. Soil depths are then sampled independently from soil cohesion and slope angle, although, empirical evidence show that a correlation may exist (e.g., Patton et al., 2018; Prancevic and Lamb, 2020). The stochastic modelling can, however, identify the interactions of these variables (see, for example, Fig. C.5 in Appendix C3), as well as those combinations of soil depths, cohesion and slope gradients that lead to slope failure, which can still be used to inform local engineers about critical combinations of these factors to be recognised in the field. Cut slopes angles are varied with a normal distribution fitted to observations, but generally constrained between 39° and 89°. The maximum cut slope height equal to 4 m (based on field observations). In this analysis, we represent the maximum number of cut slopes that can accommodate a house that is 4 m wide (+1 m of surrounding space) on a slope that is 70 m long. We therefore obtain either five or six cut slopes and a corresponding number of houses on each slope depending on the angle of the cut slope. The house width and house load ( $8 \text{ kN m}^{-2}$ ) are not varied and correspond to the size and load of informal houses constructed with shallow concrete strip or block foundations, wooden walls, and sheet-metal roofing that are typically observed in Saint Lucia (Holcombe et al., 2016).

Some probability distributions are then defined based on the aim of this specific analysis, or to represent a lack of a priori knowledge of the distribution itself. In particular:

- Slope angles are varied uniformly between 20° and 45° to represent typical scenarios of informal housing on moderate and steep slopes. The highest slope angle on which a settlement can be located without some form of engineered slope stabilisation measures is considered to be 45°.
- The height of the water table is defined as an initial hydrological condition. This water table height is varied uniformly between 0% and 90% of the slope height ( $H$  in Fig. 3.5) to account for its variability

across the region and for the variability in the initial soil moisture conditions due to antecedent rainfall events.

- The ranges of rainfall intensity and durations are based on intensity-duration-frequency relationships derived for the design of the Roseau Dam in Saint Lucia (available in paper format). Engineering consultants applied Gumbel analysis of 40 years of daily rainfall data from weather stations across the island (Klohn-Crippen 1995 – Blue lines in Fig. 3.3). From these IDFs we derive a range of rainfall intensities between 0 and 200 mm h<sup>-1</sup> and a range of rainfall durations between 0 and 72 h. As suggested by Almeida et al. (2017), the variation and uncertainty of rainfall intensity and duration are represented with uniform distributions (no a priori knowledge). We then sample independently from the two uniform distributions ('bottom-up' approach). This allows generation of a wide range of rainfall intensity-duration combinations, which should ensure that any feasible future design storm in a changing climate is captured (including rainfall that might have been observed in the past - light-grey area in Fig. 3.3 - or not - dark-grey area in Fig. 3.3). Prior to the initiation of the rainfall event, we include 168 h (7 days) of simulation with rainfall intensity equal to 0. This ensures a redistribution of water moisture in the unsaturated zone of the slope and allows hydrological equilibrium with steady-state seepage to be established. A further 168 h of zero-rainfall simulation was added after the storm in order to consider the groundwater response after the rainfall event.

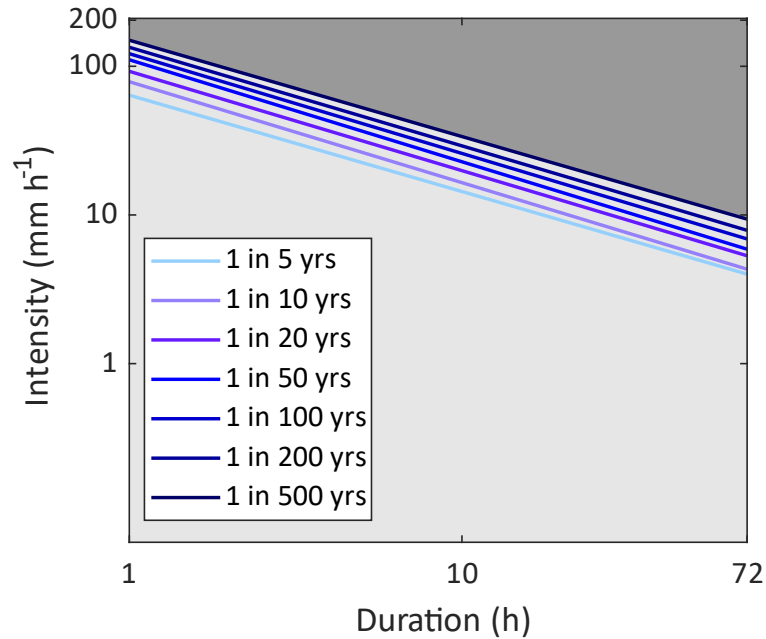


Figure 3.3: Rainfall intensity–duration–frequency (IDF) curves for Saint Lucia developed by Klohn-Crippen (1995) using Gumbel analysis of 40 years of daily rainfall data from 15 rainfall gauges. The light grey section includes rainfall events from observed data (below IDF curves); the dark grey section represents combinations of rainfall intensity-duration not recorded in the past but that might occur in the future (above IDF curves).

- Informal housing is represented by four urban properties: slope cutting, absence of roof gutters, vegetation removal, and leaking pipes and tanks. While the angle of the cut slope is varied according to its probability distribution (as previously mentioned), the vegetation, roof gutters, and water leakage are defined as present (option 1: yes) or absent (option 0: no; Fig. 3.4). When vegetation is present, it is removed on the surface of the cuts for the urban scenario. The vegetation properties used represent a tropical forest cover, here reported in Table 3.2 (the hydrological and mechanical processes of vegetation represented in CHASM are described in Section 2.2). These properties are kept fixed throughout the sampling; therefore, the effect of different types of vegetation on slope stability is not analysed. Both the tank and the pipe leakage rate are assumed to be half of  $4.2 \times 10^{-6} \text{ m}^3 \text{ s}^{-1}$ , which corresponds to the estimated leakage of 15% of the total water supply for low-income households in Saint Lucia (Anderson and Holcombe, 2013). When present, the leak is kept constant during the simulation time.

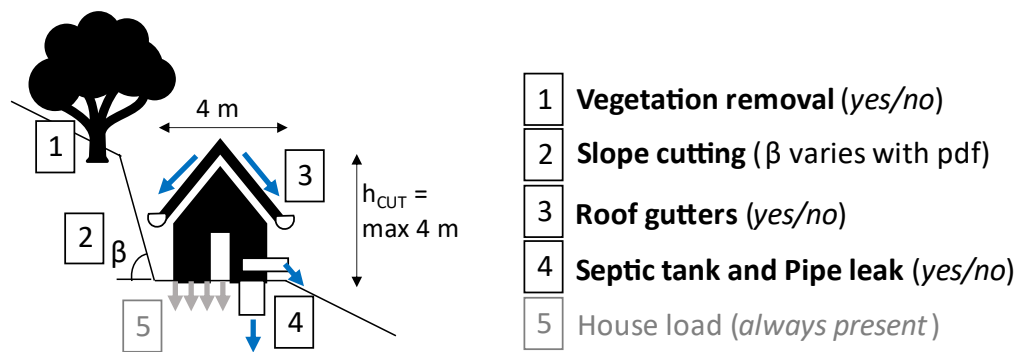


Figure 3.4: Urban properties of informal housing included in the slope stability analysis. Each house corresponds to a cut on the slope. Cut slope angle varies according to its probability distribution, defined in Table 3.1. Vegetation, roof gutters, leaking tanks/pipes are stochastically inserted or not. The house on the cut slope is always present and its load is not varied. The height of the cut slope varies relatively to the cut slope angle, but it is forced to be maximum 4 metres.

The input factors that define the discretisation of the model, such as the cell size of  $1\text{ m} \times 1\text{ m}$  and the computational time step of 60 s (both used by CHASM+'s dynamic hydrology functions), and the slip search grid location and dimensions are not varied. These values are chosen because they typically ensure numerical stability relating to the mass balance of the moisture in the domain and thus a minimum number of failed model runs. A smaller cell size would enable a more detailed representation of the slope hydrology, but it would require smaller time steps to preserve the moisture content mass balance and numerical stability. Smaller time steps would result in significantly longer simulation time. The resolution chosen is therefore a trade-off between acceptable accuracy and calculation time. The influence of the variation in these two discretisation parameters on slope stability is not explored.



Table 3.1: Input factors of CHASM+ and their probability distributions

Parameter	Symbol/Unit		Range values		
<b>Slope geometric properties:</b>					
Slope angle	$\delta$ [degrees]	U (20,45)	<b>Layer 1 *</b>	<b>Layer 2 *</b>	<b>Layer 3 *</b>
Thickness of layer	H [m]		U (1,6)	U (1,6)	
<b>Soil properties:</b>					
Effective cohesion <sup>a</sup>	c [kPa]		Ln (2.3688, 0.5698)	Ln (3.4121, 0.5774)	80
Effective friction angle <sup>b</sup>	$\phi$ [degrees]		Ln (3.2937, 0.2092)	Ln (3.1559, 0.3251)	60
Dry unit weight <sup>c</sup>	$\gamma_d$ [kN m <sup>-3</sup> ]		U (16,18)	U (18, 20)	23
Saturated moisture content <sup>d</sup>	VG $\theta_{sat}$ [m <sup>3</sup> m <sup>-3</sup> ]		N (0.413, 0.074)	N (0.413, 0.074)	N (0.413, 0.074)
Residual moisture content <sup>d</sup>	VG $\theta_{res}$ [m <sup>3</sup> m <sup>-3</sup> ]		Ln (-1.974, 0.376)	Ln (-1.974, 0.376)	Ln (-1.974, 0.376)
VG alpha parameter <sup>d</sup>	VG $\alpha$ [m <sup>-1</sup> ]		Ln (1.264, 1.076)	Ln (1.264, 1.076)	Ln (1.264, 1.076)
VG n parameters <sup>d</sup>	VG n		Ln (0.364, 0.358)	Ln (0.364, 0.358)	Ln (0.364, 0.358)
Saturated Hydraulic Conductivity	Ksat [m s <sup>-1</sup> ]		Ln (-11.055, 0.373)	Ln (-13.357, 0.373)	1xe-8
<b>Initial hydrological condition</b>					
Water table height <sup>e</sup>	DWT [%]	U (0,90)			
<b>Rainfall properties</b>					
Rain intensity	I [m h <sup>-1</sup> ]	U (0 0.2)			
Rain duration	D [h]	Ud (1 72)			
<b>Urban properties:</b>					
Cut slope angle <sup>f</sup>	$\beta$ [degrees]	N (65.18, 12.61)			
Roof gutters <sup>g</sup>	-	Ud (0 1)			
Vegetation <sup>h</sup>	-	Ud (0 1)			
Septic tank and Pipe leak <sup>i</sup>	Qt/p [m <sup>3</sup> s <sup>-1</sup> ]	Ud (0 1)			

There are 30 input factors that are stochastically varied, considering that soil properties are independently sampled for the three soil layers considered.

U = Uniform distribution; Ud = Discrete uniform; N = Normal distribution; Ln = Log-normal distribution.

\*Layer 1: Residual Soil, Weathering Grade V-VI; Layer2: Weathered material Grade III-IV; Layer3: bedrock Grade I-II; Weathering grades defined according to GEO (1988).

<sup>a</sup> Effective cohesion > 0. Effective cohesion c (layer 3) > c (layer 2) > c (layer 1).

<sup>b</sup> Effective friction angle > 0. Effective friction angle  $\phi$  (layer 3) >  $\phi$  (layer 2) >  $\phi$  (layer 1).  $\phi$  < 90 degrees

<sup>c</sup>  $\gamma_s = \gamma_d + 2$ , where  $\gamma_s$  is the saturated unit weight.  $\gamma_d$  (layer 3) >  $\gamma_d$  (layer 2) >  $\gamma_d$  (layer 1)

<sup>d</sup> Values from Hodnett and Tomasella (2002) for Sandy Clay Loam material. We impose  $n > 1$ ;  $\theta_{sat} > \theta_{res}$ ;  $\theta_{res} > 0$ .

VG: Van Genuchten parameters for defining suction moisture characteristics curve.

<sup>e</sup> Water table height is defined as a percentage of slope height measured to the toe of the slope.

<sup>f</sup> Slope of the cut forced to be between 39 and 89 degrees, and it is always greater than natural slope angle

<sup>g</sup> 0 stands for house without rain gutters; 1 stands for house with rain gutters. Roof type = double pitch

<sup>h</sup> Vegetation presence: 0 no vegetation; 1 insert vegetation in the spare spaces.

<sup>i</sup> The leak of the septic tank is equal to the leak of the pipe. When 0 is selected there is no leak, whilst with 1 there are both. The leak rate is constant and equal to 4.2e-6 m<sup>3</sup> s<sup>-1</sup>

Table 3.2: values defining the vegetation parameters for trees. The values refer to the work presented in Holcombe et al. 2016 (online Supplement, Table S5).

Parameter	Unit	Value
<b>Tree canopy parameters:</b>		
Max leaf storage	mm	5
Wet canopy evaporation	$\text{m s}^{-1}\times 10^{-7}$	2
Leaf-drip rate	% per time step	0.8
Stem portion	%	0.0012
Max trunk storage	mm	0
<b>Atmospheric parameter:</b>		
Net radiation	$\text{W m}^{-2}$	700
Average daily temperature	Degrees	30
Average daily rel. humidity	$\text{s m}^{-1}$	0.7
Canopy resistance	$\text{s m}^{-1}$	70
Soil aerodynamic resistance	$\text{s m}^{-1}$	50
Veg. aerodynamic resistance	$\text{s m}^{-1}$	40
Oxygen deficiency	m	-0.1
Pressure head Constant	m	-0.35
sink terms Constant	m	-5
Wilting point	m	-14
<b>Tree/grass parameters:</b>		<b>Trees</b>
Surcharge	$\text{kN m}^{-2}$	2
Leaf area index	$\text{m}^2 \text{m}^{-2}$	10
Canopy cover	%	0.8
Rooting depth	m	4
Max transpiration	$\text{m s}^{-1}\times 10^{-7}$	2
Root tensile strength	MPa	50
Root area ratio	$\text{m}^2 \text{m}^{-2}$	0.002

### 3.2.3 Creation of synthetic combinations of input factors and model simulation

We use Latin hypercube sampling (McKay et al., 1979) to generate 10,000 different combinations of the 30 independently varying input factors shown in Table 3.1. Figure 3.5 illustrates one example of a slope defined by a single combination of these input factors. Due to the randomness of the process, checks are undertaken to ensure that realistic combinations of factors are generated; if not, they are discarded and replaced by another randomly generated, feasible combination. These ‘feasibility’ checks are reported in the footnote of Table 3.1 (letters a–f). The stochastically generated simulations are then run in CHASM+ using the high-performance computer at the University of Bristol. The outputs considered for each simulation are the minimum factor of safety (FoS) and the slip surface where the minimum FoS is calculated. We divide the completed simulations according to whether the minimum FoS is less than 1 (slope predicted to have failed, i.e. a landslide) or greater than 1 (slope is predicted stable). We exclude the simulations predicting that the slope is failed before the start of the rainfall event, which represents inherently unstable slopes (for example steep slopes with deep soil thickness). We repeat the same procedure with and without including the urban properties. We therefore obtain two sets of model outputs: 10,000 representing urbanised slopes and 10,000 representing non-urbanised slopes.

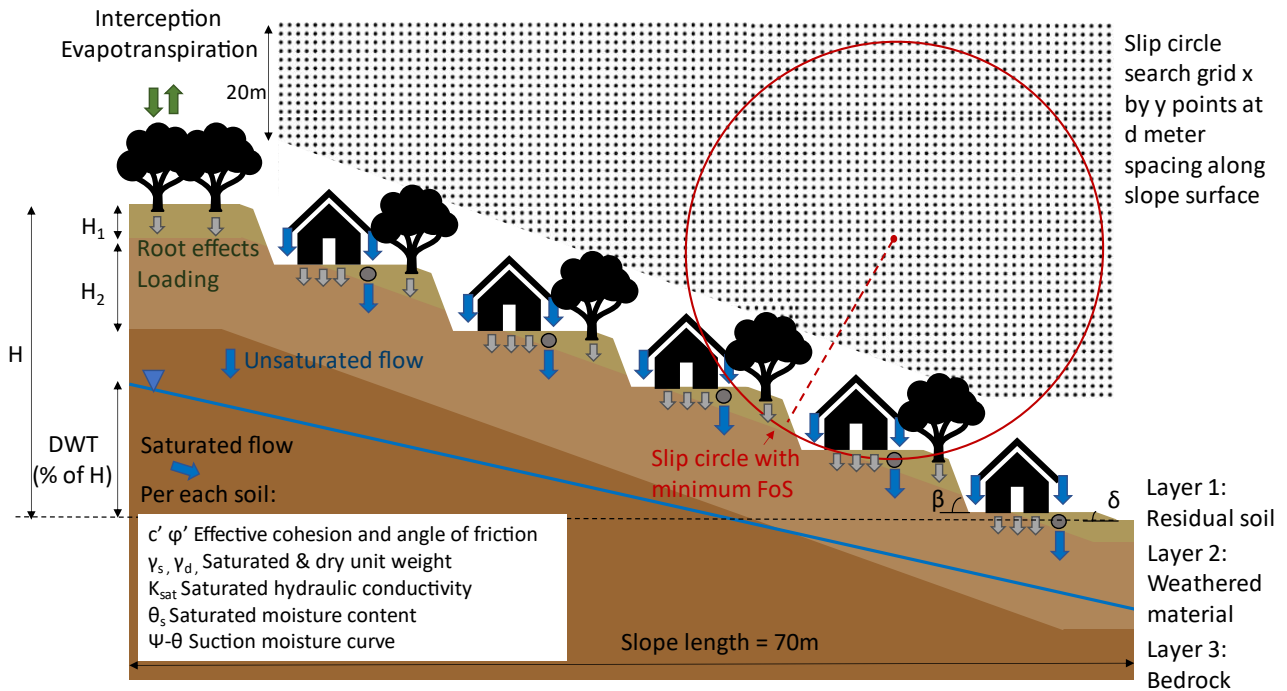


Figure 3.5: Example of slope generated by stochastically sampling from the ranges of input factors specified in Table 3.1.  $H$  is the slope height resulting from the fixed slope length and varying slope angles. The dimensions of the slip circle search grid are fixed, with initial height of 20 m, and width equal to the slope length. The grid extends downslope parallel to the slope as shown.

### 3.3 Results

In this section we analyse the  $10,000 \times 2$  outputs generated by CHASM+ for the urbanised and non-urbanised slope scenarios. As previously mentioned, we split the simulations into stable and failed according to the value of the minimum FoS (respectively, greater or less than 1). As a first analysis we compare the percentage of failed slopes against stable slopes for each of the urban properties. Figure 3.6 shows that the presence of cut slopes significantly influences the percentage of predicted slope failures: the steeper the cut slope angle, the higher the percentage of failed slopes. Vegetation removal and roof gutters instead have a negligible role in dividing the two sets. Last, septic tanks and leaking pipes have some effect, generating about 10% more failed slopes when present.

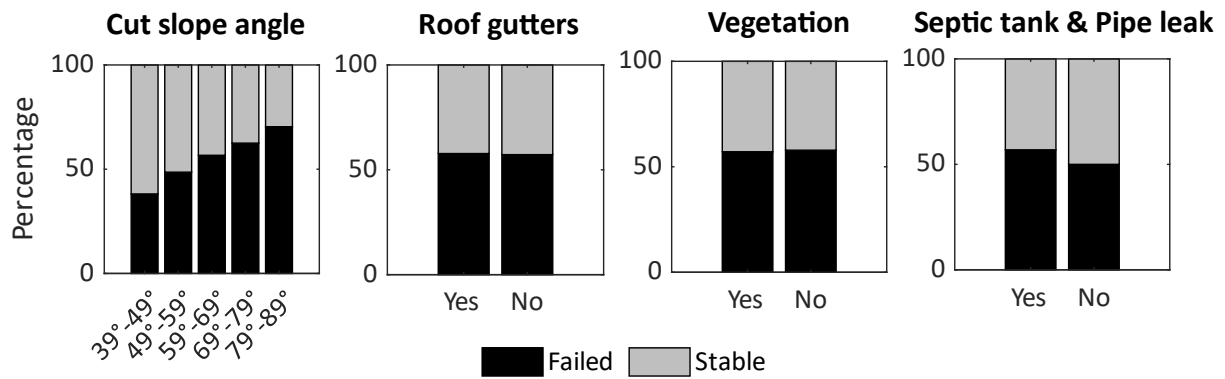


Figure 3.6: Percentage of predicted stable and failed slopes per each urban property. An urban property will be influencing slope stability if the percentage of the predicted failures changes with the variation of that urban property.

### 3.3.1 Regional sensitivity analysis

We then perform RSA on both sets of urbanised and non-urbanised slope simulations, calculating the cumulative marginal distributions of the failed and stable simulations for each input factor. The maximum distance between the two distributions (KS statistic) is computed and used as a sensitivity index (see Chapter 2, Section 2.3.1). A high value of the sensitivity index suggests that the variation in that input factor significantly influences slope stability. The results are shown in Fig. 3.7 for both urbanised and non-urbanised slopes. Figure 3.7 shows that slope stability is insensitive to many input factors and highly sensitive to few, namely effective cohesion and thickness of layer 1 (residual soil), slope angle, and rain intensity and duration. These sensitive input factors represent the main landslide drivers. The sensitivity indices of the urban properties (in orange) are consistent with the findings of Fig. 3.6, where only the variation in cut slope angle influences slope stability. Remarkably, the influence of the cut slope angle is comparable to other slope and climate properties, such as the thickness of layer 1 and the rainfall duration. When looking at the comparison between urbanised and non-urbanised slopes, it appears that the urban presence decreases the sensitivity indices of all the input factors, except for the effective cohesion of layer 1 and the rainfall intensity.

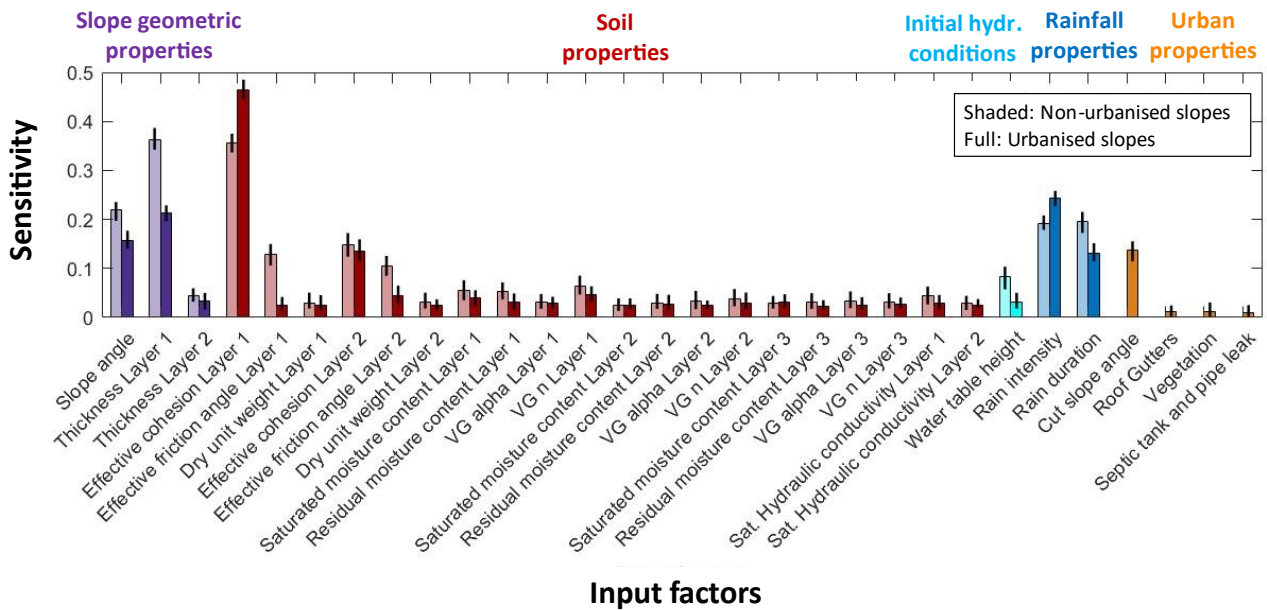


Figure 3.7: Sensitivity index for each input factor in the urbanised (full colour) and not urbanised (pale colour) cases. The bars correspond to the mean value of sensitivity for each input factor calculated with bootstrapping, while the black vertical lines at the top of the bars represent the confidence interval (Number of bootstrap resampling  $N = 100$ ; significance level for the confidence intervals 0.05).

We further explore the change in sensitivity caused by urbanisation by plotting the percentage of failed slopes for the main landslide drivers (Fig. 3.8). The figure shows how this percentage varies for the urbanised (full colour bars and lines) and non-urbanised cases (pale colour bars and lines). In general, urbanised slopes produce more failures than non-urbanised slopes, though they both display similar trends: an increased percentage of predicted landslides when we would expect the slope to become more susceptible (e.g. when slope angles are higher) or the trigger more severe (i.e. when rainfall intensity and duration are larger). For example, in Fig. 3.8b the percentage of failed slopes in the non-urbanised case linearly increases from ~5% (for soil thickness 1–2 m) to ~50% (thickness of 5–6 m). In the same figure, urbanised slopes show higher failure rates for all values, though the greatest increase occurs for soil thicknesses less than 4 m (up to +46% for the 2–3 m category). This means that the most significant increase in number of landslides occurs for thin soil thicknesses, i.e. on slopes less susceptible to failure when non-urbanised. The same can be said for slope angles less than  $25^\circ$  and rainfall duration less than 10 h, where percentages of slope failures pass from less than 15% to more than 40% when urbanisation is introduced (Fig. 3.8a and c). In the lower plots instead, more urban landslides are observed on slopes that show high percentage of failures also when urbanisation is not present (+43% for low values of soil cohesion; Fig. 3.8d; +35% for high rainfall intensities; Fig. 3.8e). The difference in failure rates with variations in input factors also explains the change in sensitivity found in Fig. 3.7: when urbanised, a slope's response varies less (less sensitive) to variations in the input factors in the

upper plots (whose sensitivity indices get smaller) and more (more sensitive) to variations in the input factors of the lower plots (whose sensitivity indices get larger).

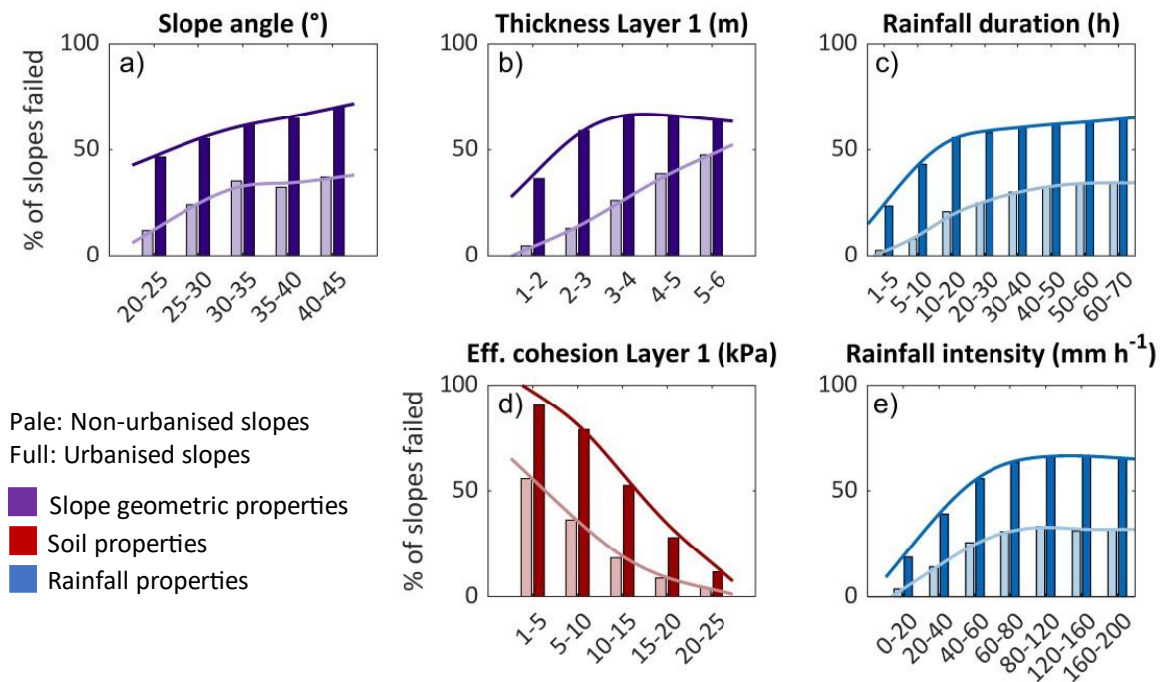


Figure 3.8: Percentage of slope failures for urbanised and non-urbanised slopes for different categories of input factors. Throughout, urbanised slopes show higher failure rates than non-urbanised slopes. In the upper plots (a), (b), (c), the distribution of failure rates for urbanised slopes are more uniform for variations of input factors than the non-urbanised case, while in the lower plots (d), (e), it is more pronounced. Panels (a-c) represent the input factors whose sensitivity indices are smaller when urbanisation is introduced in Fig. 3.7, while the (d-e) show the input factors whose sensitivity gets larger when urbanisation is introduced in Fig. 3.7.

### 3.3.2 CART analysis

We use the CART analysis to formalise the critical thresholds of input factors above or below which slopes are most likely to be predicted as stable or failed. Figure 3.9 represents the two trees for the non-urbanised (Fig. 3.9a) and urbanised case (Fig. 3.9b). As expected, the best predictors selected in CART are the same input factors previously identified as most influential (Fig. 3.7). The boxes with double colour represent the auxiliary variables that combine correlated input factors: the ratio between effective cohesion and thickness of layer 1 to account for their counterbalancing effect on slope stability (i.e. slope with more cohesive soil can be thicker without experiencing failure); the negative ratio between the logarithm of rainfall intensity and rainfall duration, which represent the slope of the rainfall threshold for triggering landslides; and the weighted average of the natural and the cut slope angles to account for the fact that slope susceptibility can significantly increase for low natural slope angles but high cut slopes angles (see Appendix B1 for details about the auxiliary variables and the change in the model's performance when they are not considered).

Using these few predictors, both trees correctly classify more than 85% of the simulations as stable or failed (details about the pruning in Appendix B2). Each branch of the tree shows the paths and thresholds of input factors that lead to slopes most likely to fail (black branch) or most likely to not fail (grey branch). At the end of each branch the black and grey bar shows the fraction of failed and stable simulations, while the thickness of the branch is proportional to the number of simulations following that path. For example, in the tree resulting from non-urbanised slopes (left-hand side), the thickest grey line shows that more than 50% of simulated slopes were stable 91.2% of the time for cohesion/thickness of layer 1 ratios greater than  $2.5 \text{ kPa m}^{-1}$ . The thick black branch instead shows that the greatest proportion of simulations predicted as failed occurred for cohesion/thickness of layer 1 ratios less than  $2.5 \text{ kPa m}^{-1}$ , rainfall intensity duration ratios ( $-\log(I)/\log(D)$ ) greater than  $0.9 \text{ m h}^{-2}$ , and slope angles greater than  $25^\circ$ .

In the trees resulting from non-urbanised slopes (right hand side), the black branch leading to the majority of failures is similar to the non-urbanised tree, but it presents higher splitting thresholds: from the top, the split happens for cohesion/thickness of layer 1 ratios less than 4.9 (instead of 2.5) and for a rainfall intensity/duration ratio of 1.06 (instead of 0.9). The branch then leads to the majority of failures for values of effective cohesion of layer 1 less than 12.6 kPa, regardless of the natural slope angle. A higher threshold in cohesion/thickness ratios indicates that when urbanisation is present, more failures occur on slopes with higher soil cohesion and/or thinner soil layers than non-urbanised slopes (compatible with Fig. 3.8b and d), while higher rainfall intensity duration ratios suggest that more failures occur for higher rainfall intensity and/or lower rainfall durations when compared to non-urbanised slopes (as shown in Fig. 3.8c and e). Finally, going back to the top and looking at the thick grey branch of the urbanised tree, it can be noted that a ratio between the effective cohesion and the thickness of layer 1 greater than 4.9 ensured 95% of slope stability only when the weighted slope angle is less than  $48^\circ$ .

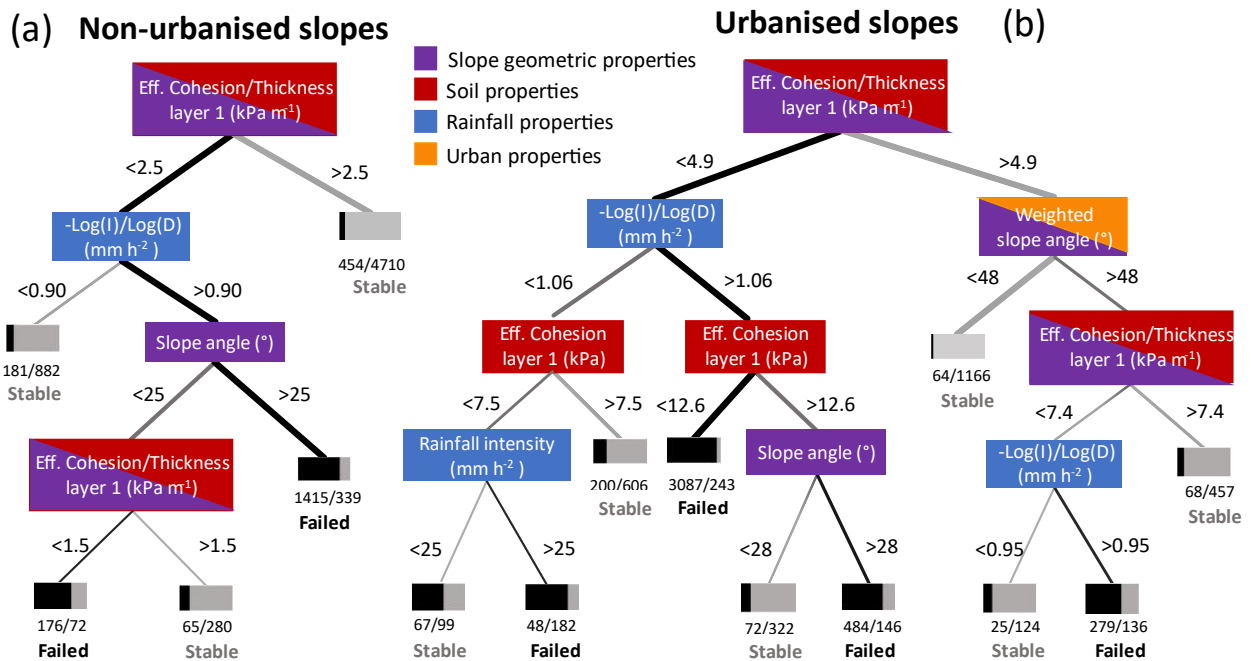


Figure 3.9: Classification tree of slope response for non-urbanised slopes (a) and urbanised slopes (b). Black branches represent the paths that lead to simulations predicted as failed, while grey branches lead to simulations predicted as stable. The bar under each leaf shows the proportion of simulations that resulted as failed (black) or stable (grey) for that leaf. The thickness of the branch is proportional to the number of simulations following that path. Note as 14% and 22% of the simulated slopes have been excluded respectively for the non-urbanised and urbanised case, because failed before the start of the precipitation.

### 3.4 Discussion

#### 3.4.1 Slope cutting is the urban construction activity most detrimental to slope stability

In this analysis, slope cutting is the urban construction activity with the strongest effect on slope stability's response (Figs. 3.6 and 3.7). Figure 3.8 indicates that when urbanisation is present, more slope failures are observed, mainly on slopes with relatively low slope angles and with low values of both soil (layer 1) thickness and cohesion (Fig. 3.8a, b and d; also reflected by higher effective cohesion/thickness ratios in CART in Fig. 3.9b). This is interpreted as being caused by cut slopes: when cut slope angles are steep, a higher effective cohesion and thus a higher soil strength are required to maintain stability, regardless of the natural slope angles; when soil layers intersect the cuts, relatively high values of soil strength are not sufficient to ensure slope stability even on thin – and therefore less landslide-prone – soil layers. The interaction between the depth of soil layer 1 and the cut slope geometry is deduced from Fig. 3.8b: almost 50% more failures are observed for a thickness of layer 1 smaller than the slope's height (4 m), i.e. when the interface of soil (layer 1) and weathered material (layer 2) outcrops in the cut slope face (as illustrated in Fig. 3.5). For these



slopes, visual inspection reveals that the slip surface is generally located between layer 1 (residual soil, weathering grade V–VI) and layer 2 (weathered material, grade III–IV). This is explained by the different soil strength of the two layers, which constrains the slip surface within the weaker layer 1, and the different hydraulic conductivities. As rainfall infiltrates, the lower hydraulic conductivity of the underlying weathered material leads to a progressive accumulation of water, promoting a perched water table. The raised pore water pressure decreases the effective soil strength and consequently the stability of the soil layer. Part of the increase in pore water pressure might be caused by the presence of water leakages at the top of the cut slope. However, the low sensitivity of the slope response to leakage (Fig. 3.7) does not allow for more considerations.

Slope cutting is therefore considered in this analysis to be the practice most detrimental to slope stability. This result is consistent with studies carried out in the humid tropics at regional scales, for which slope cutting was identified as one of the major causes of landslides (e.g. Brand et al., 1984; Froude and Petley, 2018; Holcombe et al., 2016). Cuts with slope angles greater than 60° are also considered to be at particularly high risk (e.g. Cheng, 2009), while excess of pore water pressure was shown to be a dominant process in triggering shallow failures on cut slopes (Anderson, 1983). CHASM+ therefore successfully captures these physical mechanisms, confirming, despite the uncertainties, the governing role of soil properties and soil thickness in determining slope equilibrium. The other urban construction activities considered seem to have a less significant role on landslide hazard. Previous studies found that vegetation can be both beneficial and detrimental to slope stability (So, 1971; Collison et al., 1995). Here we find that its effect is negligible, probably due to its limited presence in urbanised slopes (trees are left at the crest of each cut slope, where they add loading and may actually be detrimental to the local cut slope stability – see Fig. 3.5). Also, adding roof gutters does not seem to decrease the number of failed slopes. However, in the scenarios generated here we have only reached a maximum of 30% slope coverage by houses, i.e. about 30% of impervious surface (five to six households on 70 m slope) due to our inclusion of cut slopes for every house. Evidence shows that roof guttering effectiveness becomes evident only when the house coverage is above 50%, and thus a considerable portion of rain does not infiltrate into the slope (Anderson and Holcombe, 2013). On the other hand, leaks from septic tanks and pipes lead to 10% more failures despite the low house coverage. When higher house densities are considered, the lack of water management might become even more significant (Di Martire et al., 2012).

### 3.4.2 The rainfall threshold for triggering landslides is lower when informal housing is included

We found that when slopes are urbanised, the most significant increase in the percentage of failed slopes

occurs for rainstorm events with high intensity ( $>20 \text{ mm h}^{-1}$ ) and low duration ( $<20 \text{ h}$ ; Fig. 3.8c and e). Accordingly, our CART analysis identifies a higher threshold of rainfall intensity/duration ratio to divide the stable and failed slopes in the urbanised case (Fig. 3.9b). In landslide analysis, so-called minimum rainfall thresholds are defined as the combinations of rainfall intensity (I) and duration (D) above which we would expect landslides to start occurring. These thresholds are generally expressed by a power law relationship  $I = \gamma D^\alpha$  (Guzzetti et al., 2007) and they are constructed based on inventories of observed landslides and the rainfall that triggered them (e.g. Caine, 1980; Larsen and Simon, 1993). Many countries in the humid tropics have limited empirical data on landslides, and therefore it would be useful to be able to generate such thresholds from stochastic analyses of the type we performed here. To demonstrate how this could be done, we applied a multi-objective optimisation method to our sample of stochastically generated slopes (details about our approach in Appendix B3). We do not use the more commonly employed frequentist methods (Melillo et al., 2018; Brunetti et al., 2010) because the high frequency of failed slopes for high-intensity and long-duration events would strongly bias the position of the threshold. Figure 3.10a and b show the calculated thresholds on a log-log scale, respectively, for the non-urbanised and urbanised case (red lines). In both cases, 99.9% of the failed simulations fall above them. The thresholds present the typical descending trend found in empirical analysis, for which lower rainfall intensities are needed to trigger a landslide when rainfall durations increase. The fact that this trend can be replicated by our synthetic simulations indicates that CHASM+ and our stochastic modelling framework are giving realistic hydrological and stability responses to the rainfall forcing.

The higher the intensity and/or the duration of the rainfall event is, the more slope failures will occur in both cases. However, when informal housing is present, more failures are observed for rainfall durations less than 10 h (short events; Larsen and Simon, 1993). This pushes down the intercept of the rainfall threshold, as reflected in the change in the coefficients of the power law equations (reported in each figure). The slope of the threshold line (i.e. the exponent of the power law) is also steeper in the urbanised case, implying the presence of more failures for lower rainfall intensities throughout the duration axis. These results are compatible with the increase in small-scale landslides previously commented (failure depths less than cut slope's height): to reach saturation at shallow depths, relatively low rainfall intensities and durations can be sufficient to initiate slope failure. Figure 3.10c confirms this assumption: when slopes are urbanised (black dots), failures tend to occur with a smaller radius of slip surface and for higher values of intensity/duration ratio. The findings reflect the empirical evidence in low-income communities which report a high frequency of small-scale landslides, particularly associated with cut slopes, for high-intensity and short-duration events ('the everyday disasters'; Bull-Kamanga et al., 2003). Finally, we compare our results with the empirical rainfall threshold proposed by Larsen and Simon (1993) for Puerto Rico, which is based on landslide inventories that also include failures observed on slopes modified by construction activities (mainly slope

cuts for road network; see Larsen and Parks, 1997). When informal urbanisation is considered, the two thresholds are almost overlapping (Fig. 3.10b). This reinforces both the potential of using mechanistic models within a stochastic framework to generate synthetic thresholds in data-scarce locations and the possibility of using the resulting thresholds for regions of the humid tropics with similar geophysical, climatic, and urban properties.

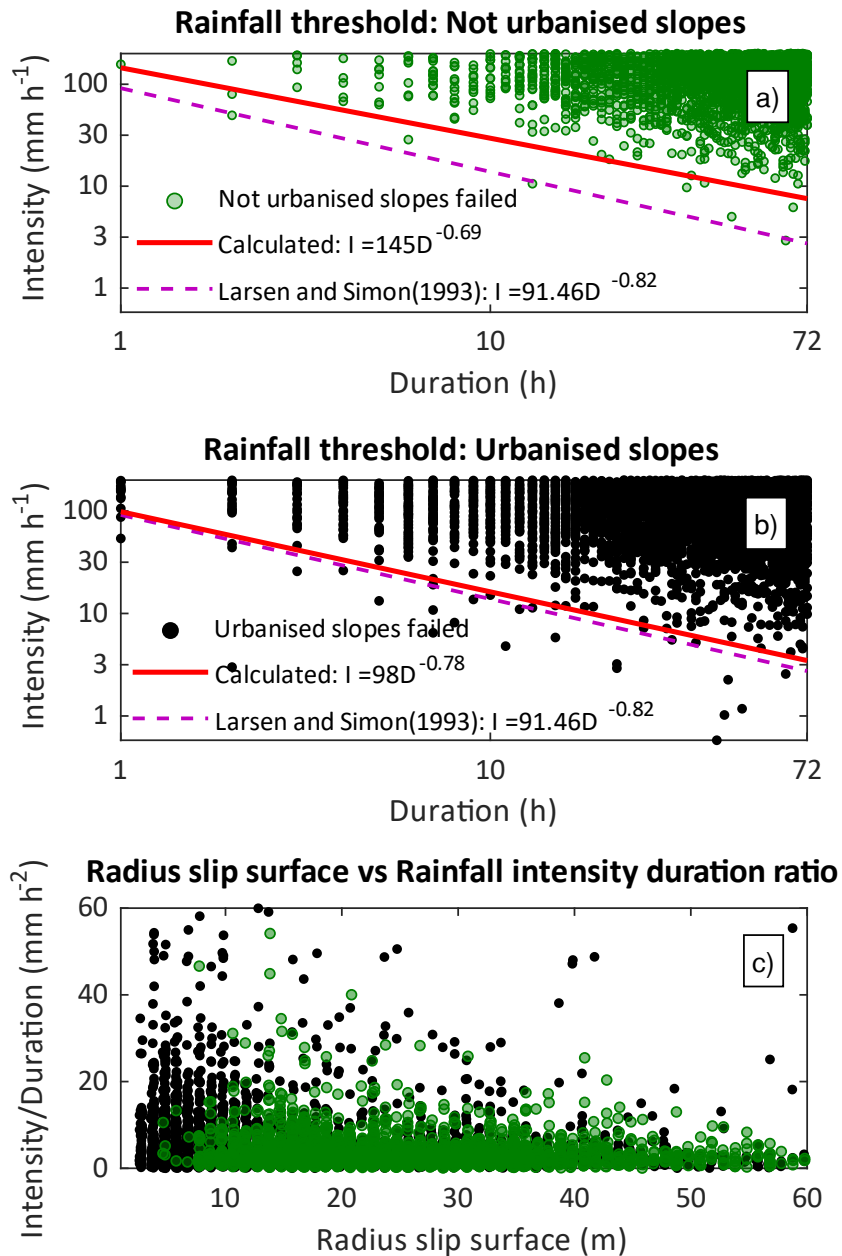


Figure 3.10: In figure (a) and (b) the red line represent the minimum rainfall thresholds calculated from our stochastic sample (99.9% of the failed slopes in the sample are above the thresholds). Figure (c) represents the radius of the slip surfaces of the recorded landslides plotted against the corresponding triggering rainfall intensity/duration ratio. Note as in (a) and (b) the x and y axis are in logarithmic base 10 scale, but the notation is linear for an easier readability.

### 3.4.3 Guidelines for landslide mitigation actions to tackle the main instability drivers

The identification of the main instability drivers and their thresholds can contribute to create objective rules to classify slopes as hazardous in a region with data scarcity. For example, in Saint Lucia our analysis suggests that slopes with effective cohesion less than 12 kPa and thickness more than 2.5 m (effective cohesion/thickness of layer 1  $< 4.9$ ) in layer 1 are particularly at risk for rainfall events with intensity/duration ratios greater than  $1.06 \text{ m h}^{-2}$  (Fig. 3.9b). These rules can shape look-up tables or priority ranking to classify human-made slopes as dangerous (Anderson and Lloyd, 1991; Cheng, 2009). Figure 3.7 shows that only few input factors particularly influence slope stability with or without urbanisation. These are effective cohesion and thickness of the layer 1 (residual soil), natural slope angles, and rain intensity and duration. The crucial role of these factors in regulating slope stability is broadly recognised (van Westen et al., 2006; Guzzetti et al., 2007a). The results presented here demonstrate how the influence of these instability drivers can be ranked and quantified. The other input factors might have a smaller direct or indirect effect, but they are not dominant. This is an expected finding in global sensitivity analysis (Wagener and Pianosi, 2019), even if different outputs (e.g. the timing of the failure) might be sensitive to different input factors (e.g. variations in the moisture suction curves, as demonstrated in Chapter 2, Section 2.4.2 for a urban landslide with fixed properties). The identification of these main landslide drivers helps to address data acquisition efforts, while the comparison between urbanised and non-urbanised simulations quantifies the different relative role (e.g. weight) of preparatory factors in landslide susceptibility assessment when informal urbanisation is present. For example, a weighted average of natural and cut slope angle can be used to identify areas (not) at risk.

All the results presented are subjected to the assumptions made in our study. The large variation in some of the input factors can lead to overestimating the hazard. Almeida et al. (2017), for example, varied the slope angles between  $27^\circ$  and  $30^\circ$  (instead of between  $20^\circ$  and  $45^\circ$ ) and hence found a lower value of the cohesion/thickness ratio to separate stable and failed slopes than we found (in the non-urbanised case). Data acquisition can help to reduce these uncertainties. However, when data are not available, our approach allows for the identification of so-called 'low regrets' mitigation measures, i.e. actions that have a positive impact on slope stability regardless of the uncertain factors. According to our analysis, the most effective action would be avoiding or well designing slope cutting since it was shown to be the urban construction activity most detrimental to slope stability. However, this is of scarce utility since informal housing often outstrips urban planning and regulations (Fekade, 2000). Better hazard awareness and construction practices should therefore be suggested. These include for example reducing surface water infiltration on slopes, especially when the topsoil layers intersect the cut slope, and the resulting perched water tables reduce

shear strength in a critical location. Slope surface and subsurface drainage can be designed to reduce the infiltration of rainwater to a level that, in effect, reduces the total rainfall intensity below the rainfall threshold calculated. Another cost-effective landslide mitigation strategy can be the planting of deep-rooting grasses, shrubs, or small trees, which increases slope strength (e.g. soil cohesion) in the top couple of metres of soil and also reduces soil moisture content through root water uptake and evapotranspiration (Holcombe et al., 2016; Ng et al., 2011; Wilkinson et al., 2002b).

Finally, Fig. 3.10b shows that when slopes are urbanised, high-intensity short-duration rainfall events lead to an increased number of small-scale landslides (failure depths less than 4 m; Fig. 3.8b; and radius of slip failure less than 10 m; Fig. 3.10c). Future climate change could potentially increase the frequency of intense precipitation events (e.g. O’Gorman and Schneider, 2009) and therefore the occurrence of these types of landslides in informal communities. However, if small-scale failures produced by anthropogenic factors are neglected in the calculation of rainfall thresholds, current rainstorms events could also be excluded as triggering factors (Crozier, 2010; Mendes et al., 2018). Small-scale, high-frequency landslide events might not lead to major disasters, but they are increasingly seen as indicators of risk accumulation, detrimental to disaster resilience and economic development (Bull-Kamanga et al., 2003). For this reason, these types of landslides deserve greater attention from the scientific community.

### 3.5 Conclusions

This chapter shows how the methodology developed in this thesis can be applied to quantify the influence of informal housing on landslide probability. The stability of slopes with different geometrical, soil and urban properties under a wide range of rainstorm conditions (including climate change) is evaluated. Then, we investigate: which are the urban construction activity most detrimental for slope stability and how their uncertainty compare to the uncertainty of the other environmental properties; how the natural slope susceptibility to failure (i.e. spatial probability) and the rainstorm conditions to trigger landslide (i.e., temporal probability) change, once informal housing is included; and how such mechanistic based evidence can inform landslide mitigation strategies and future urban practices. The analysis demonstrates that informal housing increases landslide hazard and that slope cutting is the most detrimental construction activity when compared to vegetation removal, lack of roof gutters, and presence of water leaks. Furthermore, the influence of cut slope angle on slope stability, is comparable to other slope and climate properties (the thickness of layer 1 and the rainfall duration). The presence of informal housing modifies the relative role that natural slope angle, soil cohesion, and soil thickness have in maintaining stable slopes, with increased hazard occurrence for low values of these three main landslide drivers (e.g. on slopes with angle less than 25°). The critical rainfall thresholds at which slope failure is predicted to occur are evaluated. The

rainfall threshold is lower when informal housing is present, with an increased number of small-scale landslides (+85%, with failure depth less than 4 m and radius of slip surface less than 10 m) for high-intensity and short-duration events. The rainfall threshold associated with the urbanised slopes is comparable to the one proposed by Larsen and Simon (1993) for the region of Puerto Rico, suggesting its potential validity also for other similar (data-scarce) regions of the humid tropics. Finally, the CART analysis identifies the thresholds of input factors separating stable and unstable slopes (e.g., slopes with effective cohesion less than 12 kPa and thickness less than 2.5 m have a high probability of failure). These thresholds can be used as objective criteria for guiding local engineers in identifying slopes at risk, deducing landslide mitigation actions, and targeting data acquisition to reduce model prediction uncertainty.

Future work might seek to vary the properties that were kept constant in this study, such as the degree of urbanisation and house dimensions, to evaluate their significance for slope stability. This might confirm the importance of household water management such as roof guttering and leaking water supply pipes and septic tanks when the number of households is increased. Analysis of slopes where slope cutting is replaced by other possible construction techniques (such as houses suspended on pile foundations) can identify whether the construction of future hillside settlements could be done in a manner less detrimental to slope stability. Different bioengineering techniques to mitigate hazard likelihood could also be modelled and their effectiveness evaluated.

## Chapter 4 : Mapping landslide hazard in a data scarce region under changing urbanisation and climate

This chapter is adapted from a paper in preparation that has been partially modified to improve the consistency throughout the thesis:

*Bozzolan, E., Holcombe, E., Pianosi, F., Wagener, T., Marchesini I., and Alvioli M.: Mapping landslide hazard in a data scarce region underchanging urbanisation and climate*

## 4.1 Introduction

This chapter extends the spatial scale of the analysis, considering all slopes in Saint Lucia. The aim is to quantify the change in landslide rates under different climate and land cover scenarios, and then spatially distribute the results at regional (island-wide) scale. This chapter, therefore, addresses the third research question:

- 3) How can we incorporate the understanding of slope stability gained at the hillslope scale, into regional landslide probability maps under changing urban expansion and rainfall conditions?

The generated maps are particularly novel because they include both land cover and climate change, which are generally analysed separately. As introduced in Chapter 1, this research gap can be explained by a lack of models capable of representing hydrological slope dynamics, vegetation, and urbanisation, as well as a lack of methodologies that deal with the large uncertainty that such analysis involves. Source of uncertainties can relate to (i) the inherent variability and/or errors in the measurement of the input parameters used in the slope stability modelling (i.e. aleatory uncertainties – such as soil properties or landslide inventories, Cho et al. 2007; Steger et al., 2017); or to (ii) a lack of knowledge, such as future climate trends (i.e. epistemic uncertainties; Beven et al. 2018).

Critically, the approach most commonly adopted (Gariano and Guzzetti, 2016) to include future climate projections on landslide hazard assessment extrapolates rainfall projections from downscaled global climate scenarios based on general circulation models (GCMs) (previously defined as 'top-down' approaches - Buma and Dehn, 2000; Ciabatta et al., 2016; Melchiorre and Frattini, 2012). The deep, epistemic uncertainties of GCMs predictions (discussed in Chapter 1) can lead to highly uncertain impacts of climate change on landslide hazard with a wide range of (sometimes contrasting) feasible outcomes (Melchiorre and Frattini, 2012; Ciabatta et al. 2016). GCMs projections are thus analysed without involving further uncertainties introduced by land cover change in the attempt to obtain more unequivocal slope stability response. However, in the few analyses where both future land cover and climate change are included, their combined effect has resulted in a larger change in landslide frequency than when considered separately (van Beek, 2002).

A quantitative analysis of the joint effects of land cover change (from deforestation to informal housing, in the case of this research) and climate change (rainfall) is therefore necessary for more robust predictions of future landslide hazards. This chapter addresses this type of analysis, using the methodology reported in Chapter 2, which bypasses the uncertainty introduced by the 'top-down' modelling chain, such as the choice of the green gas emission scenario, GCMs and downscaling technique, by using a bottom-up approach. As in the previous chapter, a wide range of observed and unobserved rainfall intensity-durations combinations are



stochastically generated (via MC sampling) and used to force the slope stability analysis. Slope geometrical, soil geotechnical and hydrological properties are also varied according to their probability distributions (defined in Section 3.2.2) to account for the aleatory uncertainties. Such procedure is repeated four times, each time including one dominant land cover of the study area: forest, shrub, bare and informal urbanisation. With the exception of cut slope angle and the urban density which are varied according to a probability distribution, all urban (pipe and tank leakage, and house roof gutters) and vegetation (root depth, evapotranspiration rate etc.) properties are considered fixed (e.g., pipe leakage are present or absent, but the leakage rate is not varied; vegetation is present or absent, but the root properties are not varied). This simplification (urban and vegetation properties clearly vary across Saint Lucia) facilitates the comparison of slope stability response between land covers (e.g. if the root depth is fixed, it is easier to understand its relative influence on slope stability at variations of soil depth).

The stability of the slopes of each land cover group is evaluated with CHASM+. Each slope is associated with the predicted minimum factor of safety (FoS); a Global Sensitivity Analysis (GSA) is then applied to identify the input factors that, by varying, most influence the slope stability response. To spatially distribute the CHASM+ predictions, the simulated 2D cross-sectional slopes need then to be linked to 3D mapping units. This is not a trivial task (Van Westen et al. 1997). Here, we show how this can be done by attributing only the subset of input factors found to most influence slope stability in the GSA (e.g. slope angle), to slope units (SUs), a type of mapping units that we automatically delineated using an open-source software (Alvioli et al., 2016; Alvioli et al., 2020).

The goodness of such assumption is evaluated by comparing the landslide probability maps generated for the Hurricane Tomas (2010) to the landslide records obtained after that event (and also the only one available with a significant number of records for the same rainstorm event). Finally, we generate several landslide probability maps for different rainstorm severity and under extended deforestation and informal urbanisation expansion (both recognised as the biggest contributors to risk from losses in Saint Lucia - World Bank, 2012, p. 226-235), in order to assess the joint impact of land cover and climate change on landslide probability. The chapter therefore builds upon the following three sub-questions:

- 3a) Which input factors (e.g. soil or climate properties) most influence landslide hazard at regional scale?
- 3b) How can we create regional hazard maps that account for both land cover and climate change, based on these influential input factors?
- 3c) How does the combined effect of land cover and climate change impact the frequency of landslides?

The core of the methodology used for this analysis is the one illustrated in Chapter 2. However, there are some additional pre- and post- processing steps for generating the model input factors and for creating the link with the GIS mapping. These steps are described in the next section.

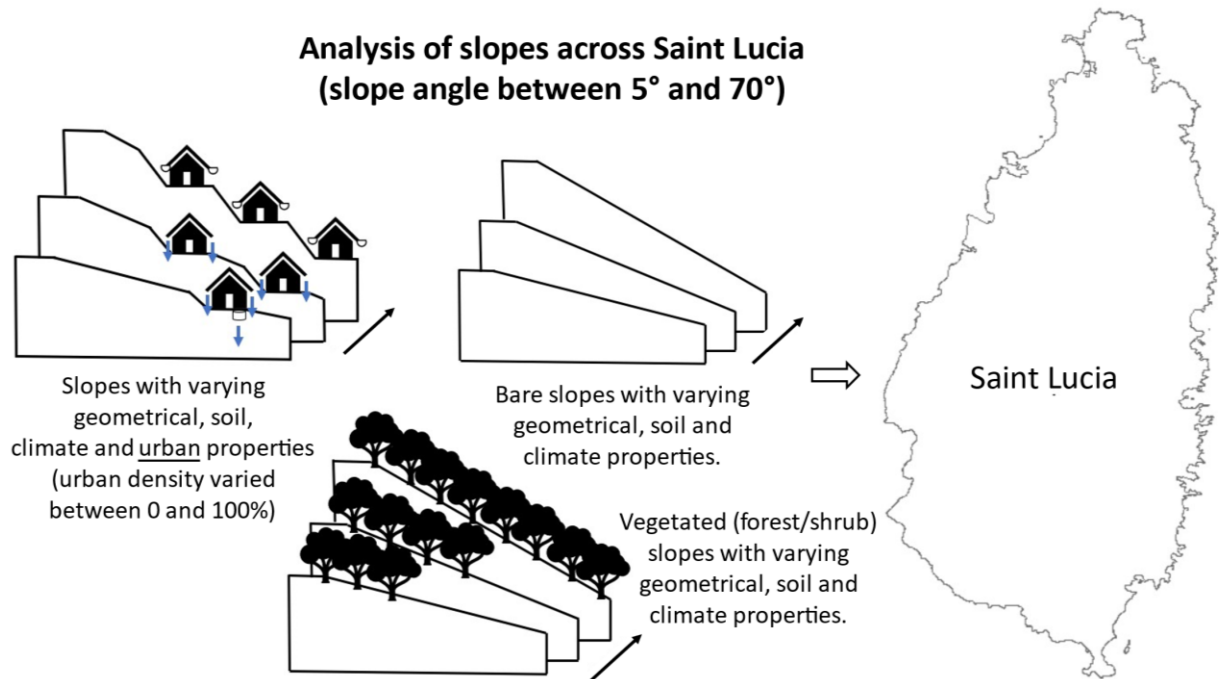


Figure 4.1: Slopes stochastically generated for the analysis of this chapter to compute regional hazard maps for Saint Lucia.

## 4.2 Method workflow and components needed

Figure 4.2 shows the main workflow of the analysis reported in this chapter.

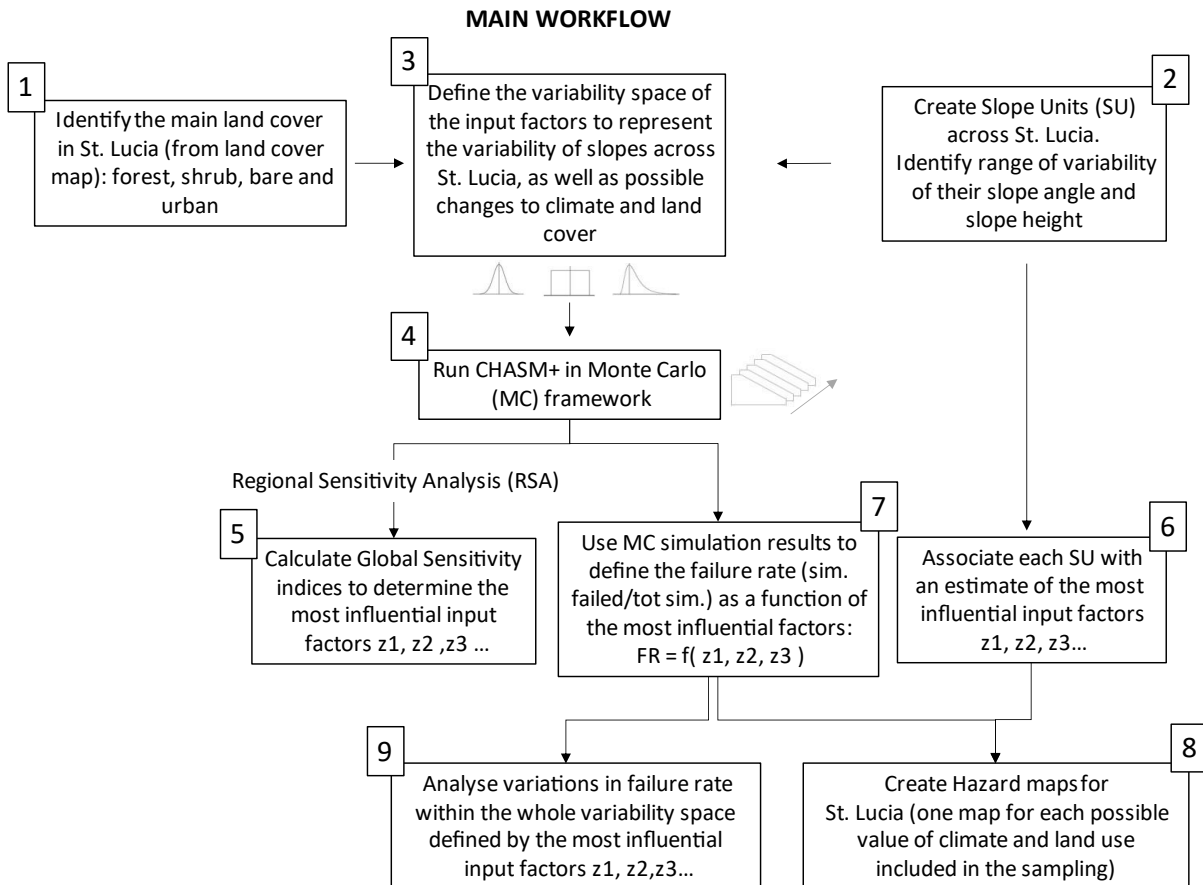


Figure 4.2: scheme of the main workflow of Chapter 4.

Specifically, the method entails the following steps:

- 1) Identify the predominant land cover types across the Saint Lucia island (e.g. forest, bare etc...) (described in Section 4.2.1)
- 2) Define the mapping unit, i.e. subdivisions of the land surface that maximize the within-unit homogeneity and the between-unit heterogeneity. In this analysis, we use slope units (SUs; Guzzetti et al. 1999), which are automatically delineated from available Digital Elevation Model (DEM) (Alvioli et al., 2016) (Section 4.2.2).
- 3) Define the inputs factors necessary to run the model and their variability space (Section 4.2.3). In our case study, the input factors are the parameters defining the slope, soil, geometry, urban characteristics, as well as rainfall forcing data. As previously mentioned, the variability space of the input factors is increased here with respect to Chapter 3, in order to represent the variability of all

slopes across Saint Lucia. Each input factor is considered a random variable and associated with a probability distribution. The probability distributions are defined based on the physical meaning of the input factors, available data and information gathered from fieldwork in Saint Lucia, literature review (as described in Chapter 3, Section 3.2.2), and by processing the DEM data.

- 4) Create synthetic combinations of input factors by stochastically sampling from their probability distributions and running CHASM+ (MC simulation). We use the minimum FoS calculated by CHASM+ to classify each simulated slope as stable ( $\text{min FoS} > 1$ ) or failed ( $\leq 1$ ). The stochastic sampling is performed for all the land cover considered, which in this case are forest, shrub, bare and urban (here representing informal housing). Note that, given that the input factors are considered independent from each other, their random sampling might generate impossible combinations, such as slopes with steep slope angles, deep soil strata and low cohesion values. These combinations are, in most cases, automatically excluded in the analysis because CHASM predicts their failure before the start of the precipitation. These excluded simulations can instead be used to identify those maximum soil depths that, at varying slope gradient and cohesion values, are still predicted in equilibrium (as will be shown in Appendix C2).
- 5) Identify the input factors that most influence slope stability using global sensitivity indices (Pianosi et al., 2016). In particular, we use a regional sensitivity analysis approach (RSA, Hornberger and Spear, 1981; described in Chapter 2, Section 2.3.1) to identify which input factors are most influential in leading to slope failure (Section 4.3.1).
- 6) Assign each SU of the region with the corresponding values of the influential input factors, according to its physical properties. This will enable us to calculate the frequency of slope failure (i.e. the landslide hazard) for each SU for any choice of land cover and rainfall event (Section 4.3.2).
- 7) Use the Monte Carlo (MC) simulations results to define a function that returns the frequency of slope failure ('failure rate' in Fig. 4.2) as a function of the most influential input factors (Section 4.3.2).
- 8) Derive different hazard maps by selecting the land cover and rainstorm of interest. (Section 4.3.2.1 and Section 4.3.2.2).
- 9) Identify for which conditions the lack of vegetation or the presence of informal housing on the slope increase landslide hazard (Section 4.3.2.3).

The characteristics of the physical environment and of the informal urban communities in Saint Lucia and relevant data were described in previous Chapter (Sections 3.2.1 and 3.2.2, respectively). In the following sections, the new data needed to extend the variability space, and the new methodological steps to map the results back into the GIS, are described in more detail.

#### 4.2.1 Available land cover map, Digital Elevation Model and landslide inventory

Figure 4.3 shows the land cover map (A) and the slope steepness map (B) used for the analysis. The land cover map refers to the year 2015, and was created by the British Geological Survey (BGS) using an object-oriented image classification based on satellite images (Jetten, 2016). The spatial resolution (pixel size) is 2 m. The map was improved by BGS using ancillary satellite data (e.g. Landsat) and manual digitalization coherent with existing maps and local knowledge (Van Westen et al., 2016). From the original map, we merge the different types of deep-rooted vegetation (e.g., mixed and lowland forest) into a single 'forest' class, and all shallow-rooted (e.g., shrubland and herbaceous agriculture) vegetation into a single 'shrub' class. The class 'urban' encompasses both buildings and roads. The slope steepness map (Fig. 4.3B) is derived from the available Digital Elevation Model (DEM) at 5 m resolution. The DEM was generated from available contour lines, subsequently modified to remove errors. However, the quality is poor, showing an inaccurate representation especially in forested areas (as shown in Fig. 5-1 of Van Westen et al., 2016). On the same figure (Fig. 4.3B) the black polygons represent the landslides recorded after the Hurricane Tomas (2010), which will be later used to evaluate the quality of the hazard map. We use the landslides inventory derived by Mott MacDonald (2013), which was found the most reliable by Van Westen (2016) after a comparison with another available inventory (Abraham and Rock, 2010). These landslides were derived from satellite image interpretation and field verification. Of the 1025 landslides recorded, only those fully contained in the SUs (714 in total) are considered in the hazard map evaluation (Section 4.2.5), so to better identify the SUs that hosted landslide initiation and exclude those containing only runoff.

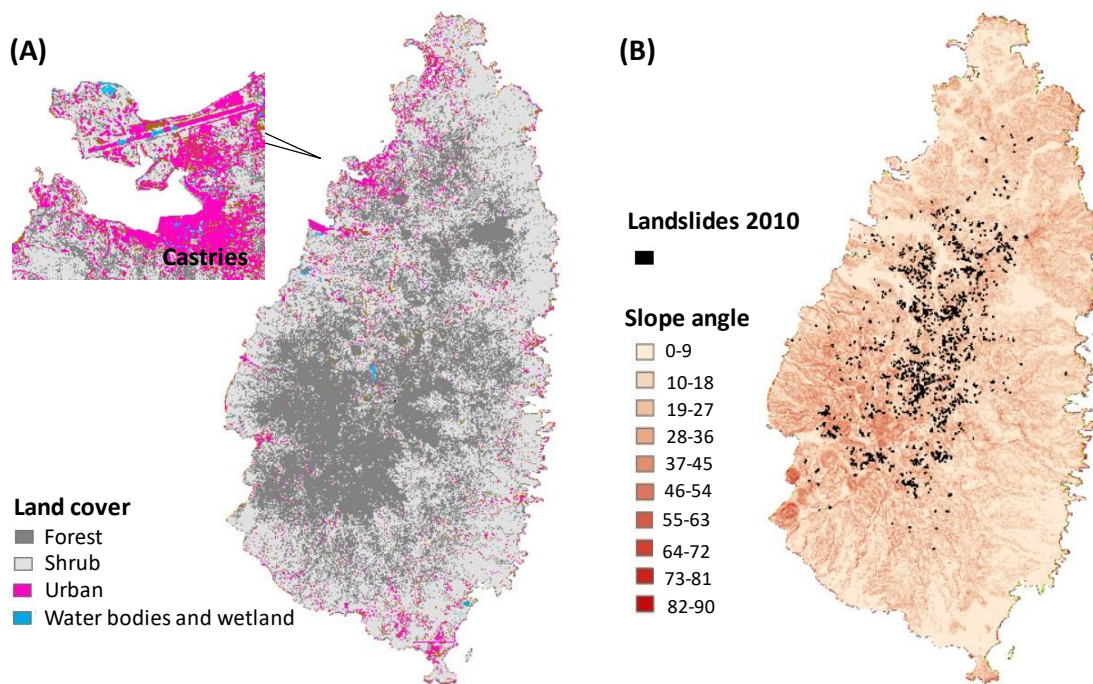


Figure 4.3: (A) Land cover map where different land cover types have been grouped into 4 classes: forest, shrub, urban and water bodies. The original version can be downloaded at <http://www.charim.net/stlucia/maps.>; (B) Slope steepness map derived from the DEM available at 5m resolution; the DEM is available at <http://www.charim-geonode.net/layers/geonode:dem>; the black polygons in Fig. 4.3 (B) represent the landslides recorded after the Hurricane Tomas (2010) by Mott MacDonald (2013). The corresponding GeoNode can be downloaded at [http://www.charim-geonode.net/layers/geonode:landslides\\_2010\\_2014](http://www.charim-geonode.net/layers/geonode:landslides_2010_2014). Of the 1025 landslides available for the year 2010, only the 714 landslides fully contained within the slope units are displayed.

## 4.2.2 Automatic creation of slope units for Saint Lucia

Landslide hazard assessment requires the preliminary selection of a suitable mapping unit (Guzzetti et al., 1999), i.e. a portion of land surface that maximises its internal homogeneity and between-units heterogeneity. In this analysis, we subdivide Saint Lucia into slope units (SUs), i.e. mapping units bounded by drainage and divide lines extrapolated from a Digital Elevation Model (DEM) (Carrara et al., 1991, 1995; Guzzetti et al., 1999). Specifically, we use the open source *r.slopeunits* software to automatically delineate SUs from the DEM. The *r.slopeunits* was developed by Alvioli et al. (2016) and employs the hydrological module *r.watershed* (Metz et al., 2010) available in GRASS GIS. The procedure follows an iterative process: first, *r.watershed* divides the digital topography of the region into large half-basins (a basin subdivided into left and right sides from the main drainage) using an initial large (user-defined) upslope contributing area (T). Then, *r.slopeunits* partitions these half-basins into smaller nested units, which maximise the internal homogeneity of their terrain aspect (i.e. maximise the grid cells facing in the same direction, so to minimise the circular variance) while respecting some size properties (e.g. minimum area). If the new, smaller, half-basins respect all the requirements then they are flagged as SUs, otherwise they are sent to the next iteration.

The procedure is repeated until the entire region is divided into SUs, which will differ in size according to the landscape morphology and complexity. Locally, r.slopeunits might produce SUs with unrealistic shape or size (e.g. very small SUs) resulting from errors in the DEM. These are removed through a 'cleaning' automatic procedure which ensures that each SU is bigger and larger respectively than a defined minimum size and width (see Alvioli et al., 2016, for more details).

The execution of the r.slopeunits algorithm requires specifying a number of tuning parameters, such as the minimum circular variance and minimum area mentioned above. The 'optimal' (unknown) combination of these tuning parameters is the one that produces a partitioning of the terrain into SUs as homogeneous as possible with the terrain aspect. In this analysis, we tested different possible values of some of these parameters while we held others to fixed values based on expert opinion (evaluated by I. Marchesini, personal communication). The final choice of the optimal combination was based on visual inspection, favouring small SUs when possible, because CHASM can only represent slopes with slope length and height less than 300 m. Specifically, the tuning parameters for the procedure of SUs extractions are (see Alvioli et al. 2016 for detail on their physical meaning and scope):

- the flow accumulation area (FA) threshold: set to 1,000,000 m<sup>2</sup>;
- the minimum surface area for the SU: we tested: [50,000 100,000 150,000 200,000 250,000 300,000] m<sup>2</sup>;
- the minimum circular variance: we tested [0.01 0.1 0.15 0.2 0.25 0.3 0.4] (values close to 0 represent grid cells all facing nearly in the same direction);
- a reduction factor: set to 5;
- the maximum surface area: not used;
- a threshold value for the cleaning procedures: set to 10,000 m<sup>2</sup>.

The SUs that we finally obtained are shown in Fig. 4.4. Each SU is defined by an elevation value (this is the relative height from toe to crest of slope, rather than the height above sea level), mean slope angle and standard deviation, and other geometrical characteristics (e.g. mean curvature) derived by the DEM. The mean slope angle (averaged between the pixels within the SU) and the elevation value of each SU will be used to define the variability space of these two input factors for the stochastic sampling.

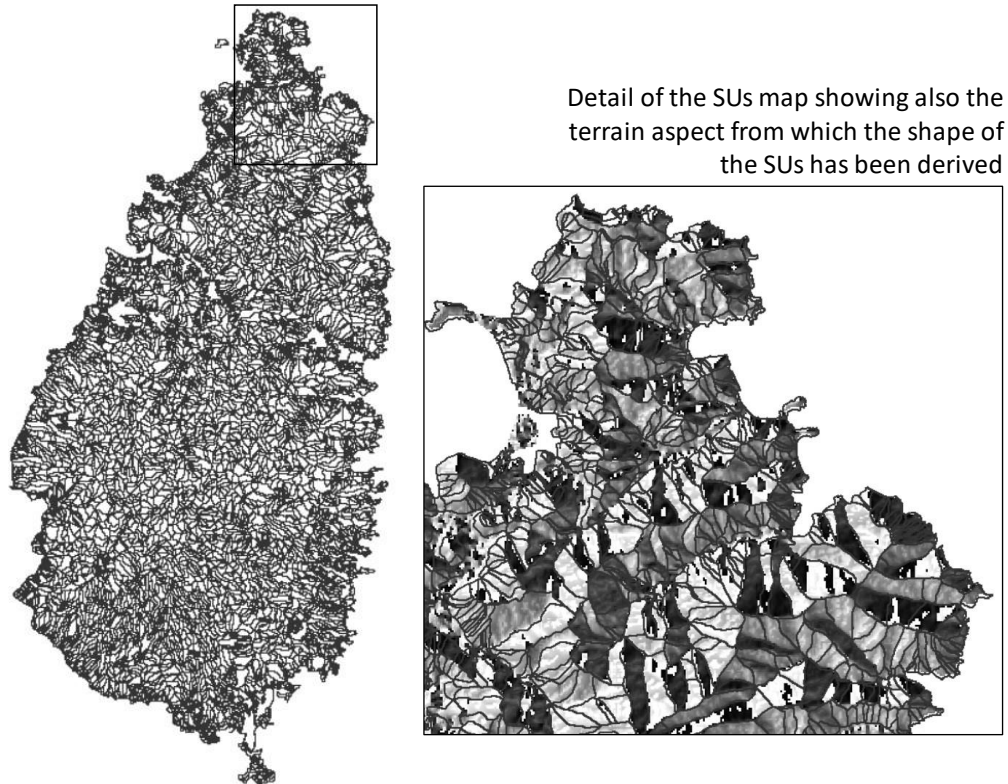


Figure 4.4: Slope Units (SUs) of Saint Lucia. On the right hand side, a zoom-in of the map, showing the SUs overlaying the terrain aspect (derived from the DEM described in Section 4.2.1). The minimum area and circular variance values are varied until the shape of the SUs is as much as possible homogeneous with the terrain aspect.

### 4.2.3 Definition of the input factors and their probability distributions

CHASM+ requires information on two-dimensional slope cross-section geometry (e.g. slope angle, slope height and slope material strata – particularly depth of weathered materials and soil that are the focus of this study), soil properties (geotechnical and hydrological), boundary conditions (e.g. initial water depth), rainfall (i.e. intensity and duration) and urban properties. The variation of these input factors can have a significant impact on the calculation of the factor of safety. Uncertainties in their definition can arise from the natural variation of soils, measurement techniques, and lack of reliable information.

In this chapter, the variation of 32 input factors, characterising our case study area, are analysed. Table 4.1 reports the full list of these input factors and the probability distributions that define their range of variability, while Fig. 4.6 shows an example of a slope derived from a combination of input factors.

The parameters of the probability distributions are defined based on various sources of information. These are described in Chapter 3, Section 3.2.2. However, in this chapter, the range of variability of some input factors is modified to address the specific purpose of the analysis. In particular:



- The slope angle is varied more widely than Chapter 3 to potentially represent all the SUs in the region. Also, the slope length is not fixed but it is varied according to the SUs height. In particular, the mean SU slope angles here considered vary between 5° and 70° (we exclude few SUs with angles between 70 and 90° because they are not considered realistic). The range of slopes heights varies between 5 m and 100 m, even if the minimum and maximum slope height found amongst the SUs are 5 m and 700 m. We constrained the maximum slope height to 100 m in order to (i) limit the computational time of running CHASM, given that the grid size for the search of the slip surface depends on the slope dimensions and large grids significantly increase simulation time (as shown in Fig. 4.6); (ii) prevent the generation of slopes with length greater than 300 m, because this exceeds the mesh size that can be modelled by CHASM. Despite these constraints, the range of slope dimensions generated is still considered to reasonably represent the SUs within the region because when the stochastic modelling and sensitivity analysis results are mapped back to the SUs we can be conservative in selecting a slope angle that represents the steepest part of each SU (based on mean angle statistics generated for each SU).
- The range of the initial water table height is varied between 50% and 100% of the slope height (instead of between 0-90%, performed in Chapter 3). This is to limit the number of simulations excluded because of issues with generating the initial hydrological conditions in certain cases. The problem can arise due to the way that CHASM allocates the initial moisture contents of unsaturated zone cells and the initial matric suction to the surface cell prior to hour 0 of the simulation. Certain combination of very low water tables and large slope heights (e.g. slope 100 m high and water table 0%) can generate a large unsaturated zone above the water table with surface matric suctions below the minimum suction values set in the soil water retention curve (SWCC – the minimum suction value corresponds to the maximum (saturated) moisture content value in SWCCs). For those cells, a saturated moisture content is assigned causing an unwanted increase of the water table (as shown in Section 2.4.2 and Appendix A2). This can be avoided by setting the minimum water table depth to 50% of the slope height.
- Urban density is varied between 0 and 100% (fixed in Chapter 3). The number of houses and the corresponding number of cutslopes are calculated according to the urban density, the length of the stochastically generated slope and the house footprint (i.e. house width + 1 m of surrounding unbuilt space + space occupied by the cutslope, which will depend on its angle).
- When vegetation (trees or shrubs) is present on the original non-urbanised slope, it is removed on the surface of the cuts for the urban scenario. In the deforestation scenario instead, trees or shrubs are removed but not replaced with informal housing. Operationally, this translates into looking at the simulations representing bare slopes instead of vegetated slopes, and the effect of deforestation

is assessed by comparing the stability of the two groups. The vegetation properties are representative of a tropical forest cover and shrub. They are reported in Table 4.2, and they are taken from the work of Holcombe et al. 2016 and Fung 2019. These properties are kept fixed throughout the sampling; therefore, the effect of different properties (e.g., root depth) on slope stability is not analysed.

The ranges of the other input factors are assigned as in the previous analysis of Chapter 3:

- the cross-sectional profile is discretised into three parallel layers of materials which are varied according to different soil thickness and soil geotechnical and hydrological properties according to the probability distributions reported in Table 4.1.
- rainfall events are defined by their intensity and duration, which vary in the ranges shown in Fig. 4.5. These rainstorms cover both events that have been observed in the past and rainfall events that might occur in the future (e.g. with higher intensity and duration than observed historically). Prior to the initiation of the rainfall event, we include 168 h (7 days) of simulation with rainfall intensity equal to 0, to ensure that a hydrological equilibrium is established. A further 168 h of zero-rainfall simulation is added after the storm in order to consider the groundwater response after the rainfall event.

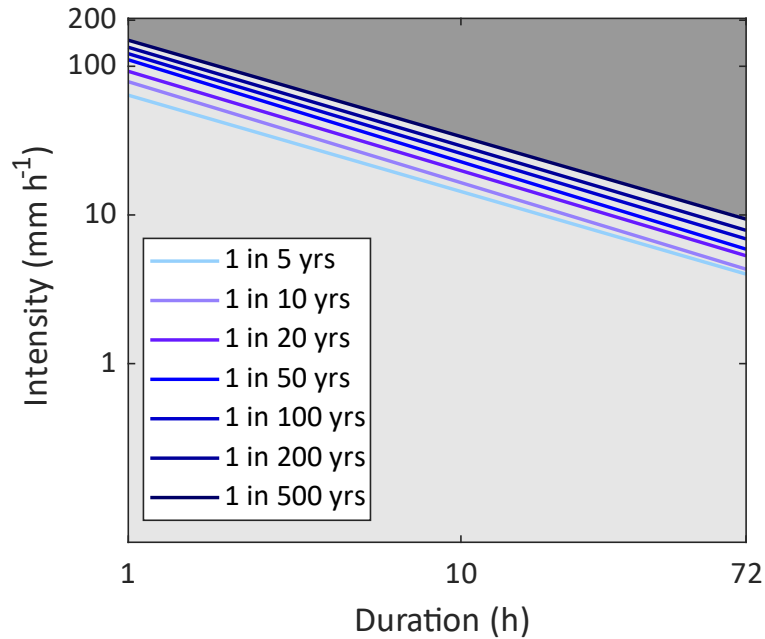


Figure 4.5: Rainfall intensity–duration–frequency (IDF) curves for Saint Lucia developed by Klohn-Crippen (1995) using Gumbel analysis of 40 years of daily rainfall data from 15 rainfall gauges. The light grey area includes rainfall events from observed data (below IDF curves); the dark grey area (above IDF curves) represents combinations of rainfall intensity-duration not recorded in the past but that might occur in the future.

- Informal housing is represented by four urban properties: slope cutting, absence of roof gutters, vegetation removal, and leaking pipes and tanks. While the angle of the cut slope is varied according to its probability distribution, the vegetation, roof gutters, and water leakage are defined as either present (option 1: yes) or absent (option 0: no; Fig. 4.6). The cut slope angle is varied between  $39^\circ$  and  $89^\circ$ , with a maximum cut slope height equal to 4 m. The house width and house load ( $8 \text{ kN m}^{-2}$ ) are not varied and correspond to the size and load of informal houses constructed with shallow concrete strip or block foundations, wooden walls, and sheet metal roofing that are typically observed in Saint Lucia (Holcombe et al., 2016). Both the tank and the pipe leakage rate are assumed to be half of  $4.2 \times 10^{-6} \text{ m}^3 \text{ s}^{-1}$ , which corresponds to the estimated leakage of 15% of the total water supply for low-income households in Saint Lucia (Anderson and Holcombe, 2013). When present, the leak is kept constant during the simulation time.

The input factors that define the spatial and temporal discretisation of the model, and the slip search grid location and dimensions are not varied. In particular, we use a cell size of  $1 \text{ m} \times 1 \text{ m}$  and a computational time step of 60 s. These values are chosen because they typically ensure numerical stability when solving the mass balance equation for the moisture over the domain, and thus a minimum number of failed model runs. A smaller cell size would enable a more detailed representation of the slope hydrology, but it would require

smaller time steps to preserve numerical stability. Smaller time steps would result in significantly longer simulation time. The resolution chosen is therefore a trade-off between acceptable accuracy and calculation time. The influence of the variation in these two discretisation parameters on slope stability is not explored.

Table 4.1: Input factors of CHASM+ and their probability distributions.

Parameter	Symbol/Unit	Range values		
		Layer 1 *	Layer 2 *	Layer 3 *
<b>Slope geometric properties:</b>				
Slope angle	$\delta$ [degrees]	U (5, 70) *		
Slope height	H [m]	U (5, 100)		
Thickness of layer	H1 – H2 [m]	U (1,6)	U (1,6)	
<b>Soil properties:</b>				
Effective cohesion <sup>a</sup>	c [kPa]	Ln (2.3688, 0.5698)	Ln (3.4121, 0.5774)	80
Effective friction angle <sup>b</sup>	$\phi$ [degrees]	Ln (3.2937, 0.2092)	Ln (3.1559, 0.3251)	60
Dry unit weight <sup>c</sup>	$\gamma_d$ [kN m <sup>-3</sup> ]	U (16,18)	U (18, 20)	23
Saturated moisture content <sup>d</sup>	VG $\theta_{sat}$ [m <sup>3</sup> m <sup>-3</sup> ]	N (0.413, 0.074)	N (0.413, 0.074)	N (0.413, 0.074)
Residual moisture content <sup>d</sup>	VG $\theta_{res}$ [m <sup>3</sup> m <sup>-3</sup> ]	Ln (-1.974, 0.376)	Ln (-1.974, 0.376)	Ln (-1.974, 0.376)
VG alpha parameter <sup>d</sup>	VG $\alpha$ [m <sup>-1</sup> ]	Ln (1.264, 1.076)	Ln (1.264, 1.076)	Ln (1.264, 1.076)
VG n parameters <sup>d</sup>	VG n	Ln (0.364, 0.358)	Ln (0.364, 0.358)	Ln (0.364, 0.358)
Saturated Hydraulic Conductivity	Ksat [m s <sup>-1</sup> ]	Ln (-11.055, 0.373)	Ln (-13.357, 0.373)	1xe-8
<b>Initial hydrological condition:</b>				
Water table height <sup>e</sup>	DWT [%]	U (50,100)		
<b>Rainfall properties:</b>				
Rain intensity	I [m h <sup>-1</sup> ]	U (0 0.2)		
Rain duration	D [h]	Ud (1 72)		
<b>Urban properties:</b>				
Cut slope angle <sup>f</sup>	$\beta$ [degrees]	N (65.18, 12.61)		
Roof gutters <sup>g</sup>	-	Ud (0 1)		
Septic tank and Pipe leak <sup>i</sup>	Qt/p [m <sup>3</sup> s <sup>-1</sup> ]	Ud (0 1)		
Urban density	U_d [%]	Ud (0, 100)		
Vegetation <sup>h</sup>	-	Ud (0 1)		

There are 32 input factors that are stochastically varied, considering that soil properties are independently sampled for the three soil layers considered.

U = Uniform distribution; Ud = Discrete uniform; N = Normal distribution; Ln = Log-normal distribution.

\*Layer 1: Residual Soil, Weathering Grade V-VI; Layer2: Weathered material Grade III-IV; Layer3: bedrock Grade I-II; Weathering grades defined according to GEO (1988).

\*U (5, 50) when slopes are urbanised. 50° is assumed to be highest slope angle on which a settlement can be located without some form of engineered slope stabilisation measures

<sup>a</sup> Effective cohesion > 0. Effective cohesion c (layer 3) > c (layer 2) > c (layer 1).

<sup>b</sup> Effective friction angle > 0. Effective friction angle  $\phi$  (layer 3) >  $\phi$  (layer 2) >  $\phi$  (layer 1).  $\phi$  < 90 degrees

<sup>c</sup>  $\gamma_s = \gamma_d + 2$ , where  $\gamma_s$  is the saturated unit weight.  $\gamma_d$  (layer 3) >  $\gamma_d$  (layer 2) >  $\gamma_d$  (layer 1)

<sup>d</sup> Values from Hodnett and Tomasella (2002) for Sandy Clay Loam material. We impose  $n > 1$ ;  $\theta_{sat} > \theta_{res}$ ;  $\theta_{res} > 0$ .

VG: Van Genuchten parameters for defining suction moisture characteristics curve.

<sup>e</sup> Water table height is defined as a percentage of slope height measured to the toe of the slope.

<sup>f</sup> Slope of the cut forced to be between 39 and 89 degrees, and it is always greater than natural slope angle

<sup>g</sup> 0 stands for house without rain gutters; 1 stands for house with rain gutters. Roof type = double pitch

<sup>h</sup> Vegetation presence: 0 no vegetation; 1 insert vegetation in the spare spaces.

<sup>i</sup> The leak of the septic tank is equal to the leak of the pipe. When 0 is selected there is no leak, whilst with 1 there are both. The leak rate is constant and equal to 4.2e-6 m<sup>3</sup> s<sup>-1</sup>

Table 4.2: parameters defining the vegetation properties for trees (land cover ‘forest’) and shrub. The values are taken from Holcombe et al. 2016 (online Supplement, Table S5) and Fung 2019. These parameters are maintained fixed throughout the modelling.

Parameter	Unit	Value	
<b>Tree canopy parameters:</b>			
Max leaf storage	mm	5	
Wet canopy evaporation	$m s^{-1} \times 10^{-7}$	2	
Leaf-drip rate	% per time step	0.8	
Stem portion	%	0.0012	
Max trunk storage	mm	0	
<b>Atmospheric parameter:</b>			
Net radiation	$W m^{-2}$	700	
Average daily temperature	Degrees	30	
Average daily rel. humidity	$s m^{-1}$	0.7	
Canopy resistance	$s m^{-1}$	70	
Soil aerodynamic resistance	$s m^{-1}$	50	
Veg. aerodynamic resistance	$s m^{-1}$	40	
Oxygen deficiency	m	-0.1	
Pressure head Constant	m	-0.35	
sink terms Constant	m	-5	
Wilting point	m	-14	
<b>Tree/grass parameters:</b>			
		<b>Trees</b>	<b>Shrub</b>
Surcharge	$kN m^{-2}$	2	0.3
Leaf area index	$m^2 m^{-2}$	10	5.8
Canopy cover	%	0.8	0.4
Rooting depth	m	4	1
Max transpiration	$m s^{-1} \times 10^{-7}$	2	1
Root tensile strength	MPa	50	32
Root area ratio	$m^2 m^{-2}$	0.002	0.002

#### 4.2.4 Creation of synthetic combinations of input factors and model simulation

We use Latin hypercube sampling (McKay et al., 1979) to generate 30,000 different combinations of the 32 independently varying input factors for each land cover type (120,000 simulations in total). Figure 4.6 illustrates one example of an urbanised slope defined by a single combination of these input factors. Due to the randomness of the process, checks are undertaken to ensure that realistic combinations of factors are generated; if not, they are discarded and replaced by another randomly generated, feasible combination. The criteria for these ‘feasibility’ checks are reported in the footnote of Table 4.1 (letters a–f). The stochastically generated slopes are then run in CHASM+ using the high-performance computers at the University of Bristol. We divide the completed simulations according to whether the minimum FoS is less than 1 (slope predicted to have failed, i.e., a landslide) or greater than 1 (slope is predicted stable). We exclude from the landslide hazard assessment the simulations predicting that the slope is failed before the start of the rainfall event, which represents inherently unstable slopes (for example steep slopes with deep soil thickness). However, these simulations will be used to estimate the maximum soil thickness to assign to each SU, as will be shown in the result section (4.3.2).

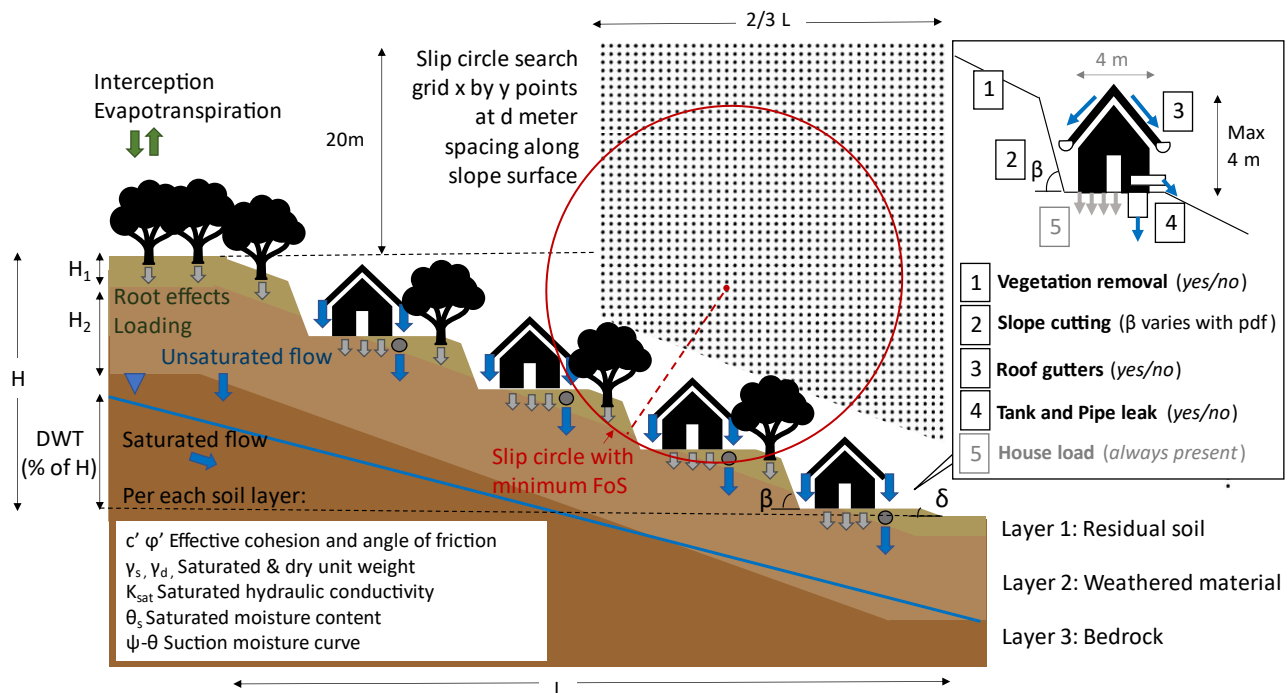


Figure 4.6: Example of urban slope generated by stochastically sampling from the ranges of input factors specified in Table 4.1. The dimension of the slip circle search grid depends on the slope height ( $H$ ) and length ( $L$ ) as shown in the figure. The grid extends downslope parallel to the slope as shown. Its size has been reduced compared to the analysis of Chapter 3 to constrain the computational time. On the right-hand side of the figure, a zoom-in box shows the urban properties included in the slope stability analysis. The urban properties that are stochastically varied are written in black, whereas those that are kept fixed are written in grey. Cut slope angle varies according to its probability distribution, defined in Table 4.1. Vegetation, roof gutters, leaking tanks/pipes are stochastically inserted or not. The house on the cut slope is always present and its load is not varied. The height of the cut slope varies relatively to the cut slope angle, but it is constrained to a maximum of 4 metres.

#### 4.2.5 Analysis of model simulations to associate each SU with a failure rate and create a hazard map

The 120,000 outputs generated by CHASM+ are analysed using Regional Sensitivity Analysis (RSA). As described in Chapter 2, Section 2.3.1, this method returns a global sensitivity index for each input factor. Based on these sensitivity indices, we can identify the subset of influential factors that mostly contribute to determine whether a slope is stable ( $FoS > 1$ ) or fails ( $FoS \leq 1$ ). In the next step, we estimate the values of these influential input factors for each SU in Saint Lucia. We can then look in our library of simulated slopes to find a prescribed number ( $M$ ) of slopes with the most similar values of the influential input factors, calculate their frequency of failure ('failure rate'), and use that frequency as an estimate of the probability of failure of our SU. By repeating the process for all the SUs, we can then build a hazard map. As simulations are

available for each land cover type and against a range of rainfall events, different hazard maps can be generated under different land use and climate (i.e. triggering rainfall event) scenarios.

#### 4.2.6 Evaluation of the quality of the hazard map

Once a landslide hazard map is delineated, its quality needs to be assessed. High quality maps will have high accuracy in representing observed data, i.e. in correctly identifying the presence or absence of landslides within SUs (Frattini et al., 2010). To define what is ‘correctly’ classified, a hazard threshold over which landslides are expected to be observed needs to be set. For example, if the hazard threshold is set at 0.5, an accurate model would predict a failure rate  $\geq 0.5$  for the SUs that contain observed landslides, and a probability  $< 0.5$  for the SUs that do not. In this analysis, we use two different techniques to assess the model’s accuracy: the success rate curve and the Receiver Operating Characteristic (ROC) curve (for discussion about these and other techniques, the reader is referred to Frattini et al., 2010). Neither of these techniques require the definition of specific hazard thresholds (e.g. 0.5 mentioned earlier; these are cut-off independent techniques) because the cumulative percentage of correctly classified SUs is calculated for all thresholds, from the highest (hazard threshold = 1) to the lowest (= 0). In the case of the success rate curves, the correctly classified SUs are plotted against their associated area. In the case of the ROC curves, the correctly and incorrectly classified SUs are used to define True and False Positive Rate, as outlined in Fig. 4.7. True positive rates are then plotted against False Positive rates. In both approaches we therefore obtain a curve similar to the one reported on the right-hand side of Fig. 4.7. Steep curves are associated with accurate maps, i.e. maps where the SUs predicted with highest probability also host the majority of the observed landslides. The quality of the hazard map can then be quantified by calculating the area under both curves: the larger the area, the better the map (Hanley and McNeil, 1982).

Per each hazard threshold (also called cut-off):

Observed	Predicted	
	Stable	Unstable
Stable	True negative (TN)	False positive (FP)
Unstable	False negative (FN)	True positive (TP)

SUs = slope units.  
 LSs = recorded landslides.  
 Observed stable = SUs without LSs  
 Observed unstable = SUs with LSs  
 Predicted stable = SUs predicted below hazard level  
 Predicted unstable = SUs predicted above hazard level

True positive rate	$TP / (TP + FN)$
False positive rate	$FP / (FP + TN)$

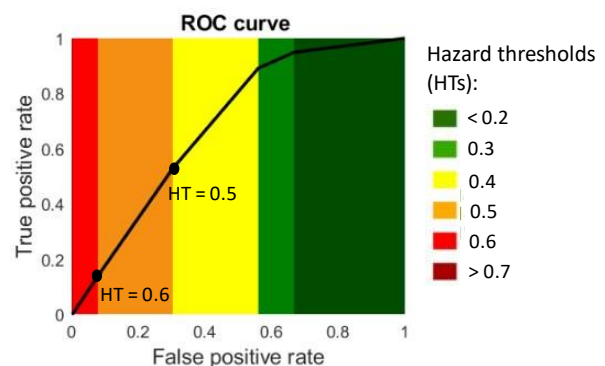


Figure 4.7: Accuracy statistics for the calculation of the ROC curve.

## 4.3 Analysis and results

### 4.3.1 Identify the most influential input factors for slope stability

In this section we analyse the 120,000 outputs generated by CHASM+ for the four land covers considered: forest, shrub, bare and urban (30,000 simulations each). We perform RSA on all sets of simulated slopes, and we compute the sensitivity index of each input factor. A high value of the sensitivity index suggests that the variation of that input factor significantly influences slope stability. Figure 4.8 shows that slope stability is insensitive to many input factors, and highly sensitive to five, namely slope angle, effective cohesion and thickness of the layer 1 (residual soil), rain duration and intensity.

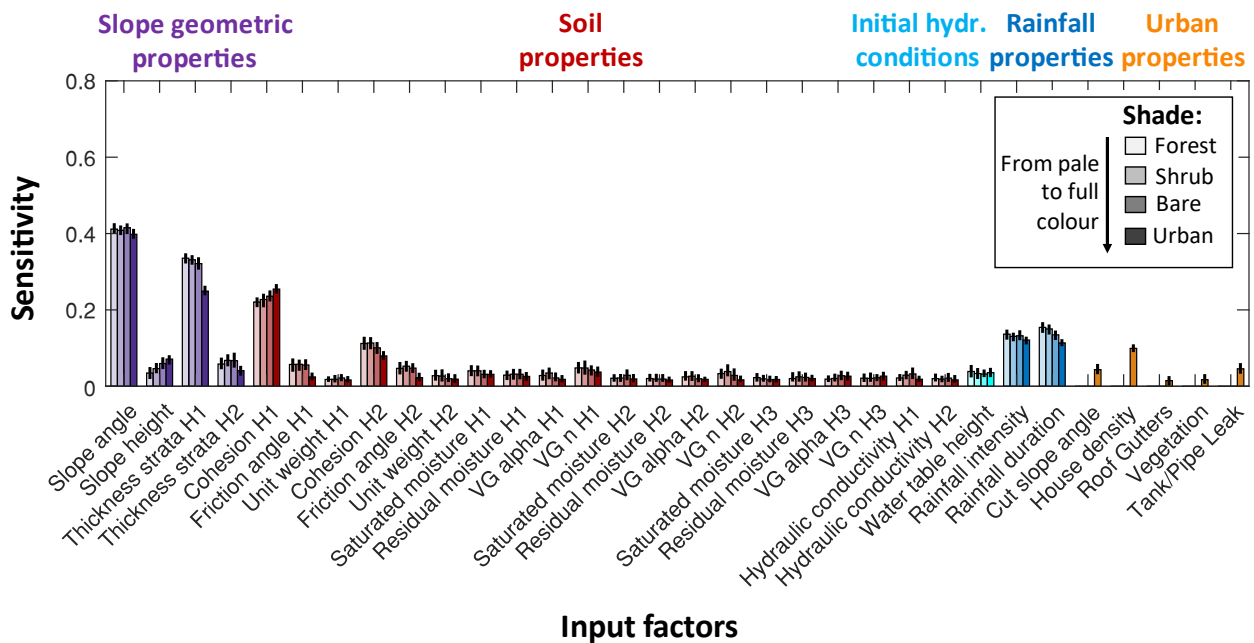


Figure 4.8: Sensitivity index for each input factor in the 4 land covers considered. The bars correspond to the mean value of sensitivity for each input factor calculated with bootstrapping, while the black vertical lines at the top of the bars represent the confidence interval (Number of bootstrap resampling  $N = 100$ ; significance level for the confidence intervals 0.05).

There is no significant difference in sensitivity index between land covers, except for the urban case. When slopes are urbanised (darkest bars in Fig. 4.8), the sensitivity of slope stability to the soil cohesion of layer 1 increases while the sensitivity to soil thickness of layer 1 and rainfall duration decreases. This is compatible with previous findings of Chapter 3, where we justified the change in sensitivity index with the fact that when slopes are urbanised, they are more prone to failure even on less susceptible soils and under less severe rainfall. The stability of urbanised slopes is also significantly influenced by variations of urban density. More considerations on this input factor are reported in Appendix C1.



### 4.3.2 Define the probability of failure for a slope unit as a function of the most influential input factors

In the previous section, five input factors are found to most influence slope stability: slope angle, effective cohesion, thickness of the layer 1 (residual soil), and rain duration and intensity. The first three are geometric and soil characteristics that vary across our domain. We must then assign these three variables to each SU. We do this as follows:

- Slope angle: conservatively defined as the 90th percentile of all slope angles extrapolated from the pixels within that SU.
- Soil thickness of layer 1: estimated from the slope angle. To make such estimation we analyse the CHASM+ simulations in which slope were predicted to fail before the rainfall events (i.e. slopes that are inherently unstable due to an unrealistic combination of input factors). RSA results, previous analyses (Chapters 3 and Section 4.3.1) and empirical evidence indicate the strong influence of slope angle, soil thickness and soil strength on stability, and the existence of a threshold that will limit the maximum thickness of soil able to be maintained on a real slope for a given angle and soil strength. We therefore back-analyse the inherently unstable slopes from the CHASM+ simulations to identify the critical soil thickness-slope angle threshold and assign the maximum soil thickness to each SU based on its angle. This method is fully described in Appendix C2.
- Soil effective cohesion of layer 1: we set it to the constant value of 8 kPa, which represents the mode of the probability distribution employed in the stochastic sampling for layer 1 (see Table 4.1). This is the best available estimate, given the lack of soil cohesion data (an inherent problem at regional scales).

Furthermore, each SU can be associated with a specific landcover as assigned according to Fig. 4.3A. For each SU, we can then search the library of stochastically generated slopes and find a group of slopes with similar characteristics, compute the proportion of slopes for which CHASM+ predicted a landslide for a chosen intensity-duration combination, and use that frequency as the ‘failure rate’ of the SU under study. For the search, we found it convenient to combine the influential input factors into ratios. We define: the soil ratio as the ratio between the soil thickness and the effective cohesion of layer 1 ( $H_1/c_1$ , m kPa<sup>-1</sup>); and a rain index as the logarithmic ratio between the storm’s duration and intensity ( $-\log(D)/\log(I)$ , h<sup>2</sup> m<sup>-1</sup>) – the higher the index the greater the magnitude of the rainfall event. The soil ratio and the rain index were previously introduced in similar slope stability analyses and they proved to be better at separating out the failed from the stable simulations (Almeida et al. 2017; and Chapter 3 of this thesis). A combination of slope angle, soil ratio and rain index identifies a point in the 3D variability space of simulated slopes, as shown in Fig. 4.9 (blue

dot). However, this point might not correspond to any particular simulated slope. We then look at other similar slopes within a window centred in that point (red cube in Fig. 4.9). The window includes a number of slope that were simulated by CHASM+ and then classified as failed or stable based on their FoS (black and grey dots). If the number of simulations  $M$  within the window is equal or greater than a fixed quantity (here  $M \geq 30$ ), the failure rate is calculated as the ratio between the failed slopes over  $M$  (failed + stable), otherwise the size of the window is increased until  $M$  is reached. The width of the initial range ((a), (s), and (r) in Fig. 4.9) and the rate of its increase depend on each input factor (specified in the box on the left-hand side of Fig. 4.9). For example, if we are interested in calculating the failure rate of a slope with angle  $30^\circ$ , the initial window is centred on  $30^\circ$  with an initial width of  $2^\circ$ , thus including simulated slopes with angles between  $29^\circ$  and  $31^\circ$ . If such an initial window does not contain  $M$  simulations, the range of slope angles is increased with a rate of  $0.5^\circ$  in each side (e.g., in the first iteration the range will contain angles between  $28.5^\circ$  and  $31.5^\circ$ ), while the range of soil ratios is increased of  $0.0125 \text{ m kPa}^{-1}$ . Note that the rate of increase of the rain index is set to zero, so that the window does not increase in size along the rain index axis, even if it contains less than  $M$  simulations. This is done to look at simulations within the window that correspond only to rainfall intensity and duration ratios similar to those selected for the hazard assessment (e.g., if we are interested in rainfall events similar to the Hurricane Tomas with rainfall intensity equal to  $28 \text{ mm s}^{-1}$  and duration of 24h, then the window is fixed at the corresponding rain index  $\pm 0.05 \text{ h}^2 \text{ m}^{-1}$ ). The rate of increase of the window along the soil ratio axis is proportionally larger than the slope angle axis. This accounts for the greater uncertainties in defining the soil thickness and cohesion of a slope than its slope angle.

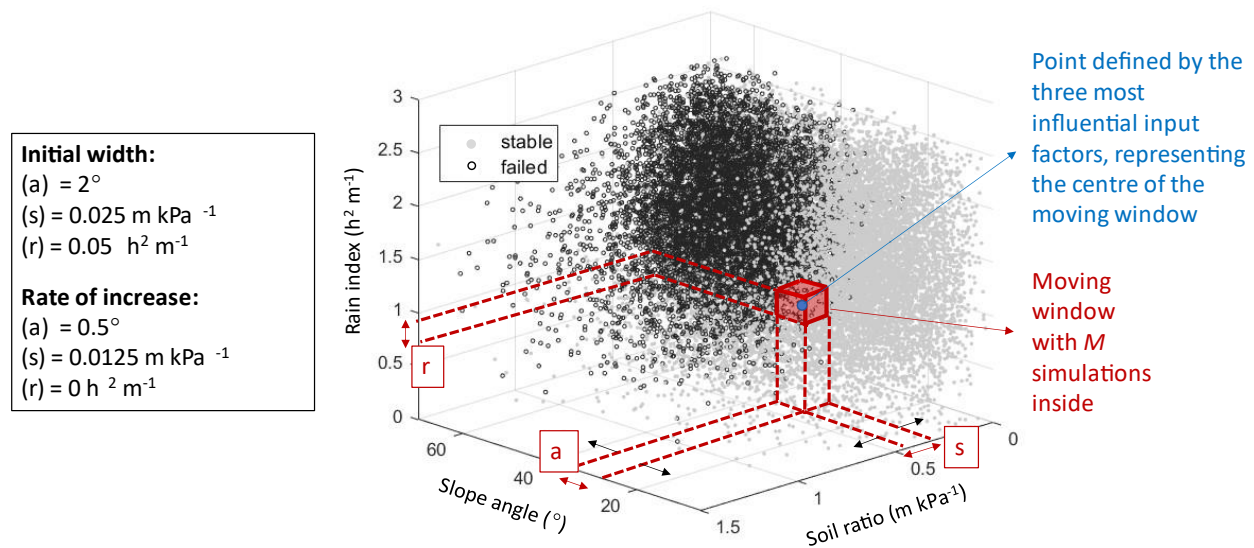


Figure 4.9: Representation of the window (red cube) used to calculate the frequency of failure across the variability space. The letters (a), (r), (s) represent the ranges of the three combined input factors whose intersection define such window. The initial width of these ranges is defined in the box on the left hand side of the figure as well as the rate of increase. Initial width and rate of increase are chosen heuristically according to the total range of variability, input factor type and after visual inspection of the results. When the window includes a number of simulations less than  $M$ , the rate of increase is used to iteratively widen the ranges (a), (r), and (s) in the direction of the black arrows until  $M$  simulations are included.

In the following sections, we use the moving window just described for three applications: to generate the hazard map for a known landslide-triggering event (i.e. Hurricane Tomas); to generate the hazard maps for different hypothetical land cover and climate change; and to explore the variation of failure rates between different land cover for variations of the most influential input factors.

#### 4.3.2.1 Generating and evaluating hazard maps for a known landslide-triggering event

We start by evaluating the hazard map corresponding to Hurricane Tomas, which in October 2010 caused severe damage due to flood and landslides throughout the country (Van Westen, 2016). The total rainfall was estimated to be 660 mm in some locations, over about a 24 hours period, corresponding to a return period between 180 and 200 years depending on the source (van Westen, 2016; Mott MacDonald, 2013). We therefore consider the simulations associated with a precipitation intensity of approximately  $28 \text{ mm h}^{-1}$  (i.e. 660 mm over 24 hours) and duration of 24 h. The set of simulations associated with the current land cover (Fig. 4.3A) is used to evaluate the hazard corresponding to this rainfall event. The result is shown in Fig. 4.10 together with the locations of the 714 landslides recorded after the hurricane (see Section 4.2.1). The quality of the hazard map is evaluated by calculating the area under the success curve rate (top right hand corner of Fig. 4.10) and under the ROC curve (bottom right hand corner of Fig. 4.10). These areas are equal

to 0.66 and 0.69 respectively. Both values indicate a better performance than a random model (area = 0.5), i.e. a model that predict stable or unstable SUs with the same rate.

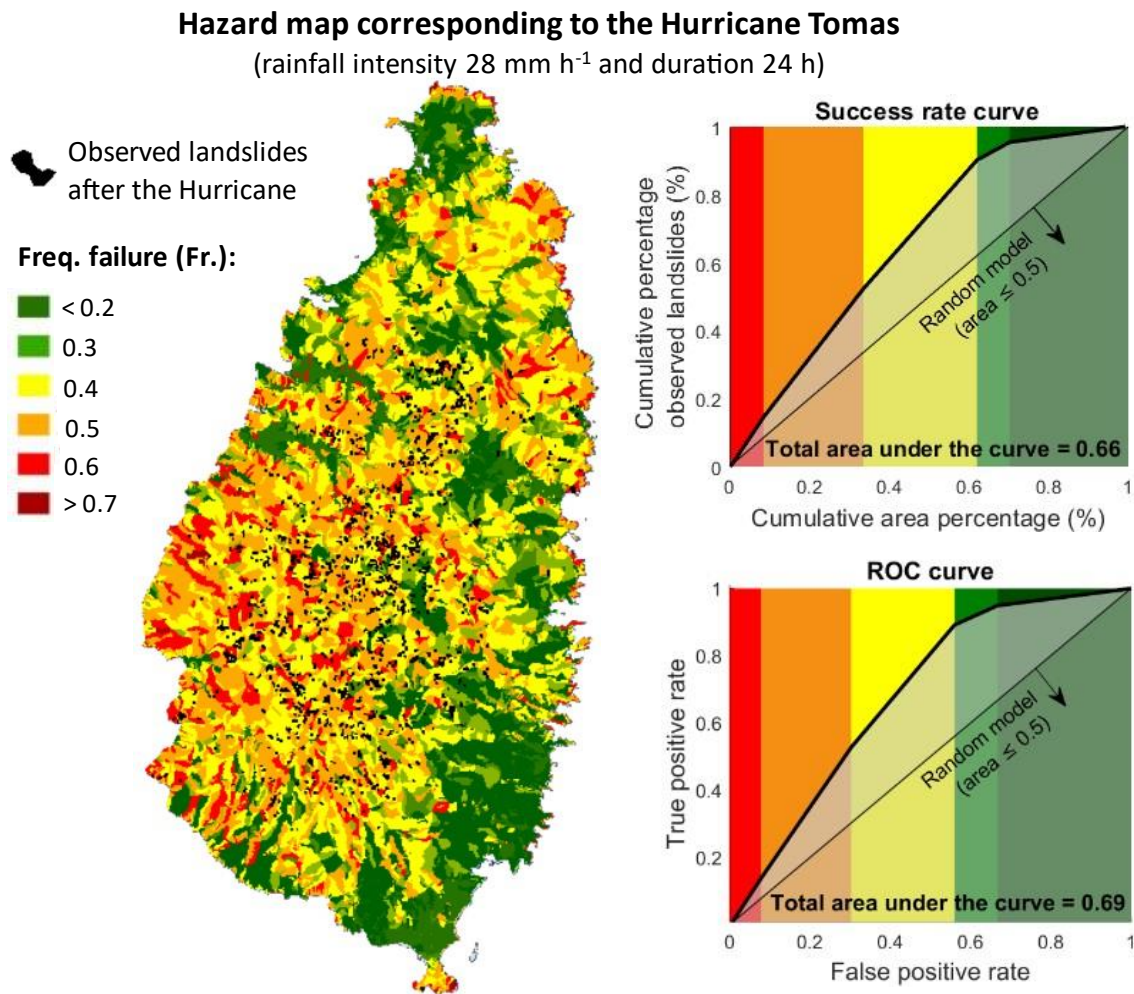


Figure 4.10: Landslide hazard map corresponding to the Hurricane Tomas rainfall event. The landslides recorded after the event (black polygons) are plotted on the map. On the top right-hand side corner, we show the success rate curve, overlying the ROC curve. These curves are used to evaluate the capability of the map to reproduce the hazardous areas under the rainstorm event. The performance of the model increases the more the curve gets closer to the point (0,1). Points that fall on the bisector are associated with a model that randomly predicts stable or unstable slope units with the same rate.

#### 4.3.2.2 Mapping landslide hazard for hypothetical climate (rainfall) and land cover change

We now explore the effects of land cover change on landslide frequency by creating hazard maps for two hypothetical scenarios: 1) where vegetation is removed (vegetated slopes are replaced with bare slopes) and 2) where urbanisation occurs on all slopes with angles less than 50°, i.e. slopes that might be affected by future urban expansion. These are extreme scenarios since land cover changes are forced also over the centrally located rainforest reserves which are currently protected. Figure 4.11 shows a set of hazard maps under such hypothetical land cover conditions for different rainfall intensity-duration combinations:

Hurricane Tomas and two hypothetical storms with slightly lower and higher intensity and duration. The arrows between the maps report the change in percentage of SUs associated with a failure rate greater than 0.5 (defined as ‘hazardous’ SUs).

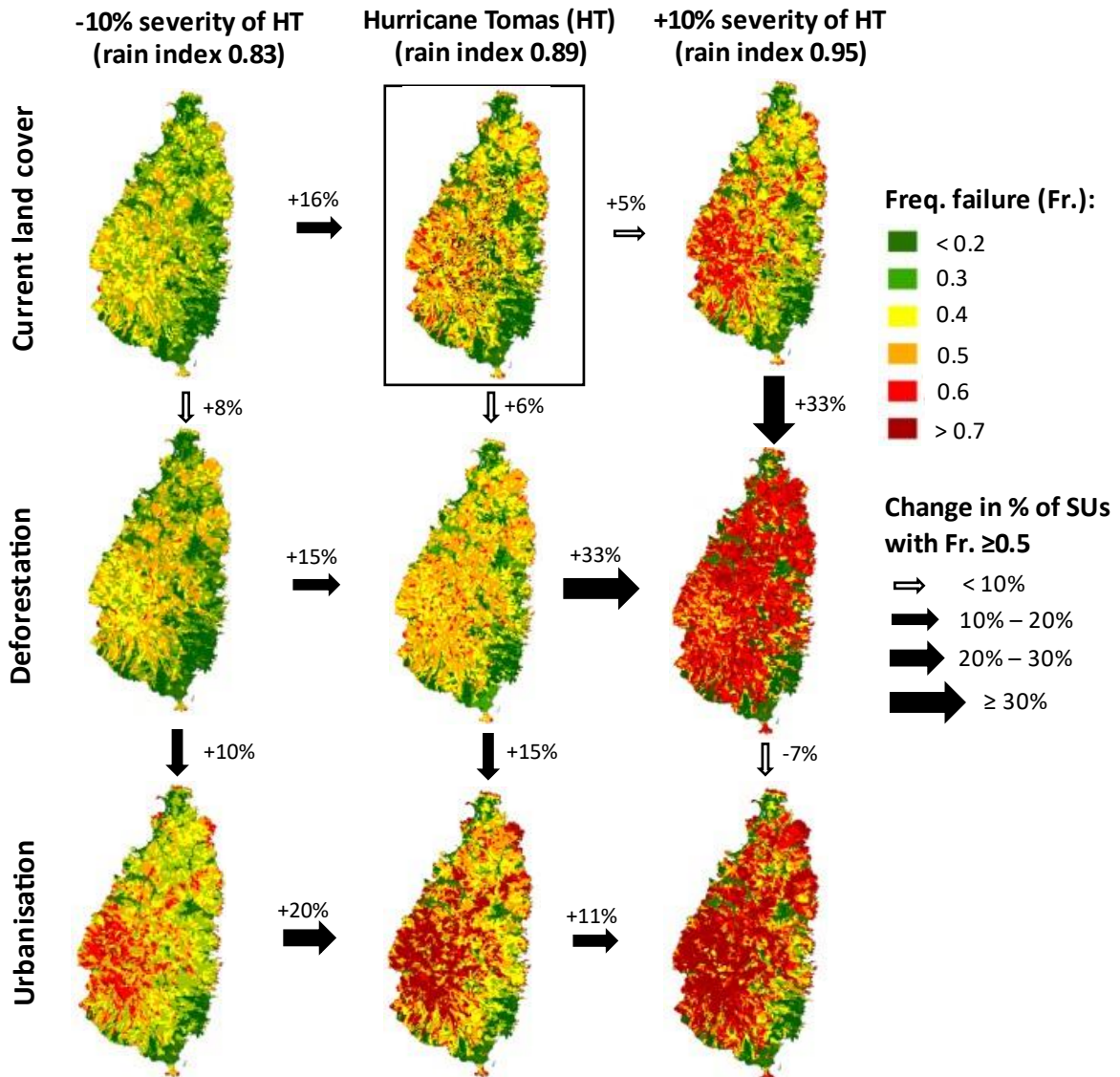


Figure 4.11: Hazard maps obtained for varying rainstorm severity and two hypothetical scenarios: 1) vegetation is removed (middle panel) and 2) informal housing is inserted (bottom panel) on all slopes with angle less than 50°. The framed map is the same reported in Fig. 4.10. The arrows between the maps highlight the change in percentage of SUs predicted with high frequency of failure ( $\geq 0.5$ ). Between the maps, each SU is defined by the same two input factors - slope angle, soil ratio but varying rain index. A moving window (see Section 4.3.2) is then used to identify the frequency of failure of the simulated slopes most similar to each SU, within the library of simulations corresponding to the SU’s landcover. The windows size used for the maps are kept equal to those used for calculating the hazard map of Fig. 4.10 in order to facilitate the comparison.

In general, more SUs are associated with high failure rates for more severe rainfalls under the hypothetical land cover scenarios. However, the greatest increase occurs when the severity of the Hurricane Tomas rainfall event is increased by 10%, with +33 and +27% of hazardous SUs under the deforested and urbanised scenarios, respectively. On the other hand, when the rainstorms are less than, or as severe as, Hurricane Tomas, the presence of informal housing leads to about 20% increase in the number of hazardous SUs, whereas deforestation has a more negligible effect (increase < 10%).

#### 4.3.2.3 Evaluate the difference in failure rates between land covers

In this section we go back to looking at the whole set of Monte Carlo simulations to explore the more general question of which conditions of vegetation cover and informal housing increase landslide hazard. The three top panels in Fig. 4.12 shows the scatter plots of sampled soil ratio, rain index and slope angle for failed (black) and stable (grey) slopes. The bottom panel show the corresponding frequency of failure calculated with a moving window. As expected, higher failure rates are found for higher slope angle and soil ratio, and for more severe rain event (high rain index). Visually, we could say that most of the failures occur for slope angles greater than 30°, rain index greater than 0.7 and soil ratio greater than 0.2. 68% of the failed simulations fall within this region, confirming the predominant role of these factors in defining slope stability (as previously shown in Fig. 4.8). Interestingly, the region of failure can be delimited by an exponential trend on multiple dimensions (see Appendix C3 for further discussion on this topic).

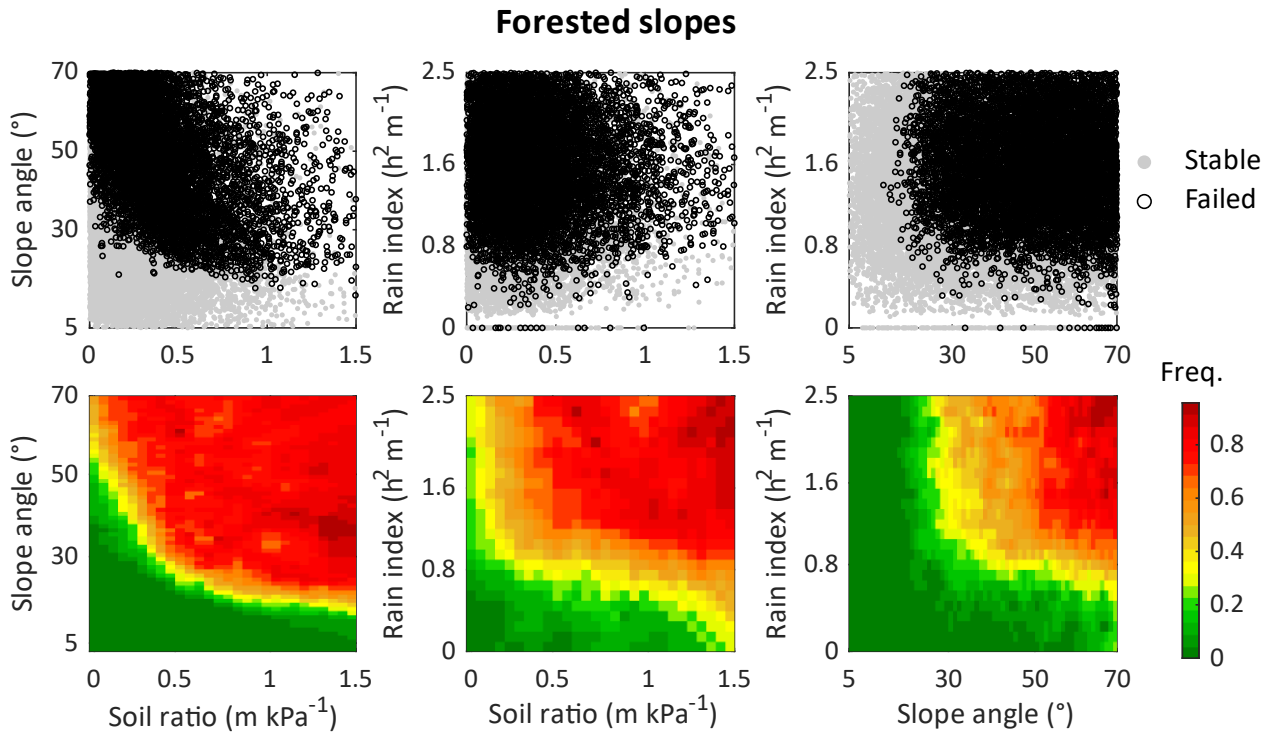


Figure 4.12: Example for forested slope: in the upper panel the scatter plot of failed (black dots) and stable (grey dots) slopes at variations of soil ratio, slope angle and rain index. The lower plots represent the frequency of failure calculated with the moving window from the corresponding scatter plots of the above panel. These scatter plots represent the 2D planes of the 3D plots shown in Fig. 4.9. The frequency of failure calculated for the other land covers are reported in the Appendix C3.

The results in Fig. 4.12 refer to the case of 'forest' land cover. Failure rates calculated for forested slopes (lower panel of Fig. 4.12) are then compared to the failure rates calculated for bare and urbanised slopes (reported in Appendix C3) by performing an image subtraction. The results are shown in Fig. 4.13. Table 4.3, instead, provides some values of rain index with the associated rainfall intensity and duration, for better interpreting the variations of failure rates observed along the rain index axis in Fig. 4.13.



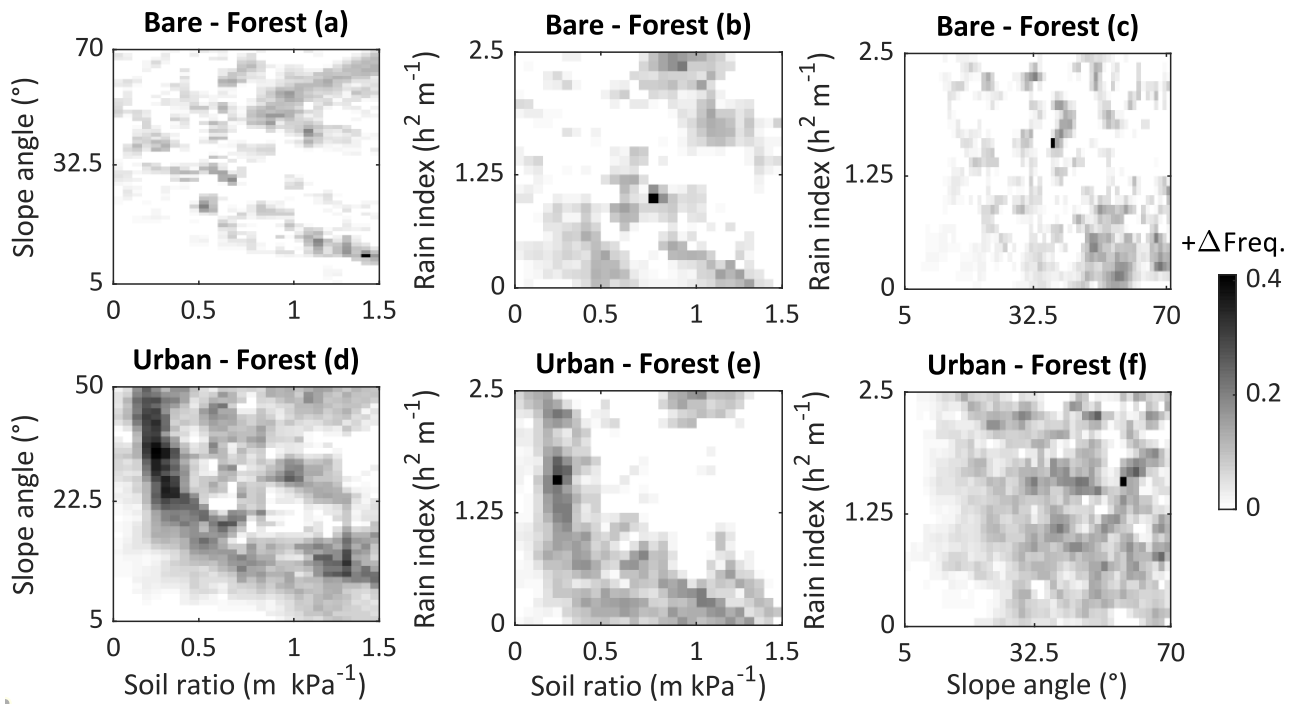


Figure 4.13: difference in frequency of failure between the three land covers considered. The title of each plot defines the calculation made in the image subtraction (e.g. bare – forest: frequency of failure of bare slopes minus frequency of failure of forested slopes). The colour identifies the increase in landslide frequency (from 0 difference in white to 40% more failures in black). The other combinations of image subtraction can be found in Appendix C4.

Table 4.3: Example of rain indices and their associated rainfall intensity and duration. The rain index is calculated as specified in Section 4.3.2 and its unit of measure is in metres. However, the rainfall intensities in the table are reported in millimetres for an easier interpretation. The rain index in bold corresponds to similar rain conditions of the Hurricane Tomas (rainfall intensity 28 mm h<sup>-1</sup> and duration 24 h).

<b>Rain index (h<sup>2</sup> m<sup>-1</sup>)</b>	Rainfall duration (h)					
	3	6	12	24	48	72
Rainfall intensity (mm h <sup>-1</sup> )						
10	0.23	0.38	0.54	0.69	0.84	0.92
20	0.28	0.45	0.63	0.81	0.98	1.10
30	0.31	0.51	0.70	<b>0.90</b>	1.10	1.22
50	0.36	0.59	0.83	1.06	1.29	1.42
100	0.47	0.77	1.08	1.38	1.68	1.85
200	0.68	1.11	1.54	1.97	2.40	2.65

Urban slopes (Fig. 4.13d, e, f) present the highest increase in percentage of failures (shown by darker colour). Specifically, frequency of failure increases by up to +40% for slopes with angles greater than 25° and soil ratio between 0.2 and 0.5, for any rainstorm severity (Fig. 4.13d and e). 20% more failures are also observed for rain indices less than 0.6 (e.g. rainstorm with intensity 30 mm h<sup>-1</sup> and duration 6 h; Table 4.3) and soil ratio greater than 0.4 (Fig. 4.13e), i.e. on slopes with high susceptibility to failing (thick soil thickness or low



cohesion values) but for not severe rainfall events. The difference in frequency of failure between forested and bare (Fig. 4.13a, b, c) is less evident. Although clusters of darker colour identify an increase of up to 25% of failures when forest is removed, for rain indices less than 1 (Fig. 4.13b and c), and slope angles greater than 35° (Fig. 4.13a and c).

## 4.4 Discussion

### 4.4.1 Thickness and cohesion of the first layer of soil, slope angle and rain properties are the most influential input factors at regional scales

Figure 4.8 shows that there are five most influential input factors which are the same for all the land covers considered: slope angle, thickness and cohesion of layer 1, and rainfall intensity and duration. The relevance of these input factors was widely recognised in other landslide mechanistic hazard assessments as well as empirical-statistical and heuristic assessments (Guzzetti et al., 2006a; Melchiorre and Frattini, 2012; Salciarini et al., 2012 van Westen et al., 2006). The other input factors might have a smaller direct or indirect effect, but they are not dominant at this scale. The fact that very few input factors control one particular model output (the FoS in our case) is not surprising, as it has been found in many other global sensitivity analysis studies (Wagener and Pianosi, 2019). Also, when looking at a smaller variability space, such as that for a single slope (Chapter 2, Section 2.4.2) or specific slope type (Chapter 3) the ranking of the influential factors might change (as shown in Appendix C5). Smaller variations of soil cohesion and soil strata, for example, might lead to more significant changes of their sensitivity between vegetated and non-vegetated covers because of the more visible effect of root reinforcement (e.g., the additional effective cohesion added by the roots is more visible on soils with low soil cohesion but less on soil with high cohesion values and here, all soils are considered together).

Figure 4.8 also shows that, at regional scale, geometrical and soil properties influence slope stability more than rainfall (which has lower sensitivity indices). These results are confirmed also by other studies (Almeida et al., 2017; Folberth et al., 2016) and suggests that climate change might have a smaller influence on landslide hazard than the slope intrinsic properties and their evolution, such as slope topography, lithology, or soil mantle formation and modification due to previous failures (Parker et al. 2016; Samia 2017). The sensitivity analysis also reveals that erroneous evaluations or uncertainty in the estimation of geometrical and soil properties might lead to wider inaccuracies in landslide hazard assessment than uncertainty in the rainfall associated with future climatic changes. Thus, improving the quality of this data seem the most important step to obtain more accurate results. While slope angle (the most influential factor) can be evaluated with increasing resolution from DEMs, soil cohesion and soil depth are generally highly

heterogeneous and difficult to sample across wide areas, and thus their evaluation is highly uncertain (Burton et al., 1998; El-Ramly et al., 2006). It becomes, therefore, crucial to improve the ability of predicting both soil thickness and soil cohesion across landscapes, through a better understanding of their relationships with the local geomorphology (Dietrich et al., 1995; Patton et al., 2018), parent materials and soil forming processes. With respect to the prediction of soil cohesion, dividing the studied area into different classes based on topography, available soil and geological maps, for then considering different soil cohesion probability distributions for each of these classes, might improve the models' accuracy in landslide prediction (Salciarini et al., 2006). This would require greater emphasis and priority to be placed on obtaining soil index properties and geotechnical testing data and, importantly, collating and curating such information in database so that statistical analysis can be undertaken (see Shephard et al., 2019). According to this analysis, obtaining such information is as relevant as the evaluation of climate change projections, at least in the region considered.

#### 4.4.2 The five most influential input factors identified create accurate hazard maps

Figure 4.10 shows the hazard map corresponding to the Hurricane Tomas, which we have generated using reasonable approximations of the five most influential input factors for slope stability (Fig. 4.8). Despite the uncertainties in the estimation of those factors, the map gives satisfactory results, with an area under the ROC curve comparable to other similar slope stability analysis that use mechanistic-based models (score 0.69 - Frattini et al., 2010; Raia et al., 2014). More accurate representation of the precipitation hyetograph (here uniform across the 24h) might lead to better results (Arnone et al., 2016). The model performance can also be influenced by other factors such as the landslide inventory chosen, its quality and resolution (SafeLand, 2011 – Deliverable D2.8). The number of misclassified SUs (which in turn influences the accuracy score) might, for example, be due to missing landslide observations (e.g. due to unrecognised landslide from the satellite images or field surveys) on SUs predicted with high probability of failure. Furthermore, the predictive model might be more efficient in correctly classifying the SU subjected to landslides, than those free of slopes failure. However, by using only one landslide inventory that represents a very intense hurricane (200 years return period), the difference in the model performance between more extreme and less extreme rainfall conditions (e.g. under more frequent, less intense rainfalls) cannot be evaluated. To reduce such uncertainty, multiple event landslide inventories should be used (Guzzetti et al. 2006). The analysis may allow, for example, evaluation of the error associated with the model's prediction for each mapping unit. An information that can complement the landslide hazard map. Once such analysis is performed, the hazard maps can be useful for identifying both the SUs predicted as most hazardous and the SUs where the hazard is underestimated (i.e. those that were predicted stable but experienced failure) with the associated error. The latter SUs may be the subject of targeted data collection. More accurate (ranges of) soil thickness and

cohesion values for those particular SUs could then be used to improve the hazard assessment by re-mapping the relevant simulation inputs and outputs from the library of simulated slopes without re-running the model, effectively providing a tool that can switch from regional to hillslope scale and vice-versa.

The methodology employed for this analysis, therefore, presents advantages compared to other methods currently in use. (i) It is capable of dealing with non-stationary conditions and determining the change in spatio-temporal pattern of landslide hazard under various land cover and climate scenarios (Gariano and Guzzetti, 2016; van Westen et al., 2006). This is not the case for other methods, such as statistically-based models, where the functional relationship between landscape attributes and past landslides might not hold under changed environmental conditions (Reichenbach et al., 2018). (ii) It can quantify both epistemic (due to lack of knowledge) and aleatory (due to inherent natural variability) uncertainties, which can then be communicated to decision makers (as recommended by Gariano and Guzzetti, 2016). (iii) The hazard assessment can be updated as frequently as required (Huabin et al., 2005). The slope failure probability can be modified if new data are available and/or if land cover and climate change. (iv) This methodology provides a way to upscale the mechanistic site-specific hydro-mechanical models to catchment/regional scales (van Westen et al., 2006). These models have the advantage of representing and assessing the physical processes that drive slope failures (including those associated with urban construction activities) which can be used to deduce effective and targeted mitigation solutions.

#### 4.4.3 When and where the combined effect of land cover and climate change mostly increases landslide hazard

Figure 4.11 shows that when more bare and urbanised slopes are present, more hazardous SUs are predicted. This is compatible with studies that compared observed or simulated landslides across different land cover types: more landslides are typically observed on bare (Reichenbach et al., 2014; Vanacker et al., 2003; Pisano et al., 2017) and on terraced slopes (Persichillo et al., 2018) than forested slopes. Most notably, the greatest increase of hazardous SUs in Fig. 4.11 occurs when the severity (represented by the rain index,  $-\log(D)/\log(I)$ ,  $\text{h}^2 \text{m}^{-1}$ ) of the Hurricane Tomas is increased by 10% (right hand side column of Fig. 4.11). Such an increase may represent one of the potential future scenarios predicted by climate models for tropical hurricanes (Knutson et al., 2015; Knutson and Tuleya, 2004). In this eventuality, extensive deforestation and informal urbanisation would lead to a significant increase of hazardous SUs compared to the current land cover conditions (+33 and +27% respectively). These results therefore confirm and quantify the importance of the simultaneous analysis of climate and land cover changes on landslide hazard, given the significant increase in the number of hazardous SUs when their combined effect is considered.

Furthermore, both Fig. 4.11 and Fig. 4.13 (panel e,f) suggest that the land cover change associated with informal housing can increase landslide hazard under current rainfall conditions, even without climate change. This is confirmed by empirical evidence in which slopes that are progressively urbanised with informal housing can experience failure for less severe rainstorms than non-urban or formally urbanised slopes, but rarely has been quantified (Crozier,1986). These results allow quantification and a representation of the effect of informal housing on landslide probability, which can be used to support actions. Mitigation solutions that aim to both improve current landslide hazard and potentially buffer the impact of future climatic changes are thus recommended (IPCC, 2012, 2014). Examples of such interventions could include: the reforestation of degraded areas, which may both decrease current landslide hazard by adding root strength and increasing the interception of potential future heavier rainfalls; and/ or the reduction of leakages from water utility infrastructures and the installation of household roof guttering and rainwater tanks (see Anderson and Holcombe, 2013, for example) which has the potential to both improve slope stability and better address drought risk. The effectiveness of each mitigation action could potentially be tested with the slope stability analysis and then integrated within the social and financial context of the area for identifying targeted landslide mitigation solutions that can be part of strategies to reduce landslide risk ALARP, As Low As Reasonably Practicable (Lange et al., 2018; Bull-Kamanga et al., 2003).

## 4.5 Limitations

All the results are subjected to the limitation of the input data and the assumptions made in our study.

Using different probability distributions for the stochastic sampling might lead to quite different global sensitivity analysis results (Paleari and Confalonieri, 2016). In this study, some of the distributions were based on standard assumptions in the literature such as lognormal distributions for effective cohesion and angle of frictions (with values derived from the Saint Lucia geotechnical dataset) whereas rainfall intensities and durations, soil depths and house loading, for example, were sampled from assumed uniform or normal distributions in the absence of further information.

To spatially distribute the results of CHASM we use the SU model to define hillslopes in Saint Lucia automatically and objectively. The delineation of a hillslope then allows the definition of its most critical cross section, which we assume to be a slope with a steep angle (90<sup>th</sup> percentile of all angles within that hillslope). However, shallow rainfall triggered landslides might also occur on moderately steep slopes because of their topographic convergence, where relatively thick soils and high soil water pressure (due to flow accumulation) act combinedly to decrease the soil mass stability (Prancevic and Lamb, 2020; Nakileza and Nedala, 2020; Bellugi et al., 2015). Here, topographic convergence is not considered in the mapping but different initial water table heights (which were not found highly influencing the slope stability response in the GSA) are

modelled and they might be used to evaluate the stability of critical cross sections within converging topographical areas under different soil saturation levels, which can then be recognised in the field.

The vegetation parameters are represented in a simplistic way (although the physical representation of vegetation in CHASM is relatively sophisticated): only two types of vegetation (forest and shrub) are simulated and the effect of variations of their physical features on slope stability is not analysed. Vegetation properties as well as soil properties might change with slope topography, geology and climate (Collison et al., 2000; Muscarella et al., 2020; Dixon and Brook, 2007), but in this analysis they are considered independent. Furthermore, the beneficial/adverse effect of vegetation on slope stability depends on factors such as soil depth and soil properties. In particular, the root system can have a significant beneficial effect on slope stability when it crosses the slip surface and anchors the soil into more stable substrate. Deep seated landslides, commonly associated with deep soils, might benefit only marginally by the presence of root reinforced soils (Stokes et al., 2009; Wilkinson 2000). In the forested slopes simulated, visual inspection reveal that most slip surfaces are located between layer 1 (residual soil, weathering grade V–VI) and layer 2 (weathered material, grade III–IV). This is explained by the different soil strength and hydraulic conductivities of the two layers, which constrains the slip surface within the weaker layer 1, as discussed in Chapter 3. Given that the depth of layer 1 varies between 1 and 6 metres and that we have been conservative in assigning soil depth to slope units (Appendix C2), the root zone fixed at 2 m, in most cases does not intersect the interface between layer 1 and 2 and thus its beneficial mechanical effect on slope stability results limited (as from the top to the middle panel of Fig. 4.11, where deforestation does not significantly increase the probability of failure of the slope units, under the same rainfall conditions).

The effect of root reinforcement (which is fixed, although it can vary widely in a region – e.g., Schmidt et al., 2001) is also more beneficial where the effective cohesion of the vegetated soil is low (Chok et al., 2015; Collison and Anderson, 1996). Such effect might be hidden by the fact that in the landslide probability mapping, the effective cohesion of layer 1 (which is the most likely to host the root zone) is fixed to a relatively high value (the mode of its probability distribution, obtained from measurements in different locations of the region) and uniformly assigned to all the SUs of Saint Lucia, – again, in the absence of any data to enable allocation of different values to different SUs.

The use of one-point statistical parameters (the mode in this case) challenges the accuracy of the assessment. Soil composition and strength, in fact, vary from one location to another, even within homogenous layers (Burton et al., 1998), and it might influence the formation of different soil depths (e.g. low soil depth might be result unstable on shallow slopes because low values of soil cohesion – as shown in Appendix C3).

The large uncertainty associated with the spatial distribution of soil cohesion and soil thickness is common for spatially-distributed analyses (Salciarini et al., 2006; Melchiorre and Frattini, 2012). However, rather than predicting absolute values of landslide probability, we aimed to give, despite the uncertainties, insights on the relative change of landslide occurrence between different scenarios. Such information is often sufficient to inform environmental planning (Van Beek and Van Asch, 2004). Furthermore, as noted in Section 4.4.2, the architecture of the new modelling methods allows for individual SUs to be re-assessed as new data is obtained, or if slope-specific assessment is required for determine site-specific stability behaviours and mitigation measures.

## 4.6 Conclusions

This chapter demonstrates how the methodology developed for this thesis can be used to generate regional landslide probability maps for Saint Lucia. These maps allow exploration of the effects of a wide range of combinations of land cover and climate change (rainfall) scenarios on landslide probability, whilst accounting for the uncertainty of all input factors.

The input factors that most influence slope stability are identified with a GSA and assigned to each SU, using some reasonable assumptions. Under such assumptions, the landslide probability map generated for the Hurricane Tomas satisfactorily identifies the observed landslides (area under ROC curve = 0.69). Additional probability maps are then presented for different storm intensities and under two hypothetical deforestation and urbanisation scenarios. The results show that if the storm intensity is increased by 10%, the hypothetical scenarios exhibit ~30% more SUs at high ( $\geq 0.5$ ) slope failure hazard than with the current landcover. However, we also show that landslide hazard is increased by ~20% under current climatic conditions if informal housing increases, and we identify for which geomorphological and climate conditions this might occur.

Most importantly, this analysis shows that, in a data-scarce context such as the one analysed, we can reasonably estimate how regional landslide probability might vary under the joint effect of future climate and land cover change (which includes both potential deforestation and expansion of informal urbanisation). The quantification of the relative change in regional landslide probability between scenarios, such as the one presented in this chapter, has the potential to support environmental and climate adaptation planning, which would not be otherwise possible in data-scarce developing countries.

# Chapter 5 : Summary and Conclusions

## 5.1 Research Summary

In a time of rapid urbanisation and changing climate, informal settlements can be a catalyst for landslide risk accumulation in the humid tropics but, with changes in slope management and construction practices, they could also play a key role in urban landslide risk mitigation and climate change adaptation. To understand how urban development within informal settlements can be made more sustainable, it is crucial to advance landslide hazard assessments by incorporating the anthropogenic component. Urban construction activities lacking engineering design or consideration of slope processes, such as those characterising informal housing, can often increase landslide hazard. Identifying the causes of landslide hazard, and the locations where it is significantly increased within informal settlements is particularly important in resource-limited contexts, where mitigation actions need to be effectively prioritised and targeted to address the local landslide drivers. Furthermore, current scientific methods for landslide hazard assessment struggle to support disaster risk reduction and sustainable development decisions in data-scarce locations and when dealing with uncertain climate projections. This thesis has introduced a new methodology that can support decision making in such contexts. This methodology has been tested in a typically data scarce, resource limited location of the humid tropics, providing mechanistic modelling-based evidence of how much, and for which slope and climate properties, informal housing becomes most detrimental for slope stability.

More specifically, this thesis makes four main contributions:

- 1) It introduces a new methodology that for the first time includes informal housing (vegetation removal, slope cutting, house loading, and point water sources) in a mechanistic slope stability analysis, also considering the uncertainties associated with slope properties and climate change. Part of the methodology development is the extension of the mechanistic model CHASM (new CHASM+) to include the effects of different forms of water management: superficial pipes, buried septic tanks and roof gutters on houses (Chapter 2 – addressing research question 1: How can we include informal housing in a slope stability analysis that also considers the uncertainties due to both poorly defined slope properties and potential future climate changes?).
- 2) It quantifies how slope susceptibility to failure is modified by the presence of informal housing. Specifically, it calculates the minimum rainfall threshold for triggering landslides from synthetic

simulations, it demonstrates the higher frequency of small-scale landslides on urbanised slopes, and it identifies the topographical, soil and rainfall properties for which informal housing becomes most detrimental for slope stability, using this information to identify appropriate hazard mitigation measures (Chapter 3 – addressing research question 2: How can we quantify the relative role of informal housing in increasing rainfall-triggered landslide hazard within a community?).

- 3) It introduces a way to generate regional hazard maps that consider both climate and land cover change (from deforestation and/or housing development), demonstrating the importance of accounting for their joint effects on slope stability analysis when supporting environmental planning under changing conditions (Chapter 4 – addressing research question 3: How can we incorporate the understanding of slope stability gained at the hillslope scale, into regional hazard maps under changing urban expansion and rainfall conditions?).
- 4) It gives insights on the relative importance of the main landslide drivers across scales, as summarised in Fig. 5.1, which can help to prioritise future research and data collection efforts, according to the purpose of the analysis (Chapter 2, 3 and 4).

### Chapter 2: site-specific hillslope scale, single rainfall event

*Fixed properties:*

- geotechnical and geometrical properties
- rainfall intensity and duration
- initial water table height
- cut slope angle

*Main landslide drivers (ranked for urbanised slopes):*

- **water table height**
- **leak from the water tank**
- shape parameters of soil water characteristic curves (SWCC)
- saturated soil moisture content defining SWCC

### Chapter 3: community scale (slope angle between 20° and 45°)

*Fixed properties:*

- leak from the tanks and pipes
- slope length
- house density

*Main landslide drivers (ranked for urbanised slopes):*

- **eff. cohesion of residual soil (layer 1)**
- **rainfall intensity**
- thickness layer 1 (residual soil)
- cut slope angle, rainfall duration and slope angle

### Chapter 4: regional scale (slope angle between 5° and 50°)

*Fixed properties:*

- leak from the tanks and pipes

*Main landslide drivers (ranked for urbanised slopes):*

- **slope angle**
- **eff. cohesion, soil thickness of residual soil (layer 1)**
- rainfall intensity and duration
- house density

Figure 5.1: Landslide drivers found to most influence urban slope stability in the three analyses performed in this thesis, and their respective spatial scales. The drivers are ranked in order of influence.



### 5.1.1 Summary of Chapter 2

The review of Chapter 1 highlights that informal housing can increase the occurrence of rainfall-triggered landslides, but it is rarely included in hazard assessments at community and regional scales. Amongst the methods available for landslide hazard assessment, site-specific mechanistic models are the most suitable for our research purposes. This is because they can represent the dominant failure processes and thus quantify the relative influence of informal housing in slope instability as well as ascertain the conditions at which it becomes most detrimental. However, depending on the level of process representation, these models can be particularly data demanding and not many field or lab measurements are available for slope topography, soil, or hydrological properties within informal settlements. Poorly defined slope properties introduce uncertainties in the modelling chain, which add to the uncertainties associated with future climates. Future climate projections are generally derived by downscaled global climate scenarios based on General Circulation Models (GCMs). However, different models might produce significantly different rainfall projections which, once introduced in the modelling chain, can produce a wide range of stability response.

This thesis therefore develops and demonstrates a new methodology to include informal housing influences (vegetation removal, slope cutting, house loading, and point water sources) in a slope stability analysis, also accounting for large uncertainties. This allows to generate outputs that bring the understanding on slope stability gained at site-specific hillslopes scale, up to community and regional scales. The first new development of the methodology is the extension of the site-specific mechanistic model CHASM (Combined Hydrology and Stability Model) to include superficial leaking pipes, buried septic tanks, and roof gutters on houses (new CHASM+). The consistency of the results provided by the newly extended software CHASM+ are successfully verified by comparing them to hypothetical scenarios and to a peer-reviewed analysis of an observed urban landslide in Brazil. CHASM+ is then run in a stochastic Monte Carlo framework to create libraries of tens of thousands of slopes with varying geometrical, soil, boundary conditions, and urban properties. This allows both the slopes' variability within the analysed area (community or region) and the associated uncertainties to be accounted for. Instead of using GCMs projections, the rainfall properties are stochastically sampled using a wide range of possible future intensity-duration combinations (bottom-up approach). This ensures that any feasible future design storm in a changing climate is captured by the sampling process. We analyse the large number of outputs using global sensitivity analysis and data mining tools. Specifically, we use Regional Sensitivity Analysis (RSA), and Classification And Regression Trees (CART). RSA and CART allow the identification of the slope, climate and urban properties most influencing slope stability as well as thresholds over which landslide hazard is significantly increased by informal housing.

### 5.1.2 Summary of Chapter 3

The new methodology is tested using the example of Saint Lucia, a typical data-scarce, resource limited location of the humid tropics. The analysis focuses on representing the population of slopes that have the potential to be particularly susceptible to landslides and which may be a location for informal urbanisation (slopes with angles between 20° and 45°). The urbanisation scenarios are modelled as having moderately densely constructed informal housing (30% slope coverage by houses). It is demonstrated that informal housing increases landslide hazard, and that slope cutting is the most detrimental construction activity when compared to vegetation removal, the lack of roof gutters and the presence of water leaks. Furthermore, this methodology allows the quantification of how the presence of informal housing modifies the relative roles that natural slope angle, soil cohesion and soil thickness in maintaining slope stability – in this Saint Lucia case study, there is an increased hazard occurrence (by up to +45%) for low values of these three main landslide drivers (e.g. on slopes with angles less than 25°). Critical rainfall thresholds at which slope failures are predicted to occur are also estimated. The rainfall (intensity-duration) threshold for triggering landslides is lower when informal housing is present, with an increased number of small-scale landslides (+85%, with failure depth less than 4 m and radius of slip surface less than 10 m) for high intensity and short duration events. This rainfall threshold is comparable to that found empirically for roads (with cut slopes) in Puerto Rico (Larsen and Simon, 1993) and for similar urbanised tropical regions. This suggests the applicability of the methodology, and potentially the some of the key findings, for other data scarce regions of the humid tropics with similar soils, topography, land cover and climate. Finally, low cost-effective ‘low regrets’ mitigation actions are suggested to tackle the main landslide drivers identified in the study area.

### 5.1.3 Summary of Chapter 4

The new modelling methodology is applied to the whole Saint Lucia and the mapping component is developed. The aim of the analysis is to generate a suite of regional landslide hazard maps that represent both land cover and climate change scenarios. This is a significant step forward because: (i) land cover and climate change are generally investigated separately at this scale, mainly because of their high uncertainties; and (ii) current spatially distributed landslide hazard assessments and hillslope-specific mechanistic analyses are not often compatible and require separate modelling approaches. The new methodology allows dynamic changes and scalability. The analysis starts by dividing the region into slope units which exhibit internally consistent topographies defined by drainage and watershed division lines (topographic ridges) and the selected level of drainage network hierarchy. According to the geometrical characteristics of the slope units and other information of the study area, we generate an ensemble of slopes with varying slope, soil and climate properties representative of each of the main land covers identified in the region: forest, shrub, bare

and urban. In particular, the urban slopes are modelled with varying urban density and informal housing characteristics (cut slopes, loading, and point water sources). The library of stochastic simulations results is then 'mapped back' to the slope units by matching the assigned slope unit properties with the failure rates of the corresponding stochastically generated slopes. To create this link, only the most influential input factors for slope stability are used: slope angle, soil thickness and soil cohesion of the top strata and rainfall intensity and duration. The hazard map so generated and representing the Hurricane Tomas rainfall event, satisfactorily identifies the observed landslides (area under Receiver Operating Characteristic curve = 0.69). More hazard maps are then presented for different storm intensities and under two hypothetical scenarios, where deforestation and informal housing are extended to all slopes that might be subjected to future urban expansion. The results show that if the rainfall intensity and duration of the Hurricane Tomas are increased by 10%, the hypothetical future land cover scenarios exhibit ~30% more hazardous slope units than the current land cover conditions. However, even without an increase in the rainstorm severity we show that regional landslide hazard is increased by ~20% under current climatic conditions when the expansion of informal housing is considered, and we identify the properties of the slopes that are most affected by this urbanisation scenario. In Chapter 4 a total of ten hazard maps are generated and discussed to demonstrate the outputs and applications of the new end-to-end modelling methodology; however, many more hypothetical scenarios (as many as can be modelled) could be explored and the relative change in landslide hazard assessed. This information can be used to address research, practice and policy questions in landslide resilience, environmental and climate adaptation planning.

### 5.1.4 Overall thesis conclusions

This thesis provides evidence of the relative influence of informal housing on the occurrence of rainfall-triggered landslides, identifying the sensitivity of slopes to the informal housing under land cover and climate change. Most importantly, it develops and demonstrates a methodology able to diagnose trends of slope response behaviour at multiple spatial scales, despite the data scarcity and uncertain future projections. This tool can identify the most detrimental urban practices for slope stability within informal communities, the rainfall conditions likely to trigger landslides, and the locations where the presence of identified urban mismanagement most increase slope instability. This is useful information to guide engineers and policy makers on landslide mitigation decisions, target data collection, prioritise actions and address further analyses in locations identified as particularly at risk. On the other hand, the information might also be used as part of community-based disaster risk reduction approaches to support the co-development and adoption of better slope management practices, ultimately promoting an increasing resilience within informal settlements.

## 5.2 Directions for future work

This thesis develops a new methodology to diagnose the conditions by which informal housing most influence landslide hazard under climate change. There are now opportunities for both the implementation of this research into practice and for future model refinements and developments. In this Section we provide: 1) a short-term outlook, answering the question: how would we use the results obtained so far in order to support end-users such as local engineers and those living in informal communities in their decision-making for landslide hazard mitigation ?; and 2) a long-term outlook, answering the question: how could we further improve the representation of landslide hazard processes within informal communities and how much additional explanatory power might this deliver for the extra data requirements or modelling complexity?.

### 5.2.1 Bringing this research into practice

In this thesis a substantial library of slope simulations (140,000) was created for the island of Saint Lucia. Each slope is described by certain geometrical and soil properties, antecedent hydrological conditions, land cover and rainfall driver, and is associated with a minimum Factor of Safety (FoS) as well as a potential failure position and size. This information could be translated into two main practical tools: (i) look-up tables for landslide hazard reduction decisions; and (ii) a digital spatial data layer to employ in GIS (Geographic Information System) mapping.

**Look-up tables as a decision tool.** In practice, it is often necessary for engineers to form a rapid assessment of stability conditions for particular slopes (and/or multiple slopes), making direct application of mechanistic models impractical. The slope simulations created in this research, summarised in the form of 'look-up' table (e.g. implemented using macros in MS Excel), could instead be used as a quick synthetic data source for such assessments (Anderson and Lloyd, 1991). This could be useful for local engineers who can often measure or estimate properties for the slope of interest such as the slope angle, approximate soil strength (e.g. from the local knowledge of the soil type and weathering grade) and soil thickness (again from local knowledge or from boreholes or observations of strata intersected by slope cuts). The combination of these factors together with the chosen rainfall conditions could be used to interrogate the look-up table and identify a range of relevant model simulations and associated Factor of Safety. If more detailed information is known (e.g., hydraulic conductivity of the soil or the results of geotechnical tests), the search could be made more specific and accurate. Changes in land cover on a particular slope can also be tested to evaluate the corresponding change in slope stability. Look-up tables based on sets of a few hundred (manually run) CHASM+ simulations have previously been made available by other researchers for quantifying the effect of bioengineering and cut slopes on landslide hazard, for example Anderson and Lloyd, 1991, Collison et al.,

1995, and Wilkinson et al., 2002. The stochastic modelling methodology applied in this thesis covers a much larger and more densely sampled parametric space, potentially representing the population of slopes under a range of landslide cover and climate conditions for a whole region. This increased number of simulations (tens of thousands) and slope representation should provide more robust estimates of slope response based on the simulated frequency of failure for a certain type of slope and set of landslide drivers. Furthermore, not only the effect of vegetation and cut slopes could be considered but also different urban densities and surface water infrastructure.

**The new geographic layer ‘HILLS’: Human Interaction Layer for Landslide hazard modelling.** Following on from the previous point, the results obtained in this analysis can be formalised into a new data layer for use in platforms like GIS. The slope and urban properties of each slope unit are either derived from available layers (e.g. DEM, OpenStreetMap) and/or defined by the user in case more precise information are known from other sources (e.g. soil thickness or the presence of hill cutting of specific slopes). Simulated slopes with similar properties can be extrapolated from the library of CHASM+ simulations using a ‘moving window’ approach such as that developed in Chapter 4, and an estimate of the minimum FoS can then be assigned to the slope units according to the rainfall conditions of interest. The user can select specific slope units and insert optional urban properties (e.g using a drop-down list), such as insert roof gutters on houses, vegetation between houses or increase urban density. This would automatically change the search within the simulated slopes, and a new FoS would be assigned, rapidly indicating the relative effect of Human Interaction on slope stability.

## 5.2.2 Possible ways to improve landslide hazard assessment: a scientific outlook

This thesis provides a methodology that allows the exploration of many possible urban and climate combinations. Chapter 4 developed and demonstrated a way to link the library of CHASM+ simulation results to regional hazard maps for Saint Lucia. The link enables the analysis of hypothetical urban expansion scenarios and the relative change in landslide probability they would induce, compared with current land cover conditions. Here, we suggest two ways this analysis could potentially be improved: (i) by combining the slope stability analysis with a hydrological model to account for locations of topographic convergence and thus water accumulation; (ii) by using available techniques to identify informal settlements within a region, and to project their potential future expansion.

**Accounting for flow accumulation due to topographical convergence.** In this thesis the two-dimensional cross sections simulated by CHASM were linked to the three-dimensional slope units (SUs) on the basis of extrapolated (conservative) values of slope angle, soil thickness and soil cohesion that were each assumed uniform within the slope unit. It might be argued that surface and sub-surface water flow accumulation,

which was found detrimental for slope stability in informal settlements lacking surface water management (Anderson and Holcombe, 2006), is not directly accounted for in our methodology. Future studies could thus investigate whether identifying the slope cross sections most susceptible to water flow convergence could improve landslide hazard predictions. Since topographic convergence or divergence is a major control on water flow at the surface (e.g. Kirby, 1971; Bogaard and Greco, 2016), topographically driven hydrological models of water flow could be used to assess the locations subjected to flow accumulation within the upper/steepest part of each catchment. Thus, while hydrological model dynamically estimates the water table conditions for a given precipitation (which we found to influence slope stability at hillslope scale – Fig. 5.1), we would extrapolate from the stochastic library, those slopes with similar topographical and hydrological conditions to evaluate the corresponding probability of failure.

**Using new techniques for informal settlements mapping and projection.** The Sustainable Development Goals (SDG) adopted by the UN member states in 2015 include the goal to “*make cities and human settlements inclusive, safe, resilient and sustainable*” (SDG 11). To monitor the achievement of this goal, the “*proportion of the urban population living in slums, informal settlements or inadequate housing*” needs to be evaluated (SDG 11.1.1). Four main approaches are generally employed for such purposes: aggregation of census data and surveys of slum (and informal community) households (e.g. Bakibinga et al., 2019); field-based mapping (e.g. van Steensel, 2016); manual delineation of imagery (e.g. Baud et al., 2010); and remote sensed image classification, including machine learning (e.g. Leonita et al., 2018). When the spatial delineation involves earth observation images, informal settlements are identified through their typical physical characteristics: a dense and irregular building density; small shape, size and height of the buildings; settlement location, generally unsuitable for construction such as steep slopes or flood zones; lack of access to infrastructure such as road network; and neighbourhood characteristics such as the proximity to railways and high-voltage power lines (Kohli et al., 2012; Kuffer et al., 2020). These data and maps of informal settlements could be particularly useful for those landslide hazard assessments that include informal housing, such as the one presented in this thesis. For example, urban density and building material would identify the number of houses and additional load to insert in the slope stability analyses, whereas census data might provide information on construction techniques and presence of water facilities (and associated level of maintenance). When analysing future urban expansion projections, statistical or cellular automata models could also be employed. These models use a set of environmental and physical conditions (such as accessibility to roads, or urban development suitability) to create urban expansion ‘rules’ for projecting informal settlements in areas currently unbuilt (Dubovyk et al., 2011; Hill and Lindner, 2010). However, these three research branches (landslide hazard assessment, informal settlements detection and projection) are not yet connected. A more holistic approach should therefore be undertaken not only between the scientific community and communities living in informal settlements (as already recommended via community-based

projects, e.g., Gaillard and Mercer, 2013) but also between scientific communities that analyse different social, physical, political and economic aspects of informal settlements. A mechanism to promote such integration could be, for example, to create an open access global database of slums data and maps, which would facilitate comparison and transfer of results across countries. Such cross-disciplinary exchange can identify interdependencies which can help to delineate possible solutions of complex problems, such as those associated with urban development of informal settlements.

### 5.3 Concluding remarks

Many studies on landslide hazard assessment have been published in the last century. However, very few of them focus on informal settlements, i.e. where landslide hazards have the highest impact. Amongst the reasons behind this limited amount of scientific research, is the lack of scientific methods that can deal with large uncertainties. In this thesis, a new approach is taken to address some of the scale and data gaps that hinder effective assessment of landslide hazard within informal settlements. The methodology introduced here balances the level of urban landslide process representation required with appropriate assumptions and simplifications, to develop a valuable tool for maximising the “actionable” knowledge (Aitsi-Selmi et al., 2015) that can be gained when data are scarce and future predictions uncertain. This methodology therefore sets the basis for bridging the current gap between science and effective mitigation actions in informal settlements, providing new scientific understanding of, and interdependencies between the natural and urban systems in contributing to landslide hazard, and producing innovative outputs useful for supporting hazard mitigation decisions for a more sustainable future within informal settlements.

## Appendix A – Supporting information for Chapter 2

### Appendix A1: Description of the new text files for running CHASM+

CHASM requires five input files to run:

- 1) Steering file: lists all the files considered for the simulation.
- 2) Soil file: defines hydraulic and mechanical properties of each soil type.
- 3) Geometry file: discretises the slope into a regular mesh. Each element of the mesh (cells) is assigned with dimensions (usually cells of 1x1m), and soil type. The water table height is defined as number of saturated cells, and the initial suction is specified on the top cell of each column.
- 4) Stability file: defines the stability method chosen (Bishop' or Janbu's stability method), the elements necessary to represent the slip search grid and the x-y coordinates of the slope profile.
- 5) Boundary conditions file: defines the boundary conditions (upslope recharge, detention capacity and max soil evaporation) as well as the frequency and duration of the precipitation event.

Two optional files are included in this analysis:

- 6) Vegetation file: defines the vegetation effect on slope hydrology and material strength.
- 7) Water leakage file: inserts point water sources to represent water leaks from superficial pipes and from buried septic tanks

To use the new CHASM+ (i.e. include surface water management and use the modified search grid) the steering file and the stability file need to be modified, and the new 'water leakage' file needs to be created. Below we give instructions on how this must be done.

Steering file. The steering file lists all the files considered for the simulation. The only modification regards the option for inserting the water leakage files. This can be done by removing the symbol '#'. If # is not removed, the text file is not read by the model.

```
geometry file:          geom.txt
soils database file:   soil.txt
stability file:       stab.txt
boundary conditions file: bond.txt
#waterleakage file:   wleak.txt
#vegetation file:     veg.txt
```

Figure A.1: Typical content of a steering file. CHASM reads the text files not preceded by the symbol #.



Water leakage file. The format of the new text file (left hand column) describing the surface water management is described in Table A.1.

Table A.1: Format of the new text file describing surface water management.

Format:	Notes:
Model_type: WATERLEAKAGE	Model name
Tank: 1	Activate tank (0 = no active; 1 = active)
Pipe: 1	Activate pipe (0 = no active; 1 = active)
Qtank: 2.0e-06	Leak from the tank (m <sup>3</sup> /s)
Qpipe: 2.0e-06	Leak from the pipe (m <sup>3</sup> /s)
Length: 2	Length (x wise) of the tank
House_type: 2	Type of roof: 1 = double pitch with gutters 2 = double pitch without gutters 3 = downslope single pitch without gutters 4 = downslope single pitch without gutters
Percent_no_Gutters: 10	Percentage of houses without roof gutters (%)
Depth^Type^Cell^P	Depth of tank (e.g. 3 m)
0 0 0 0	Type of leakage: 1 = evenly distributed 2 = localised
3 2 0 0	Cell: 0 when localised leakage is not in that cell 1 when localised leakage is that cell
3 2 1 0	P: 0 when pipe not discharging in that cell 1 when pipe discharging in that cell
0 0 0 1	
0 0 0 0	
...	
0 0 0 0	

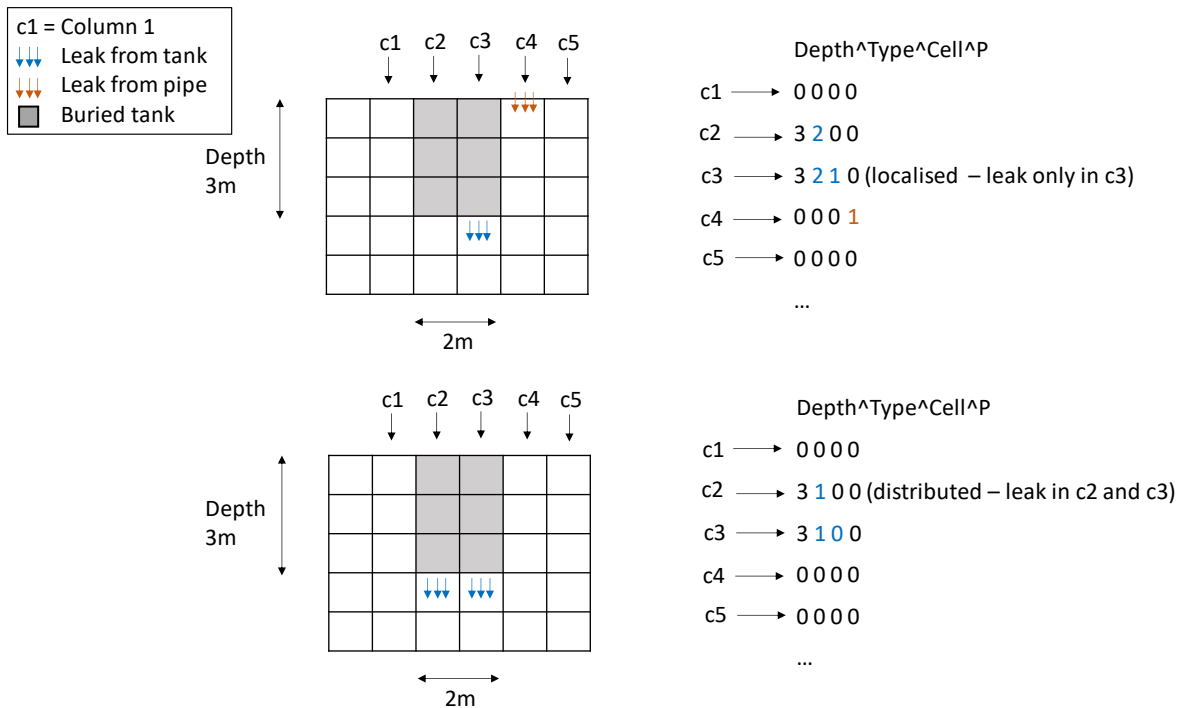


Figure A.2: Example in support of Table A.1.

Stability file. The format of the modified stability file for including the modified search grid is described in Table A.2.

Table A.2: Format of the new text file describing the modified search grid (the modifications are reported in italic)

<p><b>Format:</b> <i>BishopU</i></p> <p>41.2 23.4 1 1 10 48 39 0.5 1</p> <p>7</p> <p>0 28 2.9 26.6 11.96 22.42 ...</p>	<p><b>Notes:</b> <i>Bishop stability analysis – urban model</i></p> <p><b>Search grid parameters:</b> x and y cords for bottom left hand corner of search grid spacing between grid nodes in x and y direction (m) grid size in x and y direction <i>slope of the grid (NEW)</i> Initial radius Radius increment</p> <p>Number of slope surface coordinates specified (n)</p> <p><b>Slope surface coordinates:</b> x1, y1 x2, y2 ...</p>
--	--

## Appendix A2: Stochastic creation of input files to run CHASM

As explained in Chapter 2, we aim to generate thousands of slopes to run in CHASM+. Each slope is defined by a combination of input factors (geometrical, soil, urban and rainfall properties and initial hydrological conditions) which is generated by stochastically sampling from their probability distributions. Each combination of input factors then needs to be translated into a list of input files that CHASM+ can read to run the slope stability analysis (as those presented in Appendix A1). Seven input files are needed: steering, soil, geometry, stability, boundary conditions, vegetation and water leakage file (the description is given in Appendix A1). These input files are in a text format and they can be modified with any text editing software.

Given the large number of simulations required for the analysis, manual creation of the input files is unviable. We therefore automatically generate the input files using a Matlab code. Previous codes had been designed to include only the compulsory files (steering, soil, geometry, stability and boundary conditions). We therefore develop new functions to generate the vegetation and the water leakage files and we make some edits on the compulsory files to account for the presence of informal housing (e.g. modify the slope profile with cut slopes). In the following paragraphs the information needed to understand how to generate and modify the input files in the Matlab code is reported. For the sake of understanding, we remind the reader that the slope cross section in CHASM is divided into a regular mesh of columns and cells as shown in Fig.

A.3. The initial hydrological conditions defining the position of the water table and the surface matrix suction are specified as input data as well as the hydrological and geotechnical parameters per cell.

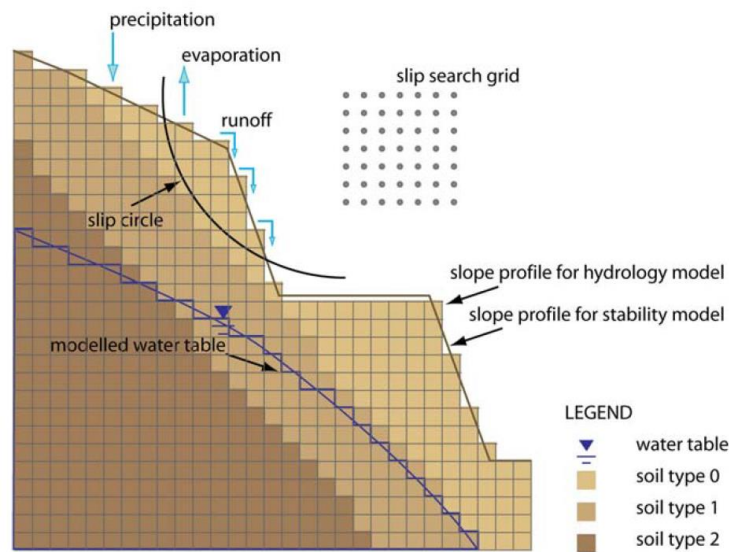


Figure A.3: Geometrical and process representation of CHASM (after Wilkinson 2000).

Informal housing on slopes is defined by input factors that are both varied and maintained fixed. The range or value of these input factors can be modified within the two main Matlab files:

- 1) Step1\_InputSampling\_VaryUrbanDegree
- 2) Generate\_input\_Urban (called by the previous script)

Within these two scripts, the modifications made to generate or modify the input files are reported and described in the following sections.

## A2.1 Geometry file

### Tasks:

- 
- Insert houses according to the urban density and urban expansion model
  - Modify the slope profiles when hill cutting is present
  - Modify the initial soil suction according to the water table height
- 

Table A.3 reports the input factors describing informal housing that are involved in the generation of the geometry file. Their combination defines the number of houses present on a slope and their position.

Table A.3: Input factors to be inserted to include cuts and/or houses on slopes. All the input factors in the table, their ranges and probability distributions, can be defined in Step1\_InputSampling\_VaryUrbanDegree.

Input factors required to include informal housing into the geometry file					
Stochastic input factors			Fixed input factors		
Name	Meaning	Range	Name	Meaning	Range
$\beta$	Angle of the cut	[0° - 89°]	$h_{max}$	Maximum height of the cut	Any
$H_d$	House density	[0% – 100%]	urban_model	Urban expansion model	[1-2-3]
Hwidth	House width	Any [m]	house_d cut_d	Space left unbuilt around the household	Any

The number of houses is calculated considering the length of the slope, the house density, and the total space that a single household occupies. Figure A.4 represents the house total footprint (letter f) for scenarios with hill cutting (1-2) and without (3).

The height of the cut is determined to accommodate entirely the house footprint, equal to the house width when its surrounding space (letter c) is fixed to zero. When the resulting height exceeds the maximum value ( $h_{max}$ ), this latter is imposed, and the house footprint is moved downslope accordingly (case 2 in Fig. A.4).

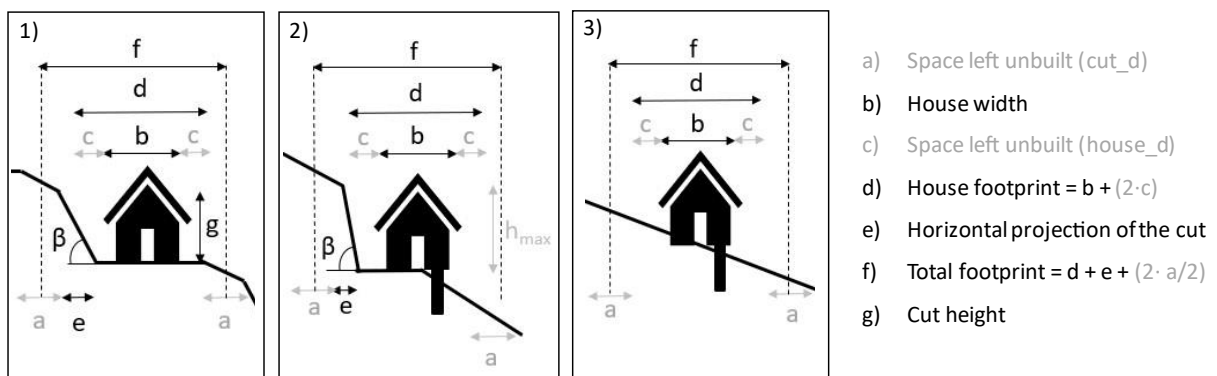


Figure A.4: representation of the input factors required for the representation of houses on slopes. The physical meaning of the letters are reported on the legend on the right hand side of the figure. The colour grey refers to those input factors that are treated as fixed within the Matlab code (as specified in Table A.3).

### A2.1.1 Modify coordinate of the slope profile when cut slopes are present

The geometry of the slope is defined by (x,y) coordinates. When cuts are present ( $\beta \neq 0$  and  $H_d \neq 0$ , Table A.4) the slope profile is modified, and the coordinates (x,y) of each cut slope instance are calculated (function: findCutSlopeCoord). Checks are undertaken to assess whether the underlying soil layers and water table

intersect the cuts. In this case, also the (x,y) coordinates of each intersection are calculated and used to adjust their profile. The function findHouseCoord detects and stores the (x,y) coordinates of each house's location. This will be used to change the soil properties underneath the houses (i.e. add the houses' weight).

### A2.1.2 Insert houses according to the selected urban expansion model

Houses are then inserted according to the urban expansion model chosen (urban\_model, in Table A.3). Figure A.5 shows the three possible ways a slope can get urbanised: starting from the bottom (urban\_model = 1), from the top (urban\_model = 2) or from the centre of the slope (urban\_model = 3).

The urban expansion models follow a progressive 'crowding up' process, explained by the numeration of the cuts in the figure. This assumes that each household prefers to maintain a certain distance from the neighbour when space is available. When the number of the households increases, the remaining terrain gaps get filled, progressively (over)crowding the slope.

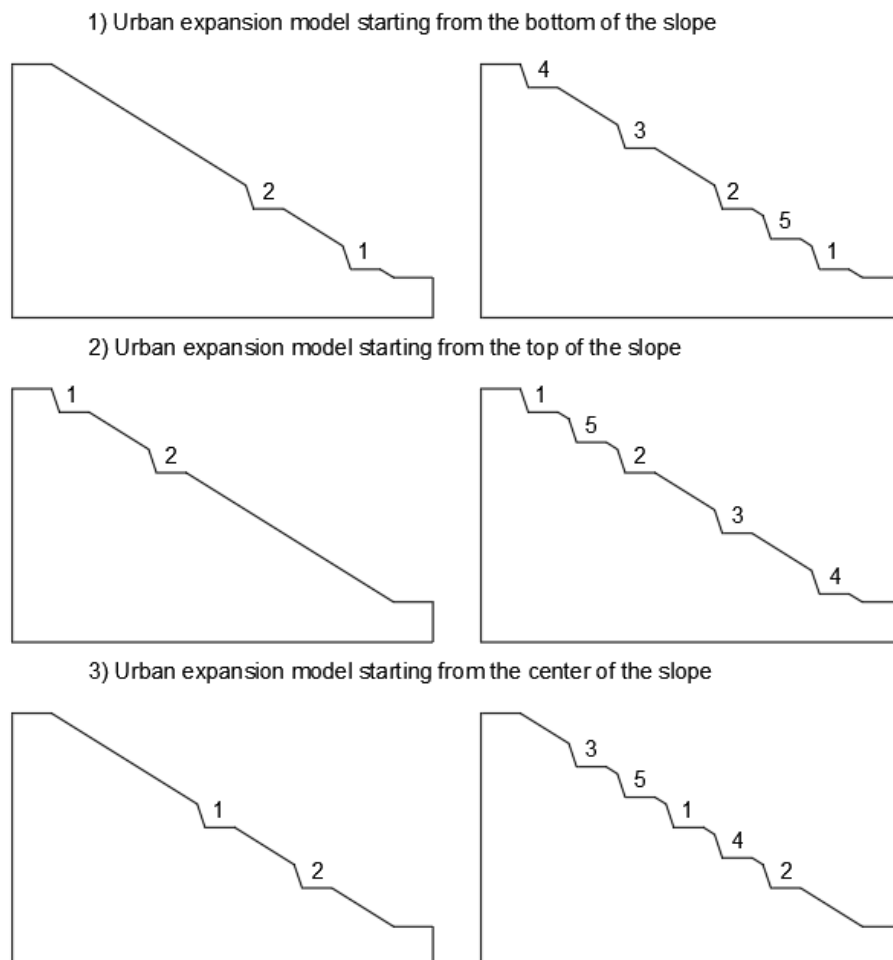


Figure A.5: representation of different urban expansion models (regulated by the input factor: urban\_model). The numbering shows how cut slopes are generated according to the urban model selected.

### A2.1.3 House loading

Each cell of each column of the slope mesh is defined by a soil type. An extra soil type is inserted in the soil file to simulate the presence of houses and the associated additional loading. Specifically, the soil underneath the house will have the same characteristics of the surrounding soil, except for a lower hydraulic conductivity and an increased dry unit weight. In this analysis, the influence of the house load on the underlying soil is considered uniform and limited to 1 metre depth (i.e. the soil properties are modified only on the cells immediately underneath the house). This can be adjusted, for example, by gradually reducing the loading pressure and the hydraulic conductivity with depth.

### A2.1.4 Modify the initial soil suction to maintain the water table height where initially set

In CHASM the initial soil suction is specified for each top cell of the slope and is used to determine the initial soil water moisture distribution in the unsaturated zone, prior to the first iteration of the dynamic hydrology function when the simulation starts. This is done by linearly decreasing the soil suction from its maximum value (assigned to the top cell) to zero, when the water table is reached (saturated soil; see the example of Fig. A.6). Each suction value corresponds to a moisture content value in the soil water characteristic curve (SWCC user-defined; Fig. A.6b), which is assigned to each cell of the slope. If a slope is high and the initial water table height relatively low, or the initial surface suction low, a great number of cells above the water table might have initial interpolated soil suction values smaller than the minimum suction imposed in the SWCC (for example, the soil suction of the cell above the water table in Fig. A.6a is equal to 0.062 m, which is smaller than the minimum suction imposed at -0.1 m in the SWCC of Fig. A.6b). This results in a saturated moisture content being assigned to those cells and the water table height automatically increases accordingly.

Example: initial suction = -0.5 m

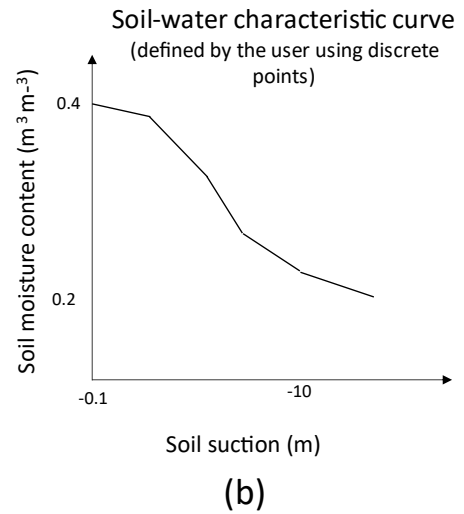
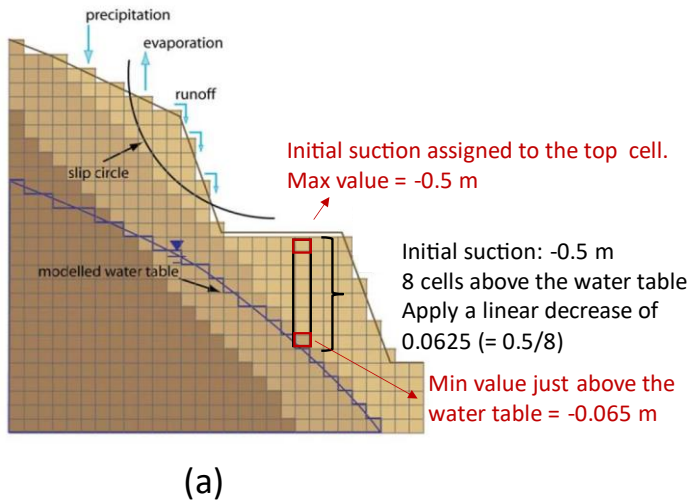


Figure A.6: (a) Example of slope with initial soil suction equal to -0.5 m. (b) Example of soil water characteristic curve (SWCC), user defined. The example shows that the cell above the water table is defined by an initial suction equal to -0.065 m which is smaller than the maximum value defined in SWCC (max value = -0.1 m). The maximum value of soil moisture content is then assigned to that cell, thus resulting saturated.

Soil suction is generally treated as a stochastic variable. Due to the randomness of the process, relatively high slopes with relatively low values of initial suction might be generated. In that case, a significant number of cells above the water table might result saturated, consequently increasing the initial water table height (as shown in Chapter 2, Section 2.4.2 while benchmarking CHASM+). This is a problem because the initial water table height of the slopes might not correspond to the initial water table height initially assigned in the stochastic process, losing the connection between inputs and outputs that we want to analyse. We therefore render the initial soil suction a function of the initial water table height. Soil suction ( $\varphi$ ) is still stochastically generated but it is equal to:

$$\varphi = \begin{cases} \varphi_i & \text{if } \varphi_c < \varphi_{\max} \\ \varphi_{\max} \cdot n & \text{if } \varphi_c > \varphi_{\max} \end{cases} \quad (\text{A2.1})$$

$\varphi$  = soil suction assigned to the top cell (m)

$\varphi_i$  = soil suction stochastically generated (m)

where:  $\varphi_c$  =  $\varphi_i/n$  where  $n$  is the number of cells above the water table

$\varphi_{\max}$  = maximum suction value in SWCC (m)

If the final  $\phi$  is greater than 40 kPa (4 m), the assumption at the base of Darcy's law are not satisfied (Lloyd, 1990) and the generated slope is discarded.

Figure A.7 gives a reference list of the functions where the processes described in the previous sections can be found.

```
Generate_input_Urban:
  • Calculate number of houses on the slope, according to the urban density and house total footprint

findHouseCoord:
  • Calculate and store the (x,y) coordinate of the houses' position

findCutslopeCoor:
  • Calculate and store the (x,y) coordinate of the slope profile when cuts are present
  • Calculate and store the (x,y) coordinates also of the underlying soil layers and water table in the case they intersect the cuts

Write_geom:
  • Insert a different soil type where houses are located, i.e. at the (x,y) coordinates found with findHouseCoord
  • Modify the initial soil suction according to the water table height. If it results greater than 40kPa, abort
```

Figure A.7: List of functions in the Matlab code generating the new geometry file.

## A2.2 Vegetation file

### Task:

---

- Generate a new text file describing the vegetation properties
- 

Vegetation is stochastically inserted or not inserted on the slope. However, the vegetation properties are fixed. In the script `Step1_InputSampling_VaryUrbanDegree` vegetation gets activated by a Boolean: 1 vegetation is present; 0 vegetation is not present.

If cut slopes are present the input factor 'vegetation\_dist' allows to differently allocate vegetation:

- `vegetation_dist = 1`, the vegetation is removed from the cut slopes (which represent the case when trees are removed during urban construction activities)
- `vegetation_dist = 2` vegetation is left on the cut slopes (which can be the case of vegetation used for landslide hazard mitigation)



Details about the properties defining vegetation are given for example in available in report 'CHASM Input and Output files' and the values used in the analyses of this thesis are reported in Chapter 3 and 4. These vegetation properties can be modified within the Matlab function: `Generate_input_Urban`.

```
Generate_input_Urban:
  • Set up parameters necessary to write the vegetation file

Write_veg:
  • Detect whether vegetation needs to be inserted
  • Detect whether vegetation needs to be inserted on the cut or not
  • Write text file
```

Figure A.8: List of functions in the Matlab code generating the new vegetation file.

## A2.3 Water leakage file

### Task:

---

- Generate a new text file describing slope water management: new water leakage file
- 

CHASM+ can represent leaking buried tank and superficial pipes as well as roof gutters on houses (Fig. A.9). To activate these processes in the slope stability analysis, the new water leakage input file needs to be present (see Appendix A1). Table A.4 lists the input factors necessary to automatically generate it. Stochastic input factors define the percentage of houses without gutters, and the percentage of houses with leaking pipes and tanks. The leak rate ( $\text{m}^3 \text{s}^{-1}$ ) is fixed as well as the tanks' dimensions. The variable 'house\_type' describes the type of roof. This can be double or single pitch (Fig. A.9, lower panel 2). The house type can also be used to determine whether the houses have gutters or not without using the percentage: if the house\_type is equal to 1 then all houses on slope have gutters; if it is equal to 2, 3 or 4, then all houses have no gutters (2 = double pitch; 3 = downslope single pitch; 4 = upslope single pitch).

Currently, the Matlab scripts automatically place the septic tanks underneath the house, whereas the pipe discharges on the side the house, as shown in Fig. A.9, upper panel 1. Details on the format of the new water leakage files are given in Appendix A1.

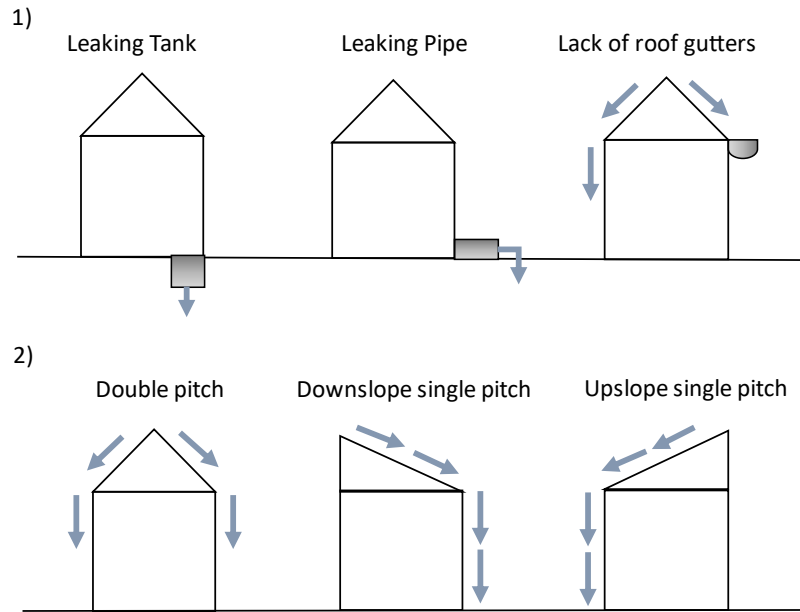


Figure A.9: representation of possible options that can be inserted to model water management at household scale

Table A.4: input factors that define the water management options shown in Fig. A.9

Input factors required to include informal housing into the geometry file					
Stochastic input factors			Fixed input factors		
Name	Meaning	Range	Name	Meaning	Range
%no_Gutters	% of houses without roof gutters	[0% - 100%]	House_type	Roof type	[1-2-3-4]
%leaking_pipe /tank	% of houses with leaking pipes and tanks	[0% - 100%]	width-Depth	Dimensions of the tank	Any
Tank	Activate tank	[0-1]	Qpipe	Leak from each pipe	Any
Pipe	Activate pipe	[0-1]	Qtank	Leak from each tank	Any

#### Generate\_input\_Urban:

- Set up parameters necessary to write the water leak file

#### Write\_leak:

- Detect whether tank and pipe leaks are active
- Read tank dimensions
- Read percentage of houses without gutters
- Insert the tank underneath the house. Insert the pipe on the side of the house. This is determined by using the house coordinated calculated in the geometry file
- Write text file

Figure A.10: List of functions in the Matlab code generating the new water leakage file.

## A2.4 Modify the stability file to include the new search grid

The Bishop's circular stability analysis in CHASM employs an automatic search of the slip surface with minimum Factor of Safety (FoS). The search grid location and size as well as the initial radius and radius increment of the circular slip surface are specified by the user. The search procedure is then automatically carried out in successive steps: the slip circle is centred on each generated grid points and the shear and strength forces are calculated along the slip surfaces generated at each radius increment. When all the available grid nodes have been tested, only the absolute minimum FoS is given as output.

To detect slip surfaces with both small and large slip circle radii, the grid dimensions have been modified to extend the grid search (see Section 2.2.1 of Chapter 2). An example is shown in Fig. A.11. A new function is then developed in the stability routine of CHASM+ that indicate when to activate such changes.

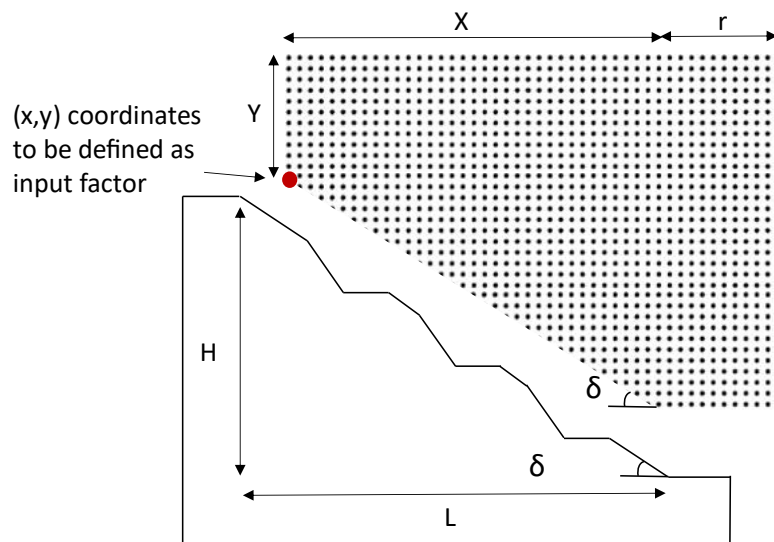


Figure A.11: representation of the new search grid, modified to look for both small and large slip surfaces.

In the stability input file, the  $(x, y)$  coordinates of the highlighted vertex (red point), the  $X$ - $Y$  dimensions of the grid, the space between the nodes and the radius increment of the circular slip surface need to be specified. The  $X$  dimension, which determines the length of the tilted portion of the grid, should be set in a way that avoids the slope profile intersection. An extra horizontal portion of the grid ' $r$ ' in Fig A.11 will be automatically added in CHASM+ (set at 15 m). An example of the new stability file is presented in Table A.2. If CHASM+ reads in the format name 'BishopU' (Bishop Urban) rather than 'Bishop', the new grid is generated.

## Appendix B – Supporting information for Chapter 3

This appendix is part of the supplementary material of a published work:

*Bozzolan, E., Holcombe, E., Pianosi, F. and Wagener, T.: Including informal housing in slope stability analysis – an application to a data-scarce location in the humid tropics, Nat. Hazards Earth Syst. Sci. Discuss., 1–20, doi:10.5194/nhess-2020-207, 2020.*

### Appendix B1: CART performance without auxiliary variables

Figure B.1 shows the percentage of misclassified simulations (i.e. the cross-validation error) for different pruning levels for the non-urbanised (a) and the urbanised case (b) when auxiliary variables are not considered. In these cases, the minimum validation error is obtained for pruning level 123 and 143 respectively ('absolute minimum' in red), which correspond to trees with 219 and 269 nodes. The arrows in the figures point to the pruning levels used to construct the CARTs with auxiliary variables (A.V.), shown in Chapter 3, Fig. 3.9a and 3.9b. If the auxiliary variables were not considered, the misclassification errors at these pruning levels would be respectively 16.7% and 17.6%, instead of 13.4% and 14.4% (as shown in Fig. B.3).

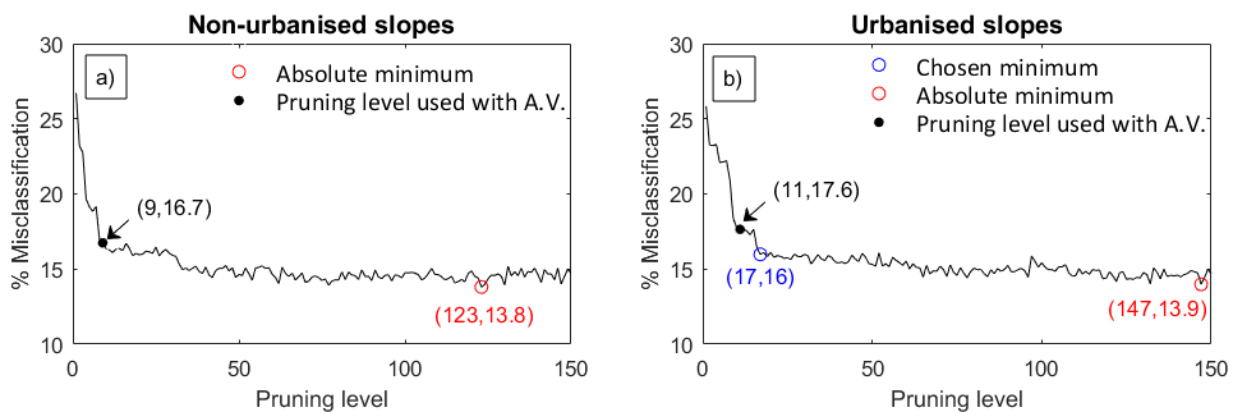


Figure B.1: Cross-validation error of the CART for increasing pruning level for non-urbanised (a) and urbanised (b) slopes. The cross-validation error is computed by randomly dividing the dataset in 10 subgroups. Ten trees are then constructed by using 9 subgroups as training set. The excluded subgroup is used to calculate the misclassification error (in percentage). The average value of the ten misclassification errors so obtained gives the cross-validation error (at given pruning level). The 'chosen minimum' (in blue) represents the pruning level and corresponding misclassification error to build the CART in Fig. B.2; in black (values pointed by the arrows), the pruning level used to build the trees reported in the Chapter 3 (Fig. 3.9 a and b) and the corresponding misclassification error resulted if the auxiliary variables (A.V.) were not considered.

Figure B.2 shows the CART obtained without considering the auxiliary variables (pruning level 17 and 16% misclassification error – ‘Chosen minimum’ in Fig. B.1). The thickest branches of the tree show for which critical thresholds of the input factors the majority of simulated slopes failed (black branch) or did not fail (grey branch). The majority of failed simulations in this case, occur for values of effective cohesion of layer 1 less than 12.4 kPa, rainfall intensities greater than 32.7 mm h<sup>-1</sup>, thicknesses of layer 1 (residual soil) more than 1.9 m, and rainfall durations greater than 5 h.

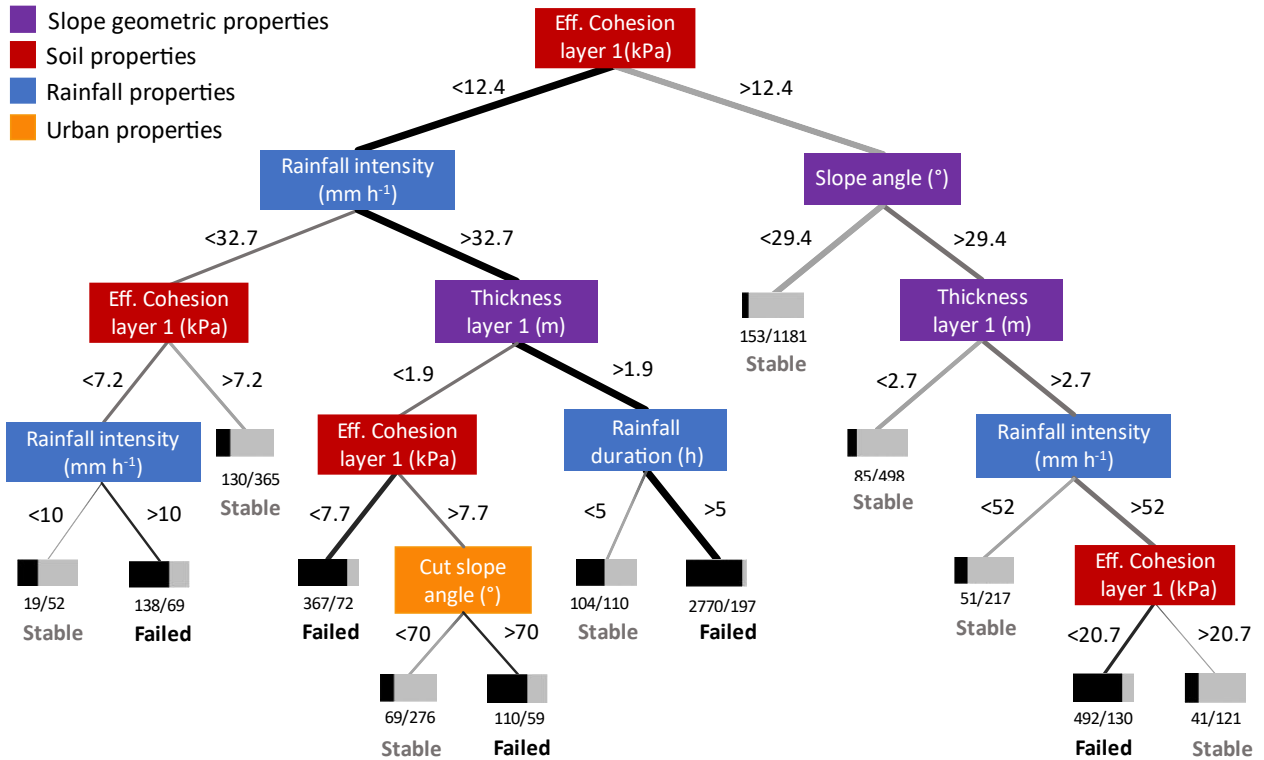


Figure B.2: CART tree obtained for urbanised slopes without considering auxiliary variables. Black branches represent the paths that lead to simulations predicted as failed, while grey branches lead to simulations predicted as stable. The bar under each leaf shows the proportion of simulations that resulted as failed (black) or stable (grey) for that leaf. The thickness of the branch is proportional to the number of simulations following that path. The pruning level used is 17, with 16% simulations misclassified (Fig. B.1).

Almeida et al. (2017) showed how cohesion and thickness of layer 1 as well as rainfall intensity and duration interact to produce slope failures. Two auxiliary variables were introduced: the ratio between effective cohesion and thickness of layer 1 and the negative ratio between the logarithm of rainfall intensity and rainfall duration. The misclassification error was similar (11%) with and without auxiliary variables, but the resulting trees had a much simpler structure. In this analysis, the misclassification error decreases of 1.91% (from 17.64% to 15.73% at pruning level 11) when these two auxiliary variables are considered.

We introduce a third auxiliary variable: a weighted average of the natural and the cut slope angles (Eq. B.1). The weights are represented by the sensitivity indices reported in Fig. 3.7 of Chapter 3 ( $w_1 = 0.15$  for slope angle;  $w_2 = 0.13$  for cut slope angle).

$$\text{Weighted Slope Angle} = \frac{w_1 * (\text{Slope angle}) + w_2 * (\text{Cut slope angle})}{w_1 + w_2} \quad (\text{B.1})$$

Weighted slope angles consider that slope susceptibility can significantly increase for low natural slope angles but high cut slopes angles. We use the sensitivity indices as weights to reflect that the natural slope angles resulted more influential than cut slope angles. An averaged sum of the two input factors would result from equal weights. In this last case, the reduction in misclassification error would be 0.3%. When the sensitivity indices are considered as weights, the reduction increases to 1.3% (from 15.73% found introducing the first two auxiliary variables to 14.4%). The weighted slope angle presented in Eq. (B.1) is therefore better performing and it is used for the CART analysis in Chapter 3.

## Appendix B2: CART pruning

We use cross-validation to avoid overfitting. Figure B.3 shows the percentage of misclassified simulations (i.e. the cross-validation error) for different pruning levels for the not urbanised and the urbanised case. The minimum validation error is obtained for pruning level 83 and 69 respectively ('absolute minimum' in red), which correspond to trees with 145 and 116 nodes. We choose much simpler trees with pruning level 9 and 11 ('chosen minimum'). These correspond to cross-validation error of 13.4% and 14.4% respectively for the two cases.

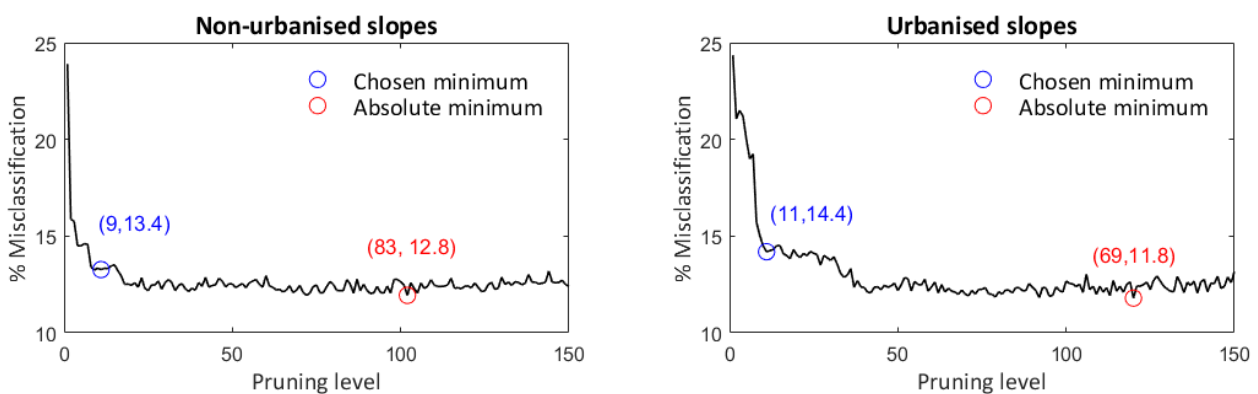


Figure B.3: Cross-validation error of the CART for increasing pruning level. The cross-validation error is computed by randomly dividing the dataset in 10 subgroups. Ten trees are then constructed by using 9 subgroups as training set. The excluded subgroup is used to calculate the misclassification error (in percentage). The average value of the ten misclassification errors so obtained gives the cross-validation error (at given pruning level).

## Appendix B3: Calculation of the rainfall threshold by multi-objective optimisation

Figure B.4 shows the slopes simulated as failed (black) and stable (grey), plotted on log-log axes of associated rainfall intensities ( $I$ ) and durations ( $D$ ). The plot shows a descending trend according to which landslides are more likely to occur for high-intensity short-durations rainfall events, and for long-duration low-intensity rainfall events. This relationship is observed in landslide inventories and it is widely used to generate rainfall empirical thresholds for landslides prediction and landslide warning systems (see Segoni et al., 2018, for a review on the topic). Intensity duration thresholds are the most common type of thresholds that can be found in literature (Guzzetti et al., 2007), and they identify the intensity-duration combinations below which landslides are not expected to occur. Intensity duration thresholds are generally expressed by a power law  $I = \gamma D^\alpha$  (Guzzetti et al., 2007) which in logarithmic axis becomes:

$$\log_{10}(I) = \gamma - \alpha \log_{10}(D) \quad (\text{B.2})$$

i.e. a linear equation where  $\gamma$  (the intercept) and  $\alpha$  (the slope) are parameters specific to the site considered.

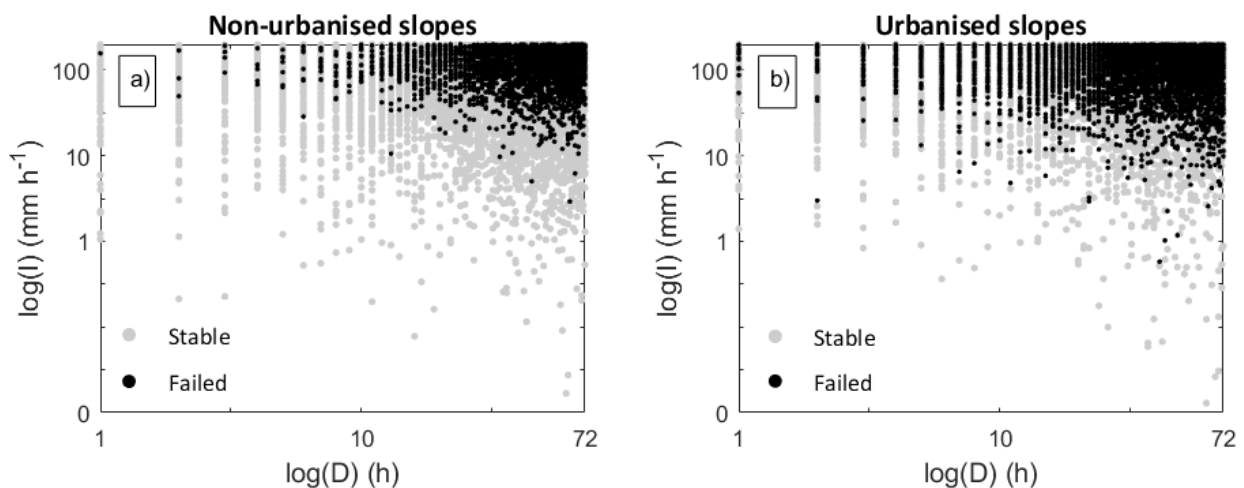


Figure B.4: Combinations of rainfall intensities ( $I$ ) and durations ( $D$ ) resulted into stable (grey dots) or failed (black dots) slopes, for the non-urbanised (a) and urbanised (b) case. The plots show how the recorded landslides follow the typical descending trend found in empirical rainfall thresholds. The x and y axis are in logarithmic base 10, but the notation is linear for an easier readability.

To formalise the threshold that best divide failed from stable slopes, the parameters  $\gamma$  and  $\alpha$  of Eq. B.2 need to be evaluated. Different methods have been suggested to calculate these two parameters (see Table 3 in Segoni et al. 2018). Amongst these, statistical methods are widely employed because they provide objective and reproducible results (Brunetti et al., 2010; Perruccacci et al. 2012; Staley, 2013; Melillo et al. 2015; Piciullo et al. 2017; Perruccacci et al. 2017; Melillo et al. 2018). Frequentist methods showed to give satisfactory results for large datasets and allowed the definition of multiple minimum thresholds based on

different exceedance levels (Peruccacci et al., 2012; Brunetti et al., 2010; Melillo et al., 2018). This can be useful in setting different landslide warning levels, each based on different probability of landslides occurrence. However, frequentist methods result unsuitable for analysing our synthetic dataset because of the high frequency of slopes failed for high intensity and high duration events (which are usually not recorded in reality) would strongly bias the position of the threshold. We therefore suggest a new approach that employs:

- the combinations of rainfall intensity and durations resulted in landslides (black dots in Fig. B.4).
- a multi-objective optimisation algorithm for the estimation of the two parameters  $\gamma$  and  $\alpha$  of Eq. B.2.

The multi-objective optimisation involves minimising or maximising multiple objective functions subject to a set of constraints. In this case, we want to draw a threshold line in the form of Eq. B.2 which identifies the space where landslides are recorded. This translates into choosing parameters  $\gamma$  and  $\alpha$  of Eq. B.2 that satisfy the following two contrasting objectives:

- 1) maximise the number of (simulated) failed slopes falling above the threshold line (Fig. B.5a)
- 2) minimise the area above the threshold line (Fig. B.5b)

To constrain the search to realistic values of rainfall intensity and duration, the optimisation only explores values of  $\gamma$  and  $\alpha$  within upper and lower boundaries specified as:

$$\gamma [-0.5; -2] \tag{B.3a}$$

$$\alpha [0.05; 2] \tag{B.3b}$$

The range of  $\alpha$  so defined includes typical slope values of empirical rainfall thresholds (Guzzetti et al., 2007), while the range of  $\gamma$  is designed to include all the rainfall intensities simulated. To perform the multi-objective optimisation, we used the generic algorithm implemented in the ‘gamultiobj’ function of the Matlab Optimisation Toolbox (Mathworks, 2018). As any multi-objective optimiser, it produces a set of Pareto-optimal solutions that realise different optimal trade-offs of the two objectives. In this case, 13 possible optimal combinations of  $(\gamma, \alpha)$  are obtained, and among them we (subjectively) chose the one that gives a threshold line with 99.9% of failed simulations above it or, in other words, with 0.1% landslide probability below it. This is the threshold line reported in Fig. 3.10a,b of Chapter 3. A different choice could be made to determine the threshold line for any exceedance probability level. An alternative to this approach could be to use a (single-objective) optimization based on ROC (receiver operating characteristics), where false positives and negatives (represented in this case by the simulated landslides below the threshold and simulated stable slopes above the threshold) are minimised (Gariano et al., 2015; Staley et al., 2013).



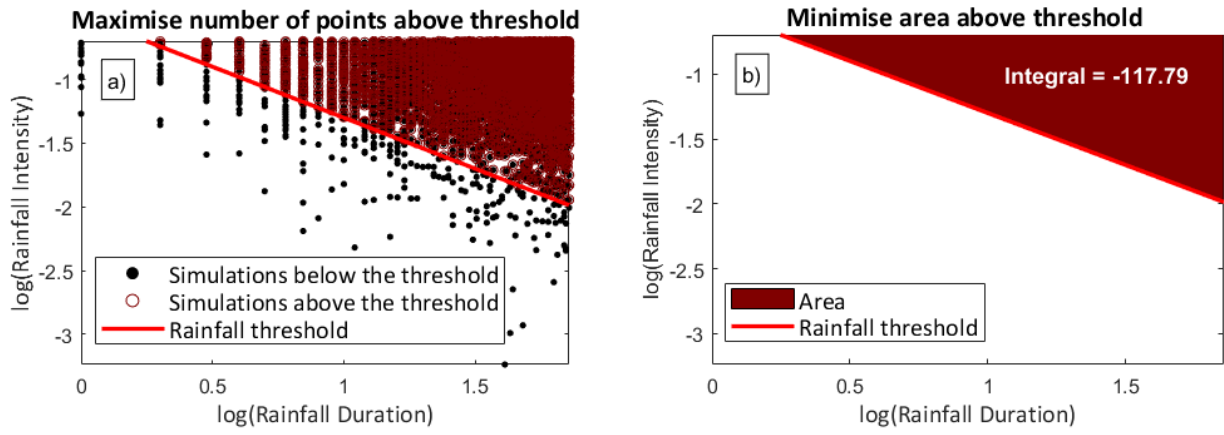


Figure B.5: Illustration of the two objectives functions used in the optimisation, for a given threshold line: (a) maximise the number of failed slopes above the threshold and (b) minimise the area above the threshold.

## Appendix C - Supporting information and results for Chapter 4

### Appendix C1: The influence of urban density on slope stability

The Global Sensitivity Analysis performed in Chapter 4, identified that variations of urban density significantly influence slope stability (Fig. 4.8). Here we define urban density as a percentage of the maximum possible housing cover, where for steeper slopes, cut slopes must occupy some of this surface cover. To identify for which values of urban density slope stability decreases, the 120,000 simulations are split into stable and failed according to the value of the minimum Factor of Safety (FoS respectively, greater or less than 1). Figure C.1a compares the percentage of slope failure between landcovers, whereas Fig. C.1b shows the percentage of slope failure at variations of percentage of urban density (from 0 to 100%). These two figures show that for urban densities less than 70% (Fig. C.1b), the failure rates of urbanised slopes are greater than those of natural slopes, i.e. greater than 25% of failure rate identified in Fig. C.1a for slopes with land cover forest, shrub and bare. For higher urban densities, failure rates instead decrease by up to 17%. Based on the observed effectiveness of community-based surface water management in the Caribbean (as reported in Anderson and Holcombe, 2013, for example) it has been shown that this effect can occur in high density informal communities where the impervious surfaces associated with houses (i.e. preventing rainwater infiltration to slope material) combined with the installation for roof guttering and rainwater harvesting from roofs, can compensate for the effects of potential household water leakages onto the slope. Thus, where more houses are present less rainwater can infiltrate into the soil.

Furthermore, the simulations generated here suggest that even when there are no roof gutters on houses there is a reduced likelihood of failure. This result requires careful interpretation because in the CHASM formulation such an effect could be because surface water runoff is not represented. In CHASM the amount of rainwater infiltrating into the slopes is at maximum equal to the soil infiltration capacity, and the exceedance gets removed from the simulation. As a result, fewer failures are simulated for high urban densities, potentially indicating an underprediction of landslide hazard when roof gutters are not present and rainfall intensity and duration are high. Nonetheless, even if these physical processes are not considered, these results are comparable to field observations within informal settlements. These field evidence suggest that in well-consolidated informal settlements (high urban densities), more rainfall is required to trigger slope failures, as less rainfall penetrates the slopes because of the paved and compacted surfaces (Smyth and Royle, 2000; Diaz, 1992). However, this is not the case in less-consolidated informal settlements (low to medium urban densities), where rainfall can infiltrate into slopes with fewer impediments. In this case, less

rainfall is required to reach the slope failure threshold than formal settlements (as demonstrated in Chapter 3, for 30% house coverage; (Smyth and Royle, 2000; Bozzolan et al., 2020).

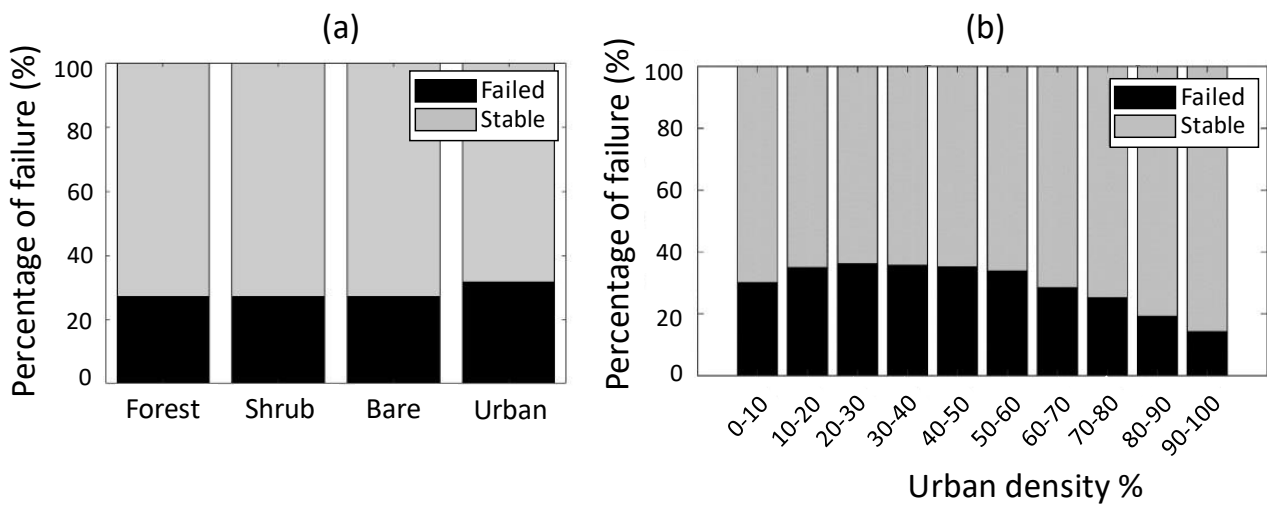


Figure C.1: Percentage of failure rates (a) between land covers and (b) for varying percentage of urban density.

## Appendix C2: Predict soil thickness by using inherently unstable slopes

The Regional Sensitivity Analysis (RSA) performed in Chapter 4 identifies thickness of the top strata of slope material (the soil, or 'layer 1', in the simulations) as one of the most influential input factors for slope stability. This is in line with the findings of a wide number of studies (Dietrich et al., 1995; Ho et al., 2012; Melchiorre and Frattini, 2012). Despite its importance, soil thickness is still not able to be effectively predicted across landscapes. This is mainly due to its high heterogeneity and to the lack of spatially distributed field data. Different models have been used to better understand soil thickness evolution within a catchment or bigger areas. The most commonly employed are mechanistic (process-based) and empirical-statistical models. Mechanistic models use mass balance equations of soil production versus soil transport to relate soil thickness and topography (Bonfatti et al., 2018; Dietrich et al., 1995); empirical and semi-empirical models, instead, statistically analyse the link between field-measured soil thicknesses and other potentially correlated factors (such as parent material, slope gradient and curvature) (Catani et al., 2010; Patton et al., 2018). When not much field information are available, proxies such as the wetness index are extrapolated from Digital Elevation Models (DEMs) are used to predict soil thickness (Lee and Ho, 2009; Ho et al., 2012). Regardless of the method adopted, there is a general consensus that soil thickness is strongly influenced by the landscape topography, with thick soils on shallower slopes and in valleys, and thin soils on steeper slopes and ridges (Heimsath et al., 1997; Patton et al., 2018).

In this analysis, we lack both sufficient field measurements and models for the prediction of soil thickness across the region. However, if we accept CHASM's ability to distinguish stable and unstable slopes in most cases (see Anderson, 1990) we have a significant number of slope stability analyses that can be used to quantify the relationship between slope angle and soil thickness. Specifically, we reanalyse the CHASM simulations that predicted failed slopes before the imposition of the rainfall event (i.e. slopes that are inherently unstable) to draw the threshold line that delimits 'possible' from 'impossible' slopes (e.g. thick soil layers on steep slopes, that would not be possible in reality). These simulation results have not been included in any of the other analyses reported in Chapters 3 and 4 because they had been filtered out during the first post-processing stage as being unrealistic.

Figure C.2 shows how these impossible slopes (black dots) are distributed according to slope angle and the natural logarithm of soil thickness so that the steeper the angle, the thinner the soil must be to ensure initial stability of the slope before rainfall occurs. This exponential decrease (linear in logarithmic scale) is in accord with observations worldwide based on measured soil thicknesses (Daleon and Lorenzo, 2018; Derosé et al., 1991; Salciarini et al., 2006). In particular, the figure shows that the logarithmic decrease of soil thickness appears to be linear for slopes with angles up to  $\sim 50^\circ$ , above which it decreases more steeply. Nonetheless, we assume a linear relationship for the whole range, also given the minor importance that very steep slopes have for potential urban expansion scenarios. A multi-objective optimisation algorithm is used to identify the 'optimal' threshold line that delimits the space where the impossible slopes are recorded. An optimal threshold is a trade-off between maximising the number of failed slopes above it and minimising the area above it to exclude outliers. The threshold line has the form:

$$\text{Ln}(H1) = a - b \cdot (\text{Slope angle}) \quad \text{C.1}$$

where H1 is the soil thickness of layer 1, whereas (a) and (b) are respectively the intercept and the slope of the threshold. To constrain the search to realistic values of soil thickness, the optimisation only explores values of (a) and (b) within upper and lower boundaries specified as:

$$a = [\text{Ln}(10), \text{Ln}(20)] \quad \text{C.2}$$

$$b = [0.025, 0.1] \quad \text{C.3}$$

The range for (b) is selected after visual inspection, to potentially include all the failed simulations above the threshold; the range of (a) is selected on the basis of soil depths measured for planar slope profiles (i.e. not convex or concave) using geophysical surveys in Saint Lucia (RRL, 1970; Holcombe, 2006) and from surveys in other regions of the Caribbean (Simon et al., 1990). To perform the optimisation, we use the 'gamultiobj' function of the Matlab Optimisation Toolbox (Mathworks, 2018). As with any multi-objective optimiser, the

function produces a set of Pareto optimal solutions that realise different optimal trade-offs of the two objectives. In this case, 30 possible optimal combinations of (a, b) are obtained. These are shown in Figure C.2 (red and grey lines). We choose a conservative mid threshold (th2), because its values are the most in line with the literature of the region, at least for slope angle lower than 50° (RRL, 1970, in Holcombe, 2006). The equation representing the relation between slope angle and soil thickness of layer 1 is therefore equal to:

$$H1 = \exp(2.91 - 0.04 \cdot (\text{Slope angle})) \tag{C.4}$$

This equation (C.4) is used to assign a conservative soil depth to each Slope Unit (SU) based on its angle as part of the process for creating the landslide hazard maps. To assess the mapping methodology a hazard map is generated representing the Hurricane Tomas rainfall event, for which there is a corresponding landslide inventory. As reported in Chapter 4, this map proved reasonably good at identifying the slopes most at risk with a Receiver Operating Characteristic (ROC) score of 0.69 (see also Fig. 4.10 in Chapter 4).

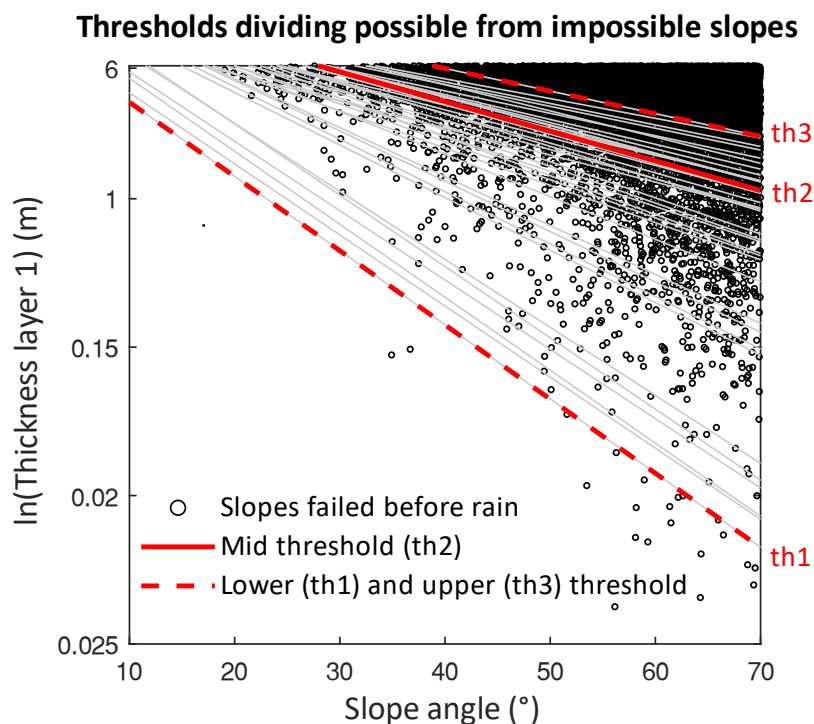


Figure C.2: Simulated slopes failed before the triggering event at variations of their slope angle and thickness of layer 1. The plots show how the recorded landslides follow a linear descending trend (i.e. exponential without the log. transformation) until ~50° for then decreasing more rapidly with steeper angles. The 30 thresholds obtained with the multi-objective optimisation tool are plotted in grey and red colour. The dashed red lines represent the lower and upper thresholds, with respectively 99% (lower th1), and 70% (upper th3) of simulations above them. The continuous red line is the threshold used in the analyses presented in Chapter 4. 85% of simulations are above this threshold and it is defined by equation C.4. The y axis of the figure is in logarithmic scale, but the notation is linear for an easier readability.

However, different soil depth thresholds could clearly lead to significantly different landslide hazard mapping results. In Fig. C.3, for example, we compare the hazard maps representing the Hurricane Tomas obtained using the lower, mid, and upper threshold of Fig. C.2 (th1, th2, and th3) and different cohesion values. Using the lower (upper) threshold, landslide hazard is low (high) regardless the soil cohesion adopted, as shown on the left (right) hand side column of Fig. C.3. The mid threshold is therefore a trade-off between the two and also gives estimated soil depths that are realistic compared with the (scarce) observations already mentioned. If detailed landslide inventories and soil cohesion data were available, this approach may help to have a better (physically-based) understanding of how soil thickness distributes across the region or within a given catchment. The hazard maps obtained with different thresholds can be compared to available landslide inventories and the threshold that maximise the map performance can be selected (e.g. choosing the threshold that maximise the area under the ROC curve of the map). In this analysis, the maximum performance (area under ROC curve = 0.71) was obtained with cohesion value equal to 8 kPa and the upper threshold (th3), which was considered to give overestimated soil thickness values. Such discrepancy might be due to the incompleteness of the landslide inventory used.

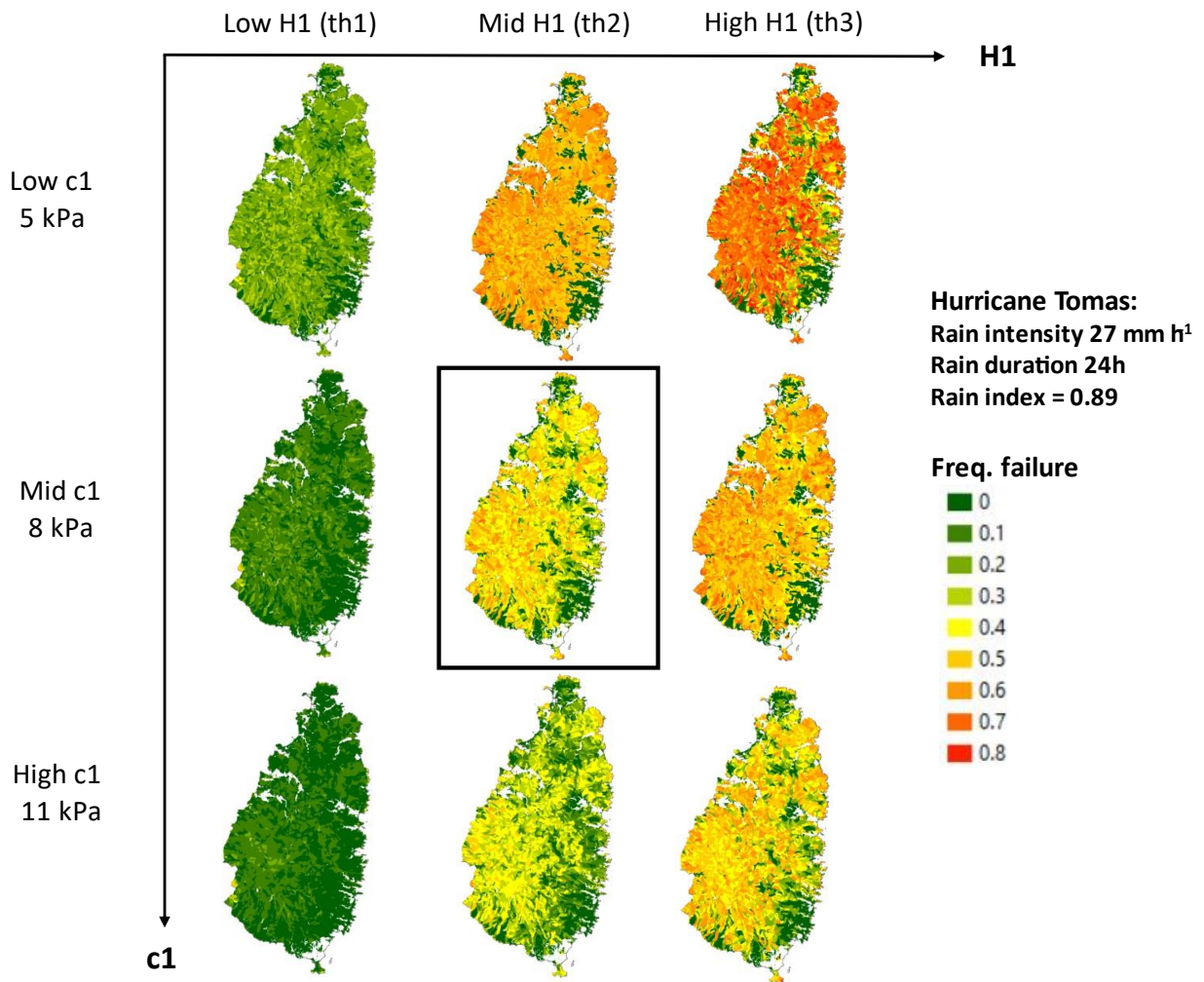


Figure C.3: Hazard maps representing the Hurricane Tomas (rain index = 0.89 – see Chapter 4), calculated using different cohesion and soil thickness values. Specifically, cohesion values equal to 8 – 5 – 11 kPa respectively represent the mode, and the mode  $\pm$  half standard deviation of the probability distribution of soil cohesion of layer 1 used for the stochastic sampling. The thresholds th1, th2, and th3 are respectively the lower, mid, and upper thresholds calculated with the optimisation algorithm and represented in Fig. C.2. The figure shows how the lower (higher) the threshold the lower (higher) the number of slopes predicted with high frequency of failure ( $\geq 0.5$ ). The framed map is the same shown in Chapter 4 (Fig. 4.10) calculated with the mid threshold (th2) and cohesion equal to 8 kPa.

### Appendix C3: Exponential relationships between the most influential input factors

Figure C.4 shows how the frequency of failure of the simulated slopes is distributed for variations and combinations of the most influential input factors, for the four different landcover scenarios considered. In all cases, the frequency of failure increases with slope angle, soil ratio (strata thickness divided by effective cohesion for layer 1 – the soil) and rain index (ratio between the logarithm of rainfall duration and intensity). Low frequency of failures ( $< 0.2$ ) are observed for slopes with angle less than  $30^\circ$ , soil ratio less than 0.5 and rain index less than 0.7 in all cases. These represent slopes with low susceptibility to landslides (Marchesini

et al., 2014). The region characterised by higher frequency of failure is divided from the region of low landslide susceptibility by an exponential trend. This trend appears in multiple dimensions. For example, high failure rates (defined as  $\geq 0.5$ ) show an exponential increase with rain index and slope angle (Fig. C.4, right hand column); however, if the rain index is deconstructed into rainfall duration and intensity, we note that failure rates also exponentially increase with these single input factors (Fig. C.5c). Figure C.5 shows the slope failure trends defined by variations of the most influential, individual input factors. To maintain stability, slopes with increasing natural angle have to exponentially reduce their soil thickness (Fig. C.5a) while slopes with increasing soil thickness has to linearly increase soil cohesion (Fig. C.5b). Finally, when rain duration increases, rain intensity has to exponentially reduce to not trigger a landslide (Fig. C.5c).

Such trends are commonly found empirically (Salciarini et al., 2006; Daleon and Lorenzo, 2018; Caine, 1980b; Larsen and Simon, 1993) indicating that CHASM gives realistic hydrological and stability responses to the rainfall forcing.



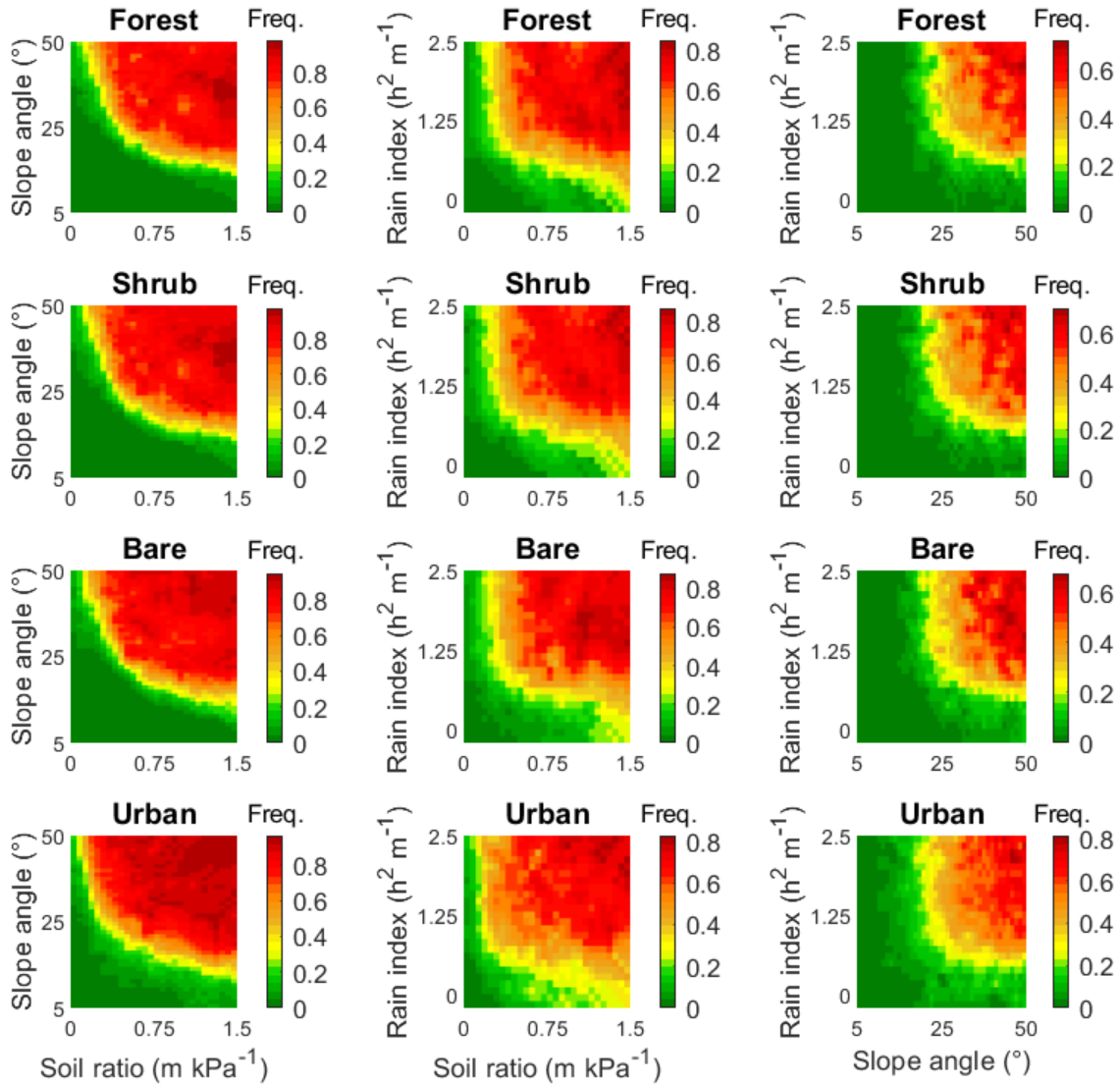


Figure C.4: Frequency of failure at variation of the most influencing combined input factors. Only slopes with angles below 50° are shown (urbanisation is not simulated for steeper slopes).

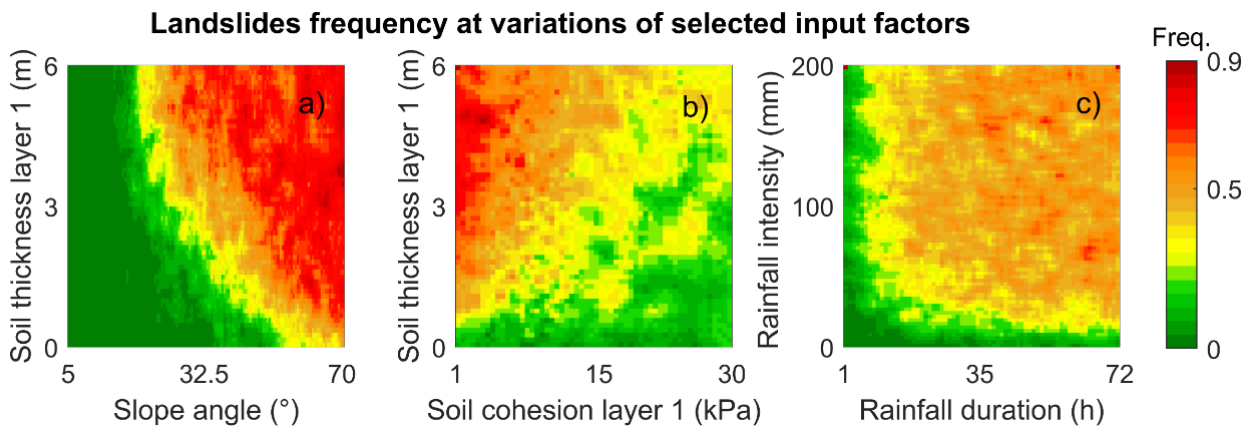


Figure C.5: Frequency of failure at variation of the most influencing non-combined input factors. The example represent the failure rates of forested slopes.

## Appendix C4: Differences in failure rates between land covers

Figure C.6 shows the difference in frequency of failure between the four land covers considered (forest, shrub, bare and urban) at variation of the most influential input factors. Darker colour identifies an increase in frequency of failure when the land cover is changed. As highlighted in Chapter 4, urban slopes (six panels at the bottom of Fig. C.6) present the highest increase in percentage of failures. Specifically, the frequency of failure increases by up to +40% for slopes with angles greater than  $25^\circ$  and soil ratio between 0.2 and 0.5, for any rainstorm severity and land cover. 20% more failures are also observed for rain index less than 0.6 and soil ratio greater than 0.4 (Fig. C.6m, p and s), i.e. on slopes with high susceptibility to failing (thick soil thickness or low cohesion values) but for not severe rainfall events. The difference in frequency of failure between slopes associated with forest, shrub and bare (top six panels) is less evident. Though, clusters of darker colour identify an increase of up to 25% when forest is replaced with shrub or bare land covers, for soil ratio greater than 0.5, slope angles greater than  $35^\circ$  and rain index less than 1 (Fig. C.6a, d, b, e, c and f). Forests therefore has a beneficial effect on the stability of slopes with relatively high susceptibility to failure (i.e. with steep angle, thick soil and/or low cohesion values) and for low to moderate rainfalls (i.e. all those characterised by rain ratio less than 1). On the other hand, there are no relevant change of failure rates between shrub and bare (Fig. C.6 g, h and i).

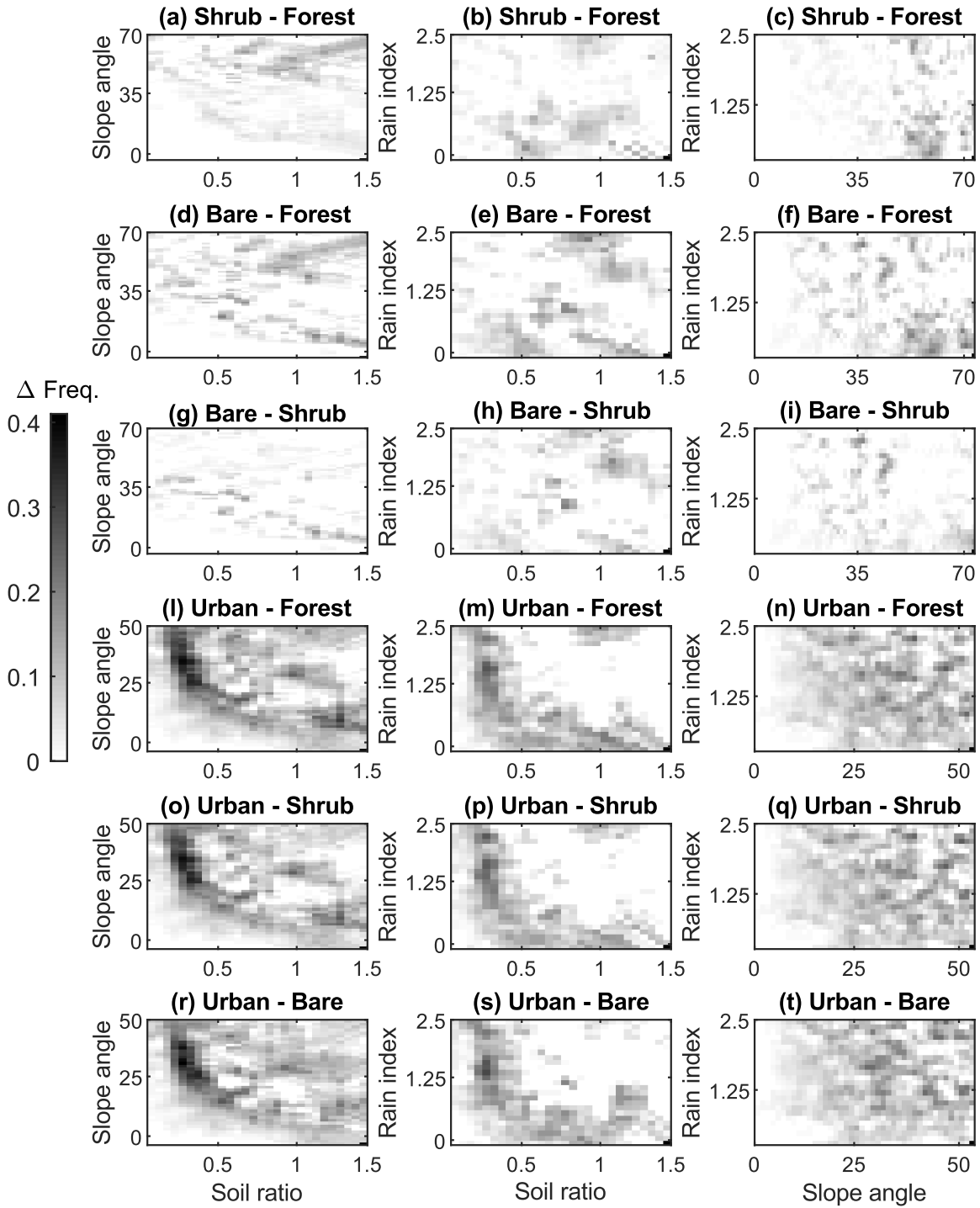


Figure C.6: difference in frequency of failure between the four land covers considered. The title of each plot defines the calculation made in the image subtraction (e.g. bare – forest: frequency of failure of bare slopes minus frequency of failure of forested slopes). The colour identifies the increase in landslide frequency (from 0 difference in white to 40% more failures in black).

## Appendix C5: Sensitivity rank for different classes of slope angle

In Chapter 4 a regional sensitivity analysis (RSA) is used to identify the input factors that most influenced slope stability at regional scale. To do so the whole variability space is considered (as defined in Table 4.1 of Chapter 4). The results show that slope angle is the most influential input factor, followed by the thickness and effective cohesion of layer 1 (i.e., the soil), rainfall duration and intensity. Shallow and steep slopes are expected to reach the same critical stability conditions ( $FoS \leq 1$ ) under different mechanical and hydrological forcing. This section explores how the sensitivity indexes change in their ranking (relative influence) when the range of slope angles is constrained (as was the case in the Chapter 3 analysis). Specifically, the simulated slopes from Chapter 4 are split into four categories: slopes with angle less than  $25^\circ$ , angles between  $25^\circ$  and  $35^\circ$ ;  $35^\circ$  and  $45^\circ$  and above  $45^\circ$ . The RSA is then applied to each of these categories.

The results are presented in Fig. C.7 for the four land covers considered: forest, shrub, bare and urban (represented in different shades). A high sensitivity index suggests that the variation of that input factor significantly influences slope stability. The figure shows that slope stability is insensitive to the majority of input factors and highly sensitive to just a few in all of the slope categories analysed. When comparing the different panels of the figure, the values of the sensitivity indexes are generally higher when angles are shallower (e.g.  $<25^\circ$  vs  $>45^\circ$ ). This is because shallow slopes are mostly inheritably stable unless adverse conditions for slope stability are imposed, making the slope's stability response particularly sensitive to variations of the input factors that determine those conditions. For example, slope angle has a high sensitivity index only in the first top panel because when it increases from  $5^\circ$  to  $25^\circ$ , slope stability rapidly decreases; failure rates are instead more similar ( $>50\%$ ) for angles between  $45^\circ$  and  $70^\circ$ , leading to lower value of sensitivity index (bottom panel of Fig. C.7).

This also means that errors or uncertainties of input factors whose variation rapidly change the frequency of slope failure can lead to wider inaccuracies in the landslide hazard assessment. Since soil thickness of layer 1 presents a high sensitivity index across all slope angle categories, its evaluation influences the accuracy of landslide hazard assessment across the whole region. Soil cohesion of layer 1 also presents high sensitivity index, but it decreases with slope angles ( $>35^\circ$ ). In fact, the stability of steep slopes ( $>45^\circ$ ) is mostly regulated by the slope geometry (soil thickness of layer 1) and by the rainfall properties. Susceptibility and hazard maps with scarce soil strength information are therefore likely to give more accurate results on steep, rather than shallow slopes. Finally, the sensitivity of slopes to the urban input factors (orange bars) is relatively high only on slopes with angles less than  $35^\circ$ . This would suggest the particular importance of including the presence of informal housing in landslide hazard assessments when such slopes are analysed.

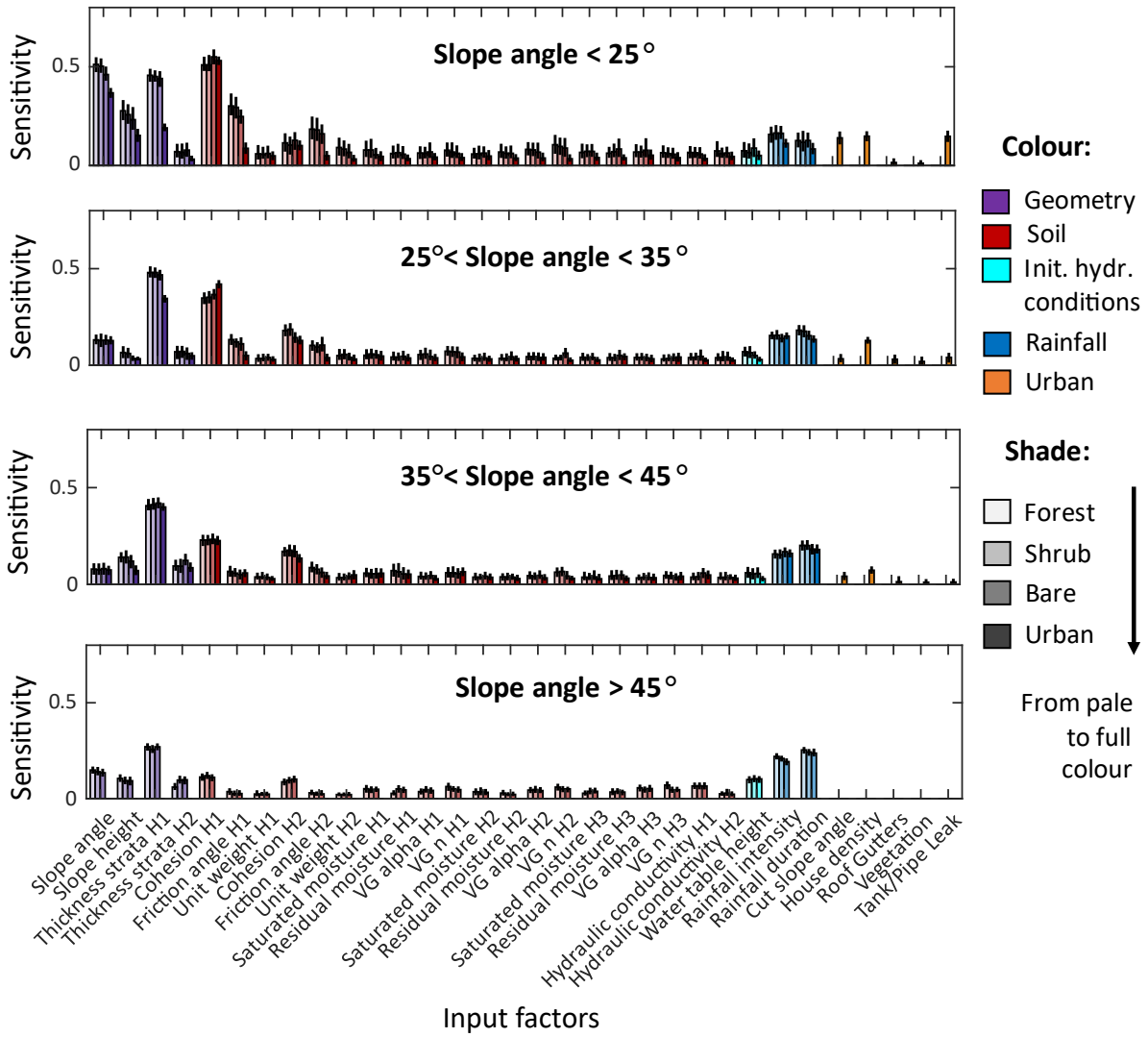


Figure C.7: Sensitivity index for each input factor in the 4 slope angle categories and land covers considered. The bars correspond to the mean value of sensitivity for each input factor calculated with bootstrapping, while the black vertical lines at the top of the bars represent the confidence interval (Number of bootstrap resampling  $N = 100$ ; significance level for the confidence intervals 0.05).

# Bibliography

- Abraham, A. and Rock, R.: Landslide inventory map for Hurricane Tomas in Saint Lucia, Digit. map, available from [http://www.charim-geonode.net/layers/geonodelandslides\\_2010](http://www.charim-geonode.net/layers/geonodelandslides_2010), 2010.
- Alcántara-Ayala, I.: Geomorphology, natural hazards, vulnerability and prevention of natural disasters in developing countries, 47, 107–124, [https://doi.org/10.1016/S0169-555X\(02\)00083-1](https://doi.org/10.1016/S0169-555X(02)00083-1), 2002.
- Alexander, D.: Urban landslides, *Prog. Phys. Geogr. Earth Environ.*, 13(2):157-, <https://doi.org/10.1177/030913338901300201>, 1989.
- Almeida, S., Ann Holcombe, E., Pianosi, F., and Wagener, T.: Dealing with deep uncertainties in landslide modelling for disaster risk reduction under climate change, *Nat. Hazards Earth Syst. Sci.*, 17, 225–241, <https://doi.org/10.5194/nhess-17-225-2017>, 2017.
- Alvioli, M., Marchesini, I., Reichenbach, P., Rossi, M., Ardizzone, F., and Fiorucci, F.: Automatic delineation of geomorphological slope units with r . slopeunits v1 . 0 and their optimization for landslide susceptibility modeling, 3975–3991, <https://doi.org/10.5194/gmd-9-3975-2016>, 2016.
- Alvioli, M., Melillo, M., Guzzetti, F., Rossi, M., Palazzi, E., Hardenberg, J. Von, Teresa, M., and Peruccacci, S.: Science of the Total Environment Implications of climate change on landslide hazard in Central Italy, *Sci. Total Environ.*, 630, 1528–1543, <https://doi.org/10.1016/j.scitotenv.2018.02.315>, 2018.
- Anagnostopoulos, G. G., Fatichi, S., and Burlando, P.: An advanced process-based distributed model for the investigation of rainfall-induced landslides: The effect of process representation and boundary conditions, *J. Am. Water Resour. Assoc. Resour. Assoc.*, <https://doi.org/10.1111/j.1752-1688.1969.tb04897.x>, 2015.
- Anderson, M., Holcombe, L., Flory, R., and Renaud, J. P.: Implementing low-cost landslide risk reduction: A pilot study in unplanned housing areas of the Caribbean, *Nat. Hazards*, 47, 297–315, <https://doi.org/10.1007/s11069-008-9220-z>, 2008.
- Anderson, M. G.: Mid-Levels Study. Report on Geology, Hydrology and Soil Properties, Geotech. Control Off. Civ. Eng. Serv. Dep. Hong Kong, 1982.
- Anderson, M. G.: Road-cut slope topography and stability relationships in St Lucia, West Indies, *Appl. Geogr.*, 3, 105–114, [https://doi.org/10.1016/0143-6228\(83\)90033-4](https://doi.org/10.1016/0143-6228(83)90033-4), 1983.
- Anderson, M. G.: A feasibility study in mathematical modelling of slope hydrology and stability, Report to Geotechnical Control Office Civil Engineering Services Department, Hong Kong, 1990.
- Anderson, M. G. and Holcombe, E.: Community-based landslide risk reduction: managing disasters in small steps, The World Bank, 2013.
- Anderson, M. G. and Holcombe, L.: Sustainable landslide risk reduction in poorer countries, *Proc. Inst. Civ. Eng. Eng. Sustain.*, 159, 23–30, <https://doi.org/10.1680/ensu.2006.159.1.23>, 2006.
- Anderson, M. G. and Howes, S.: Development and Application of a Combined Soil-Water Slope Stability Model, *Q. J. Eng. Geol.*, 18, 225–236, 1985.
- Anderson, M. G. and Kemp, M. J.: The Prediction of Pore Water Pressure Conditions in Road Cut Slopes, St Lucia, West Indies., Final Tech. Report. Overseas Dev. Agency., 1985.
- Anderson, M. G. and Lloyd, D. M.: Using a combined slope hydrology-stability model to develop cut slope design charts, *Proc. - Inst. Civ. Eng. Part 2. Res. theory*, 91, 705–718, [https://doi.org/10.1016/0148-9062\(92\)90903-d](https://doi.org/10.1016/0148-9062(92)90903-d), 1991.

- Anderson, M. G., Holcombe, E., Blake, J. R., Ghesquire, F., Holm-nielsen, N., and Fisseha, T.: Reducing landslide risk in communities : Evidence from the Eastern Caribbean, *Appl. Geogr.*, 31, 590–599, <https://doi.org/10.1016/j.apgeog.2010.11.001>, 2011.
- Arnone, E., Dialynas, Y. G., Noto, L. V, and Bras, R. L.: Accounting for soil parameter uncertainty in a physically based and distributed approach for rainfall-triggered landslides, 944, 927–944, <https://doi.org/10.1002/hyp.10609>, 2016.
- Barnard, P. L., Owen, L. A., Sharma, M. C., and Finkela, R. C.: Natural and human-induced landsliding in the Garhwal Himalaya of Northern India, 40, 21–35, [https://doi.org/10.1016/S0169-555X\(01\)00035-6](https://doi.org/10.1016/S0169-555X(01)00035-6), 2001.
- Baum, B. R. L., Savage, W. Z., and Godt, J. W.: TRIGRS — A Fortran Program for Transient Rainfall Infiltration and Grid-Based Regional Slope-Stability Analysis, 2002.
- Van Beek, L. P. H. and Van Asch, T. W. J.: Regional assessment of the effects of land-use change on landslide hazard by means of physically based modelling, *Nat. Hazards*, 31, 289–304, <https://doi.org/10.1023/B:NHAZ.0000020267.39691.39>, 2004.
- Van Beek, R.: Assessment of the influence of changes in land use and climate on landslide activity in a Mediterranean environment, 29-363 pp., 2002.
- Bello, A. A.: Reliability Assessment of Reddish Brown Tropical Soil as a Liner Material Reliability Assessment of Reddish Brown Tropical Soil as a Liner Material, <https://doi.org/10.1007/s10706-012-9558-6>, 2015.
- Bellugi, D., Milledge, D. G., Dietrich, W. E., Perron, J. T., and Mckean, J.: *Journal of Geophysical Research : Earth Surface*, <https://doi.org/10.1002/2015JF003520>.Received, 2015.
- Ben-Haim, Y.: *Info-gap decision theory: decisions under severe uncertainty*, Elsevier, 2006.
- Bernardie, S., Vandromme, R., Thiery, Y., Houet, T., Grémont, M., Masson, F., Grandjean, G., and Bouroullec, I.: Modelling landslide hazard under global change: the case of a Pyrenean valley, *Nat. Hazards Earth Syst. Sci.*, 1–34, <https://doi.org/10.5194/nhess-2019-311>, 2020.
- Beven, K.: Facets of uncertainty: Epistemic uncertainty, non-stationarity, likelihood, hypothesis testing, and communication, *Hydrol. Sci. J.*, 61, 1652–1665, <https://doi.org/10.1080/02626667.2015.1031761>, 2016.
- Beven, K., Almeida, S., Aspinall, W. P., Bates, P. D., Blazkova, S., Borgomeo, E., Freer, J., Goda, K., Hall, J., Phillips, J. C., and others: Epistemic uncertainties and natural hazard risk assessment-Part 1: A review of different natural hazard areas, *Nat. hazards earth Syst. Sci.*, 18, 2741–2768, 2018.
- Bishop, A. W.: The use of the Slip Circle in the Stability Analysis of Slopes, 5, 7–17, <https://doi.org/10.1680/geot.1955.5.1.7>, 1955.
- Bogaard, T. A. and Greco, R.: Landslide hydrology: from hydrology to pore pressure, *Wiley Interdiscip. Rev. Water*, 3, 439–459, <https://doi.org/10.1002/wat2.1126>, 2016.
- Bonfatti, B. R., Hartemink, A. E., Vanwalleghe, T., Minasny, B., and Giasson, E.: A mechanistic model to predict soil thickness in a valley area of Rio Grande do Sul, Brazil, *Geoderma*, 309, 17–31, <https://doi.org/10.1016/j.geoderma.2017.08.036>, 2018.
- Bozzolan, E., Holcombe, E., Pianosi, F., and Wagener, T.: Including informal housing in slope stability analysis – an application to a data-scarce location in the humid tropics, *Nat. Hazards Earth Syst. Sci. Discuss.*, 1–20, <https://doi.org/10.5194/nhess-2020-207>, 2020.
- Brand, E. W., Premchitt, J., and Phillipson, H. B.: Relationship between rainfall and landslides in Hong Kong, in: *Proceedings of the 4th International Symposium on Landslides*, 377–384, 1984.
- Breiman, L., Friedman, J., J, S., and RA, O.: *Classification and regression trees*, CRC Press, 1984.

- Brunetti, M. T., Peruccacci, S., Rossi, M., Luciani, S., Valigi, D., and Guzzetti, F.: Rainfall thresholds for the possible occurrence of landslides in Italy, *Nat. Hazards Earth Syst. Sci.*, 10, 447–458, 2010.
- Bull-Kamanga, L., Diagne, K., Lavell, A., Leon, E., Lerise, F., MacGregor, H., Maskrey, A., Meshack, M., Pelling, M., Reid, H., Satterthwaite, D., Songsore, J., Westgate, K., and Yitambe, A.: From everyday hazards to disasters: The accumulation of risk in urban areas, *Environ. Urban.*, 15, 193–204, <https://doi.org/10.1630/095624703101286457>, 2003.
- Buma, J. and Dehn, M.: Impact of climate change on a landslide in South East France, simulated using different GCM scenarios and downscaling methods for local precipitation, *Clim. Res.*, 15, 69–81, <https://doi.org/10.3354/cr015069>, 2000.
- Burton, A., Arkell, T. J., and Bathurst, J. C.: Field variability of landslide model parameters, *Environ. Geol.*, 35, 100–114, <https://doi.org/10.1007/s002540050297>, 1998.
- Caine, N.: The Rainfall Intensity : Duration Control of Shallow Landslides and Debris Flows Author ( s ): Nel Caine Published by : Wiley on behalf of the Swedish Society for Anthropology and Geography Stable URL : <http://www.jstor.org/stable/520449> REFERENCES Linked, *Soc. Swedish Ann. Geogr. Geogr. Phys.*, 62, 23–27, 1980a.
- Caine, N.: The rainfall intensity-duration control of shallow landslides and debris flows, *Geogr. Ann. Ser. A, Phys. Geogr.*, 62, 23–27, 1980b.
- Carrara, A., Cardinali, M., Detti, R., Guzzetti, F., Pasqui, V., and Reichenbach, P.: GIS techniques and statistical models in evaluating landslide hazard, *Earth Surf. Process. Landforms*, 16, 427–445, <https://doi.org/10.1002/esp.3290160505>, 1991.
- Carrara, A., Cardinali, M., Guzzetti, F., and Reichenbach, P.: Gis Technology in Mapping Landslide Hazard, 135–175, [https://doi.org/10.1007/978-94-015-8404-3\\_8](https://doi.org/10.1007/978-94-015-8404-3_8), 1995.
- Castro, C. P., Ibarra, I., Lukas, M., Ortiz, J., and Sarmiento, J. P.: Disaster risk construction in the progressive consolidation of informal settlements: Iquique and Puerto Montt (Chile) case studies, *Int. J. Disaster Risk Reduct.*, 13, 109–127, <https://doi.org/10.1016/j.ijdrr.2015.05.001>, 2015.
- Catani, F., Segoni, S., and Falorni, G.: An empirical geomorphology-based approach to the spatial prediction of soil thickness at catchment scale, *Water Resour. Res.*, 46, 1–15, <https://doi.org/10.1029/2008WR007450>, 2010.
- Cheng, P. F. K.: The New Priority Ranking Systems for Man-made Slopes and Retaining Walls, Special Project Report (SPR) 4/2009, *Geotech. Eng. Off. (GEO)*, Hong Kong, 6–14, 2009.
- Cho, S. E.: Effects of spatial variability of soil properties on slope stability, *Eng. Geol.*, 92, 97–109, <https://doi.org/10.1016/j.enggeo.2007.03.006>, 2007.
- Chok, Y. H., Jaksa, M. B., Kaggwa, W. S., and Griffiths, D. V.: Assessing the influence of root reinforcement on slope stability by finite elements, *Int. J. Geo-Engineering*, 6, <https://doi.org/10.1186/s40703-015-0012-5>, 2015.
- Choudhuri, K. and Chakraborty, D.: Probabilistic Bearing Capacity of a Pavement Resting on Fibre Reinforced Embankment Considering Soil Spatial Variability, 7, 1–13, <https://doi.org/10.3389/fbuil.2021.628016>, 2021.
- Chowdhury, P. A. R.: Landslide hazard assessment : summary review and new perspectives, 21–44, 1999.
- Ciabatta, L., Camici, S., Brocca, L., Ponziani, F., Stelluti, M., Berni, N., and Moramarco, T.: Assessing the impact of climate-change scenarios on landslide occurrence in Umbria Region, Italy, *J. Hydrol.*, 541, 285–295, <https://doi.org/10.1016/j.jhydrol.2016.02.007>, 2016.



- Collins, M., Chandler, R. E., Cox, P. M., Huthnance, J. M., Rougier, J., and Stephenson, D. B.: Quantifying future climate change, *Nat. Clim. Chang.*, 2, 403–409, <https://doi.org/10.1038/nclimate1414>, 2012.
- Collison, A., Wade, S., Griffiths, J., and Dehn, M.: Modelling the impact of predicted climate change on landslide frequency and magnitude in SE England, *Eng. Geol.*, 55, 205–218, [https://doi.org/10.1016/S0013-7952\(99\)00121-0](https://doi.org/10.1016/S0013-7952(99)00121-0), 2000.
- Collison, A. J. C.: Assessing the influence of vegetation on slope stability in the tropics, Ph.D. Thesis, Univ. Bristol, 1993.
- Collison, A. J. C. and Anderson, M. G.: Using a combined slope hydrology/stability model to identify suitable conditions for landslide prevention by vegetation in the humid tropics, *Earth Surf. Process. Landforms*, 21, 737–747, 1996.
- Collison, A. J. C., Anderson, M. G., and Lloyd, D. M.: Impact of vegetation on slope stability in a humid tropical environment: A modelling approach, *Proc. Inst. Civ. Eng. Water, Marit. Energy*, 112, 168–175, <https://doi.org/10.1680/iwtme.1995.27662>, 1995.
- Corominas, J., van Westen, C., Frattini, P., Cascini, L., Malet, J. P., Fotopoulou, S., Catani, F., Van Den Eeckhaut, M., Mavrouli, O., Agliardi, F., Pitilakis, K., Winter, M. G., Pastor, M., Ferlisi, S., Tofani, V., Hervás, J., and Smith, J. T.: Recommendations for the quantitative analysis of landslide risk, *Bull. Eng. Geol. Environ.*, 73, 209–263, <https://doi.org/10.1007/s10064-013-0538-8>, 2014.
- CRED: Human cost of disaster, an overview of the last 20 years 2000 - 2019., 2019.
- Crozier, M. J.: Geomorphology Deciphering the effect of climate change on landslide activity : A review, 124, 260–267, <https://doi.org/10.1016/j.geomorph.2010.04.009>, 2010.
- Cui, Y., Cheng, D., Choi, C. E., Jin, W., Lei, Y., and Kargel, J. S.: The cost of rapid and haphazard urbanization: lessons learned from the Freetown landslide disaster, 1167–1176, <https://doi.org/10.1007/s10346-019-01167-x>, 2019.
- Dahal, R. K., Hasegawa, S., Masuda, T., and Yamanaka, M.: Roadside Slope Failures in Nepal during Torrential Rainfall and their Mitigation Road construction practice in Nepal, 503–514, 2006.
- Dai, F. ., Lee, C. ., and Ngai, Y. .: Landslide risk assessment and management: an overview, *Eng. Geol.*, 64, 65–87, [https://doi.org/10.1016/S0013-7952\(01\)00093-X](https://doi.org/10.1016/S0013-7952(01)00093-X), 2002.
- Dai, F. C. and Lee, C. F.: A spatiotemporal probabilistic modelling of storm-induced shallow landsliding using aerial photographs and logistic regression, *Earth Surf. Process. Landforms*, 28, 527–545, <https://doi.org/10.1002/esp.456>, 2003.
- Dalal, S., Han, B., Lempert, R., Jaycocks, A., and Hackbarth, A.: Improving scenario discovery using orthogonal rotations, *Environ. Model. Softw.*, 48, 49–64, 2013.
- Daleon, C. F. and Lorenzo, G. A.: Empirical models for predicting the spatial variation of soil thickness and shear strength for landslide susceptibility assessment, *J. Nepal Geol. Soc.*, 55, 85–91, <https://doi.org/10.3126/jngs.v55i1.22795>, 2018.
- Darcy, H. P. G.: Les Fontaines publiques de la ville de Dijon. Exposition et application des principes à suivre et des formules à employer dans les questions de distribution d'eau, etc, V. Dalamont, 1856.
- DeGraff, J. F.: Landslide hazard on St. Lucia, West Indies, Final Report, Organization of American States, Washington, D. C., 1985.
- Dehn, M. and Buma, J.: Modelling future landslide activity based on general circulation models, 30, 175–187, [https://doi.org/10.1016/S0169-555X\(99\)00053-7](https://doi.org/10.1016/S0169-555X(99)00053-7), 1999.

- Dehn, M., Bürger, G., Buma, J., and Gasparetto, P.: Impact of climate change on slope stability using expanded downscaling, *Eng. Geol.*, 55, 193–204, [https://doi.org/10.1016/S0013-7952\(99\)00123-4](https://doi.org/10.1016/S0013-7952(99)00123-4), 2000.
- Delfin, F. G. and Gaillard, J. C.: Extreme versus quotidian: Addressing temporal dichotomies in Philippine disaster management, *Public Adm. Dev.*, 28, 190–199, <https://doi.org/10.1002/pad.493>, 2008.
- Derose, R. C., Trustrum, N. a, Blaschke, P. M., and North, P.: G E O M O R P H I C C H a N G E I M P L I E D B y Regolith - Slope Relationships on Steepland Hillslopes , Taranaki , New Zealand, 18, 489–514, 1991.
- Diaz, V. J.: Landslides in the squatter settlements of Caracas; towards a better understanding of causative factors, *Environ. Urban.*, 4, 80–89, 1992.
- Dietrich, W. E., Reiss, R., Hsu, M. -L, and Montgomery, D. R.: A process-based model for colluvial soil depth and shallow landsliding using digital elevation data, *Hydrol. Process.*, 9, 383–400, <https://doi.org/10.1002/hyp.3360090311>, 1995.
- Dilley, M., Chen, R. S., Deichmann, U., Lerner-Lam, A., Arnold, M., Agwe, J., Buys, P., Kjekstad, O., Lyon, B., and Yetman, G.: Natural disaster hotspots: A global risk analysis, 1-132 pp., 2005.
- DIWI: Materials Report. RDP-001 Soufriere-Choiseul, DIWI Consult Int. GmbH, Consult. Serv. Roads Dev. Program. Minist. Commun. Work. Transp. Public Util. Gov. Saint Lucia., 2002.
- Dixon, N. and Brook, E.: Impact of predicted climate change on landslide reactivation: Case study of Mam Tor, UK, 4, 137–147, <https://doi.org/10.1007/s10346-006-0071-y>, 2007.
- Eckhardt, K., Breuer, L., and Frede, H. G.: Parameter uncertainty and the significance of simulated land use change effects, *J. Hydrol.*, 273, 164–176, [https://doi.org/10.1016/S0022-1694\(02\)00395-5](https://doi.org/10.1016/S0022-1694(02)00395-5), 2003.
- Efron, B. and Tibshirani, R. J.: An introduction to the bootstrap, CRC press, 1994.
- El-Ramly, H., Morgenstern, N. R., and Cruden, D. M.: Probabilistic assessment of stability of a cut slope in residual soil, *Risk Var. Geotech. Eng. Inst. Civ. Eng.*, 197–204, <https://doi.org/10.1680/ravige.34860.0020>, 2006.
- Ercanoglu, M. and Gokceoglu, C.: Assessment of landslide susceptibility for a landslide-prone area (north of Yenice, NW Turkey) by fuzzy approach, *Environ. Geol.*, 41, 720–730, <https://doi.org/10.1007/s00254-001-0454-2>, 2002.
- Fekade, W.: Deficits of formal urban land management and informal responses under rapid urban growth, an international perspective, *Habitat Int.*, 24, 127–150, [https://doi.org/10.1016/S0197-3975\(99\)00034-X](https://doi.org/10.1016/S0197-3975(99)00034-X), 2000.
- Finlay, P. J., Fell, R., and Maguire, P. K.: The relationship between the probability of landslide occurrence and rainfall, 1997.
- Folberth, C., Skalský, R., Moltchanova, E., Balkovič, J., Azevedo, L. B., Obersteiner, M., and Van Der Velde, M.: Uncertainty in soil data can outweigh climate impact signals in global crop yield simulations, *Nat. Commun.*, 7, 1–13, <https://doi.org/10.1038/ncomms11872>, 2016.
- Formetta, G., Rago, V., Capparelli, G., Rigon, R., and Versace, P.: Integrated Physically based system for modeling landslide susceptibility, *Procedia Earth Planet. Sci.*, 9, 74–82, <https://doi.org/10.1016/j.proeps.2014.06.006>, 2014.
- Frattini, P., Crosta, G., and Carrara, A.: Techniques for evaluating the performance of landslide susceptibility models, *Eng. Geol.*, 111, 62–72, <https://doi.org/10.1016/j.enggeo.2009.12.004>, 2010.
- Froude, M. J. and Petley, D. N.: Global fatal landslide occurrence from 2004 to 2016, 2161–2181, 2018a.

- Froude, M. J. and Petley, D. N.: Global fatal landslides 2004 to 2016, *Nat. Hazards Earth Syst. Sci.*, 18, 2161–2181, 2018b.
- Gaillard, J. C. and Mercer, J.: From knowledge to action: Bridging gaps in disaster risk reduction, *Prog. Hum. Geogr.*, 37, 93–114, <https://doi.org/10.1177/0309132512446717>, 2013.
- Galve, J. P., Cevasco, A., Brandolini, P., and Soldati, M.: Assessment of shallow landslide risk mitigation measures based on land use planning through probabilistic modelling, 12, 101–114, <https://doi.org/10.1007/s10346-014-0478-9>, 2015.
- Gariano, S. L. and Guzzetti, F.: Landslides in a changing climate, *Earth-Science Rev.*, 162, 227–252, <https://doi.org/10.1016/j.earscirev.2016.08.011>, 2016.
- Gariano, S. L., Brunetti, M. T., Iovine, G., Melillo, M., Peruccacci, S., Terranova, O., Vennari, C., and Guzzetti, F.: Calibration and validation of rainfall thresholds for shallow landslide forecasting in Sicily, southern Italy, 228, 653–665, <https://doi.org/10.1016/j.geomorph.2014.10.019>, 2015.
- Van Genuchten, M. T.: A closed-form equation for predicting the hydraulic conductivity of unsaturated soils 1, *Soil Sci. Soc. Am. J.*, 44, 892–898, 1980.
- GEO: Geoguide 3- Guide to Rock and Soil Descriptions, *Geotech. Eng. Off.*, 177, 1988.
- Gerrard, J. and Gardner, R.: Relationships Between Landsliding and Land Use in the Likhu Khola Drainage Basin, Middle Hills, Nepal, *Mt. Res. Dev.*, 22, 48–55, [https://doi.org/10.1659/0276-4741\(2002\)022\[0048:rblalu\]2.0.co;2](https://doi.org/10.1659/0276-4741(2002)022[0048:rblalu]2.0.co;2), 2006.
- Glade, T.: Landslide occurrence as a response to land use change: A review of evidence from New Zealand, 51, 297–314, [https://doi.org/10.1016/S0341-8162\(02\)00170-4](https://doi.org/10.1016/S0341-8162(02)00170-4), 2003.
- Glade, T. and Crozier, M. J.: Landslide hazard and risk: concluding comment and perspectives, 767–774, 2005.
- Godt, J. W., Baum, R. L., Savage, W. Z., Salciarini, D., Schulz, W. H., and Harp, E. L.: Transient deterministic shallow landslide modeling: Requirements for susceptibility and hazard assessments in a GIS framework, *Eng. Geol.*, 102, 214–226, <https://doi.org/10.1016/j.enggeo.2008.03.019>, 2008.
- Gorsevski, P. V. and Jankowski, P.: An optimized solution of multi-criteria evaluation analysis of landslide susceptibility using fuzzy sets and Kalman filter, *Comput. Geosci.*, 36, 1005–1020, <https://doi.org/10.1016/j.cageo.2010.03.001>, 2010.
- Gorsevski, P. V., Gessler, P. E., Boll, J., Elliot, W. J., and Foltz, R. B.: Spatially and temporally distributed modeling of landslide susceptibility, 80, 178–198, <https://doi.org/10.1016/j.geomorph.2006.02.011>, 2006.
- Greenwood, J. R., Norris, J. E., and Wint, J.: Assessing the contribution of vegetation to slope stability, *Proc. Inst. Civ. Eng. - Geotech. Eng.*, 157, 199–207, <https://doi.org/10.1680/geng.2004.157.4.199>, 2004.
- Griffiths, D. V., Asce, M., Fenton, G. A., Asce, M., Manoharan, N., and Asce, A.: Bearing Capacity of Rough Rigid Strip Footing on Cohesive Soil : Probabilistic Study, 128, 743–755, 2002.
- Groves, D. G. and Lempert, R. J.: A new analytic method for finding policy-relevant scenarios, *Glob. Environ. Chang.*, 17, 73–85, <https://doi.org/10.1016/j.gloenvcha.2006.11.006>, 2007.
- Guzzetti, F.: Landslide fatalities and the evaluation of landslide risk in Italy, *Eng. Geol.*, 58, 89–107, [https://doi.org/10.1016/S0013-7952\(00\)00047-8](https://doi.org/10.1016/S0013-7952(00)00047-8), 2000.
- Guzzetti, F.: Probabilistic landslide hazard assessment: An example in the collazzone area, central Italy, 2005.

- Guzzetti, F., Carrara, A., Cardinali, M., and Reichenbach, P.: Landslide hazard evaluation: A review of current techniques and their application in a multi-scale study, Central Italy, 31, 181–216, [https://doi.org/10.1016/S0169-555X\(99\)00078-1](https://doi.org/10.1016/S0169-555X(99)00078-1), 1999.
- Guzzetti, F., Reichenbach, P., Ardizzone, F., Cardinali, M., and Galli, M.: Estimating the quality of landslide susceptibility models, 81, 166–184, <https://doi.org/10.1016/j.geomorph.2006.04.007>, 2006a.
- Guzzetti, F., Galli, M., Reichenbach, P., Ardizzone, F., and Cardinali, M.: Landslide hazard assessment in the Collazzone area, Umbria, Central Italy, 115–131, 2006b.
- Guzzetti, F., Peruccacci, S., Rossi, M., and Stark, C. P.: Rainfall thresholds for the initiation of landslides in central and southern Europe, *Meteorol. Atmos. Phys.*, 98, 239–267, 2007.
- Hamm, N. A. S., Hall, J. W., and Anderson, M. G.: Variance-based sensitivity analysis of the probability of hydrologically induced slope instability, 32, 803–817, <https://doi.org/10.1016/j.cageo.2005.10.007>, 2006.
- Hanley, J. A. and McNeil, B. J.: The Meaning and Use of the Area under a Receiver Operating Characteristic (ROC) Curve, *Radiology*, 143, 29–36, 1982.
- Haque, U., da Silva, P. F., Devoli, G., Pilz, J., Zhao, B., Khaloua, A., Wilopo, W., Andersen, P., Lu, P., Lee, J., Yamamoto, T., Keellings, D., Jian-Hong, W., and Glass, G. E.: The human cost of global warming: Deadly landslides and their triggers (1995–2014), *Sci. Total Environ.*, 682, 673–684, <https://doi.org/10.1016/j.scitotenv.2019.03.415>, 2019.
- Harari, N., Gavilano, A., and Liniger, H.: Where people and their land are safer: A Compendium of Good Practices in Disaster Risk Reduction, 2017.
- Heimsath, A. M., Dietrichs, W. E., Nishiizumi, K., and Finkel, R. C.: The soil production function and landscape equilibrium, *Nature*, 388, 358–361, <https://doi.org/10.1038/41056>, 1997.
- Hencher, S. R. and Lee, S. G.: Landslide mechanisms in Hong Kong, *Geol. Soc. Eng. Geol. Spec. Publ.*, 23, 77–103, <https://doi.org/10.1144/EGSP23.6>, 2010.
- Ho, J. Y., Lee, K. T., Chang, T. C., Wang, Z. Y., and Liao, Y. H.: Influences of spatial distribution of soil thickness on shallow landslide prediction, *Eng. Geol.*, 124, 38–46, <https://doi.org/10.1016/j.enggeo.2011.09.013>, 2012.
- Hodnett, M. G. and Tomasella, J.: Marked differences between van Genuchten soil water-retention parameters for temperate and tropical soils : a new water-retention pedo-transfer functions developed for tropical soils, 108, 155–180, 2002.
- Holcombe, E. A.: Modelling Landslide Risk on Highway Cut Slopes in Developing Countries, PhD thesis, Univ. Bristol, Bristol, UK., 2006.
- Holcombe, E. A., Beesley, M. E. W., Vardanega, P. J., and Sorbie, R.: Urbanisation and landslides: hazard drivers and better practices, *Proc. Inst. Civ. Eng. - Civ. Eng.*, 169, 137–144, <https://doi.org/10.1680/jcien.15.00044>, 2016.
- Hornberger, G. M. and Spear, R. C.: An approach to the preliminary analysis of environmental systems, *J. Environ. Manage.*, 12, 7–18, 1981.
- Huabin, W., Gangjun, L., Weiya, X., and Gonghui, W.: GIS-based landslide hazard assessment : an overview, 4, 548–567, 2005.
- IFRC: World Disasters Report 2020, World Disaster Report 2020, Geneva, 365 pp., 2020.
- IPCC: Summary for Policymakers. In: Managing the Risks of Extreme Events and Disasters to Advance Climate Change Adaptation, A Special Report of Working Groups I and II of the Intergovernmental Panel on

- Climate Change, Cambridge University Press, Cambridge, UK, and New York, NY, USA, 1-19 pp., 2012.
- IPCC: Synthesis Report: Contribution of Working Groups I, II and III to the Fifth Assessment Report of the Intergovernmental Panel on Climate Change, edited by The Core Writing Team, Rajendra K. Pachauri, and Leo Meyer (Geneva, Switzerland: Intergovernmental Pa, IPCC\_SynthesisReport. pdf, 2014.
- IPCC: Global warming of 1.5°C. An IPCC Special Report on the impacts of global warming of 1.5°C above pre-industrial levels and related global greenhouse gas emission pathways, in the context of strengthening the global response to the threat of climate change, IPCC\_SynthesisReport. pdf, 2018.
- Jakob, M. and Lambert, S.: Climate change effects on landslides along the southwest coast of British Columbia, 107, 275–284, <https://doi.org/10.1016/j.geomorph.2008.12.009>, 2009.
- Jetten, V.: CHaRIM Project Saint Lucia National Flood Hazard Map Methodology and Validation Report, 1-40 pp., 2016.
- Jomelli, V., Brunstein, D., Déqué, M., Vrac, M., and Grancher, D.: Impacts of future climatic change (2070-2099) on the potential occurrence of debris flows: A case study in the Massif des Ecrins (French Alps), *Clim. Change*, 97, 171–191, <https://doi.org/10.1007/s10584-009-9616-0>, 2009.
- El Kechebour, B.: Relation between Stability of Slope and the Urban Density: Case Study, *Procedia Eng.*, 114, 824–831, <https://doi.org/10.1016/j.proeng.2015.08.034>, 2015.
- Kirschbaum, D., Stanley, T., and Zhou, Y.: Spatial and temporal analysis of a global landslide catalog, 249, 4–15, <https://doi.org/10.1016/j.geomorph.2015.03.016>, 2015.
- Kirschbaum, D. B., Adler, R., Hong, Y., Hill, S., and Lerner-Lam, A.: A global landslide catalog for hazard applications: Method, results, and limitations, *Nat. Hazards*, 52, 561–575, <https://doi.org/10.1007/s11069-009-9401-4>, 2010.
- Klohn-Crippen: Roseau Dam and ancillary works. Tropical storm Debbie, *Geogr. Ann. Ser. A, Phys. Geogr.*, 1995.
- Knutson, T. R. and Tuleya, R. E.: Impact of CO<sub>2</sub>-induced warming on simulated hurricane intensity and precipitation: Sensitivity to the choice of climate model and convective parameterization, *J. Clim.*, 17, 3477–3495, [https://doi.org/10.1175/1520-0442\(2004\)017<3477:IOCWOS>2.0.CO;2](https://doi.org/10.1175/1520-0442(2004)017<3477:IOCWOS>2.0.CO;2), 2004.
- Knutson, T. R., Sirutis, J. J., Zhao, M., Tuleya, R. E., Bender, M., Vecchi, G. A., Villarini, G., and Chavas, D.: Global projections of intense tropical cyclone activity for the late twenty-first century from dynamical downscaling of CMIP5/RCP4.5 scenarios, *J. Clim.*, 28, 7203–7224, <https://doi.org/10.1175/JCLI-D-15-0129.1>, 2015.
- Kohli, D., Sliuzas, R., Kerle, N., and Stein, A.: An ontology of slums for image-based classification, *Comput. Environ. Urban Syst.*, 36, 154–163, <https://doi.org/10.1016/j.compenvurbsys.2011.11.001>, 2012.
- Kolmogorov, A.: Sulla determinazione empirica di una legge di distribuzione, 4, 83–91, 1933.
- Kuffer, M., Thomson, D. R., Boo, G., Mahabir, R., Grippa, T., Vanhuyse, S., Engstrom, R., Ndugwa, R., Makau, J., Darin, E., de Albuquerque, J. P., and Kabaria, C.: The role of earth observation in an integrated deprived area mapping “system” for low-to-middle income countries, *Remote Sens.*, 12, <https://doi.org/10.3390/rs12060982>, 2020.
- Lam, T. T. M., Sun, H. W., and K.K.S., H.: Review of Landslides in 2001, GEO Report No. 155, 2006.
- Lamb, T. S. K. and Premchitt, J.: Rainfall-runoff on slopes 1984–1988, *Civ. Eng. Serv. Rep. Hong Kong 1990.Special Proj. Rep. I 1/90.*, 1990.
- Lange, W., Sandholz, S., and Nehren, U.: Strengthening urban resilience through nature: The potential of

ecosystem-based measures for reduction of landslide risk in Rio de Janeiro, *Lincoln Inst. L. Policy*, 2018.

Larsen, M. C.: Rainfall-triggered landslides, anthropogenic hazards, and mitigation strategies, *Adv. Geosci.*, 14, 147–153, <https://doi.org/10.5194/adgeo-14-147-2008>, 2008.

Larsen, M. C. and Parks, J. E.: How wide is a road? The association of roads and mass-wasting in a forested montane environment, *Earth Surf. Process. Landforms J. Br. Geomorphol. Gr.*, 22, 835–848, 1997.

Larsen, M. C. and Simon, A.: A rainfall intensity-duration threshold for landslides in a humid-tropical environment, Puerto Rico, *Geogr. Ann. Ser. A, Phys. Geogr.*, 75, 13–23, 1993.

Laws, M. J. and Murray, J. G.: *Impacts of Poor Urban Land Development on Slope Instability*, 2001.

Lee, K. T. and Ho, J. Y.: Prediction of landslide occurrence based on slope-instability analysis and hydrological model simulation, *J. Hydrol.*, 375, 489–497, <https://doi.org/10.1016/j.jhydrol.2009.06.053>, 2009.

Lee, S., Choi, Æ. J., and Min, Æ. K.: Landslide susceptibility analysis and verification using the Bayesian probability model, 120–131, <https://doi.org/10.1007/s00254-002-0616-x>, 2002.

Lizárraga, J. J. and Buscarnera, G.: Spatially distributed modeling of rainfall-induced landslides in shallow layered slopes, 16, 253–263, <https://doi.org/10.1007/s10346-018-1088-8>, 2019.

Lloyd, D. M.: *Modelling the hydrology and stability of tropical cut slopes.*, Phd thesis, Univ. Bristol, 1990.

Lumb, P.: Slope failures in Hong Kong, *Q. J. Eng. Geol.*, 8, 31–65, <https://doi.org/10.1144/GSL.QJEG.1975.008.01.02>, 1975.

Malamud, B. D., Turcotte, D. L., Guzzetti, F., and Reichenbach, P.: Landslide inventories and their statistical properties, *Earth Surf. Process. Landforms*, 29, 687–711, <https://doi.org/10.1002/esp.1064>, 2004.

Marchesini, I., Ardizzone, F., Alvioli, M., Rossi, M., and Guzzetti, F.: Non-susceptible landslide areas in Italy and in the Mediterranean region, *Nat. Hazards Earth Syst. Sci.*, 14, 2215–2231, <https://doi.org/10.5194/nhess-14-2215-2014>, 2014.

Di Martire, D., De Rosa, M., Pesce, V., Santangelo, M. A., and Calcaterra, D.: Landslide hazard and land management in high-density urban areas of Campania region, Italy, *Nat. Hazards Earth Syst. Sci.*, 12, 905–926, <https://doi.org/10.5194/nhess-12-905-2012>, 2012.

Mathworks: *Matlab Statistics and Machine Learning Toolbox Re- lease 2018b*, Mathworks Inc., Natwick, MA, USA, 2018.

McKay, M. D., Beckman, R. J., and Conover, W. J.: Comparison of three methods for selecting values of input variables in the analysis of output from a computer code, 21, 239–245, <https://doi.org/10.1080/00401706.1979.10489755>, 1979.

Melchiorre, C. and Frattini, P.: Modelling probability of rainfall-induced shallow landslides in a changing climate, Otta, Central Norway, *Clim. Change*, 113, 413–436, <https://doi.org/10.1007/s10584-011-0325-0>, 2012.

Melillo, M., Brunetti, M. T., Peruccacci, S., Gariano, S. L., Roccati, A., and Guzzetti, F.: *Environmental Modelling & Software A tool for the automatic calculation of rainfall thresholds for landslide occurrence*, *Environ. Model. Softw.*, 105, 230–243, <https://doi.org/10.1016/j.envsoft.2018.03.024>, 2018.

Mendes, R. M.: *Study of experimental fields monitoring geotechnical and climatic variables for the implementation of the warning systems for landslides in the State of Sao Paulo*, 2014.

Mendes, R. M. and Filho, M. V.: *Real-time monitoring of climactic and geotechnical variables during*

- landslides on the slopes of Serra do Mar and Serra da Mantiqueira (Sao Paulo State, Brazil), 7, 140, 2015.
- Mendes, R. M., de Andrade, M. R. M., Graminha, C. A., Prieto, C. C., de Ávila, F. F., and Camarinha, P. I. M.: Stability analysis on urban slopes: Case study of an anthropogenic-induced landslide in Sao Jose dos Campos, Brazil, *Geotech. Geol. Eng.*, 36, 599–610, 2018.
- Mercer, J., Kelman, I., and Dekens, J.: Integrating indigenous and scientific knowledge for disaster risk reduction, *Indig. Knowl. Disaster Risk Reduct. From Pract. to Policy*, 34, 115–131, 2009.
- Metz, M., Mitsova, H., and Harmon, R. S.: Efficient extraction of drainage networks from massive, radar-based elevation models with least cost path search, *Hydrol. Earth Syst. Sci.*, 2010.
- Meusburger, K. and Alewell, C.: Impacts of anthropogenic and environmental factors on the occurrence of shallow landslides in an alpine catchment (Urseren Valley, Switzerland), *Nat. Hazards Earth Syst. Sci.*, 8, 509–520, <https://doi.org/10.5194/nhess-8-509-2008>, 2008.
- Migoñ, P.: Mass movement and landscape evolution in weathered granite and gneiss terrains, *Geol. Soc. Eng. Geol. Spec. Publ.*, 23, 33–45, <https://doi.org/10.1144/EGSP23.4>, 2010.
- Millington, R. J. and Quirk, J. F.: Permeability of Porous Media, *Nature*, 183, 387–388, 1959.
- Monsieurs, E., Kirschbaum, D., Thiery, W., van Lipzig, N., Kervyn, M., Demoulin, A., Jacobs, L., Kervyn, F., and Dewitte, O.: Constraints on Landslide-Climate Research Imposed by the Reality of Fieldwork in Central Africa, 3rd North Am. Symp. Landslides Landslides Putt. Exp. Knowledge, Emerg. Technol. into Pract. 4–8 June 2017, 158–168, 2017.
- Montgomery, D. R. and Dietrich, W. E.: A physically based model for the topographic control on shallow landsliding, 30, 1994.
- Moreda, R., Marcio, M., and Magalha, R.: Stability Analysis on Urban Slopes : Case Study ´ dos ~ o Jose of an Anthropogenic-Induced Landslide in Sa, 599–610, <https://doi.org/10.1007/s10706-017-0303-z>, 2018.
- Mott MacDonald: Landslide Risk Assessment for Saint Lucia’s Primary Road Network, Hurric. Tomas Rehabil. Reconstr. Final Feasibility Rep., 258, 2013.
- Muscarella, R., Uriarte, M., Kolyaie, S., Morton, D. C., and Zimmerman, J. K.: Effects of topography on tropical forest structure depend on climate context, 145–159, <https://doi.org/10.1111/1365-2745.13261>, 2020.
- Nakileza, B. R. and Nedala, S.: Topographic influence on landslides characteristics and implication for risk management in upper Manafwa catchment , Mt Elgon Uganda, 0, 2020.
- Ng, S. L., Chu, L. M., Li, L., and Qin, J.: Performance assessment of slope greening techniques in Hong Kong, *Asian Geogr.*, 28, 135–145, 2011.
- O’Gorman, P. A. and Schneider, T.: The physical basis for increases in precipitation extremes in simulations of 21st-century climate change, *Proc. Natl. Acad. Sci.*, 106, 14773–14777, <https://doi.org/10.1073/pnas.0907610106>, 2009.
- O’Hare, G. and Rivas, S.: The landslide hazard and human vulnerability in La Paz City, Bolivia, *Geogr. J.*, 171, 239–258, <https://doi.org/10.1111/j.1475-4959.2005.00163.x>, 2005.
- Ortuste, F. R.: Living without Sanitary Sewers in Latin America: The Business of Collecting Fecal Sludge in Four Latin American Cities, World Bank, 2–4, 2012.
- Pack, R. T.: SINMAP 2.0 - A Stability Index Approach to Terrain Stability Hazard Mapping, User’s Manual, 1999.

- Paleari, L. and Confalonieri, R.: Sensitivity analysis of a sensitivity analysis: We are likely overlooking the impact of distributional assumptions, *Ecol. Modell.*, 340, 57–63, <https://doi.org/10.1016/j.ecolmodel.2016.09.008>, 2016.
- Pardeshi, S. D., Autade, S. E., and Pardeshi, S. S.: Landslide hazard assessment : recent trends and techniques, 1–11, 2013.
- Parise, M., Calcaterra, D., and Larsen, M. C.: Introduction to Weathering and Slope Movement papers, *Q. J. Eng. Geol. Hydrogeol.*, 37, 76–76, <https://doi.org/10.1144/1470-9236/04-200>, 2004.
- Parker, R. N., Hales, T. C., Mudd, S. M., Grieve, S. W. D., and Constantine, J. A.: Colluvium supply in humid regions limits the frequency of storm-triggered landslides, *Sci. Rep.*, 6, 1–7, <https://doi.org/10.1038/srep34438>, 2016.
- Patton, N. R., Lohse, K. A., Godsey, S. E., Crosby, B. T., and Seyfried, M. S.: Predicting soil thickness on soil mantled hillslopes, *Nat. Commun.*, 9, <https://doi.org/10.1038/s41467-018-05743-y>, 2018.
- Persichillo, M. G., Bordoni, M., Meisina, C., Bartelletti, C., Giannecchini, R., D'Amato Avanzi, G., Galanti, Y., Cevasco, A., Brandolini, P., Galve, J. P., and Barsanti, M.: Shallow landslide susceptibility analysis in relation to land use scenarios, *Landslides Eng. Slopes. Exp. Theory Pract.*, 3, 1605–1612, <https://doi.org/10.1201/b21520-199>, 2016.
- Persichillo, M. G., Bordoni, M., Cavalli, M., Crema, S., and Meisina, C.: The role of human activities on sediment connectivity of shallow landslides, 160, 261–274, <https://doi.org/10.1016/j.catena.2017.09.025>, 2018.
- Peruccacci, S., Teresa, M., Luciani, S., Vennari, C., and Guzzetti, F.: Geomorphology Lithological and seasonal control on rainfall thresholds for the possible initiation of landslides in central Italy, 140, 79–90, <https://doi.org/10.1016/j.geomorph.2011.10.005>, 2012.
- Petley, D.: Global patterns of loss of life from landslides, *Geology*, 40, 927–930, <https://doi.org/10.1130/G33217.1>, 2012.
- Petley, D. N.: On the impact of urban landslides, *Geol. Soc. London, Eng. Geol. Spec. Publ.*, 22, 83–99, <https://doi.org/10.1144/egsp22.6>, 2009.
- Pianosi, F. and Wagener, T.: A simple and efficient method for global sensitivity analysis based on cumulative distribution functions, *Environ. Model. Softw.*, 67, 1–11, <https://doi.org/10.1016/j.envsoft.2015.01.004>, 2015.
- Pianosi, F., Sarrazin, F., and Wagener, T.: A Matlab toolbox for Global Sensitivity Analysis, *Environ. Model. Softw.*, 70, 80–85, <https://doi.org/10.1016/j.envsoft.2015.04.009>, 2015.
- Pianosi, F., Beven, K., Freer, J., Hall, J. W., Rougier, J., Stephenson, D. B., and Wagener, T.: Environmental Modelling & Software Sensitivity analysis of environmental models : A systematic review with practical work flow, *Environ. Model. Softw.*, 79, 214–232, <https://doi.org/10.1016/j.envsoft.2016.02.008>, 2016.
- Pisano, L., Zumpano, V., Malek, Roskopf, C. M., and Parise, M.: Variations in the susceptibility to landslides, as a consequence of land cover changes: A look to the past, and another towards the future, *Sci. Total Environ.*, 601–602, 1147–1159, <https://doi.org/10.1016/j.scitotenv.2017.05.231>, 2017.
- Poulovassilis, A.: The effect of hysteresis of pore-water on the hydraulic conductivity, *J. soil Sci.*, 20, 52–56, 1969.
- Pourghasemi, H. R., Pradhan, B., and Gokceoglu, C.: Application of fuzzy logic and analytical hierarchy process (AHP) to landslide susceptibility mapping at Haraz watershed, Iran, 965–996, <https://doi.org/10.1007/s11069-012-0217-2>, 2012.



- Prancevic, J. P. and Lamb, M. P.: Decreasing Landslide Erosion on Steeper Slopes in Soil - Mantled Landscapes *Geophysical Research Letters*, 1–9, <https://doi.org/10.1029/2020GL087505>, 2020.
- Rahardjo, H., Aung, K. K., Leong, E. C., and Rezaur, R. B.: Characteristics of residual soils in Singapore as formed by weathering, *Eng. Geol.*, 73, 157–169, <https://doi.org/10.1016/j.enggeo.2004.01.002>, 2004.
- Rahardjo, H., Ong, T. H., Rezaur, R. B., and Leong, E. C.: Factors controlling instability of homogeneous soil slopes under rainfall, *J. Geotech. Geoenvironmental Eng.*, 133, 1532–1543, 2007.
- Rahman, M. S., Ahmed, B., and Di, L.: Landslide initiation and runout susceptibility modeling in the context of hill cutting and rapid urbanization: a combined approach of weights of evidence and spatial multi-criteria, *J. Mt. Sci.*, 14, 1919–1937, <https://doi.org/10.1007/s11629-016-4220-z>, 2017.
- Raia, S., Alvioli, M., Rossi, M., Baum, R. L., Godt, J. W., and Guzzetti, F.: Improving predictive power of physically based rainfall-induced shallow landslide models: A probabilistic approach, *Geosci. Model Dev.*, 7, 495–514, <https://doi.org/10.5194/gmd-7-495-2014>, 2014.
- Redshaw, P., Boon, D., Campbell, G., Willis, M., Mattai, J., Free, M., Jordan, C., Kemp, S. J., Morley, A., and Thomas, M.: The 2017 Regent Landslide , Freetown Peninsula , Sierra Leone, 2020.
- Regmi, A. D., Yoshida, K., Dhital, M. R., and Devkota, K.: Effect of rock weathering, clay mineralogy, and geological structures in the formation of large landslide, a case study from Dumre Besei landslide, Lesser Himalaya Nepal, 10, 1–13, <https://doi.org/10.1007/s10346-011-0311-7>, 2013.
- Reichenbach, P., Busca, C., Mondini, A. C., and Rossi, M.: The Influence of Land Use Change on Landslide Susceptibility Zonation: The Briga Catchment Test Site (Messina, Italy), *Environ. Manage.*, 54, 1372–1384, <https://doi.org/10.1007/s00267-014-0357-0>, 2014.
- Reichenbach, P., Rossi, M., Malamud, B. D., Mihir, M., and Guzzetti, F.: A review of statistically-based landslide susceptibility models, *Earth-Science Rev.*, 180, 60–91, <https://doi.org/10.1016/j.earscirev.2018.03.001>, 2018.
- Richards, L. A.: Capillary conduction of liquids through porous mediums, *Physics (College. Park. Md.)*, 1, 318–333, 1931.
- Rivera, C., Tehler, H., and Wamsler, C.: Fragmentation in disaster risk management systems: A barrier for integrated planning, *Int. J. Disaster Risk Reduct.*, 14, 445–456, <https://doi.org/10.1016/j.ijdrr.2015.09.009>, 2015.
- RRL: St Lucia: An Investment Study of Road Links between Castries and Vieux Fort, *Trop. Sect. Road Res. Lab. Crowthorne, UK*, 1970.
- Rutter, A. J., Kershaw, K. A., Robins, P. C., and Morton, A. J.: A predictive model of rainfall interception in forests, I. Derivation of the model from observations in a stand of Corsican pine, *Agr. Meteorol.*, 9, 367–384, 1971.
- Salciarini, D., Godt, J. W., Savage, W. Z., Conversini, P., Baum, R. L., and Michael, J. A.: Modeling regional initiation of rainfall-induced shallow landslides in the eastern Umbria Region of central Italy, 3, 181–194, <https://doi.org/10.1007/s10346-006-0037-0>, 2006.
- Saltelli, A., Ratto, M., Andres, T., Campolongo, F., Cariboni, J., Gatelli, D., Saisana, M., and Tarantola, S.: *Global sensitivity analysis: the primer*, John Wiley & Sons, 2008.
- Samia, J., Temme, A., Bregt, A. K., Wallinga, J., Stuiver, J., Guzzetti, F., Ardizzone, F., and Rossi, M.: Implementing landslide path dependency in landslide susceptibility modelling, 2129–2144, <https://doi.org/10.1007/s10346-018-1024-y>, 2018.

- Satterthwaite, D., Archer, D., Colenbrander, S., Dodman, D., Hardoy, J., Mitlin, D., and Patel, S.: Building Resilience to Climate Change in Informal Settlements, *One Earth*, 2, 143–156, <https://doi.org/10.1016/j.oneear.2020.02.002>, 2020.
- Schmidt, K. M., Roering, J. J., Stock, J. D., Dietrich, W. E., Montgomery, D. R., and Schaub, T.: The variability of root cohesion as an influence on shallow landslide susceptibility in the Oregon Coast Range, *Can. Geotech. J.*, 38, 995–1024, <https://doi.org/10.1139/cgj-38-5-995>, 2001.
- Segoni, S., Piciullo, L., and Gariano, S. L.: A review of the recent literature on rainfall thresholds for landslide occurrence, 1483–1501, <https://doi.org/10.1007/s10346-018-0966-4>, 2018.
- Selby, M. J.: Slope Erosion due to Extreme Rainfall : A Case Study from New Zealand, *Geogr. Ann. Ser. A, Phys. Geogr. S*, 58, 131–138, 1976.
- Seneviratne, S., Nicholls, N., Easterling, D., Goodess, C., Kanae, S., Kossin, J., Luo, Y., Marengo, J., McInnes, K., Rahimi, M., and others: Changes in climate extremes and their impacts on the natural physical environment: An overview of the IPCC SREX report, 2012.
- Sepúlveda, S. A. and Petley, D. N.: Regional trends and controlling factors of fatal landslides in Latin America and the Caribbean, *Nat. Hazards Earth Syst. Sci.*, 15, 1821–1833, <https://doi.org/10.5194/nhess-15-1821-2015>, 2015.
- Shepherd, C. J., Vardanega, P. J., Holcombe, E. A., Hen-Jones, R., and De Luca, F.: Minding the geotechnical data gap: appraisal of the variability of key soil parameters for slope stability modelling in Saint Lucia, *Bull. Eng. Geol. Environ.*, 78, 4851–4864, <https://doi.org/10.1007/s10064-018-01451-5>, 2019.
- Sidle, R. C. and Ziegler, A. D.: The dilemma of mountain roads, *Nat. Geosci.*, 5, 437–438, <https://doi.org/10.1038/ngeo1512>, 2012.
- Sidle, R. C., Ziegler, A. D., Negishi, J. N., Nik, A. R., Siew, R., and Turkelboom, F.: Erosion processes in steep terrain - Truths, myths, and uncertainties related to forest management in Southeast Asia, *For. Ecol. Manage.*, 224, 199–225, <https://doi.org/10.1016/j.foreco.2005.12.019>, 2006.
- Simon, A., Larsen, M. C., and Hupp, C. R.: The role of soil processes in determining mechanisms of slope failure and hillslope development in a humid-tropical forest eastern Puerto Rico, 3, 263–286, [https://doi.org/10.1016/0169-555X\(90\)90007-D](https://doi.org/10.1016/0169-555X(90)90007-D), 1990.
- Simoni, S., Zanotti, F., Bertoldi, G., and Rigon, R.: Modelling the probability of occurrence of shallow landslides and channelized debris flows using GEOtop-FS †, 545, 532–545, <https://doi.org/10.1002/hyp>, 2008.
- Singh, R., Wagener, T., Crane, R., Mann, M. E., and Ning, L.: A vulnerability driven approach to identify adverse climate and land use change combinations for critical hydrologic indicator thresholds: Application to a watershed in Pennsylvania, USA, *Water Resour. Res.*, 50, 3409–3427, 2014.
- Smirnov, N. V.: On the estimation of the discrepancy between empirical curves of distribution for two independent samples, 2, 3–14, 1939.
- Smith, D. A.: Third World Cities in a Global Perspective: The Political Economy of Uneven Urbanisation, *Cap. Cl.*, 21, 215–216, <https://doi.org/10.1177/030981689706200126>, 1996.
- Smith, H., Coupé, F., Garcia-Ferrari, S., Rivera, H., and Mera, W. E. C.: Toward negotiated mitigation of landslide risks in informal settlements: Reflections from a pilot experience in Medellín, Colombia, *Ecol. Soc.*, 25, <https://doi.org/10.5751/ES-11337-250119>, 2020.
- Smyth, C. G. and Royle, S. A.: Urban landslide hazards: Incidence and causative factors in Niteroi, Rio de Janeiro state, Brazil, *Appl. Geogr.*, 20, 95–118, [https://doi.org/10.1016/S0143-6228\(00\)00004-7](https://doi.org/10.1016/S0143-6228(00)00004-7), 2000.

- So, C. L.: Mass Movements Associated with the Rainstorm of June 1966 in Hong Kong, *Trans. Inst. Br. Geogr.*, 53, 55, <https://doi.org/10.2307/621658>, 1971.
- Staley, D. M., Kean, J. W., Cannon, S. H., Schmidt, K. M., and Laber, J. L.: Objective definition of rainfall intensity-duration thresholds for the initiation of post-fire debris flows in southern California, 10, 547–562, <https://doi.org/10.1007/s10346-012-0341-9>, 2013.
- Steger, S., Brenning, A., Bell, R., and Glade, T.: The influence of systematically incomplete shallow landslide inventories on statistical susceptibility models and suggestions for improvements, 14, 1767–1781, <https://doi.org/10.1007/s10346-017-0820-0>, 2017.
- Stokes, A., Atger, C., Bengough, A. G., and Fourcaud, T.: Desirable plant root traits for protecting natural and engineered slopes against landslides, 1–30, <https://doi.org/10.1007/s11104-009-0159-y>, 2009.
- Terzaghi, K.: Mechanism of Landslides, in: *Application of Geology to Engineering Practice*, Geological Society of America, <https://doi.org/10.1130/Berkey.1950.83>, 1950.
- Thiebes, B.: *Landslide analysis and early warning systems: local and regional case study in the Swabian Alb, Germany*, Springer Science & Business Media, 2012.
- UN: *World Urbanization Prospects: The 2018 Revision, Online Edition (ST/ESA/SER.A/420)*, United Nations, Department of Economic and Social Affairs, Population Division, New York: United Nations., 197-236 pp., 2019.
- UN-Habitat: *The challenge of slums: global report on human settlements 2003*, *Manag. Environ. Qual. An Int. J.*, 15, 337–338, 2003.
- UN-Habitat: *Habitat Iii Issue Papers 22 – Informal Settlements*, United Nations Conf. Hous. Sustain. Urban Dev., 2015, 0–8, <https://doi.org/http://dx.doi.org/10.3402/gha.v5i0.19065>, 2015.
- UN-Habitat: *Pro-Poor Climate Action in Informal Settlements, Adress. Most vulnerable first*, 2018.
- UNDP: *Reducing disaster risk: a challenge for development. United Nations development programme.*, 2004.
- UNISDR: *Chart of the Sendai Framework for Disaster Risk Reduction, 2030*, 2015a.
- UNISDR: *Sendai Framework for Disaster Risk Reduction 2015-2030*, The United Nations Office for Disaster Risk Reduction, 2015, Geneva, 169-173 pp., 2015b.
- Vanacker, V., Vanderschaeghe, M., Govers, G., Willems, E., Poesen, J., Deckers, J., and De Bievre, B.: Linking hydrological, infinite slope stability and land-use change models through GIS for assessing the impact of deforestation on slope stability in high Andean watersheds, 52, 299–315, [https://doi.org/10.1016/S0169-555X\(02\)00263-5](https://doi.org/10.1016/S0169-555X(02)00263-5), 2003.
- Varnes, D. J. . I.-C. (Internacional A. of E. G.-C. on L. and O. M. M. on S.: *Landslide hazard zonation: a review of principles and practise*, <https://doi.org/10.1007/BF02594720>, 1984.
- Wagner, T. and Pianosi, F.: What has Global Sensitivity Analysis ever done for us? A systematic review to support scientific advancement and to inform policy-making in earth system modelling, *Earth-Science Rev.*, 194, 1–18, <https://doi.org/10.1016/j.earscirev.2019.04.006>, 2019.
- Wamsler, C.: *Mainstreaming risk reduction in urban planning and housing: A challenge for international aid organisations*, *Econ. Outlook*, 30, 151–177, <https://doi.org/10.1111/j.0361-3666.2006.00313.x>, 2006.
- Wamsler, C.: *Bridging the gaps: Stakeholder-based strategies for risk reduction and financing for the urban poor*, *Environ. Urban.*, 19, 115–142, <https://doi.org/10.1177/0956247807077029>, 2007.

- Wechsler, S. P. and Kroll, C. N.: Quantifying DEM Uncertainty and its Effect on Topographic Parameters, 72, 1081–1090, 2006.
- Van Westen, C. J.: Caribbean Handbook on Risk Information Management National Scale Landslide Susceptibility Assessment for Saint Lucia, 2016.
- Van Westen, C. J., Rengers, N., Terlien, M. T. J., and Soeters, R.: Prediction of the occurrence of slope instability phenomena through GIS-based hazard zonation, *Geol Rundsh*, 86, 404–414, 1997.
- Van Westen, C. J., van Asch, T. W. J., and Soeters, R.: Landslide hazard and risk zonation - Why is it still so difficult?, *Bull. Eng. Geol. Environ.*, 65, 167–184, <https://doi.org/10.1007/s10064-005-0023-0>, 2006.
- Van Westen, C. J.: The modeling of landslide hazards using GIS, *Surv. Geophys.*, 21, 241–255, <https://doi.org/10.1023/A:1006794127521>, 2000.
- Van Westen, C. J., Jordan, C. J., Grebby, S., Dijkstra, T., Dashwood, C., and Cigna, F.: National Scale Landslide Susceptibility Assessment for Saint Lucia, CHARIM Caribb. Handb. Risk Inf. Manag. World Bank GFDRR, ACP-EU Nat. Disaster Risk Reduct. Progr., 2016.
- Wilby, R. L. and Dessai, S.: Robust adaptation to climate change, 65, 180–185, <https://doi.org/10.1002/wea.504>, 2010.
- Wilby, R. L. and Wigley, T. M. L.: Downscaling general circulation model output: a review of methods and limitations, *Prog. Phys. Geogr.*, 21, 530–548, 1997.
- Wilkinson, P. L., Anderson, M. G., and Lloyd, D. M.: AN INTEGRATED HYDROLOGICAL MODEL FOR RAIN-INDUCED LANDSLIDE PREDICTION, 1297, 1285–1297, <https://doi.org/10.1002/esp.409>, 2002a.
- Wilkinson, P. L., Anderson, M. G., Lloyd, D. M., and Renaud, J. P.: Landslide hazard and bioengineering: Towards providing improved decision support through integrated numerical model development, *Environ. Model. Softw.*, 17, 333–344, [https://doi.org/10.1016/S1364-8152\(01\)00078-0](https://doi.org/10.1016/S1364-8152(01)00078-0), 2002b.
- Wisner, B., Blaikie, P. M., Blaikie, P., Cannon, T., and Davis, I.: At risk: natural hazards, people's vulnerability and disasters, Psychology Press, 2004.
- Wisner, B., Gaillard, J., and Kelman, I.: Framing Disaster, *Handb. Hazards Disaster Risk Reduct.*, <https://doi.org/10.4324/9780203844236.ch3>, 2015.
- Wong, H. N. and Ko, F. W. .: Landslide Risk Assessment - Application and Practice, *GEO Rep. No.*, 275, 2005.
- World Bank: Disaster risk management in Latin America and the Caribbean Region: GFDRR country notes (English), World Bank, COPERNICUS GESELLSCHAFT MBH, Washington, D.C., 226–235 pp., 2012.
- Zêzere, J., Rodrigues, M., Reis, E., and Oliveira, S.: Spatial and temporal data management for the probabilistic landslide hazard assessment considering landslide typology, *Landslides Eval. Stab. Terrain Eval. Stabilisation, Set 2 Vol.*, 117–123, <https://doi.org/10.1201/b16816-15>, 2004.
- Zhang, F., Liu, G., Chen, W., Liang, S., Chen, R., and Han, W.: Human-induced landslide on a high cut slope: a case of repeated failures due to multi-excavation, *J. Rock Mech. Geotech. Eng.*, 4, 367–374, <https://doi.org/10.3724/SP.J.1235.2012.00367>, 2012.

# Curriculum Vitae

## Elisa Bozzolan

elisa.bozzolan@bristol.ac.uk

### Education

---

11/2016 – 02/2021	PhD in Water and Environmental Engineering University of Bristol <i>Thesis: Quantifying the influence of informal housing on rainfall-triggered landslides in the humid tropics</i>
02/2014 – 08/2014	Erasmus Exchange Program University of Aberdeen, United Kingdom <i>Master thesis: Flow-Seaweed Interactions at the Blade Scale and their Significance in Aquaculture: An Experimental Study</i>
09/2012 – 09/2014	MSc in Civil and Environmental Engineering (Laura Magistrale) Università degli studi di Padova Master in: Hydraulic Engineering
09/2008 – 09/2012	BSc in Civil Engineering Università degli studi di Padova

### Teaching

---

02/2017 – 09/2020	Teaching Assistant and marking for Postgraduate modules at University of Bristol, United Kingdom: <i>Applied Soil Mechanics, Numerical Analysis using Matlab, Applied statistics</i>
-------------------	---

### Work experience

---

02/2015 – 08/2015	Studio Tecnico Ing. Avventi (Padova – Italy) Analysis and design of hydropower plants.
10/2014 – 02/2015	GGP Global Garden Products Spa (Treviso – Italy) Process Engineering office. <i>Optimization of the production processes (lean theory); quality gates management and improvement; hydraulic system analysis and costs evaluation</i>
01/2014 – 06/2014	Kairos-Consulting Company Spa (Padova – Italy) <i>Management and Representation of Company processes, conforming to the Quality certification (guideline ISO9001). Optimization of the internal organization.</i>

### Skills and extra-curricular experience

---

Languages:	Italian (Mother tongue), English (Fluent), Spanish (Fluent)
Software:	ArcGIS – CHASM – AutoCAD – Hec-Ras
Programming language:	Matlab – C++
Voluntary experience:	Bioconstruction in San Marco Sierra, Cordoba (Argentina) – 4 months.
Interests:	Volleyball players (semi-professional level for six years); friends say I could be a professional chef; painting and taking photos are my favourite hobbies.

## Software development

---

Extension of the software CHASM

Source code (C++) extended to include surface water management on slope stability analysis.

## Publications

---

### Journal (peer reviewed):

**Bozzolan E.**, Holcombe E.A., Pianosi F., Wagener T., Marchesini I., Alvioli M. (in preparation)  
*Mapping landslide hazard in a data scarce region under changing urbanisation and climate.*

**Bozzolan E.**, Holcombe E.A., Pianosi F., Wagener T. (2020)  
*Including informal housing in slope stability analysis – an application to a data-scarce location in the humid tropics*, Nat. Hazards Earth Syst. Sci. Discuss., 1–20, doi:10.5194/nhess-2020-207, 2020.

### Book chapter:

Holcombe E.A., Hen-Jones R., Vardanega P.J., Beesley M.E.W., Gilder C.E.L., **Bozzolan E.** (2021)  
*Co-Producing Data and Decision Support Tools to Reduce Landslide Risk in the Humid Tropics*. In: Sassa K., Mikoš M., Sassa S., Bobrowsky P.T., Takara K., Dang K. (eds) Understanding and Reducing Landslide Disaster Risk. WLF 2020. ICL Contribution to Landslide Disaster Risk Reduction. Springer, Cham. [https://doi.org/10.1007/978-3-030-60196-6\\_49](https://doi.org/10.1007/978-3-030-60196-6_49)

## Conference Presentation

---

### Oral presentations:

*Quantification of Urban Environment's Role in Slope Stability for Landslide Events*, AGU American Geophysical Union 2017, in New Orleans, Louisiana.

### Poster presentations:

*Do informal urban activities increase the likelihood of landslides?*, European Geosciences Union General Assembly 2018, Vienna, Austria

*When informal urban activities increase the likelihood of landslides?*, European Geosciences Union General Assembly 2019, Vienna, Austria

## Award

---

EPSRC Impact Acceleration Account 2020 – Digital Environment Sandpit Award (April 2021 – July 2021)

*A new modelling framework for evidence-based landslide hazard mitigation strategies in the humid tropics.*

The new methodology developed in this thesis will be applied in Freetown (Sierra Leone) in partnership with the UK engineering consultants Arup to demonstrate the relative role of deforestation and informal housing on landslide hazard as a basis for identifying appropriate mitigation strategies.

